Elucidating the suppression of root hair formation by a member of a novel, short ENTH protein family in *Arabidopsis thaliana*

Nina Freimuth

Dissertation

zur Erlangung des akademischen Grades
„Doctor rerum naturalium"
(Dr. rer. nat.)

in der Wissenschaftsdisziplin „Molekulare Pflanzenphysiologie"

an der Universität Potsdam
Mathematisch-Naturwissenschaftliche Fakultät
Institut für Biochemie und Biologie

Ort und Tag der Disputation:
Potsdam, 16.04.2024

Content

List of figures

List of tables

Abbreviations

(dd)H$_2$O	(double-distilled) water
(v/v)	volume per volume
(w/v)	weight per volume
A. thaliana	*Arabidopsis thaliana*
A. tumefaciens	*Agrobacterium tumefaciens*
ACT2	ACTIN2
ADP	adenosine diphosphate
ADR	adaptin-related protein
AGO1	ARGONAUTE1
AMT	AMMONIUM TRANSPORTER
ANOVA	analysis of variance
ANTH	AP180 N-terminal homology
AP	adaptor protein
APC/C	Anaphase Promoting Complex/Cyclosome
APS	ammonium persulfate
ARF	AUXIN RESPONSE FACTORS
ARF	ADP ribosylation factor
AS	acetosyringone
ATP	adenosine triphosphate
AUX1	AUXIN RESISTANT1
B. cinerea	*Botrytis cinerea*
bp	base pair
BFA	brefeldin A
bHLH	basic helix-loop-helix
BiFC	bimolecular fluorescence complementation
CALS3	CALLOSE SYNTHASE 3
CAP1	CLATHRIN ASSOCIATED PROTEIN 1
Cas9	CRISPR associated protein 9
CCS52	CELL CYCLE SWITCH52
CCV	clathrin-coated vesicles
CDC20	Cell Division Cycle20
CDH1	CDC20 Homolog1

cDNA	complementary DNA
CDS	coding sequence
CDS3	cytidinephosphate diacylglycerol synthase 3
CESA	cellulose synthase
CHC	clathrin heavy chain
CHX	cycloheximide
CLC	clathrin light chain
CME	clathrin-mediated endocytosis
CNGC5/15	CYCLIC NUCLEOTIDE GATED CHANNEL 5/15
COBL9	COBRA-LIKE9
Col-0	Columbia-0
COL5	collagen V
COPI/II	coat protein complex I/II
COP1	CONSTITUTIVELY PHOTOMORPHOGENIC 1
CPC	CAPRICE
CRISPR	clustered regularly interspaced short palindromic repeats
CRL3/4	Cul3/4 RING E3 Ligase
CUL1	Cullin1
DCL1	DICER-LIKE1
DIC	Differential Interference Contrast
DMSO	dimethyl sulfoxide
DNA	deoxyribonucleic acid
dNTP	nucleoside triphosphate
DTE	1,4-dithioerythritol
DTS	downstream target sequence
DTT	dithiothreitol
E. coli	*Escherichia coli*
EAP1	Endocytosis Adaptor of Pollen Tube 1
ECA1/4	EPSIN-LIKE CLATHRIN ADAPTOR1/4
EDS	Ehlers-Danlos syndrome
EDTA	ethylenediaminetetraacetic acid
EE	early endosome
EGL3	ENHANCER OF GLABRA3
EGTA	ethylene glycol-bis(β-aminoethyl ether)-N,N,N',N'-tetraacetic acid

EF1α	ELONGATION FACTOR-1 alpha
ENTH	EPSIN N-terminal Homology
EPSID2	EPSINOID2
ER	endoplasmic reticulum
ERU	ERULUS
ESCRT	endosomal sorting complex required for transport
ETC1	ENHANCER OF TRY AND CPC1
EXP7	EXPANSIN7
$F_{1/2/3}$	first/second/third filial generation
F actin	filamentous actin
FER	FERONIA
FZ	FIZZY
FZR	FIZZY-RELATED
GEF	guanine nucleotide exchange factor
GFP/RFP/YFP	Green/Red/Yellow fluorescent protein
GL2/3	GLABRA2/3
GLUT1	glucose transporter 1
GORI	Germinating modulator of rice pollen
GST	glutathione S-transferase
GTP	guanosine triphosphate
GUS	β-glucuronidase
H	hair
h	hour
H0	Helix 0
HECT	Homology to the E6-associated protein C-terminus
HG	homogalacturonan
HRP	horseradish peroxidase
HYL1	HYPONASTIC LEAVES 1
HEN1	HUA ENHANCER 1
HST	HASTY
ID1/2/3	EPSINOID1/2/3
IgG	Immunoglobulin G
IPTG	isopropyl β-D-1-thiogalactopyranoside
IRE	INCOMPLETE ROOT HAIR ELONGATION

JKD	JACKDAW
KCl	potassium chloride
KS	Kolmogorov–Smirnov
LB	Lysogeny broth
LE	late endosome
Lj	*Lotus japonicus*
LNA	locked nucleic acid
LRL1/2	*Lj*-RHL1-LIKE1
LRR	leucine-rich repeat
LSM	laser scanning microscopy
MCS	multiple cloning site
MED20a	MEDIATOR20a
MES	2-(N-morpholino)ethanesulfonic acid
min	minute
MIN7	HOPM INTERACTOR 7
miRNA	microRNA
mKO	monomeric Kusabira-Orange
mNeon	monomeric Neon Green
mRNA	messenger RNA
MS	Murashige & Skoog
MTV1	MODIFIED TRANSPORT TO THE VACUOLE 1
MVB	Multivesicular body
N	non-hair
N. benthamiana	*Nicotiana benthamiana*
NaCl	sodium chloride
NADPH	nicotinamide adenine dinucleotide phosphate
NaF	sodium floride
Na_3VO_4	sodium orthovanadate
NLS	nuclear localization signal
NRT1.1	NITRATE TRANSPORTER1.1
nt	nucleotide
Os	*Oryza sativa*
P. syringae	*Pseudomonas syringae*
PAGE	polyacrylamide gel electrophoresis

PCR	polymerase chain reaction
PD	plasmodesmata
PG	polygalacturonase
Pi	inorganic phosphorous
PI	propidium iodide
PLDα1	PHOSPHOLIPASE D ALPHA 1
PM	plasma membrane
PME38	PECTIN METHYLESTERASE 38
PMEI	pectin methylesterase inhibitor
Pol II	polymerase II
PR1	PATHOGENESIS-RELATED GENE 1
pre-miRNA	precursor miRNA
pri-miRNA	primary miRNA
PtdInsP	phosphatidylinositol phosphate
PTGS	post-transcriptional gene silencing
PTI	PAMP-triggered immunity
PVA12	PLANT VAP HOMOLOG 12
PVC	prevacuolar compartment
QC	quiescent center
RALF	rapid alkalinization factor
RHD6	ROOT HAIR DEFECTIVE 6
RHID	root hair initiation domain
RHL1	ROOTHAIRLESS1
Rif	rifampicin
RING	Really Interesting New Gene
RISC	RNA-induced silencing complex
RLK	receptor-like kinase
RNA	ribonucleic acid
ROP	Rho-type small GTPases of plants
ROS	reactive oxygen species
RP	regulatory particle
rpm	revolutions per minute
RSL1/2	RHD6-LIKE1/2
RT-PCR	reverse transcription polymerase chain reaction

s	seconds
SCM	SCRAMBLED
SDS	sodium dodecyl sulfate
SE	SERRATE
SEL	size exclusion limit
sgRNA	single guide RNA
SI	supplementary information
SNAP-25	synaptosome-associated protein 25 kDa
SNARE	soluble *N*-ethylmaleimide-sensitive factor attachment protein receptors
SOB	super optimal broth
Spec	spectinomycin
ssOligo	single-stranded Oligo
STTM	short tandem target mimic
SYP	syntaxin of plant
TAE	tris-acetate-EDTA
TBS-T	tris-buffered saline with TWEEN
T-DNA	transfer DNA
TE	tris-EDTA
TEMED	tetramethylethylenediamine
TGA1/4	TGACG SEQUENCE-SPECIFIC BINDING PROTEIN 1/4
TGN	*trans*-Golgi network
TMS	tomosyn
Tris	Tris(hydroxymethyl)aminomethane
TRY	TRIPTYCHON
TTG1	TRANSPARENT TESTA GLABRA1
TUBβ6	BETA-6 TUBULIN
UBQ/UBI	ubiquitin
UTR	untranslated region
UTS	upstream target sequence
VHA	V-type H^+-ATPase
VSR	vacuolar sorting receptor
VTI11/12/13	VESICLE TRANSPORT V-SNARE 11/12/13
WDL4	WAVE-DAMPENED2-LIKE4
WER	WEREWOLF

WT	wild type
Y2H	yeast-two-hybrid
YEB	yeast extract broth

Acknowledgements

Summary

This work analyzed functional and regulatory aspects of the so far little characterized EPSIN N-terminal Homology (ENTH) domain-containing protein EPSINOID2 in *Arabidopsis thaliana*. ENTH domain proteins play accessory roles in the formation of clathrin-coated vesicles (CCVs) (Zouhar and Sauer 2014). Their ENTH domain interacts with membranes and their typically long, unstructured C-terminus contains binding motifs for adaptor protein complexes and clathrin itself. There are seven ENTH domain proteins in *Arabidopsis*. Four of them possess the canonical long C-terminus and participate in various, presumably CCV-related intracellular transport processes (Song et al. 2006; Lee et al. 2007; Sauer et al. 2013; Collins et al. 2020; Heinze et al. 2020; Mason et al. 2023). The remaining three ENTH domain proteins, however, have severely truncated C-termini and were termed EPSINOIDs (Zouhar and Sauer 2014; Freimuth 2015). Their functions are currently unclear. Preceding studies focusing on *EPSINOID2* indicated a role in root hair formation: *epsinoid2* T-DNA mutants exhibited an increased root hair density and EPSINOID2-GFP was specifically located in non-hair cell files in the *Arabidopsis* root epidermis (Freimuth 2015, 2019).

In this work, it was clearly shown that loss of *EPSINOID2* leads to an increase in root hair density through analyses of three independent mutant alleles, including a newly generated CRISPR/Cas9 full deletion mutant. The ectopic root hairs emerging from non-hair positions in all *epsinoid2* mutant alleles are most likely not a consequence of altered cell fate, because extensive genetic analyses placed *EPSINOID2* downstream of the established epidermal patterning network. Thus, EPSINOID2 seems to act as a cell autonomous inhibitor of root hair formation. Attempts to confirm this hypothesis by ectopically overexpressing *EPSINOID2* led to the discovery of post-transcriptional and -translational regulation through different mechanisms. One involves the little characterized miRNA844-3p. Interference with this pathway resulted in ectopic *EPSINOID2* overexpression and decreased root hair density, confirming it as negative factor in root hair formation. A second mechanism likely involves proteasomal degradation. Treatment with proteasomal inhibitor MG132 led to EPSINOID2-GFP accumulation, and a KEN box degron motif was identified in the EPSINOID2 sequence associated with degradation through a ubiquitin/proteasome-dependent pathway. In line with a tight dose regulation, genetic analyses of all three mutant alleles indicate that *EPSINOID2* is haploinsufficient. Lastly, it was revealed that, although *EPSINOID2* promoter activity was found in all epidermal cells, protein accumulation was observed in N-cells only, hinting at yet another layer of regulation.

Zusammenfassung

In der vorliegenden Arbeit wurden funktionelle und regulatorische Aspekte des bisher wenig charakterisierten EPSIN N-Terminal Homology (ENTH)-Domäne-enthaltenden Proteins EPSINOID2 in *Arabidopsis thaliana* untersucht. ENTH-Domänen Proteine spielen akzessorische Rollen in der Bildung von Clathrin-umhüllten Vesikeln (CCVs) (Zouhar and Sauer 2014). Ihre ENTH-Domäne interagiert mit Membranen und ihr typischerweise langer, unstrukturierter C-Terminus enthält Bindungsmotive für Adapterproteinkomplexe und Clathrin selbst. In *Arabidopsis* gibt es sieben ENTH-Domänen Proteine. Vier von ihnen besitzen den langen C-Terminus und sind an verschiedenen, vermutlich CCV-bezogenen intrazellulären Transportprozessen beteiligt (Song et al. 2006; Lee et al. 2007; Sauer et al. 2013; Heinze et al. 2020; Collins et al. 2020; Mason et al. 2023). Die verbleibenden drei ENTH-Domänen Proteine haben jedoch stark verkürzte C-Termini und wurden als EPSINOIDe bezeichnet (Zouhar and Sauer 2014; Freimuth 2015). Ihre Funktion ist derzeit unklar. Vorangegangene Studien, die sich auf EPSINOID2 konzentrierten, deuteten auf eine Rolle bei der Wurzelhaarbildung hin: *epsinoid2* T-DNA-Mutanten zeigten eine erhöhte Wurzelhaardichte und EPSINOID2-GFP war speziell in Nicht-Haarzellen in der Wurzelepidermis von *Arabidopsis* lokalisiert (Freimuth 2015, 2019).

In dieser Arbeit wurde durch Analysen von drei unabhängigen mutierten Allelen, einschließlich einer neu generierten CRISPR/Cas9-Deletionsmutante, klar gezeigt, dass der Verlust von *EPSINOID2* zu einer Erhöhung der Wurzelhaardichte führt. Die ektopischen Wurzelhaare, die in allen *epsinoid2* Allelen aus Nicht-Haar-Positionen hervorgehen, sind höchstwahrscheinlich keine Folge eines veränderten Zellschicksals, da umfangreiche genetische Analysen *EPSINOID2* dem etablierten Netzwerk zur Ausbildung der epidermalen Identität nachgeschaltet platziert haben. Somit scheint EPSINOID2 als zellautonomer Inhibitor der Wurzelhaarbildung zu wirken. Versuche, diese Hypothese durch ektopische Überexpression von *EPSINOID2* zu bestätigen, führten zur Entdeckung einer post-transkriptionellen und -translationalen Regulation durch verschiedene Mechanismen. Bei einem davon handelt es sich um die wenig charakterisierte miRNA844-3p. Eine Beeinträchtigung dieses Signalwegs führte zu einer ektopischen Überexpression von *EPSINOID2* und einer verringerten Wurzelhaardichte, was bestätigt, dass es sich um einen negativen Faktor bei der Wurzelhaarbildung handelt. Ein zweiter Mechanismus beinhaltet wahrscheinlich den proteasomalen Abbau. Die Behandlung mit dem proteasomalen Inhibitor MG132 führte zur Akkumulation von EPSINOID2-GFP, und in der Sequenz von EPSINOID2 wurde ein KEN-

Box Degron Motiv identifiziert, das mit dem Abbau über einen Ubiquitin/Proteasom-abhängigen Weg verbunden ist. Im Einklang mit einer strengen Dosisregulierung zeigten genetische Analysen aller drei mutierten Allele, dass *EPSINOID2* haploinsuffizient ist. Abschließend wurde festgestellt, dass die Aktivität des *EPSINOID2* Promotors zwar in allen Epidermiszellen zu finden war, eine Proteinakkumulation jedoch nur in Nicht-Haarzellen beobachtet wurde, was auf eine weitere Ebene der Regulation hindeutet.

1. Introduction

1.1 Vesicle trafficking in the endomembrane system

The endomembrane system is a unique feature of the eukaryotic cell which includes membranous structures such as the nuclear envelope, the endoplasmic reticulum (ER), the Golgi apparatus, the *trans*-Golgi network (TGN)/early endosomes (EE), multivesicular bodies (MVB)/late endosomes (LE)/prevacuolar compartments (PVC), vacuoles/lysosomes and different types of vesicles (Robinson et al. 1998; Buchanan 2015). Subcellular trafficking of diverse cargo molecules between endomembrane compartments is a fundamental function in eukaryotic cells which involves various processes like intracellular transport between organelles, the secretory pathway and the endocytic pathway (Buchanan 2015). Anterograde (forward/secretory) transport typically delivers newly synthesized cargo from the ER to the Golgi apparatus and subsequently to the TGN, where it is sorted according to its destination. Retrograde (backward) transport recycles molecules from trafficking processes or retrieves "escaped" cargo through the Golgi back to the ER (Sanderfoot and Raikhel 1999). These dynamic and highly organized trafficking processes are facilitated by different kind of vesicles enveloped by three characteristic coat proteins depending on their respective pathway. In general, these vesicles are formed in a stepwise process at a donor membrane in which several proteins support the destabilization of the membrane, its curvature during budding and coating of the cytoplasmic vesicle side. Transport between the ER and Golgi apparatus is realized by coat protein complexes (COP) I vesicles in retrograde direction and COPII vesicles in anterograde direction. Clathrin-coated vesicles (CCVs) participate in clathrin-mediated endocytosis (CME) and post-Golgi trafficking such as vacuolar transport in plants and secretion (reviewed in Aniento et al. 2022).

The clathrin coat is made of a lattice of hexameric structures, so called triskelia, which are formed by three clathrin heavy chains (CHCs) and three clathrin light chains (CLCs) (reviewed in Kirchhausen 1993). Adaptor protein (AP) complexes and accessory proteins such as EPSIN N-terminal Homology (ENTH) domain-containing proteins facilitate recruitment and linkage to the vesicle membrane (Robinson 1996; Kay et al. 1999). AP complexes mediate clathrin assembly and recognize specific sorting signals of cargo receptors of soluble proteins such as vacuolar sorting receptors (VSRs) or transmembrane proteins (Kirchhausen et al. 1997, reviewed in Bassham et al. 2008). In plants, for example, the adaptor protein complex 1 (AP-1) is localized at the TGN where it promotes secretory and vacuolar trafficking (Park et al. 2013; Teh et al. 2013). The accessory ENTH domain proteins are also involved in CCV formation

where they have a bridging function between phosphatidylinositol phosphate (PtdInsP)-containing membranes, APs and clathrin (Chen et al. 1998; Rosenthal et al. 1999; Wendland et al. 1999; Drake et al. 2000; Itoh et al. 2001; Ford et al. 2002; Song et al. 2006; Lee et al. 2007). Correct targeting and fusion of the vesicle with the target membrane is facilitated by the interaction of specific complementary soluble *N*-ethylmaleimide-sensitive factor attachment protein receptors (SNAREs): the vesicle-SNARE (v-SNARE) in the vesicle membrane and the target-SNARE (t-SNARE) in the target membrane which form a trans-SNARE complex (Weber et al. 1998; Cooper 2000; Südhof and Rothman 2009). Correct vesicle targeting is realized by recruiting specific v-SNAREs to the vesicle during budding, which are recognized by ENTH domain proteins acting as cargo adaptors (Hirst et al. 2004; Chidambaram et al. 2004; Wang et al. 2011).

Selective transport of cargo to distinct locations in the cell is crucial for a functioning cell and organism. The underlying mechanisms regulating vesicle formation and fusion as well as participating factors have been studied extensively during the last decades but still many questions remain unresolved, especially in the field of plant cell biology (Aniento et al. 2022).

1.2 ENTH domain-containing proteins in mammalians, yeast and plants

In eukaryotes, the ENTH domain is evolutionary highly conserved and consists of ~150 amino acids that form a globular structure of eight α-helices (Kay et al. 1999; Rosenthal et al. 1999; Zouhar and Sauer 2014). It has been proposed that an additional amphipathic Helix 0 (H0), which is formed upon binding certain PtdInsP species, partially inserts itself into the membrane and as a result membrane tension is reduced which facilitates membrane curvature (Itoh et al. 2001; Ford et al. 2002; Kweon et al. 2006; Gleisner et al. 2016). For example, it has been shown that the ENTH domain of rat epsin 1 preferentially binds PtdIns(4,5)P$_2$ (Itoh et al. 2001) and this interaction induces H0 formation and insertion into the membrane (Kweon et al. 2006). Typical ENTH domain proteins exhibit a long unstructured C-terminus that includes multiple motifs for AP complex and clathrin interactions (Chen et al. 1998; Rosenthal et al. 1999; Drake et al. 2000; Drake and Traub 2001).

Phylogenetic analyses of mammalian, yeast and plant ENTH domain proteins appear to cluster these proteins into two functionally distinct families: the epsin family which is involved in endocytosis and the epsinR (epsin-related) (Mills et al. 2003)/Clint (clathrin interacting protein localized in the trans-Golgi region) (Kalthoff et al. 2002b)/enthoprotin (Wasiak et al. 2002) family which participates in transport from the TGN (Legendre-Guillemin et al. 2004; Holstein

and Oliviusson 2005). The first family involves mammalian epsin1 and epsin2 which bind CHC and the α-adaptin subunit of AP-2, and yeast homologs Ent1p and Ent2p, all four involved in CME (Chen et al. 1998; Rosenthal et al. 1999; Wendland et al. 1999; Drake et al. 2000). The second family includes mammalian epsinR/Clint/enthoprotin, which interacts with the TGN-enriched PtdIns(4)P, colocalizes with AP-1 and participates in CCV formation at the TGN/endosomes (Hirst et al. 2003; Mills et al. 2003), and yeast Ent3p, which binds AP-1 and co-localizes with clathrin at the TGN and/or endosomes (Duncan et al. 2003).

Additionally to PtdInsP, it has been reported that the ENTH domain can interact with the Habc domain of SNARE proteins through conserved basic residues in α-helix 8 of the ENTH domain that form salt bridges to acidic Habc residues (Chidambaram et al. 2004; Hirst et al. 2004; Miller et al. 2007; Wang et al. 2011). For example, mammalian epsinR interacts with Vti1b, syntaxin 7 and 8 and yeast Ent3p with Vti1p, Pep12p and Syn8p (Chidambaram et al. 2004; Hirst et al. 2004; Chidambaram et al. 2008).

In a phylogenetic analysis of *Arabidopsis thaliana* (*A. thaliana*) ENTH domain proteins, seven proteins have been identified containing a true ENTH domain (Figure 1) (Zouhar and Sauer 2014). EPSIN1 is ubiquitously expressed and participates in vacuolar transport of soluble proteins from the TGN to the PVC as well as in a subset of secretory transport (Song et al. 2006; Heinze et al. 2020). It interacts with clathrin and AP-1 through its C-terminus and its ENTH domain interacts with the TGN-localized VESICLE TRANSPORT V-SNARE 11 (VTI11) (Song et al. 2006; Heinze et al. 2020). EPSIN2 is localized at the plasma membrane (PM) and incipient cell plate, but currently no role in endocytosis or cytokinesis has been demonstrated (Heinze et al. 2020). It interacts C-terminally with α-adaptin and δ-adaptin and N-terminally with PtdIns(3)P and the TGN-localized VTI12 (Lee et al. 2007). MODIFIED TRANSPORT TO THE VACUOLE 1 (MTV1) is a more phylogenetically distant ENTH domain protein which binds clathrin and AP-4, localizes to the TGN and is involved in vacuolar and secretory trafficking (Sauer et al. 2013; Heinze et al. 2020). The function of EPSIN3 is not known yet, but, like EPSIN2 it localizes to the PM and cell plate (Heinze et al. 2020). The remaining three identified ENTH domain proteins form a yet uncharacterized subfamily. Unlike the EPSINs and MTV1, they contain a very short C-terminus thereby lacking binding motifs for clathrin or AP complex interaction. In previous, non-peer-reviewed work, these short ENTH domain proteins were termed EPSINOID1 (ID1, AT3G23350), EPSINOID2 (ID2, AT3G46540) and EPSINOID3 (ID3, AT1G08670) (Freimuth 2015). Analyses of their spatio-temporal expression patterns with β-glucuronidase (GUS)-tagged fusion proteins in *Arabidopsis* revealed that *EPSINOID1* is only weakly expressed in the anthers of flowers (Sauer and Freimuth,

unpublished). *EPSINOID3* was also found in anthers, and in seedlings, it displayed a specific localization in the later root endodermis, concomitant with the onset of casparian strip formation (Freimuth 2015). *EPSINOID2* showed ubiquitous expression in aboveground tissue in leaves and in ovaries or ovules and a specific expression in the meristematic zone of the root epidermis in seedlings (Freimuth 2015, 2019). Function and localization of EPSINOID2 as well as characterization of its mutants has been investigated in previous research and was further addressed in this work (Freimuth 2019).
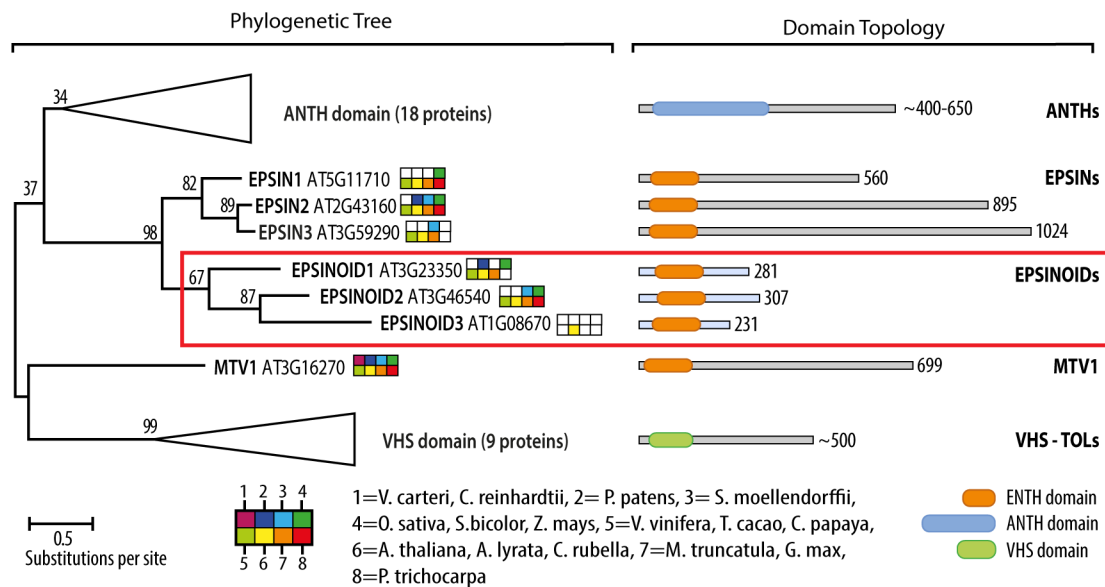
Figure 1: Phylogenetic tree and domain topology of *Arabidopsis* ENTH domain-containing proteins. Red rectangle highlights the three short EPSINOIDs. Modified from Zouhar and Sauer 2014.

1.3 EPSINOID2

Early analyses of stable transgenic *Arabidopsis* plants showed a striped expression pattern of GUS-tagged *EPSINOID2* (*ID2::ID2-GUS*) in the transition from meristematic to elongation zone of the root in seedlings (Freimuth 2015). It resembled the pattern of non-hair cell fate marker GLABRA2 (GL2) (Masucci et al. 1996; Hung et al. 1998) (Figure 2A). Stably transformed GFP-tagged *EPSINOID2* (*ID2::ID2-GFP*) expressed under its endogenous promoter confirmed a specific signal in non-hair (N) cell files of the root epidermis (Figure 2B) (Freimuth 2019). This pattern corresponds with microarray analyses with cell-type specific messenger RNA (mRNA) showing a higher expression of *EPSINOID2* in non-hair compared to hair (H) cells (Birnbaum et al. 2003). Additionally, another study showed increased expression of *EPSINOID2* in hairless mutants (Bruex et al. 2012). On a subcellular level, EPSINOID2-GFP showed a mostly cytosolic signal and it additionally co-localized with the

cell plate marker mCherry-RabA1g (Geldner et al. 2009) at the cell plate in dividing cells (Freimuth 2019). Analyses of two independent transfer DNA (T-DNA) insertion mutants *epsinoid2-1* (*id2-1*) and *epsinoid2-2* (*id2-2*), which were confirmed as knock-out and knock-down by semiquantitative reverse transcription polymerase chain reaction (RT-PCR), respectively, exhibited an increased root hair density compared to Col-0 (Figure 2C-E). Further detailed analyses showed that the increased root hair number was mainly in consequence of ectopic root hair formation (hairs originating from non-hair position) and to a lesser extent from shortened root hair cells (Figure 2F) (Freimuth 2015, 2019). The specific expression in N cells combined with the hairy mutant phenotype raised the question whether *EPSINOID2* might be a negative regulator of root hair formation.

Initial analyses showed that constitutive overexpression of *EPSINOID2* phenocopies the hairy mutant phenotype (Figure 2G) which might not be a result of co-suppression on transcript level since *EPSINOID2* mRNA levels were increased in *35S::ID2* (Figure 2H) (Freimuth 2019). Additionally, the knock-out mutant *id2-1* displayed characteristics of a dominant mutation and the knock-down mutant *id2-2* of a semi-dominant mutation suggesting haploinsufficiency (Freimuth 2019). These analyses indicate an unusual genetic regulation of *EPSINOID2* and that its function might be sensitive to expression or protein levels. In previous work, several attempts with transgenic *EPSINOID2-GFP*, untagged *EPSINOID2* or *EPSINOID2* including its 3'UTR expressed under its endogenous promoter could not complement the hairy mutant phenotype (Freimuth 2019).

In preliminary studies, plausible candidates of the vesicle generation and fusion machinery such as clathrin light chain 2 (CLC2), the t-SNARE syntaxin of plants 123 (SYP123) and the v-SNARE VTI11 were tested for EPSINOID2 interaction using Bimolecular Fluorescence Complementation (BiFC) and pull-down assays which gave inconclusive results and demand further investigations.
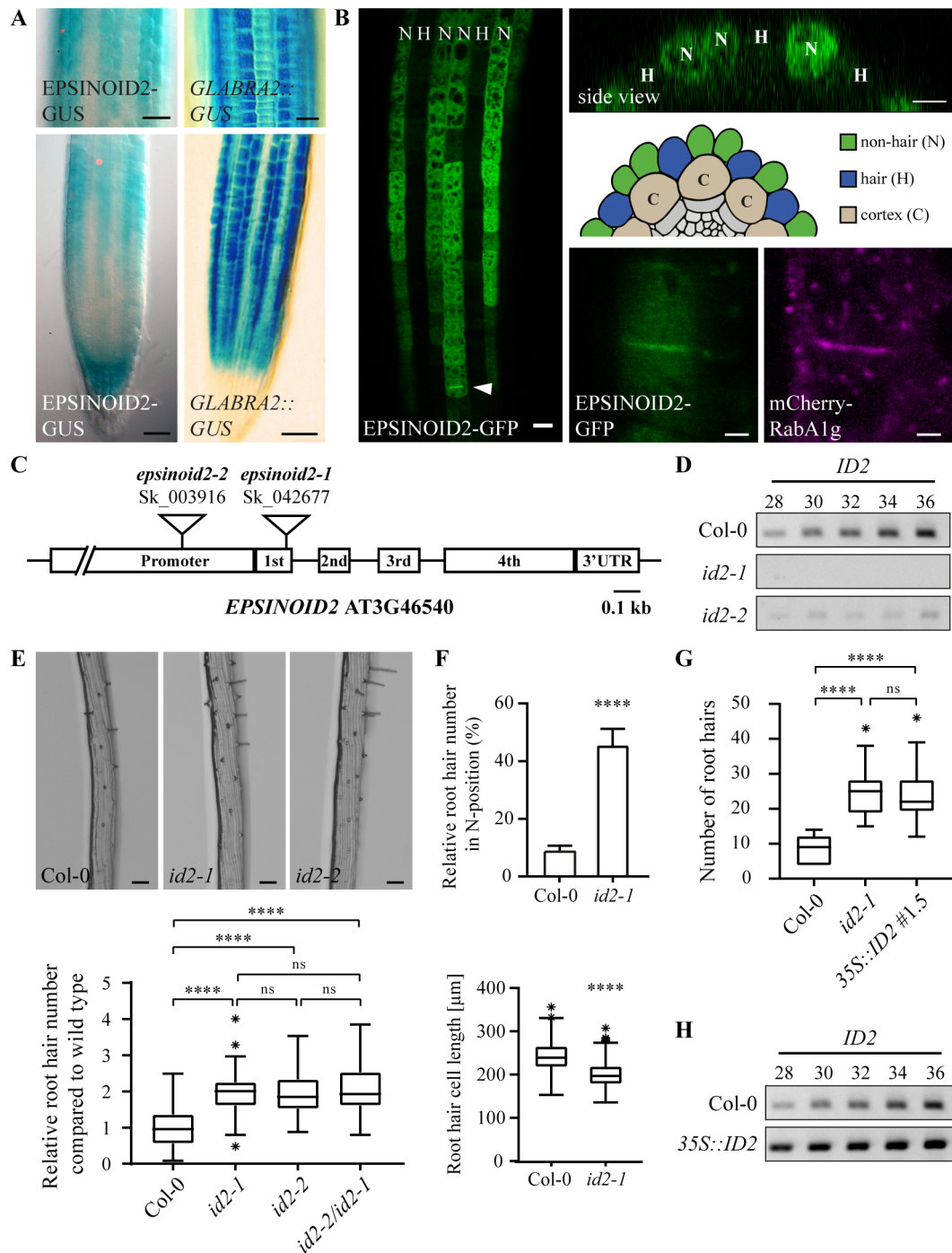
Figure 2: Preliminary research data of *EPSINOID2* expression and mutant phenotypes.

(A) In 7-day-old *Arabidopsis* seedlings, ID2-GUS showed a striped pattern in the meristematic zone of the root (left, modified from Freimuth 2015). Scale bars = 50 μm. This pattern is reminiscent of *GL2::GUS* expression pattern in roots (right, modified from Hung et al. 1998). Scale bar in upper image = 20 μm. Scale bar in lower image = 50 μm. (B) ID2-GFP confirms a specific signal in non-hair cell files of the root epidermis in 5-day-old *Arabidopsis* seedlings, particularly recognizable in the side view with a signal in N cells. Schematic cross-section represents the cellular organization of the *Arabidopsis* root (modified from Balcerowicz et al. 2015). Subcellularly, ID2-GFP showed a mostly cytosolic signal and a co-localization at the cell plate with mCherry-RabA1g. Scale bars = 10 μm. (C) Schematic representation of the *EPSINOID2* gene with two independent T-DNA insertion lines *id2-1* (SALK_042677) and *id2-2* (SALK_003916). In the *id2-1* mutant, the T-DNA is inserted 28 bp from the 3' end of the first exon whereas the insertion position in the *id2-2* mutant is in the promoter region 257 bp upstream

9

of the ATG (GeneBank: BH171194). Gene position on chromosome 3: 17134091 - 17135587 bp. Boxes with numbers represent exons. Introns are indicated as lines between the exons. (D) Semiquantitative RT-PCR of cDNA from 7-day-old *Arabidopsis* seedlings identified *id2-1* as a knock-out and *id2-2* as a knock-down mutant. (E) Root hair analyses of 7-day-old seedlings of homozygous *id2-1* and *id2-2* mutant as well as the F1 offspring of their crosses revealed an increased root hair density compared to Col-0 (88 < n < 135). (F) In-depth analyses showed that *id2-1* exhibited 5 times more ectopic root hairs (on average 45 %) than wild type (on average 9 %) and root hair cells were 17 % shorter in *id2-1* (mean = 200 μm) than in Col-0 (mean = 242 μm) (n = 300). (G) An initial root hair analysis of 7-day-old *Arabidopsis* seedlings expressing *35S::ID2* revealed a hairy phenotype similar to *id2-1* mutant (17 < n < 34) suggesting transgene-mediated co-suppression. (H) Semiquantitative RT-PCR showed increased *EPSINOID2* mRNA in *35S::ID2* contradicting a co-suppression on transcript level.

1.4 Cellular organization and epidermal cell differentiation in *Arabidopsis* roots

The cellular organization and radial symmetry of the *Arabidopsis* root is determined in the meristem where specific cell types arise from four species of initial cells (epidermal/lateral root cap initials, cortex/endodermis initials, columella initials and stele initials). Repeated divisions result in continuous cell files arranged in concentric layers of epidermis, cortex, endodermis and pericycle surrounding the central cylinder (Figure 3A) (Dolan et al. 1993b; Scheres et al. 2002). Cortex and endodermis cell lineages originate from cortex/endodermis initials which first divide anticlinally followed by periclinal divisions (Dolan et al. 1993b). Epidermal/lateral root cap initials divide transversally and then anticlinally, giving rise to epidermal and lateral root cap cells. Viewed in cross-section, the epidermal layer consists of 16 to 23 epidermal cells which develop into two different cell types (Duckett et al. 1994). This epidermal cell fate depends on the relative position to the underlying cortical cells: cells that lie over the anticlinal cortical cell wall ("H" position) develop into root hair cells (trichoblasts; Leavitt 1904) whereas cells in contact with a single cortical cell ("N" position) become non-hair cells (Dolan et al. 1993b). Typically, the epidermal layer surrounds 8 cortical cells and therefore gives rise to 8 hair cells with remaining 8-15 non-hair cells separating hair cells with one or two non-hair cells (Figure 3A) (Dolan et al. 1993b; Duckett et al. 1994). This characteristic cellular organization is represented in Figure 2B (Balcerowicz et al. 2015). Trichoblasts can be distinguished from non-hair cells at a very early stage in root development by a higher cytoplasmic density and cell division rate as well as reduced vacuolation and cell length compared to atrichoblasts (Cormack 1949; Dolan et al. 1993b; Galway et al. 1994; Berger et al. 1998b).

In *Arabidopsis*, root hair development involves three processes: cell fate determination, root hair initiation and root hair tip growth (reviewed in Grierson et al. 2014). Epidermal cell fate is

regulated by the differential coordinated expression of several genes (Figure 3B) and already initiated during embryonic root development (Berger et al. 1998a; Lin and Schiefelbein 2001). Post-embryonic non-hair or hair cell specialization depends on the action of two transcription factors, the R2R3 class MYB transcription factor WEREWOLF (WER) (Lee and Schiefelbein 1999) and the R3 MYB transcription factor CAPRICE (CPC) (Wada et al. 1997) that can both bind to a regulatory central basic helix-loop-helix (bHLH)-WD40 transcription complex (Bernhardt et al. 2003; Song et al. 2011). This complex consists of the homologues GLABRA3 (GL3), ENHANCER OF GLABRA3 (EGL3) (Bernhardt et al. 2003) and MYC1 (Bruex et al. 2012), that are bHLH transcription factors of partially redundant function, bound to the WD40 transcription factor TRANSPARENT TESTA GLABRA1 (TTG1) (Galway et al. 1994; Walker et al. 1999; Payne et al. 2000). In non-hair cells, WER binds this complex leading to transcriptional activation of the homeodomain transcription factor GLABRA2 (GL2) (Di Cristina et al. 1996) which suppresses expression of hair cell-specific genes and activates expression of non-hair cell-specific genes to promote non-hair cell differentiation (Masucci et al. 1996; Hung et al. 1998; Payne et al. 2000; Bernhardt et al. 2003; Tominaga et al. 2007; Song et al. 2011). *gl3/egl3*, *wer* and *ttg1* mutants cause suppression of *GL2* expression which leads to ectopic root hair formation similar as in *gl2* mutants (Galway et al. 1994; Di Cristina et al. 1996; Masucci et al. 1996; Lee and Schiefelbein 1999; Bernhardt et al. 2003). Interestingly, the resulting effects of *wer* and *ttg1* mutation differ from that of *gl2* mutation: *wer* and *ttg1* mutations cause changes in all early cellular characteristics of non-hair cell differentiation (cell division rate, cytoplasmic density and vacuolation rate), while *gl2* mutation only affects the late cell morphology (Galway et al. 1994; Masucci et al. 1996; Berger et al. 1998b; Lee and Schiefelbein 1999). These studies support the proposed model of WER and TTG1 being early players in cell fate determination and GL2 acting more downstream. The WER-GL3/EGL3-TTG1 complex additionally induces *CPC* (Bernhardt et al. 2003; Kang et al. 2013) which lacks the transcriptional activation domain (Wada et al. 1997; Tominaga et al. 2007) and moves to adjacent epidermal cells (Wada et al. 2002; Kurata et al. 2005; Kang et al. 2013) where it competes with WER for binding the GL3/EGL3-TTG1 complex (Tominaga et al. 2007; Song et al. 2011). The resulting CPC-GL3/EGL3-TTG1 complex is inactive and cannot activate *GL2* causing expression of hair cell-specific genes and hair cell differentiation (Kurata et al. 2005; Tominaga et al. 2007; Song et al. 2011). Hence, CPC acts as a negative regulator of GL2 and positive regulator of hair cell fate (Lee and Schiefelbein 2002; Wada et al. 2002; Song et al. 2011). Surprisingly, *GL3* and *EGL3* are preferentially expressed in H cells as a result of positive regulation by CPC in H cells and negative regulation by WER and TTG1 in N cells, however,

GL3 protein accumulates in N position (Bernhardt et al. 2005; Kang et al. 2013). Therefore, it has been proposed that GL3 and EGL3 move from H cells into N cells where they promote non-hair cell differentiation (Bernhardt et al. 2005).

Upstream of this transcription factor network acts the leucine-rich repeat receptor-like kinase (LRR-RLK) SCRAMBLED (SCM) that mediates the information about the relative cell position by perceiving an unknown signal from cortical cells resulting in appropriate gene expression patterns in both cell types (Kwak et al. 2005; Kwak and Schiefelbein 2007). SCM affects the relative abundance of WER in N and H cells by negatively regulating *WER* expression in H cells which leads to an accumulation of the WER-GL3/EGL3-TTG1 complex in N cells (Kwak and Schiefelbein 2007). Additionally, *SCM* itself is regulated by the WER-GL3/EGL3-TTG1 complex reducing SCM presence in N cells thereby amplifying SCM signaling in H position (Kwak and Schiefelbein 2008). This demonstrates that the establishment of root hair patterning requires a complex regulatory network involving interactions, lateral inhibition and feedback loops to ensure proper epidermal cell fate (reviewed in Schiefelbein et al. 2014).

It has been proposed that GL2 acts as a genetic switch between cell specification and differentiation by suppressing root hair cell-specific genes (Lin et al. 2015). In particular, GL2 inhibits a regulatory cell differentiation network of several bHLH transcription factors directly targeting *ROOT HAIR DEFECTIVE 6* (*RHD6*) (Masucci and Schiefelbein 1994; Menand et al. 2007), *RHD6-LIKE1* (*RSL1*) (Menand et al. 2007), *RSL4* and its related bHLH transcription factor *RSL2* (Yi et al. 2010), as well as *Lotus japonicus ROOTHAIRLESS1* (*Lj-RHL1*)-*LIKE1* (LRL1), and LRL2 (Karas et al. 2009), in N cells (Lin et al. 2015). In H cells, however, GL2 is inactivated, and root hair cell differentiation can proceed which is positively regulated by RHD6 (Masucci and Schiefelbein 1994).

After epidermal cell specification is determined, root hair cells expand by diffuse growth followed by root hair initiation. In this process, an initiation site is established close to the basal end of the epidermis cell. A so called root hair initiation domain (RHID) is formed followed by directed secretory trafficking of hydrolytic enzymes and cell wall components (reviewed in Balcerowicz et al. 2015). Rho-type small GTPases of plants (ROP) have been reported to accumulate at the initiation site (Molendijk et al. 2001; Jones et al. 2002; Denninger et al. 2019), for example, ROP2 which is recruited by guanine nucleotide exchange factor 3 (GEF3) to the RHID (Denninger et al. 2019). Additionally, the receptor-like kinase FERONIA (FER) is involved in ROP activity at the initiation site (Duan et al. 2010). After ROP localization, cytoplasmic pH at the initiation site increases whereas cell wall pH drops which has been

proposed to activate expansins such as EXPANSIN7 (EXP7) causing local cell wall loosening (Bibikova et al. 1998; Cosgrove 2000; Cho and Cosgrove 2002). This results in bulge formation where ER elements and filamentous (F) actin accumulate (Baluska et al. 2000). ROP also mediates the NADPH oxidase RHD2 which is responsible for local accumulation of reactive oxygen species (ROS) at the emerging and elongating root hairs (Foreman et al. 2003).

Bulge formation is followed by root hair tip growth which involves highly coordinated processes such as maintenance of cytosolic calcium gradient, ROS production, pH regulation, cytoskeleton dynamics, constant polarized membrane trafficking and cell wall remodeling (reviewed in Mendrinna and Persson 2015).

As mentioned before, the non-hair cell-specific expression of *EPSINOID2* in the meristematic zone of the root epidermis is reminiscent of *GL2* and both *id2-1* and *gl2* mutants, exhibit ectopic root hair formation (Masucci et al. 1996; Freimuth 2019). As GL2 acts as a negative regulator of root hair cell specification, obtained *EPSINOID2* data raised the question whether it is involved in root hair development, for example, by participating in early processes such as the establishment of cell identities or at a later stage by suppressing root hair formation. Considering the expression pattern of *EPSINOID2* in the transition of the meristematic and elongation zone, an involvement in cell fate specification is more probable than in root hair morphogenesis. Thus, placement of EPSINOID2 into this molecular framework was one of the key questions to be answered in this work.
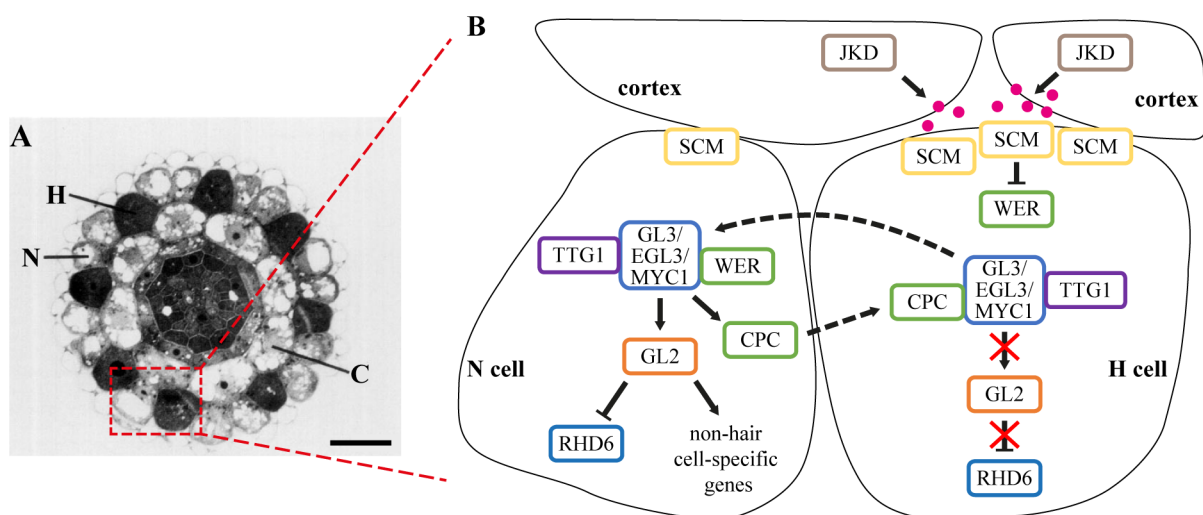
Figure 3: Cellular organization and epidermal cell fate determination in *Arabidopsis*.
(A) Cross section of wild-type *Arabidopsis* root stained with toluidine blue. Cortical layer (C) with 8 cells is surrounded by the epidermal layer with 23 cells from which 8 differentiating root hair cells (H) located over the anticlinal wall of two cortical cells are intensely stained indicating dense cytoplasm. N: non-hair cells. Scale bar = 20 μm. Modified from Galway et al. 1994. (B) Simplified schematic representation of epidermal cell fate network in *Arabidopsis*. In non-hair (N) cells, WEREWOLF (WER) together with the central transcription complex

consisting of TRANSPARENT TESTA GLABRA1 (TTG1) and GLABRA3 (GL3)/ENHANCER OF GLABRA3 (EGL3)/MYC1 function as an activator complex activating *GLABRA2* (*GL2*) expression which promotes non-hair cell fate. This complex also induces *CAPRICE* (*CPC*) which moves to neighboring cells where it interferes with WER binding to the central transcription complex which therefore cannot activate *GL2* expression and promotes hair (H) cell fate. JACKDAW (JKD) and SCRAMBLED (SCM) mediate positional signaling, presumably involving an unknown ligand (magenta circles). SCM represses *WER* expression in H cells. GL3 and EGL3 move to N cells leading to accumulation of the central transcription complex in non-hair cells. Dashed arrows indicate cell-to-cell movement. Model adapted from Grierson et al. 2014 and Balcerowicz et al. 2015.

1.5 Micro RNA (miRNA) biogenesis and activity in plants

Plants possess a variety of mechanisms to adapt their physiology and development to environmental conditions in which they regulate gene expression post-transcriptionally and post-translationally (reviewed in Floris et al. 2009). In post-transcriptional regulation, the mRNA population can be influenced quantitatively and qualitatively by different processes such as alternative splicing, RNA silencing through small RNAs, action of RNA regulation particles (stress granules or processing bodies) and translational regulation (reviewed in Guerra et al. 2015). RNA silencing and translational regulation can both be mediated by miRNAs.

MiRNAs are endogenous small non-coding RNA molecules of 20–25 nucleotides (nt) length that regulate gene expression at post-transcriptional levels in eukaryotes (Lagos-Quintana et al. 2001, reviewed in He and Hannon 2004). Plant genomes harbor hundreds of *MIRNA* (*MIR*) genes, many of them forming families associated with development and/or stress responses (reviewed in Budak and Akpinar 2015).

MiRNAs have an impact on various biological processes such as plant development and stress response by targeting a large diversity of genes (reviewed in Dong et al. 2022 and Zhang et al. 2022). So far, many miRNAs have been identified that are involved in root growth in response to abiotic stresses, for example, miRNA167 regulating lateral root growth in response to nitrogen (Gifford et al. 2008). MiRNAs are also participating in regular root development such as root elongation, for example, miRNA156 by affecting meristem activity or miRNA165/166 by controlling xylem patterning (Carlsbecker et al. 2010; Barrera-Rojas et al. 2020).

MIR genes are usually transcribed by DNA-dependent RNA polymerase II (Pol II) in the nucleus which is recruited by mediator proteins such as MEDIATOR20a (MED20a) giving rise to primary miRNA transcripts (pri-miRNA) which are 5' capped, 3' polyadenylated and form a secondary structure including a hairpin (Figure 4A) (Lee et al. 2004; Xie et al. 2005; Kim et al. 2011). This pri-miRNA consists of a terminal loop, an upper stem, the miRNA 5p-3p (former: miRNA/miRNA*) region, a lower stem and two arms. MiRNA derived from the 5'

end of the hairpin is called "5p" and the one from the 3' end "3p". It is then processed by a protein complex consisting of endonuclease DICERLIKE1 (DCL1), RNA binding protein HYPONASTIC LEAVES 1 (HYL1) and zinc-finger protein SERRATE (SE) resulting in a precursor miRNA (pre-miRNA). This carries the hairpin which is subsequently cut again by the complex producing a 20-25 bp miRNA 5p-3p duplex (reviewed in Wang et al. 2019). To increase stability, both 3' ends are methylated by HUA ENHANCER 1 (HEN1) (Park et al. 2002; Yu et al. 2005) and the miRNA duplex is exported into the cytoplasm by HASTY (HST) (Park et al. 2005) where it separates. The guide strand of the mature miRNA is loaded onto ARGONAUTE1 (AGO1) forming the RNA-induced silencing complex (RISC) whereas the second so-called passenger miRNA is degraded (reviewed in Wang et al. 2019). The RISC is guided to the target mRNA which is recognized via base pairing resulting in target cleavage or translational inhibition (reviewed in Yu et al. 2017).

As mentioned above, initial results from transgenic lines overexpressing *EPSINOID2* under the constitutive 35S promoter led to an increased root hair density compared to wild type (Figure 2G) which was unexpected since the *id2-1* mutant showed the same phenotype. It was assumed that this was caused by transgene-mediated post-transcriptional gene silencing (PTGS), also called co-suppression, however, the analyzed overexpression line *35S::ID2* showed increased mRNA levels compared to Col-0 (Figure 2H) (Napoli et al. 1990; van der Krol et al. 1990; Freimuth 2019). This led to the hypothesis of a possible post-transcriptional or -translational down regulation of *EPSINOID2*, affecting its protein abundance through inhibition of mRNA translation by a miRNA or ubiquitination and degradation (Guerra et al. 2015).

In fact, miRNA data obtained by high-throughput pyrosequencing identified the little studied miRNA844-3p with the sequence UUAUAAGCCAUCUUACUAGUU targeting *EPSINOID2* in its 3rd exon (position 464-484 from the 5' end of the cDNA) (Figure 4B) (Rajagopalan et al. 2006). Additionally, several studies revealed upregulation of *EPSINOID2* in mutants affecting miRNA biogenesis. Microarray data from *dcl1-15* mutant embryos uncovered a 13-fold upregulation of *EPSINOID2* with *MIR844* as the corresponding *MIR* gene and small RNA sequencing (RNA-seq) data showed a 3.5-fold upregulation of *EPSINOID2* in *dcl1-5* embryos (Seefried et al. 2014; Plotnikova et al. 2019). Additionally, microarray data from *med20a* mutants revealed a 2-fold upregulation of *EPSINOID2* (Kim et al. 2011). RNA-seq data from *ago1-3* mutant seedlings also presented a 2-fold upregulation of *EPSINOID2* (Arribas-Hernández et al. 2016).

All these data indicate a possible regulation of *EPSINOID2* by a miRNA, specifically miRNA844-3p, which could explain earlier observations of the hairy root phenotype in

overexpression lines despite high transcript levels. In this work, several approaches were taken to gain more insight into miRNA844-3p action on *EPSINOID2*.
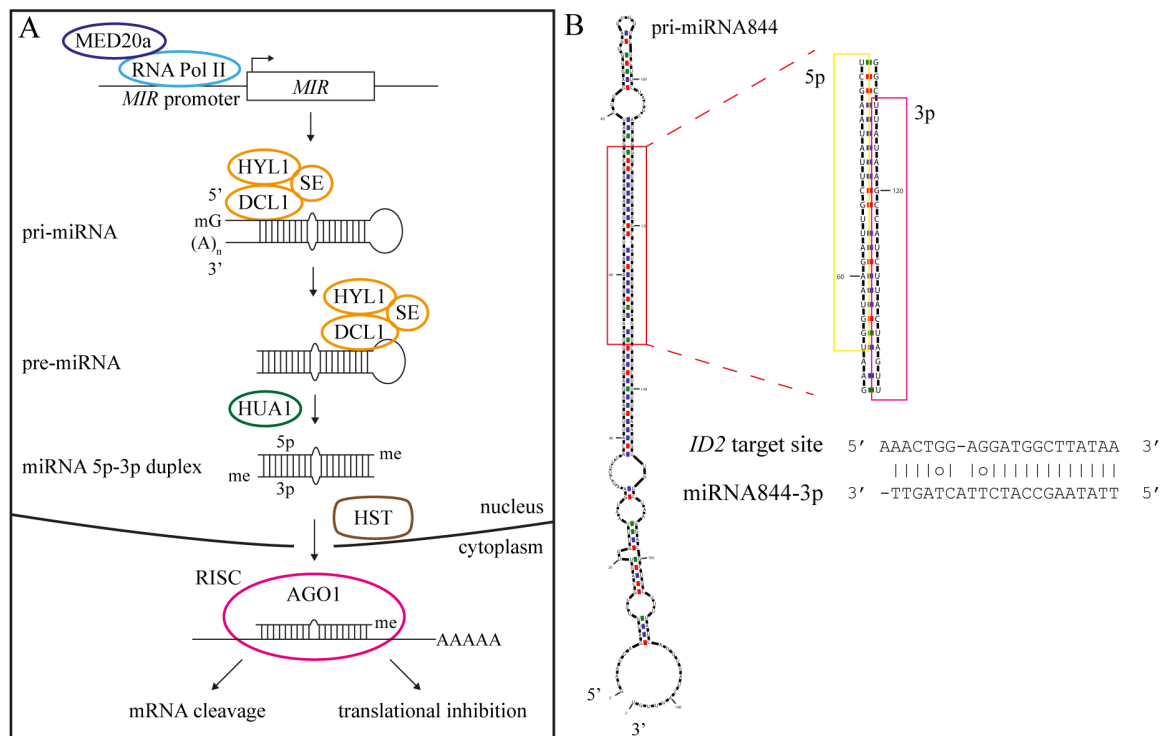
Figure 4: MiRNA biogenesis in plants.

(A) Simplified schematic overview of miRNA biogenesis in plants. *MIR* genes are transcribed by RNA Pol II which is recruited by mediator proteins e.g., MED20a. Primary transcript pri-miRNA is processed by DCL1, HYL1 and SE in two steps cleaving off the 5' and 3' ends (pre-miRNA) and afterwards the distal loop. 3' ends are methylated by HUA1 for stabilization. The resulting miRNA 5p-3p duplex is exported from the nucleus into the cytoplasm with the help of HST where the mature guide strand is loaded onto AGO1, thereby forming the RISC. The RISC promotes gene silencing by either cleaving the target mRNA or inhibiting the translation. (B) MiRNA844 stem loop with miRNA844-5p and miRNA844-3p identified by Rajagopalan et al. 2006 (reproduced by using mfold (Zuker 2003), http://www.unafold.org/mfold/applications/rna-folding-form.php, obtained on April 2021). In this study, *EPSINOID2* was also predicted as target of miRNA844-3p (position 464-484 from the 5' end of the cDNA).

1.6 Proteasomal degradation of proteins

Post-translational mechanisms of plants to regulate their physiological and developmental processes, for example, in response to environmental stimuli, involve the modulation of protein activity, subcellular localization or turnover which can include post-translational protein modifications such as phosphorylation or ubiquitination (reviewed in Guerra et al. 2015). One major factor in protein turnover is protein degradation by the ubiquitin-26S proteasome pathway (reviewed in Xu and Xue 2019). This system ensures specific spatio-temporal

activities of proteins and is the major protein degradation pathway. It involves ubiquitination of a target protein which is mainly executed by the sequential activity of three enzyme complexes (Figure 5) (Hershko and Ciechanover 1998). In the first step, an E1 enzyme binds ubiquitin in an ATP-dependent manner and activates it by adenylation of the C-terminal carboxyl group (Haas et al. 1982). In the second step, ubiquitin is transferred to an active site cysteine of E2 ubiquitin-conjugating enzyme (Stewart et al. 2016) which is then in the final step bound by an E3 ligase that mediates the transfer of ubiquitin to a substrate by linkage to an ε-amino group of a lysine (Hershko et al. 1983; Reiss et al. 1988). Ubiquitin can be repeatedly added to the substrate and these polyubiquitinated proteins are then targeted for ubiquitin-dependent proteasomal degradation (Kurepa and Smalle 2008). In *Arabidopsis*, over thousand E3 ligases have been predicted to be encoded in the genome (Vierstra 2009). There are four major classes of E3 ligases in plants depending on their domains and complex formation: monomeric and multimeric (or Cullin-based) Really Interesting New Gene (RING)-finger, U-box E3 ligases and Homology to the E6-associated protein C-terminus (HECT) E3 ligases (reviewed in Weinmann and Crews 2020 and Al-Saharin et al. 2022). The multimeric or Cullin-based RING-finger class is divided into four different subclasses: SCF (Skp1, Cullin1 (CUL1), F-box), CRL3 (Cul3 RING E3 Ligase), CRL4 (Cul4 RING E3 Ligase) and the APC/C (Anaphase Promoting Complex/Cyclosome) complex (Weinmann and Crews 2020).

APC/C E3 ligases have a major role in cell cycle regulation by targeting essential cell cycle proteins such as cyclins (Sudakin et al. 1995). However, it has been shown that APC/C is involved in many other developmental processes such as cell differentiation in *Arabidopsis* (Blilou et al. 2002) and root growth in rice (*Oryza sativa*) (Lin et al. 2020), as well as in abiotic stress responses, such as leaf senescence in response to N deficiency in *Arabidopsis* (Fan et al. 2023). APC/C E3 ligases are large complexes consisting of several subunits with different functions, among them two small protein families Cell Division Cycle20 (CDC20)/FIZZY (FZ) and CDC20 Homolog1 (CDH1)/FIZZY-RELATED (FZR), in plants known as CELL CYCLE SWITCH52 (CCS52), acting as co-activators of APC/C and being involved in substrate recognition and binding (Visintin et al. 1997; Tarayre et al. 2004; Kevei et al. 2011).

In a final process, polyubiquitinated proteins are recognized and unfolded by the 19S regulatory particle (RP)/cap of the 26S proteasome and subsequently channeled into the 20S core protease for degradation (Figure 5) (reviewed in Ali and Baek 2020).
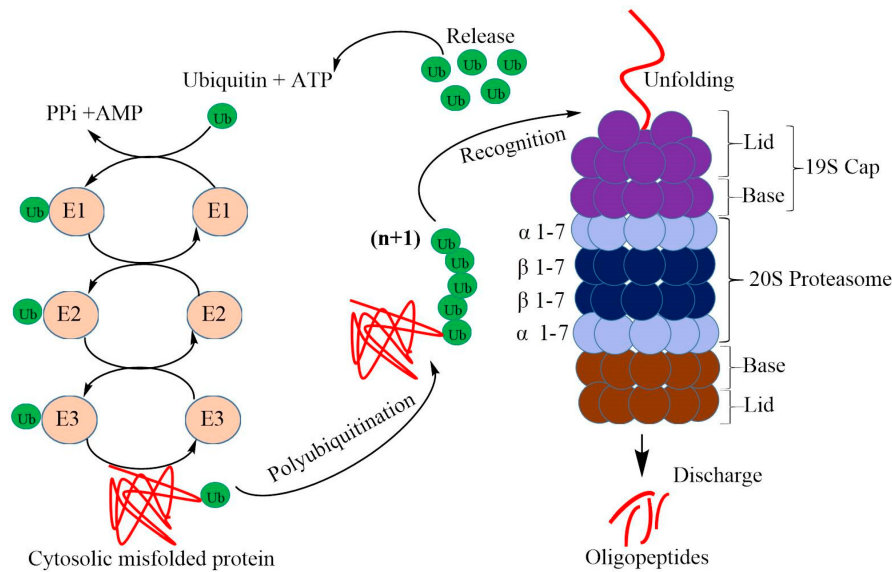
Figure 5: Ubiquitin-dependent proteasomal degradation in plants.
Simplified schematic overview of the ubiquitin-dependent proteasomal degradation pathway in plants (Ali and Baek 2020). Ubiquitin is transferred to a substrate by the sequential action of enzymes (E1, E2 and E3). The addition of ubiquitin is repeated several times resulting in a ubiquitin chain. Polyubiquitinated proteins are then targeted for degradation by the 26S proteasome which consists of the 19S cap mediating substrate recognition and unfolding and the 20S core protease for degradation. E1: ubiquitin-activating enzyme, E2: ubiquitin-conjugating enzyme, E3: ubiquitin-ligating enzyme.

1.7 Objectives

The role of *Arabidopsis* ENTH domain proteins in CCV formation and post-Golgi trafficking has been studied for decades now and in the past few years research in this field made a lot of progress in characterizing EPSINs and MTV1 and their localization, their interactors in CCV formation, their involvement in different pathways as well as their function in stress response (Song et al. 2006; Lee et al. 2007; Sauer et al. 2013; Collins et al. 2020; Heinze et al. 2020; Mason et al. 2023). However, about the recently identified short homologs that were named EPSINOIDs in previous work only little is known (Zouhar and Sauer 2014; Freimuth 2015). In preliminary work, spatio-temporal expression and subcellular localization of EPSINOID2 as well as phenotypic variation of mutant and overexpression lines were analyzed (Freimuth 2015, 2019). This work focused on further characterizing *EPSINOID2* as the causative gene for the observed root hair phenotype and the complex post-transcriptional and -translational regulation of *EPSINOID2*. For this, a third, CRISPR/Cas9 full deletion mutant was generated and extensively studied. Many different approaches were applied to explore post-transcriptional regulation of *EPSINOID2* activity by miRNA844-3p. Investigation of further regulation on EPSINOID2 protein level was also of interest. Additionally, comprehensive genetic analyses

18

were performed to place *EPSINOID2* into the hair/non-hair patterning framework. Three different approaches were used in the search for EPSINOID2 interactors and possible candidates were tested *in vitro* to gain more insight into EPSINOID2 function.

2. Materials and methods

All equipment, chemicals, compositions of buffers and solutions, bacterial strains and primers sequences are listed in the supplementary information (SI), materials and methods (section 6.2).

2.1 Plant material and growth conditions

For all analyses, *A. thaliana* Columbia-0 (Col-0) was used as wild type and all transgenic lines are in Col-0 background unless stated otherwise. For functional analysis, a T-DNA insertion mutant allele of *EPSINOID2* (AT3G46540; SALK_042677, *id2-1*) was used (Figure 2C). A schematic map in Figure **2**C shows the location of two T-DNA insertion sites in the *EPSINOID2* gene. The second independent T-DNA insertion line *epsinoid2-2* (SALK_003916, *id2-2*) was used in previous work and is only shown for completeness. Additionally, an *epsinoid2-3* (*id2-3*) mutant was generated by using the CRISPR/Cas9 system to completely delete the *EPSINOID2* gene (see section 2.2 and 3.3).

For root hair analyses of heterozygous *id2-3*, approximately 4- to 5-week-old plants of Col-0 and homozygous *id2-3* ($^-$/.) were crossed and the heterozygous F$_1$ (*id2-3* $^+$/.) was analyzed.

During the cloning process of new constructs carrying the genomic region of *EPSINOID2*, it was revealed by sequencing that in previously generated *ID2::ID2-GFP/-GUS* lines, 207 bp of the 4th exon were missing. For this work, we generated new stable transgenic *ID2::ID2-GFP/-GUS* lines containing the full *EPSINOID2* gene (see section 2.3). The untagged overexpression line *35S::ID2* in Col-0 background was generated in previous work (Freimuth 2019).

To investigate the subcellular localization, our established *ID2::ID2-GFP* line was crossed with several markers for subcellular compartments: *UBQ10::mCherry-RabA1g* (Wave129R, Geldner et al. 2009), *VHA-a1::VHA-a1-RFP* (VHA-a1-RFP, Dettmer et al. 2006), *35S::mKO-CLC* (mKO-CLC, Fujimoto et al. 2010), *UBQ10::mCherry-RabF2b* (Wave2R, Geldner et al. 2009) as well as *UBQ10::mCherry-SYP32* (Wave22R, Geldner et al. 2009).

The following root hair marker lines and root hair mutants were obtained from NASC stock center: *SCM::SCM-GFP* (*SCRAMBLED*, AT1G11130, Kwak and Schiefelbein 2008), *WER::GFP* (*WEREWOLF*, AT5G14750, Lee and Schiefelbein 1999), *scm-2* (SALK_086357), *wer-1* (Lee and Schiefelbein 1999), *cpc* (*caprice*, AT2G46410, SAIL_310_C06), *gl3* (WiscDsLox412G05), *gl3-1 egl3-1* (Bernhardt et al. 2003), *myc1-1* (SALK_057388), *gl2-2* (SALK_130213C) and *gl2-3* (SALK_039825C). The marker lines *GL3::GL3-YFP* (*GLABRA3*, AT5G41315, Bernhardt et al. 2005), *MYC1::GFP* (AT4G00480, Bruex et al. 2012) and

GL2::GFP (*GLABRA2*, AT1G79840, Lin and Schiefelbein 2001) were kindly provided by John Schiefelbein. The translational reporter *CPC::CPC-Neon* was generated according to Wada et al. (2002) which is described in detail in section 2.5. *WER::WER-GFP* (Ryu et al. 2005) was kindly provided by Prof. Dr. Markus Grebe. Homozygous root hair mutants and marker lines were established. To analyze potential changes in *EPSINOID2* expression patterns in different root hair mutant backgrounds, the *ID2::ID2-GFP* construct was introduced into the homozygous root hair mutants. Selected T_3 plant lines were backcrossed into Col-0 to re-establish *EPSINOID2* wild-type pattern. To see whether the expression of root hair markers changed in *epsinoid2* mutant background, all homozygous marker lines were crossed with *id2-1* mutant and homozygous plants for both root hair marker and *id2-1* mutation were analyzed at the Zeiss LSM 880 Airyscan Fast (Zeiss) using the 40x objective (see below for details). Homozygous double or triple mutants of *id2-1* and root hair mutants were generated to compare root hair densities.

Several stable transgenic lines regarding miRNA844 and the *mir844* mutant (Table 1) were generated and analyzed as described in section 2.7.

All plant material is summarized in Table 1 and more detailed in Table S 1.

Table 1: Overview of (previously) generated and provided transgenic *Arabidopsis* lines.

Plant material	Ecotype	Description/Application
***epsinoid2* mutants**		
id2-1	Col-0	T-DNA insertion mutant allele (SALK_042677)
id2-3	Col-0	full deletion mutant (CRISPR/Cas9)
***EPSINOID2* transformants**		
ID2::ID2-GUS in Col-0	Col-0	Analysis of expression pattern
ID2::ID2-GFP in Col-0	Col-0	Translational reporter line for analyses of expression pattern and subcellular localization
ID2-1100::NLS-GFP in Col-0	Col-0	Transcriptional reporter line, 1099 bp promoter length
35S::ID2 in Col-0	Col-0	Overexpression line, 2x35S-Ω promoter
35S::ID2-GFP in Col-0	Col-0	Overexpression line, 35S promoter
UBI10::ID2-GFP in Col-0	Col-0	Overexpression line, Ubiquitin-10 promoter
35S::ID2-miR^R in Col-0	Col-0	miRNA-resistant overexpression line, 2x35S-Ω promoter
35S::ID2-miR^R-GFP in Col-0	Col-0	GFP-tagged miRNA-resistant overexpression line
ID2::ID2-miR^R in Col-0	Col-0	miRNA-resistant *EPSINOID2* expressed under its own promoter
ID2::ID2-miR^R-Neon in Col-0	Col-0	GFP-tagged miRNA-resistant *EPSINOID2* expressed under its own promoter
ID2::ID2-3xGFP in Col-0	Col-0	*ID2-3xGFP* expression to analyze potential cell-to-cell movement

Plant material	Ecotype	Description/Application
MYC1::ID2-miR^R-GFP in Col-0	Col-0	ectopic GFP-tagged miRNA-resistant *EPSINOID2* expression under hair cell-specific promoter *MYC1*
Complementation line		
ID2::ID2-miR^R id2-3	Col-0	*id2-3* crossed with *ID2::ID2-miR^R*
Root hair markers		
SCM::SCM-GFP	Col-0	*SCRAMBLED* (*SCM*, AT1G11130) marker
WER::WER-GFP	Col-0	*WEREWOLF* (*WER*, AT5G14750) marker
WER::GFP	Col-0	*WEREWOLF* (*WER*, AT5G14750) marker
CPC::CPC-Neon in Col-0	Col-0	*CAPRICE* (*CPC*, AT2G46410) marker
GL3:.GL3-YFP	Col-0	*GLABRA3* (*GL3*, AT5G41315) marker
MYC1::GFP	Col-0	*MYC1* (AT4G00480) marker
GL2::GFP	Col-0	*GLABRA2* (*GL2*, AT1G79840) marker
Root hair marker crosses/transformants		
id2-1 x SCM::SCM-GFP	Col-0	*SCM* marker in *id2-1* mutant background
id2-1 x WER::WER-GFP	Col-0	*WER* marker in *id2-1* mutant background
id2-1 x WER::GFP	Col-0	*WER* marker in *id2-1* mutant background
CPC::CPC-Neon in *id2-1*	Col-0	*CPC* marker in *id2-1* mutant background
id2-1 x GL3:.GL3-YFP	Col-0	*GL3* marker in *id2-1* mutant background
id2-1 x MYC1::GFP	Col-0	*MYC1* marker in *id2-1* mutant background
id2-1 x GL2::GFP	Col-0	*GL2* marker in *id2-1* mutant background
Root hair mutants		
scm-2	Col-0	T-DNA insertion in third intron (SALK_086357)
wer-1	Col-2	point mutation in codon 93 (TGG → TGA)
cpc	Col-0	T-DNA insertion in second exon (SAIL_310_C06)
gl3	Col-0	T-DNA insertion in fifth exon (WiscDsLox412G05)
gl3-1 egl3-1	Col-0, L*er*	*gl3-1*: point mutation in codon 378 (CAG → TAG) *egl3-1*: point mutation in codon 26 (TGG → TGA)
myc1-1	Col-0	T-DNA insertion in second intron (SALK_057388)
gl2-2	Col-0	T-DNA insertion in second intron (SALK_130213C)
gl2-3	Col-0	T-DNA insertion in second intron (SALK_039825C)
***epsinoid2* & root hair double/triple mutants**		
id2-1 scm-2	Col-0	*id2-1* crossed with *scm-2*
id2-1 wer-1	Col-0, Col-2	*id2-1* crossed with *wer-1*
id2-1 cpc	Col-0	*id2-1* crossed with *cpc*
id2-1 gl3	Col-0	*id2-1* crossed with *gl3*
id2-1 gl3-1 egl3-1	Col-0, L*er*	*id2-1* crossed with *gl3-1 egl3-1*
id2-1 myc1-1	Col-0	*id2-1* crossed with *myc1-1*
id2-1 gl2-3	Col-0	*id2-1* crossed with *gl2-3*

Plant material	Ecotype	Description/Application
***EPSINOID2* transformants in root hair mutants**		
ID2::ID2-GFP scm-2	Col-0	*ID2::ID2-GFP* transformed into *scm-2*
ID2::ID2-GFP wer-1	Col-0, Col-2	*ID2::ID2-GFP* crossed with *wer-1*
ID2::ID2-GFP cpc	Col-0	*ID2::ID2-GFP* transformed into *cpc*
ID2::ID2-GFP gl3	Col-0	*ID2::ID2-GFP* transformed into *gl3*
ID2::ID2-GFP gl3-1 egl3-1	Col-0, L*er*	*ID2::ID2-GFP* transformed into *gl3-1 egl3-1*
ID2::ID2-GFP myc1-1	Col-0	*ID2::ID2-GFP* transformed into *myc1-1*
ID2::ID2-GFP gl2-2	Col-0	*ID2::ID2-GFP* transformed into *gl2-2*
***MIR844* transformants and mutants**		
35S::STTM844 in Col-0	Col-0	Short tandem target mimic of miRNA844-3p target, 2x35S-Ω promoter
35S::MIR844 in Col-0	Col-0	Overexpression of *MIR844*, 2x35S-Ω promoter
MIR844::ER-GFP in Col-0	Col-0	Transcriptional reporter line for *MIR844*
MIR844::GUS in Col-0	Col-0	Transcriptional reporter line for *MIR844*
mir844	Col-0	CRISPR/Cas9 full deletion mutant of *MIR844*
35S::NLS-GFP-miR844sensor in Col-0	Col-0	miRNA844-3p sensor construct
35S::NLS-GFP-miR844^{R}sensor in Col-0	Col-0	miRNA844-3p resistant sensor construct
Other transformants		
PME38-600::PME38-mNeon in Col-0	Col-0	Translational reporter line for *PME38* with 612 bp endogenous promoter
Marker lines for subcellular compartments		
UBQ10::mCherry-RabA1g	Col-0	Wave129R (Geldner et al. 2009), endosomal and cell plate marker
VHA-a1::VHA-a1-RFP	Col-0	VHA-a1-RFP (Dettmer et al. 2006); TGN marker
35S::mKO-CLC	Col-0	mKO-CLC (Fujimoto et al. 2010); TGN marker
UBQ10::mCherry-RabF2b	Col-0	Wave2R (Geldner et al. 2009); LE/PVC marker
UBQ10::mCherry-SYP32	Col-0	Wave22R (Geldner et al. 2009); Golgi marker
Crosses of *EPSINOID2* with subcellular marker lines		
ID2::ID2-GFP x UBQ10::mCherry-RabA1g	Col-0	*ID2::ID2-GFP* crossed with endosomal and cell plate marker *UBQ10::mCherry-RabA1g*
ID2::ID2-GFP x VHA-a1::VHA-a1-RFP	Col-0	*ID2::ID2-GFP* crossed with TGN marker *VHA-a1::VHA-a1-RFP*
ID2::ID2-GFP x 35S::mKO-CLC	Col-0	*ID2::ID2-GFP* crossed with TGN marker *35S::mKO-CLC*
ID2::ID2-GFP x UBQ10::mCherry-RabF2b	Col-0	*ID2::ID2-GFP* crossed with LE/PVC marker *UBQ10::mCherry-RabF2b*
ID2::ID2-GFP x UBQ10::mCherry-SYP32	Col-0	*ID2::ID2-GFP* crossed with Golgi marker *UBQ10::mCherry-SYP32*

Seeds were sterilized twice with 70 % ethanol followed by absolute ethanol or quickly with

70 % ethanol followed by 3 % sodium hypochlorite and stratified for two days. Seedlings were grown upright on 0.5x Murashige & Skoog (MS) medium containing 1 % sucrose, 0.22 % 2-(N-morpholino) ethanesulfonic acid (MES) and 0.8 % phyto-agar with a pH 5.8 in percival chambers under long day conditions (16 h light at 22°C/8 h dark at 18°C) for 5 or 7 days depending on the subsequent analysis. On soil, plants grew in a plant growth chamber under long day conditions (8 h at 18°C, 16 h at 23°C).

2.2 Generation of *epsinoid2-3* and *mir844* full deletion mutants

The *id2-3* mutant was generated by using the CRISPR/Cas9 system. To eliminate the *EPSINOID2* gene, two different single guide RNAs (sgRNAs) were designed targeting the 5'UTR (Upstream Target Sequence 1 & 2, UTS1/2) and the 4th exon or 3'UTR (Downstream Target Sequence 1& 2, DTS1/2) of the *EPSINOID2* gene, respectively (Figure 6), using CHOPCHOP (chopchop.cbu.uib.no, Labun et al. 2019) and CRISPRdirect (crispr.dbcls.jp, Naito et al. 2015). These sgRNAs were mixed and matched resulting in four different combinations (UTS1-DTS1, UTS1-DTS2, UTS2-DTS1 and UTS2-DTS2). Each sgRNA was included in primers to amplify the sgRNA cassette out of the pCBC-DT1T2 vector (kindly provided by Prof. Dr. Michael Lenhard), combine two sgRNAs as described above and clone each combination into the pHEE401E (Wang et al. 2015, kindly provided by Prof. Dr. Michael Lenhard) using the Golden Gate reaction (Xing et al. 2014). The adapted protocol was provided by Daphne Goring from University of Toronto. These four constructs were introduced into *Arabidopsis* Col-0 using *Agrobacterium*-mediated transformation. T$_1$ lines were selected on hygromycin-containing media and genotyped for *EPSINOID2* deletion. Homozygosity was confirmed in T$_2$ by genotyping and sequencing at LGC Genomics GmbH in Berlin. Homozygous plants were additionally checked for Cas9, to obtain homozygous *id2-3* deletion lines without the Cas9, and for off-targets predicted by Cas-OFFinder (www.rgenome.net/cas-offinder, Bae et al. 2014).

To generate a *mir844* full deletion mutant, two different sgRNAs recommended by CHOPCHOP with putative cutting sites a few bases upstream of the 3' end and 35 bp of the 5' end of the *MIR844* (AT2G23347) gene were used (Figure 6). All subsequent steps were performed as described for the *id2-3* deletion. There were no predicted off-targets by Cas-OFFinder. Detailed information about the protocol, primers and sequences can be found in the supplementary information (SI), materials and methods.
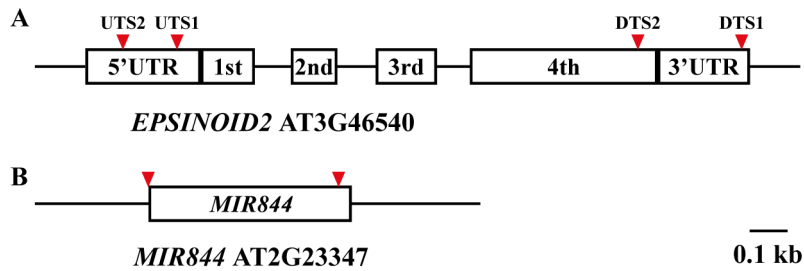
Figure 6: Creating full deletion mutants using CRISPR/Cas9.

Schematic view of the *EPSINOID2* (A) and *MIR844* (B) gene with the putative cutting sites (red rectangle) of the Cas9 protein. Boxes with numbers represent exons. Introns are indicated as lines between the exons. UTR: Untranslated region, UTS: Upstream Target Sequence, DTS: Downstream Target Sequence.

2.3 Generation of stable transgenic *EPSINOID2* lines

Constructs for stable transgenic *ID2::ID2-GUS/-GFP* lines were generated by using the sequence-specific recombination system Gateway by amplifying the *EPSINOID2* gene including 1.1 kb promoter region from Col-0 DNA and cloning it into the Gateway pDONR221 via BP reaction (detailed protocol in SI, section 6.2) which results in a pENT221 harboring the *ID2::ID2* construct. This was followed by LR reaction and thereby introducing the construct into the pGWB3 (C-terminal GUS tag) or pGWB4 (C-terminal GFP tag) destination vector, respectively. For GFP-tagged *EPSINOID2* overexpression lines, a previously generated pENT221 containing *EPSINOID2* coding sequence (Freimuth 2015) was cloned via LR reaction into pGWB405 (Cauliflower mosaic virus (CaMV) 35S, C-terminal GFP tag, addgene #74799) and additionally an existing *UBI10::ID2-GFP* from previous work (unpublished) was used. For a miRNA-resistant version of *EPSINOID2*, the putative miRNA844-3p target site was altered by changing as many bases as possible without changing the outcoming amino acids. Codons were used according to GenScript codon usage frequency table and optimization tool (https://www.genscript.com, 11.10.2019). For genomic miRNA-resistant *EPSINOID2*, a 331 bp long part of the *EPSINOID2* gene containing the modified target sequence was synthesized by Eurofins and assembled with the amplified pENT221-*ID2::ID2* excluding the same 331 bp sequence using NEBuilder HiFi DNA Assembly. The assembled pENT221-*ID2::ID2-miR^R* was then cloned into binary vector pGWB401 (Nakagawa et al. 2007) and pGWB401-mNeon (a modified pGWB401 (addgene #74795) in which mNeon was introduced as a C-terminal tag) resulting in *ID2::ID2-miR^R* and *ID2::ID2-miR^R-mNeon*. For miRNA-resistant overexpression constructs, *EPSINOID2* coding sequence including the altered target site and Gateway-compatible overhangs at the 5' and 3' end was synthesized by Eurofins and subsequently cloned via LR reaction into pGWB402Ω and pGWB405 resulting in *35S::ID2-*

miR^R and *35S::ID2-miR^R-GFP*, respectively.

To test whether EPSINOID2 protein moves between root epidermal cells, genomic *EPSINOID2* was tagged with 3xGFP. For this, pGWB401 was modified. pGWB401 was linearized with AfeI which creates a blunt cut behind the attR2 recombination site and assembled via NEBuilder HiFi DNA Assembly with 3xGFP which was amplified from the pGGC025 vector (addgene #48830, Lampropoulos et al. 2013) with primers containing corresponding overhangs to the ends of linearized pGWB401. The resulting pGWB401-3xGFP was then used as destination vector for LR reaction with pENT221-*ID2::ID2* creating the *ID2::ID2-3xGFP* construct.

All these constructs were transformed into *Arabidopsis* Col-0 by *Agrobacterium*-mediated transformation and stable, homozygous lines were obtained by selection with appropriate antibiotics. Additionally, *ID2::ID2-GFP* was stably transformed into several root hair mutants which are listed in Table 1.

2.4 Generation of *EPSINOID2* transcriptional reporter line

To analyze the promoter activity of *EPSINOID2*, a transcriptional reporter line was generated. The promoter region 1099 bp upstream from *EPSINOID2* start codon was amplified from Col-0 DNA using appropriate primers with Gateway overhangs and cloned via BP into pENT221 and subsequently via LR into pGWB565 (kindly provided by Tsuyoshi Nakagawa, Sultana et al. 2019) resulting in the *ID2::NLS-GFP* construct. This construct was stably transformed into Col-0 via floral dipping. Homozygous T$_3$ lines were analyzed at the Zeiss LSM 880 Airyscan Fast (see below for details).

2.5 Generation of a *CAPRICE* translational reporter line

To obtain a *CPC* translational marker line, genomic *CPC* including 1.2 kb of its endogenous promoter (according to Wada et al. 2002) was amplified using primers CPC-GW-F and CPC-GW-R containing Gateway-compatible overhangs (Table S 12) and introduced via Gateway cloning as described before into the pGWB401-mNeon destination vector. The resulting *CPC::CPC-mNeon* construct was then transformed into Col-0 and *id2-1* using floral dipping. Selected homozygous T$_3$ lines were analyzed at the Zeiss LSM 880 Airyscan Fast (see below for details).

2.6 Generation of stable transgenic *MIR844* lines

Short tandem target mimic construct (STTM)

To inhibit miRNA844-3p activity, a *STTM844* construct was generated according to Yan et al. (2012). This construct consists of two partially complementary miRNA844-3p target sites linked by a 48 nt spacer and both target sites contain three additional nucleotides (CTT) corresponding to positions 10 and 11 from the 5' end of the miRNA844-3p (Yan et al. 2012) (Figure 11). A CaMV poly(A) signal was added downstream of the STTM sequence. The *STTM844* sequence was synthesized as GeneStrands at Eurofins Genomics in two parts since it could not be done in one because of repetitive sequences. The first part (*STTM844a*) consisted of a Gateway overhang for BP reaction at the 5' end, followed by one miRNA844-3p target site including the three additional CTT and the 48 nt spacer. The second part (*STTM844b*) was designed with an 18 nt overhang at the 5' end which overlaps with the 3' end of the first part followed by the second miRNA844-3p target site, a CaMV poly(A) signal and a Gateway overhang for BP reaction at the 3' end. Both *STTM844* parts were assembled using NEBuilder HiFi DNA Assembly and subsequently cloned into pDONR221 via BP reaction. The resulting pENT221-*STTM844* was verified by sequencing and cloned into pGWB402Ω via LR reaction. The verified *35S::STTM844* construct was introduced into *Arabidopsis* Col-0 using *Agrobacterium*-mediated transformation. Root hair density was analyzed in homozygous T_3 plants as described below.

MIR844 overexpression constructs

To overexpress miRNA844, the whole genomic sequence of the *MIR844* gene which gives rise to the primary miRNA (pri-miRNA) was amplified from Col-0 DNA with appropriate primers containing Gateway cloning overhangs. In a BP reaction, this sequence was cloned into pDONR221. In a LR reaction, the verified pENT221-*MIR844* was subsequently cloned into pGWB402Ω. The final *35S::MIR844* construct was confirmed by sequencing and stably transformed into *Arabidopsis* Col-0 using the floral-dip method (SI, section 6.2). Homozygous T_3 plants were selected, and number of root hairs were determined as described above.

MIR844 reporter constructs

To gain insight into the expression of miRNA844-3p, the endogenous promoter region 866 bp upstream of the *MIR844* gene was amplified with primers miR844-PR-F and -R and cloned with the Gateway cloning system as described before into the destination vector pGWB562

27

(kindly provided by Tsuyoshi Nakagawa, Sultana et al. 2019) resulting in a *MIR844::ER-GFP* construct which was subsequently introduced into *Arabidopsis* Col-0 using the floral dipping method (SI, section 6.2). Selected homozygous T_3 plants were analyzed at the Zeiss LSM 880 Airyscan Fast (see below for details).

MiR844 sensor constructs

To investigate miRNA844-3p activity, sensor constructs were generated. The putative miRNA844-3p target sequence of *EPSINOID2* as well as a miRNA-resistant version were integrated into the 3'UTR of a GFP fused to an N-terminal nuclear localization sequence (NLS) expressed under a 35S promoter. First, the *35S::NLS-GFP* vector had to be created using the Gateway cloning system. For this, the 35S promoter was amplified from pGWB405 using appropriate primer containing Gateway overhangs (Table S 12). The amplicon was extracted from an agarose gel and cloned via BP reaction into pDONR221. The verified pENT221-*35S* was then cloned into pGWB565 (kindly provided by Tsuyoshi Nakagawa, Sultana et al. 2019) via LR reaction resulting a destination vector containing *35S::NLS-GFP*. To introduce the miRNA844-3p and resistant target sites, the protocol for "Bridging double-stranded DNA with a single-stranded DNA oligo using NEBuilder HiFi DNA Assembly" was used. *35S::NLS-GFP* plasmid was digested with SacI at 37°C for 20 min and subsequently extracted from an agarose gel. Two single-stranded oligos (ssOligo) were designed (Figure 7A), containing the miRNA844-3p target site and the miRNA-resistant target site, respectively. Both target sites are flanked with 5' and 3' overlap sequences with the respective ends of the digested vector. ssOligos were diluted and assembled with the linearized *35S::NLS-GFP* vector according to the NEB protocol (Figure 7B, protocol in section 6.2) resulting in a miRNA844-3p sensor (*35S::NLS-GFP-miR844-sensor*) and a miRNA844-3p-resistant sensor (*35S::NLS-GFP-miR844^R-sensor*). Both constructs were stably transformed into *Arabidopsis* Col-0 using *Agrobacterium*-mediated transformation. For both constructs, homozygous lines were selected in the T_3 generation. Five 5-day-old seedlings per line were imaged at the Zeiss LSM 880 Airyscan Fast with the 40x objectives (see below for details). Fluorescence intensity was then measured using ImageJ. For each image, an area cells of the same size including the epidermal was selected with the rectangle tool and the rest of the image was cleared ("clear outside"). A threshold of 10 % was set for each image and a selection was created. With this setting only the nuclei with the upper 10 % fluorescence intensities were measured giving a mean value for each image. Mean intensities were tested for normal distribution, statistically analyzed using one-way ANOVA and visualized in a Tukey box plot as described before.

A

ssOligo containing miR844-3p target site

CTGTACAAGTAAGCTTAGAGCT\\AACTGGAGGATGGCTTATAA\\CGAATTTCCCCGATCGTTCAAAC

ssOligo containing miR844-3p-resistant target site

CTGTACAAGTAAGCTTAGAGCT\\AAtTGGcGtATGGCaTAcAA\\CGAATTTCCCCGATCGTTCAAAC

Purple: 5' sequence of *35S::NLS-GFP* vector cut with SacI

Red: miR844-3p/-resistant target site

Blue: 3' sequence of *35S::NLS-GFP* vector cut with SacI

B
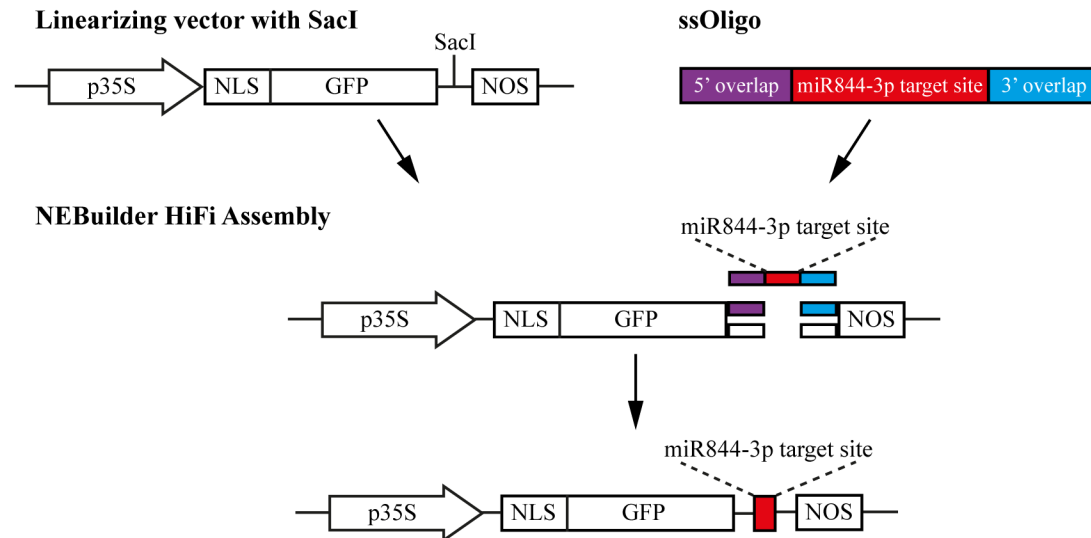
Figure 7: Creating a miRNA844-3p sensor construct.

(A) Sequences of ssOligos used to create miR844-3p and miR844-3p-resistant sensor constructs. (B) Schematic overview of cloning steps to create sensor constructs using NEBuilder HiFi DNA Assembly with ssOligos.

2.7 Generation of the *MYC1::ID2-miR^R^-GFP* construct for tissue specific expression

To express miRNA-resistant *EPSINOID2* under the hair cell-specific *MYC1* (AT4G00480) promoter, a DNA assembly method was used to replace the *EPSINOID2* promoter in the pENT221-*ID2::ID2-miR^R^* construct generated in section 2.3 with the *MYC1* promoter. The *MYC1* promoter was amplified from Col-0 DNA (2581 bp fragment upstream of *MYC1* start codon, according to Zhao et al. 2012) using primers overlapping with the first exon of *EPSINOID2* and the backbone of pENT221. To remove the *EPSINOID2* promoter, appropriate primers also binding to the pENT221 backbone and the first *EPSINOID2* exon were used to amplify the whole the pENT221-*ID2::ID2-miR^R^* vector without the *EPSINOID2* promoter (3889 bp fragment). Primers are listed in Table S 12. The pENT221-*ID2-miR^R^* product was digested with 1 µl DpnI for 1 h at 37°C to remove plasmid DNA and purified using the Monarch DNA Gel Extraction Kit (NEB). DNA concentration of both products was estimated using the GeneRuler 1kb DNA ladder (SI, section 6.2). Assembly of *MYC1* promoter and pENT221-*ID2-*

miR^R was done using the NEBuilder HiFi DNA Assembly Cloning Kit (NEB, detailed protocol in SI, section 6.2). The assembled product was confirmed by sequencing. The destination vector pGWB401-GFP was generated as described for pGWB401-3xGFP in section 2.3, only amplifying one GFP from pGGC025 and introducing it into pGWB401. By using the LR reaction, the verified pENT221-*MYC1::ID2-miR^R* plasmid was cloned into pGWB401-GFP resulting in *MYC1::ID2-miR^R-GFP* which was subsequently transformed into Col-0 using *Agrobacterium*-mediated transformation. The expression pattern was analyzed in T$_2$ generation at the Zeiss LSM 880 Airyscan Fast (see below for details).

2.8 Root hair analyses

Number of root hairs

To analyze the number of root hairs, *Arabidopsis* seedlings were grown on upright MS plates for 7 days as described above. Each analysis was repeated independently at least three times. In each experiment, at least 15 roots per genotype were analyzed, unless stated otherwise. For every root z-stacks were taken with the Zeiss Axio Zoom.V16 using a 25x magnification (objective: Plan-NEOFLUAR Z 1.0x/0.25 FWD 56mm). To process the z-stacks the "Extended Depth of Focus" and "Image Export" functions of the Zen software were used. The resulting .tif files had an image size of 1388 x 1040 pixels which was equivalent to 3.6 x 2.7 mm and were analyzed with the ImageJ plugin ObjectJ. 1 mm above the root tip, in a section of 2 mm all root hairs were counted. Acquired data were statistically analyzed and graphs were created with the Prism software. First, datasets were tested for normality using the implemented set-up consisting of the D'Agostino-Pearson test, the Shapiro-Wilk test and the Kolmogorov–Smirnov test (KS test). Each experiment comprised a measured variable (number of root hairs per root) in three or four unpaired groups (roots of one genotype). To test if the number of root hairs between respective genotypes was significantly different, appropriate statistical tests were applied. For normally distributed datasets parametric one-way analysis of variance (ANOVA) and for data sets with a non-Gaussian distribution the nonparametric Kruskal-Wallis test was used. Since there was a considerable variation in absolute root hair numbers between experiments, datasets of each experiment were standardized by normalization to the mean of the respective Col-0 data and subsequently the three biological replicates (n = 3) were pooled. Pooled datasets were visualized in a Tukey box plot (whiskers are 1.5 interquartile range, outliers are represented as asterisks). Significance levels are indicated as asterisks above brackets connecting respective compared data (* p<0.0332, ** p<0.0021, *** p<0.0002, ****

p<0.0001).

Table 2: Overview of analyzed genotypes in the root hair analyses.

In all analyses Col-0 was used as wild type control and either *id2-1* or *id2-3* as *epsinoid2* mutant control, respectively. $^{-}/_{-}$: homozygous, $^{+}/_{-}$: heterozygous

Analyzed genotypes	Number of experiments
id2-3 $^{-}/_{-}$	3
id2-3 $^{+}/_{-}$	3
ID2::ID2-GFP #12.3	3
35S::ID2 #1.5	3
35S::ID2-GFP #1.1	3
35S::ID2-miR^R ##2.1 + 3.8	3
35S::ID2-miR^R-GFP #5.2	3
35S::STTM844 ##2.1 + 3.1	3
35S::MIR844 ##7.3 + 10.4	1
id2-1 x scm-2	3
id2-1 x wer-1	3
id2-1 x cpc	3
id2-1 x gl3	3
id2-1 x gl3-1 egl3-1	3
id2-1 x myc1-1	3
id2-1 x gl2-3	3
mir844 #8.2.11	3
ID2::ID2-miR^R id2-3 #1.1	2

Ectopic root hairs & root hair cell length

To count ectopic root hairs and to measure root hair cell length, 7-day-old seedlings of Col-0 and the mutant *id2-3* were analyzed at the Zeiss Axio Imager.M2 using a Plan-Apochromat 10x/0.45 M27 lens and Differential Interference Contrast (DIC) optics. Seedlings were grown as described above. For both measurements, ten roots for each genotype were analyzed in three independent experiments. To verify whether a root hair was in hair (H) or non-hair (N) position (ectopic), ten root hairs that could be viewed from above were chosen across the entire root. By focusing on the underlying cortical cell plane, it was checked whether the root hair is located over the anticlinal wall between two cortical cells (H position) or over a single cortical cell (N position) (Dolan et al. 1993b). Number of hairs in H and N position were summed and percentage of hairs in N position was calculated. Additionally, the cell length of ten fully matured hair-carrying cells across the root was measured. Datasets with each n = 100 were tested for normality and statistically analyzed with Prism as described above. Means of all three

biological replicates (n = 3) were averaged and pooled. Mean ectopic root hairs and root hair cell length were visualized with standard deviation in a bar plot or Tukey box plot, respectively.

Root length & root diameter

To obtain root length and diameter, 7-day-old Col-0 and *epsinoid2* mutant seedlings from root hair density experiments were used. For root length, whole plates were scanned with a HP Deskjet flatbed scanner. Length of at least 21 roots was measured from root junction to root tip using ImageJ plugin ObjectJ with the polyline tool. For root diameter, images from root hair density analyses and ObjectJ were used. Diameter of at least 17 roots was measured 1 mm, 2 mm and 3 mm above the root tip and averaged for each root. Both analyses were repeated three times and datasets were pooled, tested for normality, analyzed statistically, and visualized as described above.

2.9 Semiquantitative reverse transcription polymerase chain reaction (RT-PCR)

Semiquantitative RT-PCRs were used to confirm *id2-3* as a full deletion mutant, to check whether *EPSINOID2* homologs *EPSINOID1* and *3* were potentially upregulated for compensation in the *id2-3* mutant and to compare transcript levels of *EPSINOID2* overexpression and miRNA-resistant lines. For this, 7-day-old seedlings from respective lines were weighed and ground in liquid nitrogen. RNA was extracted using the RNeasy Plant Mini Kit (QIAGEN), concentrations were measured with a NanoDrop OneC spectrophotometer (Thermo Fisher Scientific), and RNA quality was checked in an agarose gel electrophoresis run. RNA was then treated with DNaseI (Thermo Fisher Scientific). To check for genomic DNA contamination, a test PCR with intron-specific primers was run (SI, section 6.2).

For cDNA synthesis, RevertAid H Minus First Strand cDNA Synthesis Kit (Thermo Fisher Scientific) was used. Additionally, a "-RT" control with Col-0 RNA was included in which water instead of the reverse transcriptase was utilized. The cDNA served as template in the semiquantitative RT-PCR.

To test the cDNA and primers, 1:10 diluted cDNA plus a water control was used in a test PCR with primers for reference genes *BETA-6 TUBULIN* (*TUBβ6*; AT5G12250) and *ELONGATION FACTOR-1 alpha* (*EF1α*; AT5G60390) as well as with primers for *EPSINOID2*. Primers are listed in Table S 12 and PCR protocols are described in the SI, section 6.2.

To detect the *EPSINOID2* transcript in the semiquantitative RT-PCR, the primer pair EPSINOID2-RTPCR-F & -R which anneal in the third and fourth exon were used, amplifying

a 422 bp fragment of the coding sequence (Table S 12). PCR protocol and program are described in detail in the SI, section 6.2. PCR products were visualized using agarose gel electrophoresis.

2.10 Pull-down assays for mass spectrometry (MS/MS) analyses

To search for EPSINOID2 interactors using MS/MS in collaboration with AG Börnke at the IGZ Großbeeren, pull-down assays were done as preparation. Recipes for plant extraction buffer and washing buffer were provided by Jennifer Bortlik from AG Börnke at the IGZ Großbeeren who subsequently performed mass spectroscopic analyses of the retained proteins (Table S 5).

N-terminally GST-tagged *EPSINOID2* and *GST-MCS* (empty pGEX-2T-GW vector only containing a multiple cloning site) which serves as a control were generated in previous work (Freimuth 2015, 2019). For C-terminally GST-tagged *EPSINOID2*, LR reaction was performed with pENT221-*ID2-CDS* from previous work (Freimuth 2015) and a modified pGEX-2T-GW destination vector in which the N-terminal GST was removed and a C-terminal GST was added (pGEX-C-GST), followed by all subsequent cloning steps. All three verified constructs containing *GST-MCS*, *GST-ID2* and *ID2-GST* were transformed into electrocompetent *E. coli* BL21(DE3)pLysS cells. Bacterial expression and extraction of recombinant proteins is described in detail in SI, section 6.2. GST-tagged bait proteins were bound to glutathione-bound beads on columns. Plants extracts from 7-day-old Col-0 seedlings served as prey. The detailed pull-down assay protocol is described in the SI, section 6.2. Samples were sent to the IGZ for analysis.

2.11 Construct for yeast-two-hybrid (Y2H) screen

To perform a Y2H screen, a fusion protein of EPSINOID2 and the binding domain (BD) had to be generated to use EPSINOID2 as bait protein. For this, the previously generated pENT221-*ID2-CDS* was used to clone *ID2-CDS* into the gateway-compatible Y2H vector pGBT9-GW (kindly provided by Dr. Frederik Börnke from the IGZ).

33

2.12 Construct for EPSINOID2 antibody generation

To generate a specific antibody against EPSINOID2, an appropriate protein fragment which is only present in EPSINOID2 had to be found since EPSINs and EPSINOIDs share high similarity in their ENTH domain. Therefore, multiple sequence alignment with EPSIN1, EPSIN2, EPSIN3, EPSINOID1, EPSINOID2 and EPSINOID3 using BLASTp was performed in which a sequence of 65 amino acids (aa) (YRKCNSNFTKNYDEDDQENTMVSPNDANLFPQPLVADPSEESRTGMKENMDPEDD ENTEVNPLLG, Y208-G272) was identified that did not align with the other ENTH domain proteins. To confirm that, reciprocal BLASTp of these 65 aa against the *Arabidopsis* database was performed which returned EPSINOID2 as the only match. This fragment was chosen as template for an antibody generation. The corresponding 195 bp of the 4th exon were amplified from the existing pENT221-*ID2-CDS* using primers ID2-Y208-GW-F and ID2-G272-GW-R containing Gateway-compatible overhangs (Table S 12) and cloned into the pGEX-2T-GW destination vector via Gateway cloning as described before. The resulting GST-Y208-G272 protein fragment was subsequently expressed in BL21 cells in a small batch as described in the supporting information and tested for correct size in a Coomassie-stained SDS gel as well as with an anti-GST antibody in a western blot.

For antibody generation, the protein fragment was expressed as before in a bigger batch, extracted from cells and purified. Immunization of rabbits (2 individuals) and affinity purification against the antigen were carried out by Davids Biotechnologie, Regensburg.

2.13 Generation of constructs for interaction studies

All coding sequences of potential interactors were amplified from Col-0 cDNA with appropriate primers (Table S 12) containing Gateway overhangs for BP reaction, except for *PME38-CDS* which was synthesized with Gateway overhangs as GeneStrand at Eurofins Genomics since all attempts to amplify its sequence failed. Additionally, coding sequences for *CHC1*, *MIN7*, *WDL4*, *IRE*, *SEC6, BETA1-COP* and *VHA-A1* could not be obtained and analyses for these candidates were postponed. Using Gateway cloning, all constructs were introduced into the pIX-HALO destination vector (Joseph Ecker lab, SALK institute, ABRC stock CD3-1742, kindly provided by the group of Prof. Dr. Isabel Bäurle).

Table 3: Overview of potential interactors cloned into pIX-HALO vector.

Potential interactor	Full name	AGI	Coding sequence in bp	Protein size in kDa (incl. HALO tag)	Identified in
ACT2	ACTIN 2	AT3G18780	1132	78	pull-down-MS/MS
AP3D	ADAPTOR PROTEIN 3 DELTA	AT1G48760	2607	133	Y2H
BETA1-COP	BETA1 COAT PROTEIN	AT4G31480	2913	143	Y2H
CAP1	CLATHRIN ASSOCIATED PROTEIN 1	AT4G32285	1905	106	Y2H
CCS52B/FZR3	CELL CYCLE SWITCH PROTEIN 52 B, FIZZY-RELATED 3	AT5G13840	1443	90	Y2H
CHC1	CLATHRIN HEAVY CHAIN 1	AT3G11130	5115	228	pull-down-MS/MS
CNGC15	CYCLIC NUCLEOTIDE GATED CHANNEL 15	AT2G28260	2034	115	Y2H
CNGC5	CYCLIC NUCLEOTIDE GATED CHANNEL 5	AT5G57940	2151	118	Y2H
ECA4/PICALM4	EPSIN-LIKE CLATHRIN ADAPTOR	AT2G25430	1959	108	Y2H
IRE	INCOMPLETE ROOT HAIR ELONGATION	AT5G62310	3504	185	Y2H
MIN7	HOPM INTERACTOR 7	AT3G43300	5274	230	pull-down-MS/MS
PLDα1	PHOSPHOLIPASE D ALPHA 1	AT3G15730	2430	129	IP-MS/MS, pull-down-MS/MS
PME38	PECTIN METHYLESTERASE 38	AT4G00190	1422	88	IP-MS/MS
PVA12	PLANT VAP HOMOLOG 12	AT2G45140	718	62	pull-down-MS/MS
RSW10	RADIAL SWELLING 10	AT1G71100	801	66	Y2H
SEC6	SEC6	AT1G71820	2325	123	Y2H
SYP122	SYNTAXIN OF PLANTS 122	AT3G52400	1026	73	-
SYP123	SYNTAXIN OF PLANTS 123	AT4G03330	918	69	-
VHA-A	VACUOLAR ATP SYNTHASE SUBUNIT A	AT1G78900	1869	106	pull-down-MS/MS
VHA-A1	VACUOLAR PROTON ATPASE A1	AT2G28520	2451	128	-
VTI11	VESICLE TRANSPORT V-SNARE 11	AT5G39510	663	61	-
VTI12	VESICLE TRANSPORT V-SNARE 12	AT1G26670	666	61	-

Potential interactor	Full name	AGI	Coding sequence in bp	Protein size in kDa (incl. HALO tag)	Identified in
VTI13	*VESICLE TRANSPORT V-SNARE 13*	AT3G29100	588	58	-
WDL4	*WAVE-DAMPENED2-LIKE4*	AT2G35880	1296	81	pull-down-MS/MS

2.14 *In vitro* translation and pull-down assays

To study *in vitro* protein-protein interaction, bacterial expressed GST-tagged EPSINOID2 (described in SI, section 6.2) served as bait protein and *in vitro* translated N-terminally HALO-tagged potential interactors as prey proteins. As a control, GST-MCS was used. For *in vitro* translation, the TnT T7 Quick coupled system (Promega) was used and subsequently a modified pull-down assay was applied (Sauer 2014), both described in detail in the supporting information (section 6.2). A potential interaction was then visualized on a western blot by immunostaining with antibodies for HALO as well as GST and Horseradish peroxidase (HRP)-conjugated secondary antibodies (Table S 10).

2.15 Generation of stable transgenic *PME38* lines and mutants

To analyze the expression pattern of the potential interactor *PME38* (AT4G00190), two translational reporter lines were generated. The genomic region of *PME38* including 1049 bp and 612 bp of its promoter region was amplified using appropriate primers with Gateway-compatible overhangs. Both sequences were cloned via BP into pENT221 as described before. The generation of pENT221-*PME38-1000::PME38* failed and was not continued. pENT221-*PME38-600::PME38* was subsequently introduced into pGWB401-GFP (generated in section 2.7) via LR as described before resulting in the final construct *PME38-600::PME38-GFP* which was the transformed into Col-0 using the floral dip method.
Seedlings of the T_2 generation were analyzed at the Zeiss LSM 880 Airyscan Fast (Zeiss).

2.16 GUS staining

To analyze the expression of GUS-tagged *EPSINOID2*, 7-day-old homozygous *ID2::ID2-GUS* seedlings were stained with 1x GUS buffer containing 1 mg/ml X-Gluc for 1 h at 37°C (Table S 5). Seedlings were then incubated for a few minutes in 70 %, 50 %, 25 % and 10 % ethanol, followed by incubation in ddH$_2$O. Samples were embedded in mounting media (Table S 5) and

imaged at a Zeiss Axiophot2 with objective EC-Plan Neofluar 10x NA 0.3 or 20x NA 0.5 using brightfield illumination. Images were captured with an adapted Canon EOS 350 digital camera; white balance was kept identical for all images.

2.17 In situ RNA hybridization

For in situ RNA hybridization, *EPSINOID2* coding sequence including its stop codon was amplified from cDNA with ID2-CDS-KpnI-F and ID2-CDSStop-XbaI-R primers which generate a KpnI and XbaI cutting site at the beginning and end of the sequence, respectively (Table S 12). The amplicon and the vector backbone pBluescript II Sk (+) were then digested with KpnI and XbaI and subsequently ligated using the T4 DNA ligase (NEB). The ligation mix was digested with PstI to destroy remaining empty pBluescript II Sk (+) plasmids. In situ RNA hybridization including tissue preparation was performed by Magdalena Musialak-Lange from Vanessa Wahls group (AG Metabolism and Development) at the MPI-MP, Potsdam. Resulting cross-sections and longitudinal sections of 7-day-old Col-0 and *id2-3* roots were imaged at the Zeiss Axiophot2 as described above.

2.18 Confocal laser scanning microscopy

Live cell imaging to explore expression patterns and subcellular (co-)localization was performed with confocal laser scanning microscopy at the Zeiss LSM 880 Airyscan Fast (Zeiss) using the argon laser for exciting GFP at 488 nm and YFP at 514 nm and the DPSS laser for exciting mCherry at 561 nm and appropriate single- or double wavelength beam splitters. Depending on the signal intensity and laser line, laser intensity attenuators were set to 4-8 percent. Quasar 34 channel spectral GaAsP detector was utilized in 1 or 2 channel configuration and windows for emission wavelength started 5 nm below the peak emission of each fluorophore and were set in an approximately 40 nm range. Gain was set between 750-880 V with no offset or digital amplification and was adjusted to prevent overexposition of the sensor. Pinhole typically ranged between 1.0 to 1.23 airy units, depending on the signal characteristics. To analyze expression and/or localization of ID2-GFP, ID2-miR[R]-Neon and root hair marker lines, the objectives LD LCI Plan-Apochromat 40x/1.2 Imm Korr DIC M27 and LD LCI Plan-Apochromat 25x/0.8 Imm Korr DIC M27 were used, with water as immersion medium. For better visualization of relative positions of epidermal cells to cortex cells, roots were incubated with 1 µg/ml propidium iodide (PI) to stain cell walls. To obtain side view images of the root

epidermis and cortex cells, confocal Z-stacks with a fixed 0.1 µm interval were taken using the line-scan mode.

Subcellular (co-)localization of EPSINOID2 was analyzed using the Airy Scan detector.

To better understand subcellular localization and dynamic characteristics, 7-day-old seedlings were treated with 50 µM BFA or DMSO mock treatment for 1 h in liquid 0.5x MS medium.

For analysis of EPSINOID2 protein degradation, 5-day-old seedlings of the established *ID2::ID2-GFP* line were treated for 3 h with 50 µM MG132, 100 µM Cycloheximide (CHX) and, MG132 plus CHX in combination at same concentrations. DMSO was used as mock treatment and roots were subsequently imaged using the same setup as described above for ID2-GFP with the 40x objective. Experiments were repeated three times and, in each experiment, 7 to 11 seedlings per treatment were imaged. Fluorescence intensity was measured using ImageJ. For this, fluorescent area was selected with the polygon tool and then intensity was measured giving a mean value for each image. For each treatment, mean intensities were averaged and then normalized to the total mean of the DMSO treatment. Data from three experiments were pooled, tested for normal distribution, statistically analyzed using one-way ANOVA and visualized in a Tukey box plot as described before.

3. Results

3.1 *EPSINOID2* is expressed in non-hair cell files of the root epidermis

It was revealed that in previously analyzed stable transgenic lines (Freimuth 2015, 2019) which express GUS- and GFP-tagged *EPSINOID2* under 1.1 kb of the endogenous promoter (*ID2::ID2-GUS/-GFP*), 207 bp of the 4th exon of *EPSINOID2* corresponding to 41 amino acids were missing. This line was hence renamed in ID2-Δ41-GFP and retired. To overcome potential problems regarding the localization or functionality, new stable transgenic lines were established containing the full genomic region of the *EPSINOID2* gene (ID2-GUS/-GFP). These lines confirmed the expression pattern of *EPSINOID2* that was shown in previous work (Freimuth 2015, 2019). ID2-GUS was detected in leaves, particularly in trichomes, and, depending on the age of the flower, in the ovary or ovules (not shown). In 5-day-old *Arabidopsis* seedling roots, it showed a striped pattern in the transition region from the meristematic to the elongation zone (Figure 8A). ID2-GFP displayed a specific signal in non-hair (N) cell files of the root epidermis, especially seen in the side view: single hair (H) cell files are in contact with two underlying cortical cells (C) and separated by one or two non-hair cell files which are located over a single cortical cell (Figure 8B, Duckett et al. 1994). A comparison of the expression pattern of the new stable transgenic line *ID2::ID2-GFP* and the old one *ID2::ID2-Δ41-GFP* can be found in the supporting information (Figure S 1), no obvious differences were visible. This expression pattern also corresponds with the results of microarray analyses with cell-type-specific mRNA, showing a higher expression of *EPSINOID2* in non-hair cells compared to hair cells (Birnbaum et al. 2003).
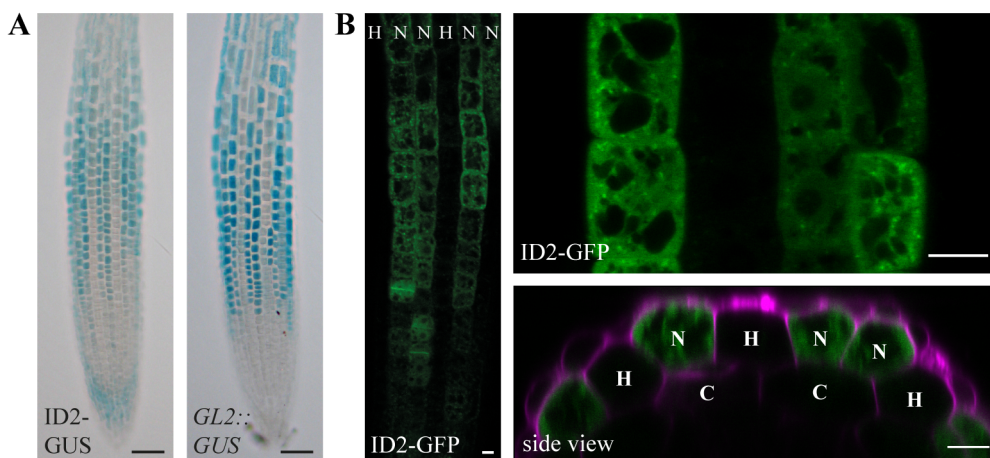
Figure 8: EPSINOID2 is specifically located in non-hair cells of the root epidermis.
EPSINOID2 gene expression in *Arabidopsis* roots of 5-day-old seedlings. (A) GUS-tagged *EPSINOID2* showed a striped pattern in the transition of the meristematic and elongation zone of the root epidermis, reminiscent of the

expression pattern of non-hair marker *GL2::GUS*. Scale bar = 50 µm. (B) Expression of *ID2::ID2-GFP* confirmed a specific signal in non-hair cell files (N) in the meristematic zone of the root epidermis. Non-hair specificity is supported by the side view showing a signal in epidermal cells located over a single cortical cell (C). Cell walls were stained with propidium iodide. Scale bars = 10 µm.

3.2 EPSINOID2 is associated with endosomal structures and the cell plate

On a subcellular level, ID2-GFP appears to be mostly cytosolic and it localizes to the growing cell plate in dividing cells as reported before (Freimuth 2019). Interestingly, in the new line with full length ID2-GFP the signal in the cytosol exhibits a lot more distinct punctate structures reminiscent of endosomal structures (Figure S 1). This was confirmed by crosses with the endosomal and cell plate marker mCherry-RabA1g (Wave129R, Geldner et al. 2009) that belongs to the RABA1 GTPases which are involved in secretory trafficking (Figure 9A). ID2-GFP signal colocalized to the mCherry-RabA1g signal at the cell plate and partly with endosomal structures. Colocalization analyses with other established markers for subcellular structures were performed and showed that ID2-GFP also colocalizes with the TGN marker VHA-a1-RFP (Figure 9B) (Dettmer et al. 2006). After treatment with the fungal toxin brefeldin A (BFA), which inhibits certain ADP-ribosylation factor–guanine-nucleotide exchange factors (ARF-GEFs) (Helms and Rothman 1992; Donaldson et al. 1992; Peyroche et al. 1999) interfering with the endocytic pathway (Nebenführ et al. 2002), ID2-GFP and mCherry-RabA1g (Figure 9F) as well as ID2-GFP and VHA-a1-RFP (Figure 9G) were aggregated in so-called BFA compartments, suggesting that EPSINOID2 is associated with BFA-sensitive endosomal structures, such as, for example, the TGN. Additionally, ID2-GFP colocalizes with the TGN-associated clathrin light chain marker mKO-CLC (Figure 9C) (Fujimoto et al. 2010). Furthermore, crosses of ID2-GFP with markers for other punctate structures, such as the late endosomal (LE)/PVC marker mCherry-RabF2b (Figure 9D) (Wave2R, Geldner et al. 2009) as well as the Golgi marker mCherry-SYP32 (Figure 9F) (Wave22R, Geldner et al. 2009) did not show any colocalization. Similar results have been shown for TGN-associated EPSIN1 and MTV1, which are involved in vacuolar and secretory transport, colocalizing with VHA-a1-RFP and mKO-CLC but not mCherry-RabF2b and mCherry-SYP32 (Heinze et al. 2020). Together, these results strongly suggest an association of EPSINOID2 with TGN-associated endosomal structures and furthermore points towards an involvement in post-Golgi trafficking.
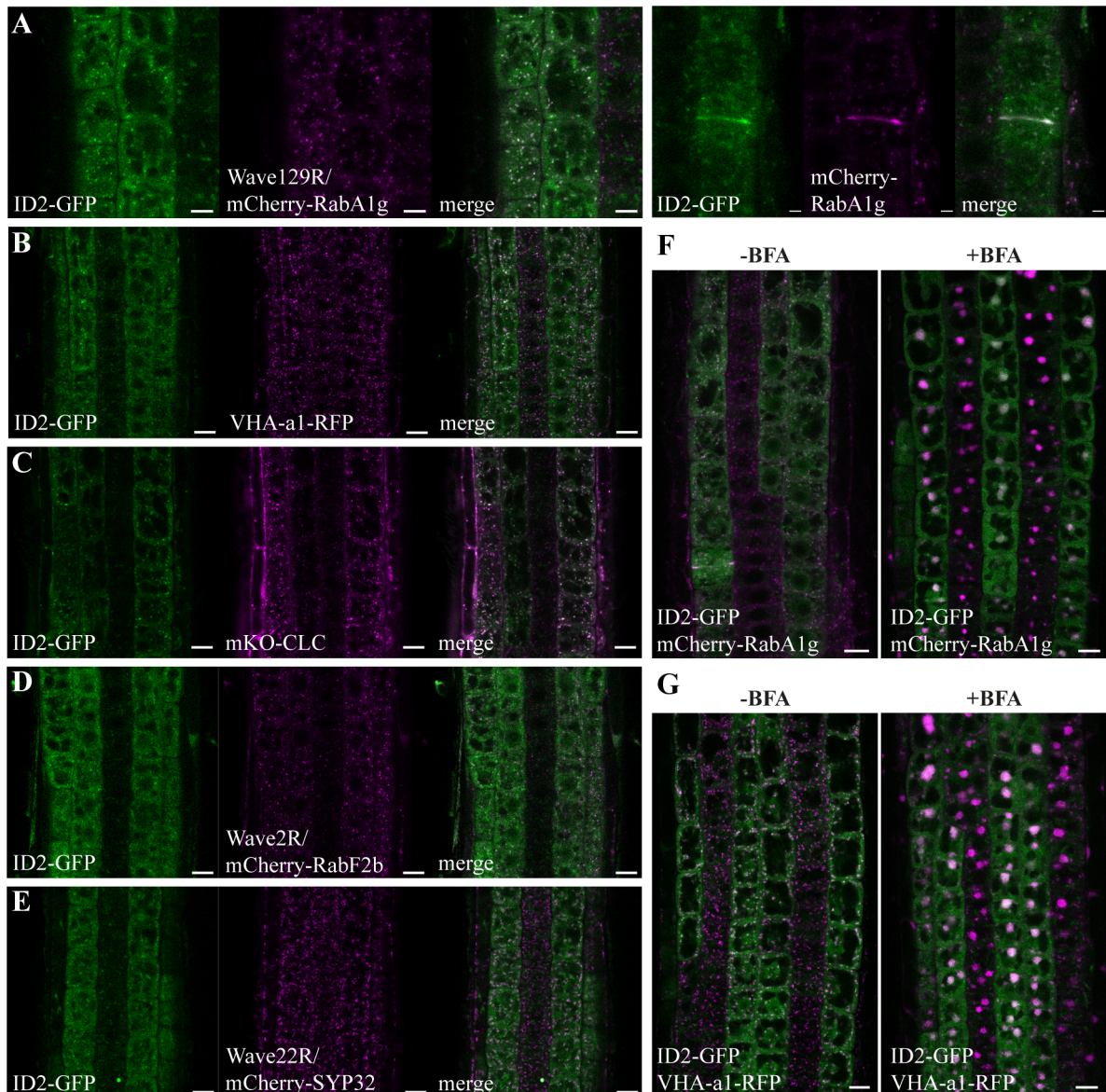
Figure 9: EPSINOID2 colocalizes with endosomal structures.

Subcellular localization of ID2-GFP in root epidermis cells in 5-day-old *Arabidopsis* seedlings. (A) Partial colocalization of ID2-GFP with the endosomal marker mCherry-RabA1g which also colocalized at the cell plate. (B) ID2-GFP colocalized with the TGN marker VHA-a1-RFP. (C) Colocalization of ID2-GFP with the TGN-associated mKO-CLC. (D) No colocalization of ID2-GFP and the LE/PVC marker mCherry RabF2b. (E) ID2-GFP did not colocalize with Golgi marker mCherry-SYP32. (F) ID2-GFP and mCherry-RabA1g aggregated in BFA compartments after 1 h BFA treatment. (G) After BFA treatment, both ID2-GFP and VHA-a1-RFP accumulated in BFA compartments. Scale bars = 10 μm.

3.3 *epsinoid2* loss-of-function mutants exhibit ectopic root hair formation

In previous work, two independent T-DNA insertion lines, the knock-out mutant *id2-1* and knock-down mutant *id2-2*, showed a significantly increased root hair density compared to the wild type (Figure 2) (Freimuth 2019). Further previous analyses indicate that both ectopic root

hair formation (hairs originating from non-hair cells) and, to a lesser extent, reduced length of hair cells contribute to the hairy mutant phenotype (Figure 2) (Freimuth 2019). In this work, the causative nature for the hairy mutant phenotype due to lack of *EPSINOID2* was further confirmed by a mutant with a full deletion of the *EPSINOID2* gene generated with the CRISPR/Cas9 system (Figure 10A). In this *id2-3* mutant, the whole genomic region of *EPSINOID2* including 64 bp of its 5'UTR and 223 bp of its 3'UTR were cut out. This was verified by sequencing and the Cas9 cassette was removed by outcrossing. The *id2-3* mutant was further verified as a knock-out by semiquantitative RT-PCR in which no *EPSINOID2* transcript was detected (Figure 10B) whereas housekeeping genes *BETA-6 TUBULIN* (*TUBβ6*) and *ELONGATION FACTOR-1 alpha* (*EF1α*) showed normal mRNA levels (Figure S 3B). Additionally, in situ RNA hybridization of *EPSINOID2* mRNA in 5-day-old seedlings of this line showed no staining in longitudinal or transverse section of the root (Figure 10C). The transverse section also demonstrates that the primary root structure is not altered in terms of cell file number in *id2-3*. *Arabidopsis* wild-type primary roots have a very conserved number of cortex cell files which is normally 8 (Dolan et al. 1993a). Root diameter as a result of increased number of cortex cells as well as root elongation can differ in response to nutrient availability or in other stress responses (Ma et al. 2001; López-Bucio et al. 2003). The number of cortex cells (Figure 10C) and root length (Figure S 2A) as well as root diameter (Figure S 2B) were not altered in *epsinoid2* mutants, indicating that the root hair phenotype is unlikely a secondary effect of a stress response. To rule out compensation of *EPSINOID2* loss by the two homologous *EPSINOID1* and *3*, semiquantitative RT-PCR with specific primers for these two genes were performed. *EPSINOID3*, which is specifically expressed in the endodermis (Freimuth 2015), did not display an upregulation in *id2-3* mutants (Figure S 3A). *EPSINOID1* transcript was completely absent in either Col-0 or the *id2-3* mutant (Figure S 3A) which is not surprising since *EPSINOID1* is not expressed in roots (Freimuth 2015), only weakly in anthers of flowers (Sauer and Freimuth, unpublished). Additionally, *id1 id2 id3* triple mutants did not show an additional abnormal phenotype (Sauer and Freimuth, unpublished). Root hair analyses of 7-day-old *id2-3* seedlings revealed a similar mutant phenotype as *id2-1* with approximately 35 % more root hairs than the wild type (Figure 10D). The *id2-3* mutant also showed 4 times more ectopic root hairs (on average 33 %) (Figure 10E) and reduced hair cell length (on average 203 μm) compared to Col-0 which had on average 8 % ectopic root hairs and a mean hair cell length of 251 μm (Figure 10F).

These results from *id2-3* support the obtained *id2-1* and *id2-2* data from previous studies that loss of *EPSINOID2* is indeed the cause for ectopic root hair formation.
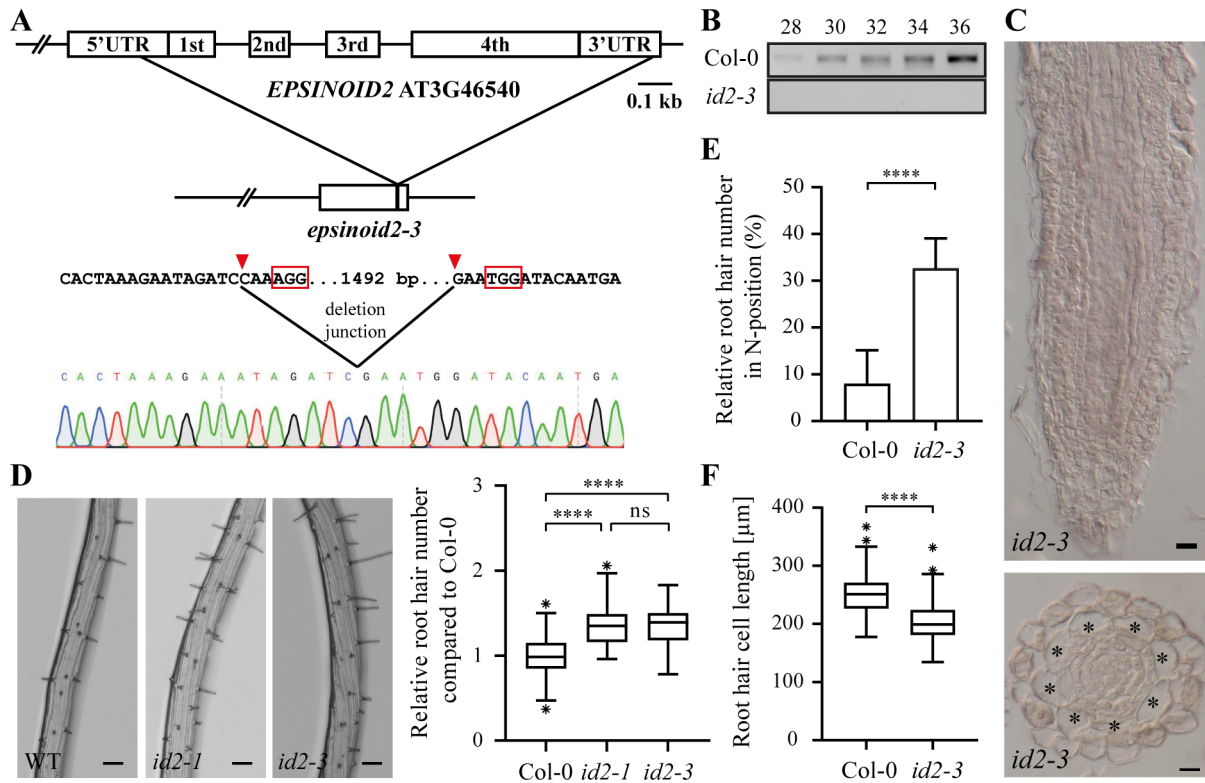
Figure 10: *EPSINOID2* **full deletion causes an increased root hair density.**

(A) Schematic view shows the *EPSINOID2* gene and its full deletion including 64 bp of its 5'UTR and 223 bp of its 3'UTR in the *id2-3* mutant. Red rectangles mark the PAM sequence and red arrows the cutting site of Cas9. (B) Semiquantitative RT-PCR confirmed *id2-3* to be a knock-out. (C) In 5-day-old *Arabidopsis* seedlings, in situ RNA hybridization of *EPSINOID2* mRNA verified the *id2-3* deletion mutant as a knock-out. Additionally, transverse section of the root showed a normal number of cortical cells (marked with asterisks) suggesting *id2-3* mutation does not disrupt the overall cellular organization of the primary root. (D-E) Three independent experiments were performed with 7-day-old *Arabidopsis* seedlings. Asterisks in boxplots indicate outliers and asterisks above brackets significance level. (D) *id2-3* as well as *id2-1* showed approximately 35 % more root hairs than Col-0 (71 < n < 88). Root hair density was determined in a 2 mm range 1 mm above the root tip. Images of the roots represent the analyzed section. Scale bars = 100 µm. Three independent experiments were normalized to wild type and pooled. (E) On average, Col-0 showed 8 % ectopic root hairs (N position) whereas *id2-3* exhibited 33 %. In three independent experiments, ten hairs were checked for their position relative to the underlying cortical cells in ten roots and summed. Experiments were pooled and percentage of hairs in N position was calculated. (F) Root hair cells in *id2-3* seedlings were approximately 19 % shorter (mean = 203 µm) than in wild type (mean = 251 µm). Root hair cell length of ten cells was measured in ten roots pre experiment three times independently, the data were then pooled.

3.4 EPSINOID2 appears to be targeted by miRNA844-3p

The non-hair cell-specific expression pattern of *EPSINOID2* and the hairy mutant phenotype indicate a potential role as a negative regulator in root hair formation. To address this question, an overexpression line with untagged *EPSINOID2* under the 2x35S-Ω promoter from previous

work was analyzed. Additionally, a stable transgenic line overexpressing GFP-tagged *EPSINOID2* under the 35S promoter was generated. Surprisingly, all lines overexpressing *EPSINOID2* phenocopied the hairy mutant phenotype (Figure 11A) and in GFP-tagged lines, a signal could not be detected except for occasionally in lateral root cap cells (Figure 11D). In previous work, semiquantitative RT-PCR of *35S::ID2* revealed higher mRNA levels in overexpressing lines (Figure 2), suggesting an actual overexpression of *EPSINOID2* which indicates that the overexpression phenotype is not a result of transgene-mediated co-suppression at transcript level (Napoli et al. 1990; van der Krol et al. 1990; Larkin et al. 1994). It could have been possible that the 2x35S-Ω promoter might have been too strong. Therefore, a stable transgenic line expressing *ID2-GFP* under the weaker UBI10 promoter was analyzed which, however, also did not show a signal (Figure 11D).

It was hypothesized that overexpression of *EPSINOID2* could also lead to post-transcriptional or -translational down regulation, such as inhibition of mRNA translation by microRNA (miRNA) or ubiquitination and degradation (Guerra et al. 2015), thus affecting protein abundance. MiRNAs can repress gene expression by binding complementary target mRNA which promotes their cleavage (slicing) or inhibits their translation. In line with this hypothesis, literature research revealed a study that identified miRNA844-3p with the sequence UUAUAAGCCAUCUUACUAGUU targeting *EPSINOID2* in its 3rd exon (Rajagopalan et al. 2006). Additional reports of *EPSINOID2* upregulation in several miRNA biogenesis mutants support a potential miRNA-based regulation (described in detail in section 1.5). To investigate this, miRNA-resistant versions of the genomic and coding sequence were generated by introducing silent mutations into the miRNA target site (Figure 11B).

The coding sequence of miRNA-resistant *EPSINOID2* was either GFP-tagged (*35S::ID2-miR^R-GFP*) combined with the 2x35SΩ or untagged with the 35S promoter (*35S::ID2-miR^R*), respectively. These constructs were introduced into wild type. Overexpression of miRNA-resistant *EPSINOID2* in Col-0 background showed a strong ubiquitous signal (Figure 11D), which was initially expected in the normal overexpression line, indicating a miRNA844-3p dependent regulation of *EPSINOID2*. This is also supported by analyses of the root hair density of the tagged and untagged miRNA-resistant overexpression lines showing significantly fewer root hairs than *id2-1* and even 22 % (*35S::ID2-miR^R-GFP* #5.2) and 37 % (*35S::ID2-miR^R* ##2.1 & 3.8) fewer than the wild type, respectively (Figure 11C). These results suggest that *EPSINOID2* is a target of miRNA844-3p.

To further corroborate miRNA844-3p regulation of *EPSINOID2*, a Short Tandem Target Mimic (STTM) construct was created (Figure 11E). STTM is a technique to inhibit a specific

mature miRNA activity, in our case miRNA844-3p, without altering the state of the additional miRNA generated from the endogenous pri-miRNA duplex (here: miRNA844-5p) (Yan et al. 2012). This construct consists of two partially complementary miRNA target sites linked by a 48 nt spacer and both contain three additional nucleotides (CTT) corresponding to positions 10 and 11 from 5' end of the mature miRNA, so that a bulge can be formed (Tang et al. 2012). The target mimicry can bind to the miRNA844-3p but it will not be cleaved, therefore inhibiting the miRNA844-3p activity (Yan et al. 2012). This construct was introduced into wild type and root hair density was analyzed. Two independent *35S::STTM844* lines #2.1 and #3.1 showed 24 % and 14 % fewer hairs than Col-0, respectively, a slight but significantly decrease in root hair density, similar to the results with the miRNA-resistant constructs (Figure 11F). This supports a regulation of *EPSINOID2* by miRNA844-3p and indicates that *EPSINOID2* negatively regulates root hair formation.

Semiquantitative RT-PCR showed an increased *EPSINOID2* transcript level in *ID2::ID2-GFP* and *35S::ID2-GFP* compared to Col-0 which was even higher in the miRNA-resistant overexpression line suggesting that *EPSINOID2* is indeed overexpressed in all three lines (Figure 11G). However, on protein level ID2-GFP could not be detected in *35S::ID2-GFP* in a western blot, neither with a generated EPSINOID2 antibody nor with a commercial GFP antibody, in line with the absent GFP signal (Figure 11H). In contrast, two independent *ID2::ID2-GFP* lines (#6.3 and #12.3) showed higher levels of ID2 protein which is concurrent with the intensity of the GFP signals observed in each line where #6.3 was weaker than #12.3 (not shown). These results also confirm that the generated EPSINOID2 antibody is working to detect ID2-GFP. Furthermore, *35S::ID2-miR^R-GFP* showed the highest protein level of ID2-GFP (Figure 11G and H). This indicates that *EPSINOID2* could be targeted by miRNA844-3p by translational inhibition. Additionally, in *35S::STTM844* #2.1 a weak upregulation of *EPSINOID2* was detected on mRNA level as well as at the protein level (Figure 11G and H). This further supports a regulation of *EPSINOID2* by miRNA844-3p which seems to be partly prevented by the *STTM844* construct. Upregulated *EPSINOID2* on transcript and protein level together with the decreased root hair density in *35S::ID2-miR^R/-GFP* and *35S::STTM844*, in which miRNA844-3p supposedly cannot act on *EPSINOID2* or is sequestered, respectively, indicates that *EPSINOID2* indeed negatively regulates root hair formation. It remains to be said that endogenous EPSINOID2 could not be detected in wild type, likely because of its low endogenous expression level or high turnover.
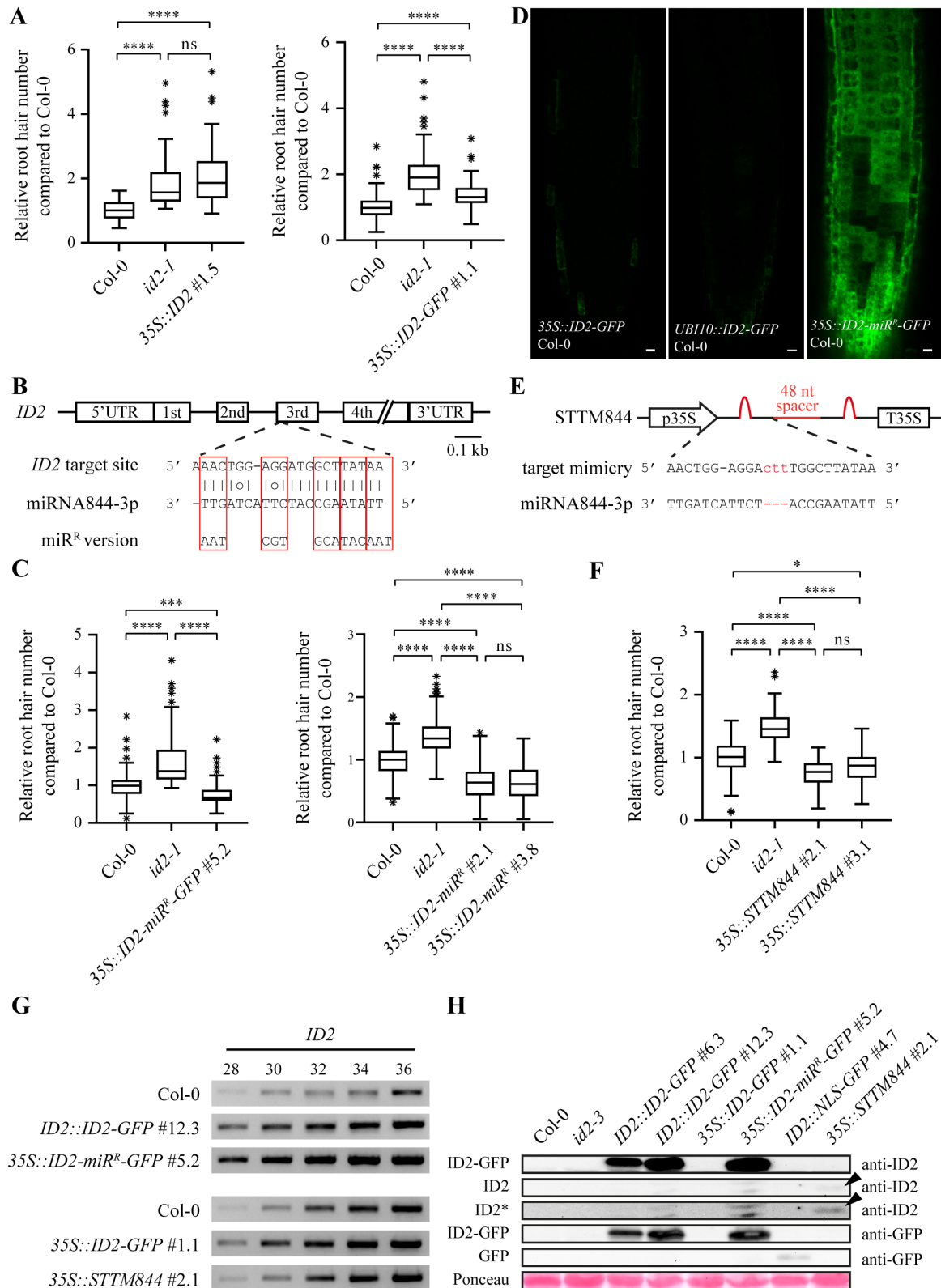
Figure 11: *EPSINOID2* is likely a target of miRNA844-3p.

(A, D, F) Root hair density in a 2 mm range 1 mm above the root tip in 7-day-old *Arabidopsis* seedlings. Three independent experiments were normalized to wild type and pooled. Asterisks in boxplots: outliers. Asterisks above brackets: significance level. (A) Both overexpression lines expressing *EPSINOID2* under 2x35S-Ω (58 < n < 76) and GFP-tagged *EPSINOID2* under 35S promoter (96 < n < 135) phenocopied the hairy *id2-1* mutant phenotype. (B) Schematic view shows target site of miRNA844-3p at the end of the second exon of *EPSINOID2*. Silent

mutations were introduced into that sequence to prevent miRNA844-3p regulation. (C) Untagged (59 < n < 161) and GFP-tagged (95 < n < 105) miRNA-resistant overexpression of *EPSINOID2* led to decreased root hair density compared to *id2-1* mutant and even Col-0 suggesting a regulation of *EPSINOID2* by miRNA844-3p. (D) Overexpression of *EPSINOID2* under a strong (35S) and weaker (UBI10) promoter did not show a GFP signal in 5-day-old seedling roots, only slightly in lateral root cap cells which is in line with the hairy mutant phenotype. Overexpression of miRNA-resistant *ID2-miR^R-GFP* showed a ubiquitous signal in almost all cells supporting the hypothesis of *EPSINOID2* being regulated by miRNA844-3p. Scale bars = 10 μm. (E) Schematic view shows the Short Tanden Target Mimic (STTM) construct in which two copies of the partially complementary miRNA844-3p target sites contain three additional nucleotides (CTT) corresponding to positions 10 and 11 from 5' end of the mature miRNA844-3p, forming a bulge, and which are linked by a 48 nt spacer (Tang et al. 2012). The target mimicry can bind to the miRNA844-3p but it will not be cleaved, therefore inhibiting the miRNA844-3p activity. (F) Two independent lines overexpressing *STTM844* showed significantly fewer hairs than the *id2-1* mutant and wild type indicating *EPSINOID2* overexpression as a result of sequestered miRN844-3p leads to a decreased root hair density (68 < n < 139). (G) RNA was extracted from 5-day-old *Arabidopsis* seedling roots, except for *35S::ID2-GFP #1.1* where whole seedlings were used. Semiquantitative RT-PCR confirmed the overexpression of *EPSINOID2* on mRNA level in *ID2::ID2-GFP* and *35S::ID2-GFP* and an even stronger one in the miRNA-resistant overexpression line. Additionally, a slight overexpression of *EPSINOID2* was detected in *35S::STTM844* which is in line with the results from the root hair analyses. (H) Proteins were extracted from 5-day-old *Arabidopsis* seedlings. Western blots showed a higher level of ID2-GFP in *ID2::ID2-GFP* and *35S::ID2-miR^R-GFP* as well as of ID2 in *35S::STTM844* whereas no signal could be detected in *35S::ID2-GFP*. Endogenous ID2 appears to be undetectable. Protein sizes: ID2-GFP: 63 kDa, ID2: 35 kDa, GFP: 27 kDa. Detection of ID2 and ID2-GFP with the generated EPSINOID2 antibody and a commercial GFP antibody. ID2* shows the same blot area as ID2 with an increased intensity for better visualization of the weak band in *35S::STTM844* indicated by black arrows. Ponceau represents a loading control.

To gain more insight into miRNA844 expression and activity, several approaches were applied. First, the *MIR844* (AT2G23347) gene was cut out of the Col-0 genome using the CRISPR/Cas9 system as described for *id2-3*. Two sgRNAs were selected, one binding four bases upstream of *MIR844* and the other 35 bp from the 5' end, so that almost the complete *MIR844* gene was deleted which was confirmed by sequencing (Figure 12A). Semiquantitative RT-PCR showed a slight increase of *EPSINOID2* transcript level in *mir844* compared to wild type (Figure 12B). Overall, the *mir844* mutant did not show any obvious phenotypic differences to wild type. It was expected that loss of *MIR844* would give a decreased root hair density compared to Col-0. Surprisingly, *mir844* exhibited around 21 % more root hairs than wild type but fewer than *id2-1* (76 %) (Figure 12C).

Overexpression of miRNA844 has been addressed before which did not show any obvious phenotypic variation from wild type (Lee et al. 2015). However, it was not clear if analysis of root hair density was included in this study. Therefore, homozygous lines overexpressing

MIR844 under a 35S promoter were established and root hair density was analyzed. Two independent overexpression lines did not show a significant difference in number of root hairs with a range of on average 9 % fewer hairs in line #7.3 and 9 % more hairs in line #10.4. compared to Col-0 (Figure 12D). These results contradict former observations where interfering with miRNA844-3p activity led to *EPSINOID2* upregulation and decreased root hair density. However, *MIR844* deletion and overexpression affects the full *MIR844* gene which also codes for a second mature miRNA844-5p (UGGUAAGAUUGCUUAUAAGCU) (Fahlgren et al. 2007). This could explain the presented root hair phenotypes since both mature miRNAs could have more targets affecting directly or indirectly root hair density.

To find out where *MIR844* is expressed, two different transcriptional reporter lines, *MIR844::ER-GFP* and *MIR844::GUS*, were created but both lines did not show any detectable signal (not shown). Expression levels of *MIR844* could be too low to detect. In the study that identified the new miRNA844 by high-throughput pyrosequencing, miRNA844-3p was represented with only 8 reads and miRNA844-5p with 5 reads, which was very low compared to an already known and well-studied miRNA165a with 514 reads which is detectable with a transcriptional reporter line (Rajagopalan et al. 2006; Carlsbecker et al. 2010).

To study miRNA844-3p activity, a sensor construct was designed in which the 3'UTR of a nuclear-localized GFP contained the *EPSINOID2* target sequence of miRNA844-3p expressed under the 35S promoter. An additional construct was created in which the altered target sequence of *ID2-miR^R* constructs was introduced. Initial analyses of several stable transformants did not give a conclusive result. Three independent lines of the *35S:.NLS-GFP-miR844-sensor* (## 1.1, 5.5 and 8.2) displayed differing signal intensities under the same growing and imaging conditions (Figure 12E). Whereas line #5.5 showed a quite strong signal in almost all cells, the signal in line #8.2 was very weak but restricted to nuclei and in line #1.1 completely absent. However, in the stronger sensor line #5.5 the signal intensity variation was very high and on average slightly higher than in *35S:.NLS-GFP-miR844^R-sensor* #2.8 (Figure 12E). Assuming a very low *MIR844* expression and considering a very strong 35S promoter activity, only small changes in GFP signal are not surprising and might even be undetectable. However, in sensor line #1.1 it appears that this might be a result of transgene-mediated silencing which is not unusual for 35S promoter constructs. Nevertheless, only five seedlings per construct were analyzed, making a final assessment impossible at this point.
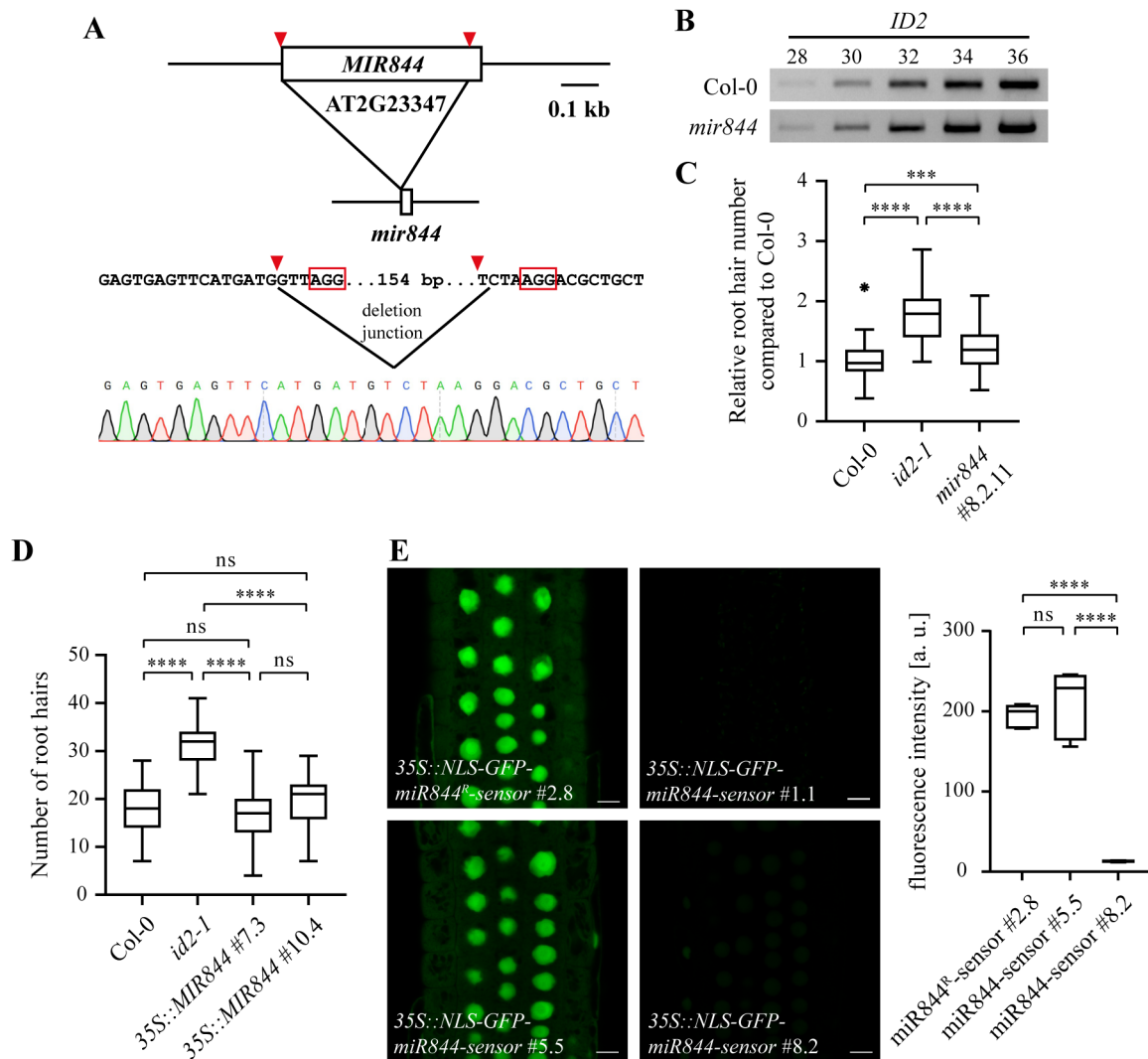
Figure 12: Changes in miRNA844 expression and activity give inconclusive results.
(A) Schematic view shows the *MIR844* gene and its full deletion in the *mir844* mutant. Red rectangles mark the PAM sequence and red arrows the cutting site of Cas9. (B) Semiquantitative RT-PCR showed an accumulation of *EPSINOID2* mRNA in roots of *mir844* mutant seedlings. (C + D) Root hair density of 7-day-old *Arabidopsis* seedlings was obtained as described before. Asterisks in boxplots indicate outliers and asterisks above brackets significance level. (C) On average, *mir844* mutants exhibited an increased root hair density of 21 % compared to wild type but lower than *id2-1* mutant which displayed 76 % more root hairs than Col-0 (81 < n < 93). Three independent experiments were normalized to wild type and pooled. (D) Two independent stable *35S::MIR844* overexpression lines did not show as significant difference in root hair density compared to wild type (25 < n < 37). (E) 5-day-old seedlings expressing *NLS-GFP-miR844-sensor* under the 35S promoter in three independent transgenic lines show differing GFP signal intensities. However, the stronger signal in line #5.5 appears to be very variable with no difference in fluorescence intensity compared to the miR844^R-sensor. Scale bars = 10 μm.

3.5 *EPSINOID2* promoter appears to be active in both H and N root epidermis cells

To confirm the expression pattern driven by the endogenous *EPSINOID2* promoter, a transcriptional reporter line *ID2::NLS-GFP* was generated. Contrary to the signal of the

translational reporter line *ID2::ID2-GFP*, which shows a specific signal in N cells of the root epidermis, the promoter of *EPSINOID2* appears to be active in both N and H cell files (Figure 13A). These findings indicate a possible post-transcriptional or -translational regulation which could occur at different levels. In situ RNA hybridization revealed a staining in all epidermal cells in the meristematic and transition to elongation zone indicating *EPSINOID2* mRNA presence in both cell types which suggests that *EPSINOID2* mRNA is neither degraded in H cells and nor moves from H to N cells (Figure 13B). Thus, it is more likely that *EPSINOID2* is affected at another level. Together with the results of the miRNA-resistant lines, there could be three different possible scenarios: i) miRNA844-3p prevents *EPSINOID2* translation in H cells, ii) EPSINOID2 protein moves from H cells to N cells or iii) EPSINOID2 protein is immediately degraded in H cells.
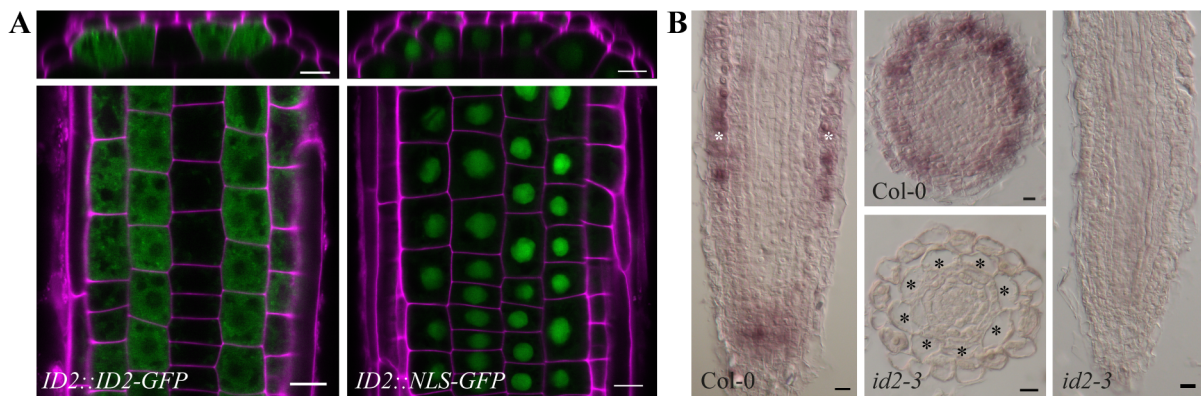
Figure 13: Promoter activity and *EPSINOID2* mRNA differ from ID2-GFP protein localization.
(A) *NLS-GFP* expressed under *EPSINOID2* endogenous promoter revealed that promoter activity is ubiquitous in root epidermal cells whereas the ID2-GFP signal was detected specifically in non-hair cell files. Cell walls were stained with propidium iodide. Scale bars = 10 μm. (B) In situ RNA hybridization showed staining of *EPSINOID2* mRNA in epidermal root cell (indicated by white asterisks in longitudinal section) which is in both hair and non-hair cells detectable in wild type and absent in the *id2-3* mutant (visualized in transverse section; Col-0 transverse section was skewed to adjust for compression artifacts). This indicates that *EPSINOID2* mRNA is not degraded or moving from hair cells. Scale bars = 10 μm.

To address these three hypotheses, several approaches were applied. To check whether miRNA844-3p acts on *EPSINOID2* in H cells, a mNeon-tagged miRNA-resistant genomic version of *EPSINOID2* expressed under its endogenous promoter was introduced into wild type. The results of three independent stably transformed lines are inconclusive showing in some cases ID2-miR[R]-Neon signal in a striped pattern in non-hair cell files as the non-resistant version but also in other cases very scattered with signal in both cell types (Figure 14A). This rather indicates that miRNA844-3p might not be responsible for downregulation of *EPSINOID2* in H cells, only in N cells.

To gain insight whether EPSINOID2 protein moves between cells, genomic *EPSINOID2* expressed under its endogenous promoter was tagged with 3xGFP and introduced into wild type. To get an initial idea, two independent segregating T_2 lines #2 and #3 were analyzed. Both lines show differing signal intensities which was also the case for the *ID2::ID2-GFP* lines #6.3 and #12.3 as mentioned before. But more importantly GFP signal appears to be present not only in non-hair cells but additionally in some hair cells where ID2-GFP also localized to the cell plate as shown for the ID2-GFP subcellular localization in the *ID2::ID2-GFP* line (Figure 14B). These results do neither confirm nor disprove a possible movement of the EPSINOID2 protein. Further analyses are required, as these studies were carried out towards the end of the project. The third question of a possible degradation of EPSINOID2 was addressed by treatments of 5-day-old seedlings of the *ID2::ID2-GFP* line with proteasomal inhibitor MG132 and protein synthesis inhibitor cycloheximide (CHX), both in combination and DMSO as a control. Treatments with MG132 caused a mean 72 % increase of ID2-GFP signal compared to the DMSO control whereas CHX led to an averaged 11 % decrease (Figure 14C). The CHX treatment appears to not have worked properly since it did not cause a significant decrease of ID2-GFP signal. However, it still seemed to have a little effect which is supported by the results of the combined treatment in which the signal was 23 % higher than in the control but weaker than in the MG132 treated samples. This indicates that MG132 treatment does indeed affect proteasomal degradation of EPSINOID2 and that CHX treatment did not completely disable protein synthesis probably due to weak activity. Additionally, either applied CHX concentration or MG132 treatment duration might have been not sufficient to reach their full potential. Nevertheless, these results indicate proteasomal degradation of EPSINOID2 affecting its protein abundance. However, EPSINOID2 protein degradation is most likely not the cause for the differences in *EPSINOID2* mRNA and protein presence in the root epidermis since MG132 treated roots did not show a changed pattern of ID2-GFP which was still in N cells but not in H cells. There is further evidence that EPSINOID2 is targeted for proteasomal degradation: Analysis of the EPSINOID2 protein sequence using the eukaryotic linear motif (ELM) prediction tool revealed a so-called KEN box motif (.KEN.) in its C-terminus at amino acid position 253-257 (MKENM). Additionally, this motif appears to be conserved in many EPSINOID2 homologs of other plant species (Figure 14D). The KEN sequence has been shown to be recognized by the CDH1 subunit of the APC/C E3 ubiquitin ligase complex leading to target ubiquitination and subsequent proteasome-dependent degradation (Pfleger and Kirschner 2000). These findings support a potential proteasomal degradation of EPSINOID2.
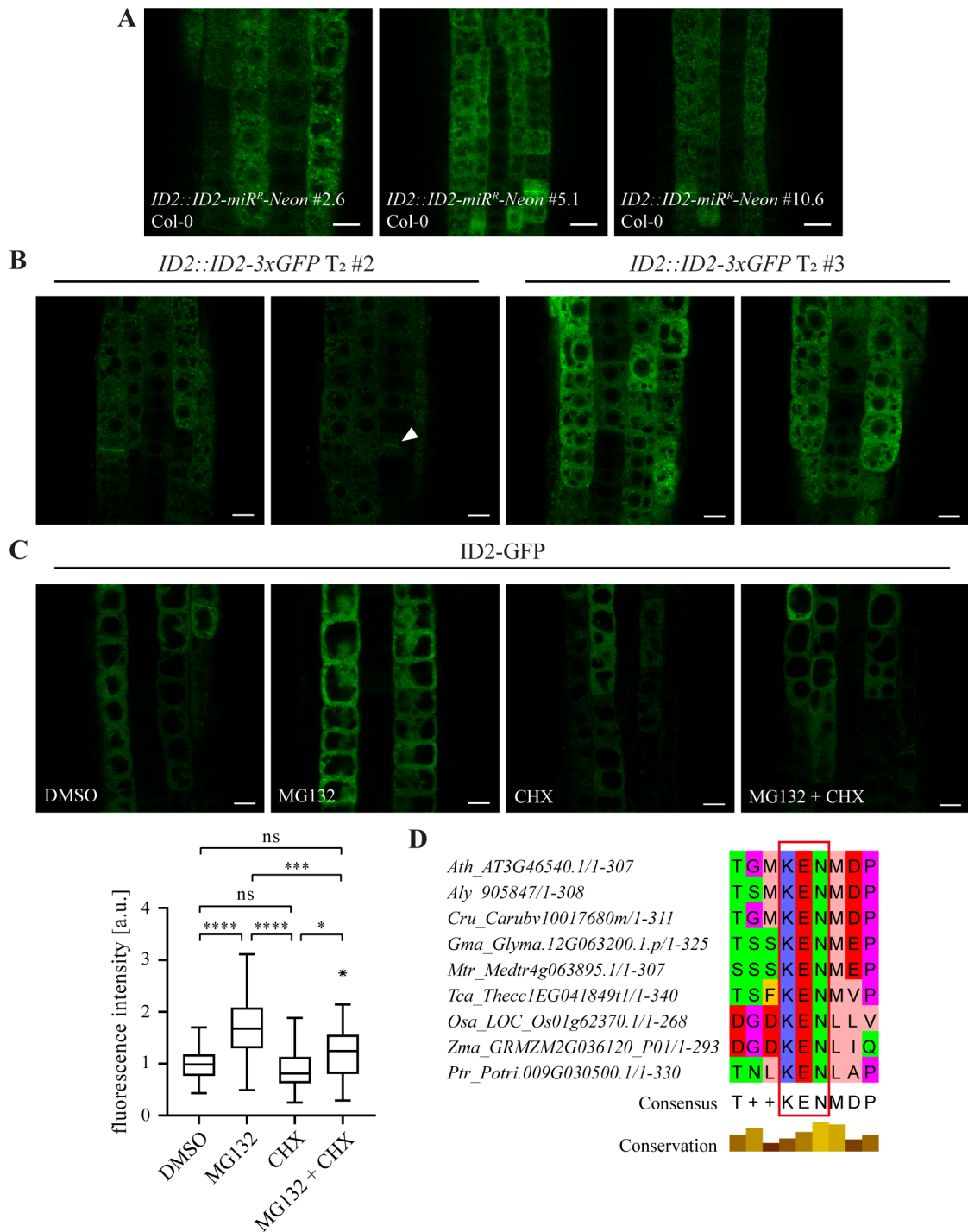
Figure 14: Possible mechanisms of *EPSINOID2* post-transcriptional regulation.

(A-C) 5-day-old *Arabidopsis* seedling roots were analyzed. Scale bars = 10 μm (A) Three independent *ID2::ID2-miR^R-Neon* lines showed slightly differing expression patterns in the meristematic zone of the root with some weak signal in H cells in #2.6 and even weaker in #5.1 which does not allow a final conclusion about regulation of *EPSINOID2* in H cells by miRNA844-3p. (B) Two independent still segregating T₂ lines of *ID2::ID2-3xGFP* exhibit differences in signal intensity. Both lines do not show a clear striped pattern but also weak to moderate signal in H cells. Note the specific ID2-3xGFP signal localized to the growing cell plate in an H cell (indicated by an arrow). This points towards a possible protein movement of EPSINOID2. (C) *ID2::ID2-GFP* seedlings were treated with 50 μM MG132 and 100 μM CHX for 3 h and for each treatment 7-11 roots were analyzed. Three independent experiments were performed. Fluorescence intensity was measured using ImageJ. Mean intensities

were normalized to DMSO control, pooled, and statistically tested for significance (n = 33-34). Results are displayed in a Tukey box plot. Asterisks above box indicates outlier. Asterisks above bars indicate significance level. MG132 treatment results in a mean 73 % higher signal intensity compared to the DMSO control. CHX showed on average 11 % less fluorescence intensity whereas roots treated with both MG132 and CHX exhibit 23 % higher signal intensity than the control but less than the MG132 treated roots indicating a potential regulation of EPSINOID2 protein by proteasomal degradation. (D) Nine protein sequences that were used for phylogenetic analyses in Zouhar and Sauer (2014) were analyzed in a multiple sequence alignment using Muscle with JalView. KEN box motif could be found in all analyzed EPSINOID2 homologs. First three letters represent species followed by the EPSINOID2 homolog locus and length of the sequence. Zappo color scheme from JalView was used which colors the amino acids according to their physicochemical properties.

3.6 *EPSINOID2* appears to be a haploinsufficient gene

In preliminary work, it was already shown that the knock-out mutant *id2-1* showed a similar increase in root hair density in its heterozygous state as in the homozygous one which suggests a dominant mutation whereas the knock-down mutant *id2-2* exhibited an intermediate root hair density between wild type and homozygous *id2-2* indicating a semi-dominant mutation, in line with the fact that *id2-2* is not a complete null allele (Figure 15A) (Freimuth 2019).

In this work, the full deletion mutant *id2-3* was also analyzed in its heterozygous state to confirm former observations. Homozygous *id2-3* was crossed with Col-0 and root hair densities were analyzed in three independent experiments. Heterozygous *id2-3* exhibited 56 % more root hairs than wild type similar to the homozygous *id2-3* mutant with 65% more root hairs with no significant difference between both states (Figure 15B). This indeed confirms that *epsinoid2* knock-out mutation is a dominant mutation and indicates that *EPSINOID2* is a haploinsufficient gene. Additionally, this suggests that EPSINOID2 protein abundance might be important for its correct function.
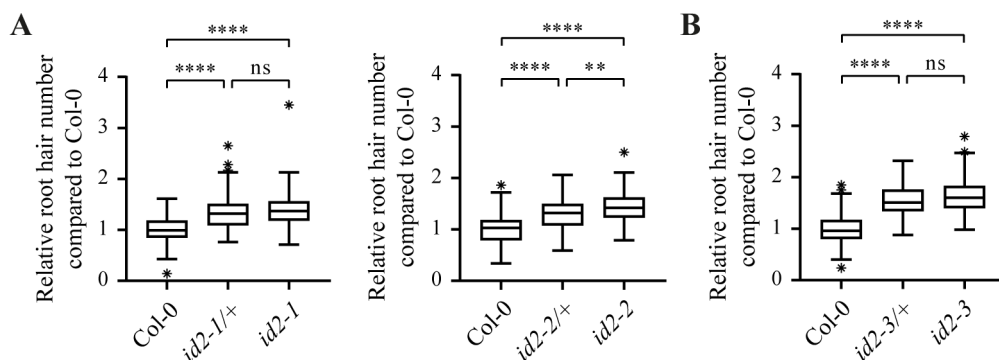
Figure 15: Root hair densities in different *epsinoid2* mutants in homo- or heterozygous states.
Root hair analyses of three (*id2-2* and *id2-3*) and four (*id2-1*) independent experiments, normalized to Col-0 and pooled. Asterisks above boxes indicate outliers and asterisks above brackets significance level. (A) Root hair

analyses obtained in previous studies (Freimuth 2019). Heterozygous *id2-1* showed no difference in root hair density (on average 33 % more than Col-0) to homozygous *id2-1* (34 %) indicating a dominant mutation (152 < n < 160) whereas heterozygous *id2-2* showed on average 31 % more root hairs than wild type but fewer than the homozygous *id2-2* (45 % more than Col-0) suggesting a semi-dominant mutation (132 < n < 137). (B) Heterozygous *id2-3* exhibited a similar root hair density (on average 56 % more than wild type) as homozygous *id2-3* (65 %) with no significant difference indicating a dominant mutation (74 < n < 129).

3.7 MiRNA-resistant *EPSINOID2* partially rescues the mutant root hair phenotype

In preliminary work, several attempts were made to rescue the hairy mutant phenotype of *id2-1*. The old *ID2::ID2-Δ41-GFP* and *ID2::ID2-Δ41* were introduced into *id2-1* but both showed an increased root hair density with no difference to *id2-1* (Freimuth 2019). At that point it was not revealed that 41 amino acids of the C-terminus were missing. Nevertheless, even the construct with full untagged *EPSINOID2* sequence including its 3'UTR did not rescue the hairy phenotype either (Freimuth 2019). Therefore, all complementation lines generated so far were not functional or downregulated by unknown mechanisms.

In this work, we took another approach using a stably transformed *ID2::ID2-miR^R* line without a tag and crossed it into the *id2-3* mutant. We chose the *id2-3* mutant to reduce the amount of T-DNA since *id2-1* also carried the SALK T-DNA ruling out a possible negative effect by that T-DNA. Additionally, we used the miRNA-resistant version since this seemed to influence root hair density in overexpression lines implying a certain functionality of the introduced construct which was also strengthened by choosing the untagged version. Initial results showed that this construct can partially rescue the hairy phenotype. *ID2::ID2-miR^R id2-3* exhibited only a 20 % increased root hair density compared to wild type whereas *id2-3* showed 50 % more root hairs (Figure 16). This is still not a full complementation. Complications with former rescue lines and the new attempt showing only a partial rescue is in line with all obtained results so far that *EPSINOID2* is regulated on different levels and protein abundance seems to be crucial for its function. This could be the reason why a full complementation could not be established so far.
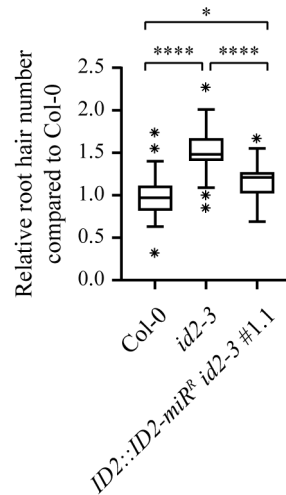
Figure 16: Root hair analyses of miRNA-resistant *EPSINOID2* complementation line.
Root hair analyses of 7-day-old seedlings were performed twice. Experiments were normalized to Col-0, pooled, statistically analyzed and visualized in a Tukey boxplot (31 < n < 65). *ID2::ID2-miR^R id2-3* partially rescues the *id2-3* hairy mutant phenotype showing only 20 % more hairs than wild type whereas *id2-3* displays 50 % more hairs than Col-0.

3.8 *EPSINOID2* is not involved in hair/non-hair cell fate decisions in the root epidermis

Given the specific expression pattern and the hairy mutant phenotype, the potential role of *EPSINOID2* in the molecular framework of hair/non-hair cell fate in the root epidermis was investigated. Epidermal cell fate is determined by a differential position-dependent coordinated expression of several genes in meristematic cells: WER together with the central transcription complex consisting of GL3/ EGL3/MYC1 and TTG1 activates GL2 promoting non-hair cell fate whereas hair cell fate is determined by CPC which interferes with WER binding to the GL3/EGL3/MYC1-TTG1 complex in hair cells. SCM mediates positional signaling for accumulation of the central transcription complex in non-hair cells (reviewed in Grierson et al. 2014). To determine at which point of this complex regulatory protein network *EPSINOID2* might play a role, several approaches were initiated.

To find out if the epidermal patterning is altered in the *id2-1* mutant, crosses of *id2-1* with several established cell fate markers were generated. Localization of the translational reporter *SCM::SCM-GFP* (Kwak and Schiefelbein 2008), *WER::WER-GFP* (Ryu et al. 2005), *CPC::CPC-Neon* (generated according to Wada et al. 2002) and *GL3::GL3-YFP* (Bernhardt et al. 2005) and expression pattern of the transcriptional reporters *WER::GFP* (Lee and Schiefelbein 1999), *MYC1::GFP* (Bruex et al. 2012) and *GL2::GFP* (Lin and Schiefelbein 2001) were analyzed in 5-day-old *Arabidopsis* seedlings (Figure 17A-G). To determine if the transcriptional marker is ectopically expressed, seedlings were also stained with propidium

iodide and Z stacks were taken and processed to generate a side view (similar to a partial transverse section). To identify possible genetic interactions between *EPSINOID2* and epidermal cell fate factors, *id2-1* was crossed with *scm-2* (Kwak et al. 2005), *wer-1* (Lee and Schiefelbein 1999), *cpc* (Sessions et al. 2002), *gl3* (Woody et al. 2007), *gl3-1 egl3-1* (Bernhardt et al. 2003), *myc1-1* (Alonso et al. 2003) and *gl2-3* (Alonso et al. 2003) and root hair densities were determined in 7-day-old seedlings (Table 4 and Figure 18A-F). To assess whether *EPSINOID2* is a downstream component of described cell fate determinants, *ID2::ID2-GFP* expression pattern was analyzed in root hair mutant backgrounds (Figure 19A-G).

The LRR-RLK SCM is an early factor in epidermal cell fate, which is required for position-dependent epidermal cell-type patterning by acting differentially on the downstream transcription factor network in H and N cells (Kwak et al. 2005; Kwak and Schiefelbein 2008). SCM-GFP accumulates at the plasma membrane in both H and N cells in the meristematic zone of the root epidermis in wild-type seedlings (Kwak and Schiefelbein 2008), which is not altered in *id2-1* mutant background (Figure 17A). The *id2-1* mutant showed approximately the same mean root hair number as the *scm-2* mutant and as well as the double mutant *id2-1 scm-2* with no significant difference (Table 4 and Figure 18B). According to Kwak et al. 2005, *scm-1* does not show an increased root hair density compared to wild type but altered distribution of N and H cells. The latter characterization also applies for *scm-2* but there is no report about root hair density. However, *scm-2* was reported to be a knock-out whereas *scm-1* only showed reduced mRNA which could explain differences in root hair density. Since there were no differences in root hair densities in both *id2-1* and *scm-2* single mutants as well as in the double mutant, it is not clear whether there is a genetic interaction between *EPSINOID2* and *SCM* as there is no additivity or suppression of both phenotypes and epistasis cannot be ruled out. However, *SCM* expression appears to be unaffected of EPSINOID2 absence indicating EPSINOID2 has no impact on SCM function. It is more likely that *EPSINOID2* is acting downstream of this early cell fate factor which is supported by the expression pattern of *ID2-GFP* in *scm-2* mutant background. The signal of ID2-GFP appeared to be disordered in *scm-2* (Figure 19A). It seems that the usual expression pattern of *ID2-GFP* in N cell files is disrupted in some cells in a random manner. This might be due to the altered distribution of N and H cells in *scm-2* mutants where *ID2-GFP* would be expressed in ectopic N cells due to a changed position-independent cell type organization. In fact, this altered seemingly random signal distribution resembles the GFP activity of *WER::GFP* in *scm-2* which is also expressed in N cells (Kwak et al. 2005). Together with the non-altered localization of SCM-GFP in *id2-1* background and the unchanged phenotype of *id2-1 scm-2* mutant, this indicates that *EPSINOID2* is acting downstream of *SCM*.

Directly downstream of SCM is the R2R3-type MYB transcription factor WER which is repressed by SCM in H cells and an early non-hair cell fate determinant upstream of the other cell fate factors (Lee and Schiefelbein 1999; Ryu et al. 2005; Kwak and Schiefelbein 2008). *WER::GFP* and *WER::WER-GFP* are both expressed in N cells in the meristematic root epidermis with the difference that *WER::WER-GFP* shows a GFP signal in the nucleus (Lee and Schiefelbein 1999; Ryu et al. 2005). This pattern was not disturbed in *id2-1* mutant background indicating that *EPSINOID2* is not required for correct *WER* expression (Figure 17C and E). The double mutant *id2-1 wer-1* showed no significant difference in root hair density to the *wer-1* single mutant but a significantly higher root hair density than *id2-1* mutant (Table 4 and Figure 18C). These results suggest that *WER* is required for non-hair fate in wild type as well as in *id2-1* mutants. A signal of ID2-GFP in *wer-1* mutant background was almost undetectable. In *wer-1* mutants, hair cells are mis-specified and most epidermal cell identities are changed into H cell (Lee and Schiefelbein 1999), which would explain the lacking *ID2-GFP* expression (Figure 19B). These results point towards *EPSINOID2* being a downstream component of *WER*.

The hair fate specifying R3-type MYB transcription factor CPC is induced by WER in N cells, moves to H cells where in turn it negatively regulates *WER* expression and outcompetes WER binding to the central transcription complex GL3/EGL3/MYC1-TTG1 thereby promoting hair fate (Lee and Schiefelbein 2002; Wada et al. 2002). In our generated stable transgenic *CPC::CPC-Neon* line in Col-0 background, fluorescence could be detected in the nuclei of all epidermal cells in the meristematic zone of the root as reported by Wada et al. (2002). This signal was not changed in *id2-1* mutant background (Figure 17B) suggesting *EPSINOID2* does not affect *CPC* expression. For the *id2-1 cpc* double mutant, a SAIL T-DNA insertion line was used for which a root hair phenotype has not been published before. However, a decreased root hair density was reported for other *cpc* single mutants (Wada et al. 1997). The *id2-1 cpc* double mutant showed no significant difference in root hair number to the *cpc* single mutant which displayed a decreased root hair density compared to wild type and of course compared to the hairy *id2-1* mutant (Table 4 and Figure 18D). This suggests that *CPC* is essential for hair fate in both wild type and *id2-1* mutants. *CPC* is required to promote hair cell fate and in *cpc* mutants almost all epidermal cells are converted into non-hair cells (Wada et al. 2002). *ID2-GFP* expression in *cpc* mutant background revealed GFP accumulation in all epidermal cells regardless of the position to the underlying cortical cell (Figure 19C). Supported by the results of unaltered *CPC* expression in *id2-1* background and decreased root hair density in *id2-1 cpc* double mutant, this indicates that *EPSINOID2* is acting downstream of *CPC*.

The two homologous bHLH transcription factors GL3 and EGL3 are partially redundant as part of the central transcription complex regulating non-hair cell specification (Bernhardt et al. 2003). GL3-YFP predominantly accumulates in nuclei of N cells in the meristematic zone of the root epidermis in wild type (Bernhardt et al. 2005). It did not show a different localization in *id2-1* mutants (Figure 17D) indicating that *EPSINOID2* does not influence GL3 localization. The *gl3* single mutant had slightly but significantly fewer root hairs than the *id2-1* single mutant. The *id2-1 gl3* double mutant, however, resembled the *gl3* single mutant and showed a significantly decreased root hair density compared to *id2-1* (Table 4 and Figure 18E). The *gl3-1 egl3-1* double mutant and *id2-1 gl3-1 egl3-1* triple mutant exhibited very hairy roots with significantly higher densities than *id2-1* and Col-0. The *id2-1 gl3-1 egl3-1* triple mutant displayed a slight increase in root hairs compared to the *gl3-1 egl3-1* double mutant (Table 4 and Figure 18F). It was previously demonstrated that both single mutants *gl3-1* and *egl3-1* show normal root hair densities and a normal pattern of epidermal cell identities, but the *gl3-1 egl3-1* double mutant displays an increased root hair density due to a reduction of non-hair cell-type frequencies (Bernhardt et al. 2003). It must be noted that a different *gl3* single mutant (Wisconsin T-DNA insertion line) than the mutants in previous studies was used. In this works root hair analyses, *gl3* showed an increase in root hairs compared to wild type instead of a normal density as reported for *gl3-1*. It could be concluded that the Wisconsin *gl3* mutant has more root hairs due to a reduced number of non-hair cells as shown in the *gl3-1 egl3-1* double mutant, but not as severe. This is encouraged by the minor changes in *ID2-GFP* expression in *gl3* mutant background, which was slightly disrupted (Figure 19D). However, in *gl3-1 egl3-1* double mutant background, where most of the cell identities changed into H cells, the ID2-GFP signal was almost undetectable (Figure 19E). These results support the hypothesis of *EPSINOID2* acting downstream of cell specification by *GL3*.

The GL3/EGL3 homolog MYC1 is acting partly redundant to GL3 and to a lesser extent EGL3 and specifies non-hair cell fate in root epidermal cells (Bruex et al. 2012; Zhao et al. 2012). The *MYC1::GFP* reporter shows a specific expression in H cells in wild type (Bruex et al. 2012) which was also not altered in *id2-1* mutant background (Figure 17F). This suggests that *EPSINOID2* does not affect *MYC1* expression. The *id2-1 myc1-1* double mutant exhibited significantly more root hairs than *id2-1* single mutant with no significant difference to the *myc1-1* single mutant (Table 4 and Figure 18G). These results suggest that *MYC1* is needed for non-hair fate in wild type and *id2-1* mutants. The *myc1-1* mutant shows an increased root hair density due to more ectopic root hairs cells compared to wild type (Bruex et al. 2012; Zhao et al. 2012). Accordingly, the *ID2-GFP* expression pattern was slightly disrupted in *myc1-1*

(Figure 19F) resembling the pattern in *gl3*, suggesting *EPSINOID2* acts downstream of *MYC1*. The homeodomain transcription factor GL2 is acting more downstream in the cell fate network, is required for non-hair cell differentiation and regulated by the central transcription complex directed by WER and CPC (Masucci et al. 1996; Lee and Schiefelbein 2002; Wada et al. 2002). *GL2::GFP* is preferentially expressed in N cells in wild type and this pattern was not changed in *id2-1* (Figure 17G) (Lin and Schiefelbein 2001). This indicates *GL2* expression is not dependent on EPSINOID2 presence. The *id2-1 gl2-3* double mutant did not show a significant difference in root hair density to the *gl2-3* single mutant but a significantly higher root hair density than *id2-1* single mutant (Table 4 and Figure 18H). These results suggest that *GL2* is required for non-hair fate in wild type as well as in *id2-1* mutants. In *gl2-2* mutants, most of the epidermal cells form root hairs (Masucci et al. 1996). In line with the assumption that EPSINOID2 is acting downstream of cell fate players, the expression of *ID2-GFP* was very weak and scattered in *gl2-2* mutant background (Figure 19G).

Taken together, these results indicate that EPSINOID2 acts downstream of the epidermal cell fate network and is not required for epidermal patterning. More likely, it appears *EPSINOID2* expression is dependent on the N cell identity established by its components.
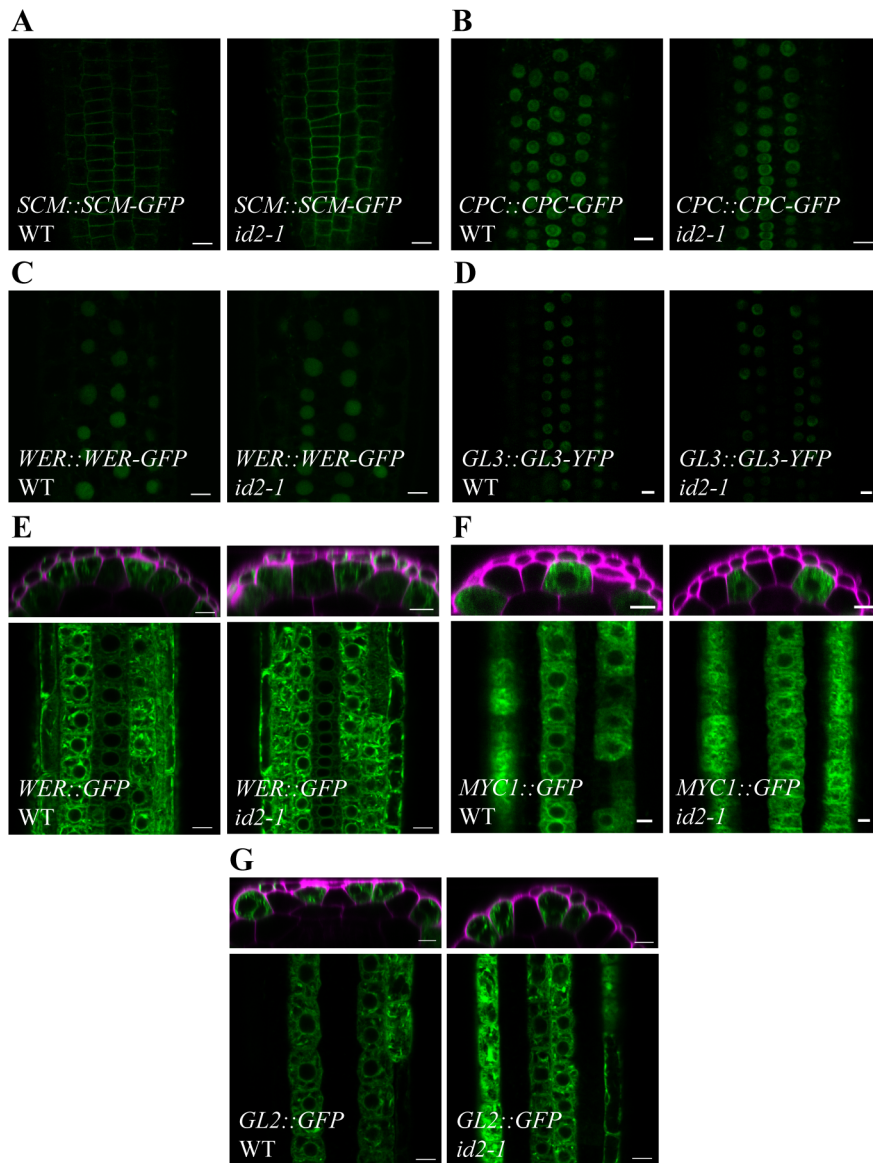
Figure 17: Expression of root epidermal marker lines is not altered in *id2-1* mutant background.

Expression patterns of translational (A-D) and transcriptional (E-G) reporter lines in 5-day-old *Arabidopsis* seedlings. Scale bars = 10 µm. (A) In wild type, SCM-GFP accumulates at the plasma membrane in both H and N cells of the root epidermis. This distribution did not change in *id2-1* mutant background. (B) The newly generated *CPC::CPC-Neon* line in wild type background showed a signal in nuclei of all epidermal cells in the meristematic zone as reported by Wada et al. (2002). This signal was not altered in *id2-1* background. (C) Wild-type GL3-YFP accumulation in N cell nuclei of meristematic epidermal root cells appears to be the same in *id2-1* mutants. (D) WER-GFP localization in nuclei of all epidermal cells in the meristematic zone of the root in Col-0 is not changed in *id2-1* mutant background. (E-G) Root cell walls were visualized with propidium iodide staining in the side view (magenta). (E) In wild type, the *WER::GFP* reporter is expressed in N cells of the meristematic root epidermis. This expression appears to be not changed in *id2-1* background. (F) In the *MYC1::GFP* reporter, GFP accumulates in H cells in Col-0 which is not altered in *id2-1*. (G) *GL2::GFP* is expressed in epidermal N cells in wild-type background. This expression pattern remains the same in *id2-1* mutant background.

Table 4: Root hair density of single root hair and double mutants.

Line	Root hair density* (hairs/2 mm)	Phenotype
Col-0	22.2 ± 3.1	normal
id2-1	34.2 ± 5.0	hairy
scm-2	32.9 ± 7.0	hairy
id2-1 x scm-2	32.5 ± 5.8	hairy
wer-1	71.2 ± 12.0	hairy
id2-1 x wer-1	67.6 ± 15.7	hairy
cpc	12.7 ± 1.6	fewer hairs
id2-1 x cpc	15.1 ± 2.5	fewer hairs
gl3	30.9 ± 6.3	hairy
id2-1 x gl3	29.5 ± 5.0	hairy
gl3-1 egl3-1	55.3 ± 12.8	hairy
id2-1 x gl3-1 egl3-1	75.6 ± 12.1	hairy
myc1-1	40.4 ± 2.3	hairy
id2-1 x myc1-1	37.4 ± 1.9	hairy
gl2-3	43.8 ± 3.8	hairy
id2-1 x gl2-3	44.8 ± 3.4	hairy

*values represent mean ± standard deviation

Figure 18: Root hair analyses of *id2-1* and root hair double and triple mutants.

Analyses of root hair density of *id2-1* crosses with root hair mutants in 7-day-old seedlings. Root hair density was determined as described before. Root images represent the mean root hair density of the analyzed area of the respective genotype. Scale bars = 100 μm. In all root hair analyses, Col-0 displayed a mean root hair number of 22.0 ± 2.5 and *id2-1* mutant of 33.5 ± 4.5, both represented in (A). (B) *scm-2* single mutants showed an increased

root hair density compared to wild type but approximately the same as *id2-1* single mutant as well as *id2-1 scm-2* double mutants. (C) *id2-1 wer-1* double mutants exhibited an increased root hair density compared to wild type and *id2-1* single mutant with no significant difference to *wer-1* single mutant. (D) *cpc* and *id2-1 cpc* double mutants showed approximately the same root hair density but significantly fewer root hairs than wild type and *id2-1* single mutants. (E) Both *gl3* single and *id2-1 gl3* double mutants showed significantly more root hairs than wild type but fewer than *id2-1* single mutants. (F) *id2-1 gl3-1 egl3-1* triple mutant exhibited slightly but significantly more root hairs than the *gl3-1 egl3-1* double mutant. Both showed a higher root hair density than the *id2-1* single mutant. (G) *id2-1 myc1-1* double mutants exhibited an increased root hair density compared to wild type and *id2-1* single mutants and no difference to *myc1-1* single mutants. (H) *gl2-3* single mutants showed more root hairs than wild type and *id2-1* single mutants but approximately the same root hair density as the *id2-1 gl2-3* double mutants.
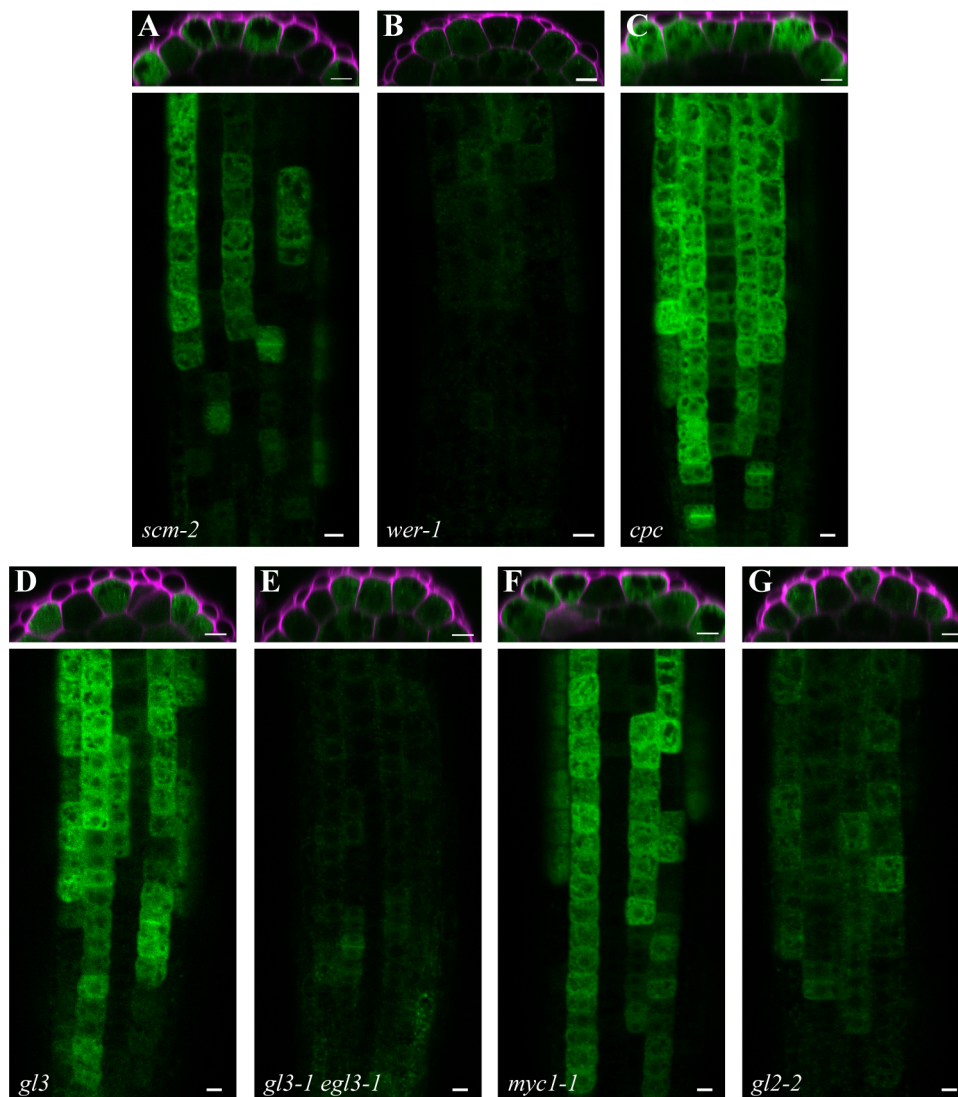
Figure 19: Expression of *ID2::ID2-GFP* in root hair mutant background.
Expression patterns of *ID2::ID2-GFP* in 5-day-old root hair mutant seedlings. Cell walls were stained with propidium iodide in side view images. Scale bars = 10 μm. (A) In *scm-2* mutants, N and H cell distribution is altered which could explain that *ID2-GFP* expression appears to be disrupted in *scm-2* mutant background. (B) In *wer-1* mutants, most N cells change into H cells which would explain the almost absent signal of ID2-GFP assuming *EPSINOID2* acts downstream of *WER*. (C) In *cpc* mutant, *ID2-GFP* appears to be expressed in almost

all epidermal cell which might be due to most of the cells harboring N cell identity in *cpc* mutants. (D) In *gl3* mutants, most of the epidermal cells keep their identity and ID2-GFP signal was only slightly disrupted. (E) *ID2-GFP* expression was extremely weak and disrupted in *gl3-1 egl3-1* background in which most cells' identity is changed into H cell. (F) The *GL3* and *EGL3* homolog *MYC1* displayed a similar root hair phenotype as *gl3*. In *myc1-1* mutants, *ID2-GFP* expression pattern is reminiscent of that in *gl3* mutant background. (G) ID2-GFP signal was very low and scattered in *gl2-2* mutant background in which most cells harbor root hair identity.

3.9 Interaction partners of EPSINOID2

To assess potential interaction partners of EPSINOID2, three different approaches were used. A commercial ULTImate Y2H SCREEN *Arabidopsis thaliana* was ordered from Hybrigenics Services SAS, France, for which EPSINOID2 fused to the binding domain was used. For that, *ID2-CDS* was cloned into the gateway-compatible Y2H vector pGBT9-GW which was sent to the company. This Y2H screen resulted in a list of 41 potential interactors categorized into four different confidence scores. Proteins that are localized in different cellular compartments than EPSINOID2, such as chloroplast or mitochondria, were removed from that list. For initial analyses, 10 candidates were picked either because of their score, their spatial expression, their subcellular localization, or involvement in cellular transport mechanisms (Table 5).

A second approach to search for interactors was a pull-down assay, in which GST-tagged EPSINOID2 as bait and *Arabidopsis* Col-0 plant extract as prey was used, followed by MS/MS analysis which was performed by Jennifer Bortlik from Frederik Börnke's group at the IGZ Großbeeren. The resulting list of 84 proteins was processed at the IGZ where contaminants, known false positives, such as sticky proteins and proteins that were also present in control samples, were removed. Furthermore, proteins localized in incompatible subcellular compartments or ribosomal proteins were eliminated, resulting in 6 candidates that were selected according to the above-mentioned criteria (Table 5).

In a third approach, seeds of the established *ID2::ID2-GFP* line were sent to Bert De Rybel at VIB Center for Plant Systems Biology at the Ghent University where IP-MS/MS experiments were performed. The resulting list was pre-processed in Ghent where contaminants, sticky proteins and ribosomal proteins were eliminated. From the remaining 120 potential interactors, proteins were removed with differing subcellular localization than EPSINOID2. Finally, 2 candidates, PHOSPHOLIPASE D ALPHA 1 (PLDα1) and PECTIN METHYLESTERASE 38 (PME38), were chosen for further analysis (Table 5).

Between the interactor lists from the pull-down-MS/MS from the IGZ and the IP-MS/MS from Ghent, 5 overlaps were identified from which 4 were already ruled out for interaction studies

according to above mentioned criteria (Figure 20A). PLDα1 was identified in both analyses making an interaction more likely which is also why it was chosen for further investigations. Between the list from the pull-down-MS/MS from the IGZ and the Y2H from Hybrigenics were two overlaps which were also already eliminated as candidates for above mentioned reasons. Additionally, some SNARE proteins were selected to test their interaction with EPSINOID2: Two t-SNAREs SYNTAXIN OF PLANTS 122 and 123 (SYP22/123), which are both involved in secretory transport (Assaad et al. 2004; Ichikawa et al. 2014), and three v-SNAREs VESICLE TRANSPORT V-SNARE 11, 12 and 13 (VTI11, VTI12 and VTI13) (Table 5). It has been shown that the ENTH domain can interact with SNARE proteins through their Habc domain (Chidambaram et al. 2004; Miller et al. 2007; Wang et al. 2011). For *Arabidopsis* EPSIN1 and the v-SNARE VTI11 as well as EPSIN2 and VTI12 such interactions have already been reported (Song et al. 2006; Lee et al. 2007). In yeast, the required interaction motif in the ENTH domain has been identified by co-crystallization studies (Wang et al. 2011). This conserved motif was found in the ENTH domain of EPSINOID2 in previous work (Figure 20B) (Freimuth 2019) in which some of these SNARE candidates have been tested in bimolecular fluorescence complementation (BiFC) experiments and additionally in pull-down assays where GST-ID2 served as bait and GFP-SYP123 as prey. Since the results of these experiments were inconclusive, interaction was tested again with this approach.

Table 5: Overview of selected potential interactors of EPSINOID2.

Potential interactor	Full name	AGI	Identified in
SYP122	SYNTAXIN OF PLANTS 122	AT3G52400	-
SYP123	SYNTAXIN OF PLANTS 123	AT4G03330	-
VHA-A1	VACUOLAR PROTON ATPASE A1	AT2G28520	-
VTI11	VESICLE TRANSPORT V-SNARE 11	AT5G39510	-
VTI12	VESICLE TRANSPORT V-SNARE 12	AT1G26670	-
VTI13	VESICLE TRANSPORT V-SNARE 13	AT3G29100	-
PME38	PECTIN METHYLESTERASE 38	AT4G00190	IP-MS/MS
PLDα1	PHOSPHOLIPASE D ALPHA 1	AT3G15730	IP-MS/MS, pull-down-MS/MS
PVA12	PLANT VAP HOMOLOG 12	AT2G45140	pull-down-MS/MS
CHC1	CLATHRIN HEAVY CHAIN 1	AT3G11130	pull-down-MS/MS
WDL4	WAVE-DAMPENED2-LIKE4	AT2G35880	pull-down-MS/MS
MIN7	HOPM INTERACTOR 7	AT3G43300	pull-down-MS/MS
VHA-A	VACUOLAR ATP SYNTHASE SUBUNIT A	AT1G78900	pull-down-MS/MS
ACT2	ACTIN 2	AT3G18780	pull-down-MS/MS

Potential interactor	Full name	AGI	Identified in
CNGC5	CYCLIC NUCLEOTIDE GATED CHANNEL 5	AT5G57940	Y2H
CNGC15	CYCLIC NUCLEOTIDE GATED CHANNEL 15	AT2G28260	Y2H
AP3D	ADAPTOR PROTEIN 3 DELTA	AT1G48760	Y2H
SEC6	SEC6	AT1G71820	Y2H
ECA4/PICALM4	EPSIN-LIKE CLATHRIN ADAPTOR	AT2G25430	Y2H
CAP1	CLATHRIN ASSOCIATED PROTEIN 1	AT4G32285	Y2H
RSW10	RADIAL SWELLING 10	AT1G71100	Y2H
CCS52B/FZR3	CELL CYCLE SWITCH PROTEIN 52 B, FIZZY-RELATED 3	AT5G13840	Y2H
BETA1-COP	BETA1 COAT PROTEIN	AT4G31480	Y2H
IRE	INCOMPLETE ROOT HAIR ELONGATION	AT5G62310	Y2H

All selected candidates were cloned into the pIX-HALO vector and resulting HALO-tagged proteins were translated *in vitro*. Since in several approaches, no coding sequences could be obtained for *CHC1*, *MIN7*, *WDL4*, *IRE*, *SEC6, BETA1-COP* and *VHA-A1*, cloning attempts for these candidates were discontinued due to time constraints. PVA12, VHA-A, CNGC5, CNGC15, ECA4 and CAP1 were successfully cloned and translated *in vitro* but pull-down assays were not performed yet.

In vitro translation of AP3D failed. For VTI11, VTI12, VTI13, SYP122, SYP123, ACT2, RSW10, PLDa1, PME38 and CCS52B/FZR3 potential interactions were analyzed in pull-down experiments using GST-tagged EPSINOID2 as bait and the HALO-tagged protein of interest as prey, which was detected with an anti-HALO antibody in western blots.

There were no interactions detected for GST-ID2 and HALO-tagged VTI11,VTI12, VTI13, SYP122, SYP123 and ACT2 as the eluate did not contain any respective HALO-tagged protein (Figure 20C). The result for SYP123 confirms the previous negative pull-down result with GFP-SYP123 and GST-ID2 and this supports the former argument that a detected interaction in BiFC was most likely a false positive. For VTI11, a signal in BiFC was also shown in previous work suggesting a possible interaction with EPSINOID2 which could not be confirmed in this pull-down. A faint band of HALO-RSW10 was detected in the eluate with GST-ID2 suggesting a weak but potential interaction (Figure 20C). However, there was also a strong band detected in the eluate with GST alone indicating that HALO-RSW10 most likely interacted with GST instead of ID2. The higher amount of GST protein compared to GST-ID2 could explain the stronger band in the GST sample suggesting there is no interaction between RSW10 and EPSINOID2. There were also faint bands of HALO-PLDα1 visible in both eluates GST and GST-ID2 with similar intensities (Figure 20C). However, here as well the amount of GST was

higher than that of GST-ID2. In this case this could mean that HALO-PLDα1 sticks a bit to GST but not as much as to GST-ID2 indicating a possible interaction with EPSINOID2. HALO-PME38 showed a weak band in GST-ID2 eluate suggesting an interaction between these two proteins but also a faint band in the GST eluate was detected (Figure 20C). Comparing the intensities of both bands with the loaded amount of protein, this indicates that there is a slight stickiness of HALO-PME38 to GST, but it potentially interacts with EPSINOID2. Pull-down experiments to test the interaction of EPSINOID2 with PME38 were repeated two more times (not shown), always showing a stronger interaction with GST-ID2 indicating a weak but true interaction *in vitro*. A very intense band of HALO-CCS52B (FZR3) was detected in the GST-ID2 eluate (Figure 20C). There was also a faint band visible in the GST eluate but again comparing both protein amounts in the loading control, it is highly likely that HALO-CCS52B interacts with ID2. These experiments were also repeated two more times giving the same results (not shown) indicating an interaction between EPSINOID2 with CCS52B/FZR3.
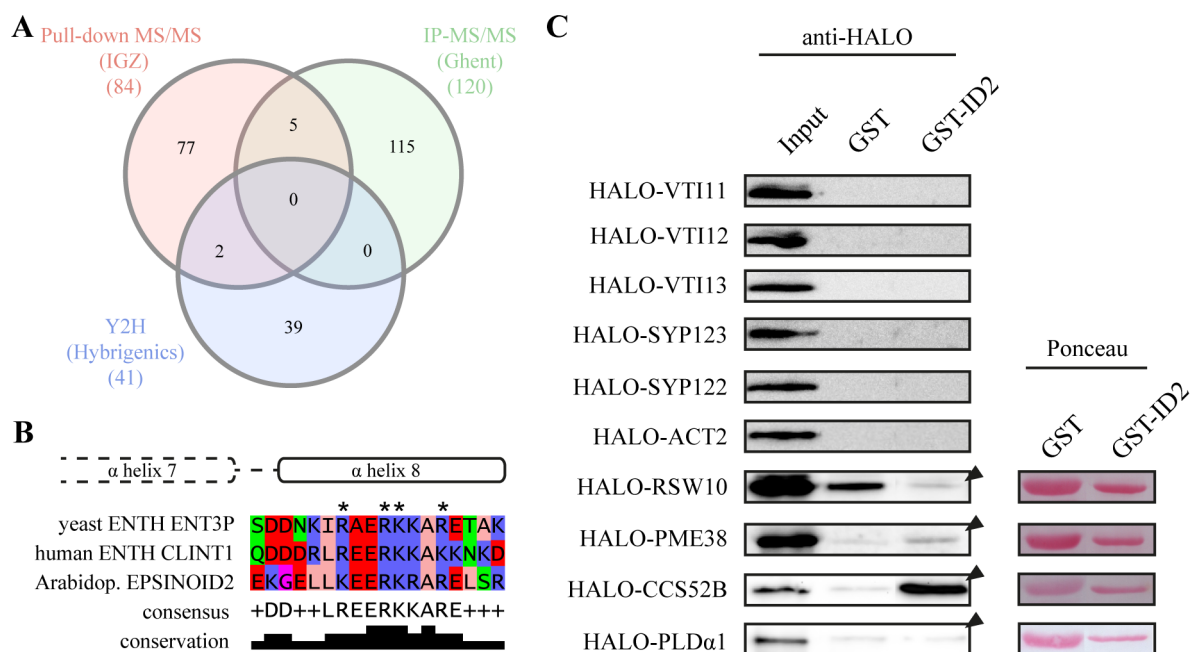
Figure 20: Insights into potential interactors of EPSINOID2.

(A) Venn-diagram of all three obtained result lists with potential EPSINOID2 interactors created with InteractiVenn (Heberle et al. 2015). (B) Sequence alignment of yeast Ent3p, human CLINT1 and *Arabidopsis* EPSINOID2 shows conserved basic residues (asterisks) in the conserved SNARE interaction motif which was identified in previous work (Freimuth 2019). (C) Pull-down assays with HALO-tagged *in vitro* translated proteins (prey) and GST-tagged ID2 as well as GST alone (bait) were analyzed in immunoblots with an anti-HALO antibody. Ponceau staining represents loading control. Input: HALO-tagged proteins; GST and GST-ID2 represents eluate. Proteins were detected at their appropriate sizes including the HALO tag: VTI11: 61 kDa, VTI12: 61 kDa, VTI13: 58 kDa, SYP122: 73 kDa, SYP123: 69 kDa, ACT2: 78 kDa, RSW10: 66 kDa, PME38: 88 kDa, CCS52B: 90 kDa, PLDα1: 129 kDa.

As demonstrated in section 3.5, EPSINOID2 could be targeted for proteasomal degradation since the ID2-GFP signal accumulates after MG132 treatment (Figure 14C). Additionally, a conserved KEN box motif, which is recognized by CDH1/CCS52/FZR proteins, was found in EPSINOID2 C-terminus at position 253-257 (Figure 14D) supporting this hypothesis. In *Arabidopsis*, there are three CDH1 homologs, two of the A-type subclass CCS52A1/FZR2 (AT4G22910) and CCS52A2/FZR1 (AT4G11920) and one of the B-type subclass CCS52B/FZR3 (AT5G13840) (Cebolla et al. 1999; Tarayre et al. 2004; Fülöp et al. 2005). The positive *in vitro* interaction test of EPSINOID2 and CCS52B further strengthens the hypothesis of EPSINOID2 regulation by proteasomal degradation. However, further analyses are required to confirm this interaction *in vivo*.

As already mentioned in section 1.4, root hair initiation and tip growth requires delivery of plasma membrane and cell wall material and modification of the cell wall (reviewed in Mendrinna and Persson 2015) which involves pectin and the activity of pectin methylesterases (Schoenaers et al. 2018). Although this activity occurs in hair cells and EPSINOID2 located in non-hair cells, an *in vivo* interaction of EPSINOID2 with a pectin methylesterase such as PME38 could be possible in terms of the putative negative regulation of root hair formation by EPSINOID2. Nevertheless, here as well additional analyses of *in vivo* interaction are essential.

4. Discussion

This work used genetic and biochemical approaches to gain more insight into the possible role of the novel short ENTH domain protein EPSINOID2 in root hair formation and its complex post-transcriptional and -translational regulation by different kinds of mechanisms.

Phenotypic characterization of a third full deletion mutant *id2-3* generated by using CRISPR/Cas9 further confirmed *EPSINOID2* as the causative gene for the hairy root phenotype. The diversity of *EPSINOID2* regulation on different levels was uncovered with several approaches to investigate miRNA844-3p action on *EPSINOID2* and to understand EPSINOID2 protein activity. Exhaustive genetic testing placed *EPSINOID2* downstream of the root epidermal cell fate network. Initial *in vitro* analyses with possible interactors of EPSINOID2 revealed two plausible candidates for future studies.

4.1 EPSINOID2 is a potential repressor of root hair formation

Accumulation of EPSINOID2 protein in N cells

The specific expression of *EPSINOID2* pattern in non-hair cell files of the root epidermis in *Arabidopsis* seedlings was confirmed with two different stable transgenic lines *ID2::ID2-GUS* and *ID2::ID2-GFP*. In aboveground tissue, EPSINOID2 was also detected in leaves, particularly in trichomes, and, depending on the age of the flower, in ovaries or ovules in *ID2::ID2-GUS* lines. These two reporter constructs use the identical genomic sequence of *EPSINOID2* with differing tags, however, microarray data confirm a higher expression of *EPSINOID2* in non-hair cells (Birnbaum et al. 2003) and cell-type-specific gene expression data that can be accessed by the eFP browser (Winter et al. 2007) also display a higher expression in non-hair cells in the elongation zone (Figure S 6) (Brady et al. 2007a; Cartwright et al. 2009). Nevertheless, Birnbaum et al. (2003) isolated cells with epidermal cell identity using *GL2::GFP* which is specifically expressed in non-hair cells meaning that obtained epidermal data represents atrichoblasts. Brady et al. (2007a) applied *GL2::GFP* specifically for isolating non-hair cells and *COBRA-LIKE9::GFP* (*COBL9::GFP*) for trichoblasts, which is downstream of epidermal cell fate determination and expressed in the elongation zone (Schindelman et al. 2001; Brady et al. 2007b). The transcriptional reporter *ID2::NLS-GFP* with the same promoter region as in the translational reporter lines revealed promoter activity in both non-hair and hair cells and also RNA in situ hybridization experiments showed mRNA presence

in both cell types. This indicates that *EPSINOID2* is expressed in all epidermal cells, however, EPSINOID2 protein localization appears to be restricted to non-hair cells in the root epidermis.

Loss of *EPSINOID2* causes an increased root hair density

Data from preliminary work revealed a hairy mutant phenotype in two independent SALK T-DNA insertion lines, knock-out mutant *id2-1* and knock-down mutant *id2-2*, mainly caused by ectopic root hair formation (Freimuth 2019). Since no complementation line could be established, and T-DNA insertion lines often carry more than one insert, it was still possible that the hairy phenotype was not caused by loss of *EPSINOID2*.

Therefore, a third mutant *id2-3* was created using CRISPR/Cas9 in which the whole genomic region of *EPSINOID2* was deleted and which was verified as a knock-out by semiquantitative RT-PCR and RNA in situ hybridization. Extensive analyses of this *id2-3* full deletion mutant confirmed the hairy mutant phenotype resulting from ectopic root hair formation and shorter root hair cells. Increased root hair density is often a result of abiotic stress such as phosphate starvation which has additional effects on the root architecture, such as increased root diameter and number of cortex cells, and decreased primary root length (Bates and Lynch 1996; Ma et al. 2001; Williamson et al. 2001). However, further analyses revealed that *epsinoid2* mutants do not show differences in root diameter or root length compared to wild type and no aberrant number of cortex cells which argues against a systemic effect. Additionally, transcriptome analyses showed increased transcript levels of *EPSINOID2* in hairless *cpc try* mutants and decreased levels in hairy *gl3 egl3* as well as *wer myb23* mutants (Figure S 5) (Bruex et al. 2012). These results strongly support a cell autonomous effect on non-hair cells of the root epidermis. Although aboveground tissue also displayed *EPSINOID2* expression, suggesting additional functions, *epsinoid2* mutants did not show obvious abnormal growth phenotypes or changes in fertility or yield. Nevertheless, a systemic effect cannot be ruled out, although it is not very likely.

It has been demonstrated that single mutants of the long ENTH domain proteins *epsin1*, *epsin2* and *epsin3* did not show any obvious growth defects except for *mvt1* which exhibited a reduced rosette size (Heinze et al. 2020; Tegtmeier 2022). However, higher order mutants revealed a dwarf phenotype in *epsin1 mtv1* who represent a partially functional redundant pair in vacuolar and secretory transport that show overlapping ubiquitous expression in almost all tissues (Heinze et al. 2020).

Obtained data form previous work showed that spatio-temporal expression of *EPSINOID2* does not overlap with the two homologs, *EPSINOID1* and *3*, and analyzed *id1 id2 id3* triple mutants

did not show additional aberrant phenotypes (Freimuth 2015; Sauer and Freimuth, unpublished). Furthermore, semiquantitative RT-PCR performed in this work did not show elevated transcript levels of *EPSINOID1* or *EPSINOID3* in *id2-3* mutant roots indicating there is no functional redundancy between these homologs and *EPSINOID2*.

The specific abundance of EPSINOID2 in non-hair cells and the hairy mutant phenotype thus indicate a possible involvement of EPSINOID2 in root hair formation, most likely acting as a repressor.

To address this question, overexpression of *EPSINOID2* was the next logical approach which, somewhat unexpectedly, revealed a possible regulation of *EPSINOID2* by a miRNA. This is discussed further in section 4.4.

4.2 EPSINOID2-GFP associates with endosomal structures

The mostly cytosolic signal of a inadvertently truncated version of ID2-GFP has been shown before, as well as the localization at the cell plate in dividing cells which has been confirmed in this work by colocalization with the endosomal and cell plate marker mCherry-RabA1g (Geldner et al. 2009; Freimuth 2019). The newly generated line with full length ID2-GFP exhibited, apart from a cytosolic signal, more distinct punctate structures similar to endosomal structures which displayed colocalization with mCherry-RabA1g, TGN marker VHA-a1-RFP, TGN-associated clathrin light chain marker mKO-CLC but not late LE/PVC marker mCherry-RabF2b and Golgi marker mCherry-SYP32 (Dettmer et al. 2006; Geldner et al. 2009; Fujimoto et al. 2010). BFA treatment led to aggregation of ID2-GFP and mCherry-RabA1g as well as VHA-a1-RFP in BFA compartments, respectively. These results suggest that EPSINOID2 is associated with endosomal structures.

A similar but more prominent punctate pattern as well as colocalization with VHA-a1-RFP and mKO-CLC has been shown for other *Arabidopsis* ENTH domain proteins such as EPSIN1 and MTV1 that are associated with the TGN (Heinze et al. 2020). This punctate signal is not restricted to plant ENTH proteins. For example, human epsinR which is involved in endosomal/TGN trafficking does also show these structures and colocalizes with TGN but not Golgi or lysosomal markers (Mills et al. 2003). In contrast, a localization at the cell plate was observed for EPSIN2 and EPSIN3 which are predominantly located at the plasma membrane (Heinze et al. 2020). Like ID2-GFP, all four ENTH domain proteins show an additional cytosolic signal (Heinze et al. 2020; Tegtmeier 2022). A dual localization in cytosol and endosomal compartments is not uncommon. For example, yeast ESCRT (endosomal sorting

complex required for transport) machinery components Vacuolar protein sorting 23 (Vsp23) and Mvb12 are transiently recruited from a cytosolic pool to endosomal membranes (Katzmann et al. 2003; reviewed in Hurley and Emr 2006; Curtiss et al. 2007). Another example are exocyst subunits which have been identified in cytosolic as well as plasma membrane pools in yeast and plants (reviewed in Heider and Munson 2012). The exocyst is an evolutionary conserved protein complex involved in exocytotic events such as polarized growth and secretion where it participates in tethering of vesicles to target membranes and regulation of SNARE assembly (reviewed in Heider and Munson 2012). In *Arabidopsis*, exocyst subunits SEC6, SEC8, SEC15b and EXO70A1 show cytoplasmic localization as well as strong association with the growing cell plate (Fendrych et al. 2010). This is reminiscent of the subcellular localization of EPSIN2 and EPSIN3 (Tegtmeier 2022). Interestingly, GFP-tagged EPSINOID2 showed a cytosolic localization but also associates with endosomal structures as well as the cell plate. However, cellular defects such as in cell plate formation were not observed in *epsinoid2* mutants in contrast to *exo70A1* mutants that fail to properly assemble the cell plate (Fendrych et al. 2010). It has been shown that members of the large ANTH family which share a similar domain with ENTH domain proteins also participate in clathrin-mediated trafficking such as *Arabidopsis* Epsin-like Clathrin Adaptor 1 (ECA1) , ECA4 and CAP1 (Ford et al. 2001, reviewed in Feng et al. 2022). ECA4 also localizes to the TGN, PM and cell plate (Song et al. 2012; Nguyen et al. 2018).

The eukaryotic machinery for clathrin-dependent vesicle generation involves APs for anchoring clathrin to the membrane through interaction with PIPs and ANTH as well as ENTH domain proteins which are helping in this process also through interaction with PIPs and cargo (Takatori and Tomita 2019; Nagano et al. 2023). Many orthologs of the involved proteins have been identified in different organisms, for example, ENTH domain protein mammalian epsinR, yeast Ent3p and *Arabidopsis* EPSIN1 which often share orthologous interaction partners such as clathrin and AP-1 and similar functions or subcellular localization (Duncan et al. 2003; Hirst et al. 2003; Mills et al. 2003; Song et al. 2006; Heinze et al. 2020, reviewed in Legendre-Guillemin et al. 2004; Craene et al. 2012; Zouhar and Sauer 2014; Takatori and Tomita 2019).

The binding motifs for APs and clathrin are usually present in the long unstructured C-terminus of the ENTH and also ANTH domain proteins (Kalthoff et al. 2002a) which is absent in EPSINOID2 including known interaction platforms. This raises the question about how EPSINOID2 would participate in vesicle trafficking since it presumably cannot bind APs or clathrin. Aside from PIPs, ENTH domains can bind the Habc domain of SNAREs which has been demonstrated for yeast Vti1p and Ent3p (Miller et al. 2007; Wang et al. 2011). Additional

interactions between ENTH domain proteins and SNAREs were shown for mouse vti1b and epsinR and *Arabidopsis* VTI11 and EPSIN1 as well as VTI12 and EPSIN2 (Chidambaram et al. 2004; Song et al. 2006; Lee et al. 2007). Acidic residues in the Habc domain of SNAREs can bind to a conserved motif of basic residues in α-helix 8 of the ENTH domain (Wang et al. 2011). This motif was also identified in EPSINOID2 indicating a potential interaction with SNAREs (Freimuth 2019). This interaction might be even in a negatively regulatory manner. For example, a cytosolic protein called tomosyn (TMS) was identified in animals that contains an R-SNARE motif with a synaptobrevin-like sequence. TMS binds syntaxin1a and synaptosome-associated protein 25 kDa (SNAP-25) thereby preventing the formation of a SNARE complex with synaptobrevin (reviewed in Ashery et al. 2009). This interaction also leads to a translocation of TMS to the plasma membrane (Widberg et al. 2003; Gladycheva et al. 2007). Recently, an *Arabidopsis* ortholog of TMS (AtTMS) was characterized harboring an R-SNARE motif that is highly conserved in plants and animals and shows high sequence similarity to synaptobrevin (Li et al. 2019). It has been demonstrated that AtTMS is recruited by SYP1s (SYP124, SYP125, SYP131, or SYP132) to the PM where it interacts with these SYPs outcompeting R-SNAREs such as VAMP721 and VAMP722 for assembling in a SNARE complex with SYP132 thereby inhibiting secretion in pollen development (Li et al. 2019). It has been proposed that AtTMS does not act as a true R-SNARE since it lacks the transmembrane domain but functions as a negative regulator of secretion, possibly in a fine-tuning process (Li et al. 2019). This is an excellent example of two proteins sharing a similar domain competitively interacting with other proteins in the same machinery or pathway thereby conferring regulation to a specific process. It is possible that this might be the role of EPSINOID2 with its highly conserved ENTH domain but missing C-terminus. However, pull-down assays with v-SNAREs VTI11, VTI12 and VTI13, the latter involved in root hair growth, as well as with two candidate t-SNAREs SYP122 and SYP123 did not show any interaction between EPSINOID2 and these SNARE proteins, although this does not generally rule out a potential interaction (Song et al. 2006; Lee et al. 2007; Larson et al. 2014; Hirano et al. 2020). Other candidates could be SYP121 that is involved in pollen tube growth as well as in root hair development or SYP111 (KNOLLE) which is associated with the cell plate (Lauber et al. 1997; Cui et al. 2022). Considering that the SNARE interaction platform is located in the EPSINOID2 N-terminus it could be worthwhile testing abovementioned candidates again with C-terminally tagged EPSINOID2 since the used N-terminal GST could prevent an interaction.

Additionally, it has recently been shown that ANTH domains and ENTH domains can interact with each other. Yeast ANTH domain protein Sla2 and ENTH domain protein Ent1p, which

are both involved in clathrin-mediated endocytosis through coupling of the plasma membrane to the actin cytoskeleton, showed PI(4,5)P$_2$-dependent interaction *in vitro* and it was demonstrated that disruption of this interaction *in vivo* led to endocytic defects (Skruzny et al. 2012; Skruzny et al. 2015). Additionally, yeast ANTH domain protein Sla2p and its mammalian ortholog Hip1R negatively regulate actin assembly through interaction with certain actin polymerization factors (mouse cortactin and yeast Pan1p) during endocytosis (Toshima et al. 2006; Le Clainche et al. 2007). So far, an interaction between ENTH and ANTH domain proteins or even between two ENTH domain proteins in *Arabidopsis* has not been investigated. This might be worth looking into if EPSINOID2 may interact, for example, with long EPSINs or ANTH domain proteins negatively regulating their action in a specific process.

Taken together these results strongly suggest an association of EPSINOID2 with TGN-associated endosomal structures and furthermore points towards an involvement in post-Golgi trafficking. Possible scenarios of EPSINOID2 action in vesicle transport could include non-productive competitive binding with factors of the vesicle generation machinery thereby preventing required interactions for proper vesicle formation or sequestration or mis-targeting of factors. In general, if EPSINOID2 represses root hair formation by interfering with root hair forming components, it is likely that it prevents their delivery to their site of action.

4.3 EPSINOID2 acts downstream of epidermal cell fate determination

Placement of *EPSINOID2* in the root epidermal cell fate network

Considering the specific appearance of EPSINOID2 in non-hair cell files in the transition of the meristematic and elongation zone of the root, a potential involvement in cell fate determination is plausible. The transcription factor GL2 is also restricted to atrichoblasts where it acts as negative regulator of hair cell fate and loss of *GL2* also results in ectopic root hair formation (Di Cristina et al. 1996; Masucci et al. 1996). Mutants of other transcription factors involved in non-hair cell differentiation such as GL3, EGL3 and WER also display increased root hair density (Lee and Schiefelbein 1999; Bernhardt et al. 2003).

In this work, comprehensive genetic testing was applied to gain more insight into *EPSINOID2* placement and potential role in epidermal cell fate determination networks. Crosses of *id2-1* with established transcriptional and translational reporter lines of cell fate markers *SCM::SCM-GFP* (Kwak and Schiefelbein 2008), *WER::WER-GFP* (Ryu et al. 2005), *WER::GFP* (Lee and Schiefelbein 1999), *CPC::CPC-Neon* (generated according to Wada et al. 2002), *GL3::GL3-YFP* (Bernhardt et al. 2005), *MYC1::GFP* (Bruex et al. 2012) and *GL2::GFP* (Lin and

Schiefelbein 2001) revealed that loss of *EPSINOID2* does not affect either expression or abundance of the respective cell fate player. However, ID2-GFP localization pattern was disrupted in established *scm-2* (Kwak et al. 2005), *wer-1* (Lee and Schiefelbein 1999), *cpc* (Sessions et al. 2002), *gl3* (Woody et al. 2007), *gl3-1 egl3-1* (Bernhardt et al. 2003), *myc1-1* (Alonso et al. 2003) and *gl2-2* (Alonso et al. 2003) cell fate mutants according to reported changes in epidermal cell identity.

Scm-2 knock-out mutants exhibit altered distribution of N and H cells (Kwak et al. 2005), and accordingly ID2-GFP showed a very disordered, ectopic signal likely as a result of a position-independent cell type organization. A similar altered signal distribution was also shown for *WER::GFP*, *CPC::GUS* and *GL2::GUS* in *scm-2* mutant background (Kwak et al. 2005), all normally expressed in N cells (Masucci et al. 1996; Lee and Schiefelbein 1999; Wada et al. 2002) and acting downstream of SCM in cell fate determination (Bernhardt et al. 2003; Kwak and Schiefelbein 2007; Kang et al. 2013). In *wer-1* mutants, most epidermal cells adopt hair cell identity (Lee and Schiefelbein 1999), which would explain the very weak ID2-GFP signal if ID2-GFP appearance was linked to N cell identity. It has been reported that N cell-specific expression of downstream components of WER, *CPC::GUS* and *GL2::GUS* was extremely minimized in *wer-1* mutant background (Lee and Schiefelbein 2002). In contrast, in *cpc* mutants, identity of most epidermal cells is changed into N cell (Wada et al. 2002) and accordingly ID2-GFP signal is present in all epidermal cells in both N and H position. This was also demonstrated for *WER::GFP* and *GL2::GUS* in *cpc* mutants which are negatively regulated by *CPC* (Lee and Schiefelbein 2002). It has been shown that epidermal cell identities are not changed in *gl3-1* and *egl3-1* single mutants, respectively, however, the *gl3-1 egl3-1* double mutant displays a strong decrease in cells with non-hair identity which is presumably based on the partial redundancy of these two homologues transcription factors (Bernhardt et al. 2003). In line with this, ID2-GFP exhibits an almost normal signal pattern in *gl3* mutant background but an almost undetectable signal in *gl3-1 egl3-1* double mutant background, indicating ID2-GFP abundance is connected to N cell identity. Similar observations were made for *CPC::GUS* and *GL2::GUS*, both downstream components of GL3/EGL3, which did not show differing expression patterns in *gl3-1* or *egl3-1* single mutant background, respectively, but a strong reduction in *gl3-1 egl3-1* double mutant background (Lee and Schiefelbein 2002; Bernhardt et al. 2003). The *myc1-1* mutant, which is another homologues bHLH transcription factor of GL3 and EGL3, exhibits ectopic H cells (Bruex et al. 2012; Zhao et al. 2012). ID2-GFP showed a similar weak pattern disruption as in *gl3* mutant background. In *gl2-2* mutants, epidermal cell identity is mostly changed into hair cell (Masucci et al. 1996) and accordingly, ID2-GFP signal

was very weak and scattered in *gl2-2* mutant background. Reporter lines of five direct targets downstream of GL2, *RHD6::GUS*, *RSL1::GUS*, *RSL2::GUS*, *LRL1::GFP* and *LRL2::GUS*, which are usually expressed in H cells, showed promoter activities in all epidermal cells in *gl2-5* mutant background (Lin et al. 2015).

All these results indicate that EPSINOID2 is acting downstream of the epidermal cell fate machinery and does not affect epidermal patterning, moreover, it seems that EPSINOID2 appearance is dependent on the established epidermal N cell identity. This is also supported by the double mutants of *id2-1* combined with cell fate players which exhibited similar root hair densities as the respective cell fate player single mutant in almost all cases. Together this indicates that loss of *EPSINOID2* has no impact on the function of the analyzed cell fate determinants. However, it must be noted that the *id2-1 gl3-1 egl3-1* triple mutant displayed a higher root hair density than the *gl3-1 egl3-1* double mutant suggesting additivity indicating that *EPSINOID2* functions independently from *GL3/EGL3*. However, *id2-1 gl3* double mutants did not show this effect which could suggest that *EPSINOID2* acts in a different pathway than *EGL3* but not *GL3* which is supported by an initial analysis of *id2-1 egl3-1* double mutants that did also show more root hairs than both single mutants (not shown). It would be interesting to explore how an *EGL3* reporter would act in *id2-1* mutant background or how ID2-GFP signal would change in *egl3-1* mutant background. Additionally, it could be worthwhile to have a closer look at a possible genetic interaction of *EPSINOID2* and *CPC* homolog *TRIPTYCHON* (*TRY*) which acts partially redundant to *CPC* but is solely involved in a feedback loop where it is positively controlled by GL2 in N cells (Simon et al. 2007).

Nevertheless, all these results point towards EPSINOID2 acting downstream of epidermal cell specification where it negatively affects root hair formation. Consequently, investigations of EPSINOID2 and interference with components downstream of patterning events would be necessary to find out at which point EPSINOID2 prevents root hair formation.

Alternative scenarios of EPSINOID2 involvement in root hair suppression

There are several scenarios about EPSINOID2 action. In one scenario, EPSINOID2 could interfere with components that act downstream of GL2 and are participating in the process of root hair initiation. EPSINOID2 could, for example, prevent delivery of factors needed for RHID or bulge formation thereby executing or maintaining the non-hair fate. Directly downstream of GL2 are several transcriptions factors RHD6, RSL1, RSL4, RSL2, LRL1 and LRL2, however, all of them are located in H cells: RHD6 and its homolog RSL1 are expressed before root hairs are initiated and are located in nuclei of trichoblasts (Menand et al. 2007),

RSL2 and RSL4 are expressed in growing root hairs, also located in nuclei (Yi et al. 2010; Pires et al. 2013), and LRL1 and LRL2 are located in H cells promoting root hair growth (Lin et al. 2015). This spatial separation not only on tissue level but also on subcellular level makes an action of EPSINOID2 on these proteins highly unlikely.

Several factors involved in root hair initiation, for example, ROP2 and ROPGEFs, such as GEF3 and GEF4 (Denninger et al. 2019), as well as their interactor RLK FER which regulates NADPH oxidase-dependent ROS-mediated root hair growth (Duan et al. 2010), would also represent candidates where EPSINOID2 action could, for example, prevent their delivery to their site of action. However, again, all the factors, except for FER, are specifically present in hair cells (Duan et al. 2010; Denninger et al. 2019). *FER* is broadly expressed throughout the plant and located at the PM (Duan et al. 2010) and is involved in female fertility by regulating pollen tube reception (Escobar-Restrepo et al. 2007), suppression of cell elongation of the primary root in which FER is activated by a secreted peptide RALF (rapid alkalinization factor) (Haruta et al. 2014), hormone signaling (Deslauriers and Larsen 2010; Yu et al. 2012) and abiotic as well as biotic stress response (Stegmann et al. 2017; Feng et al. 2018). FER could be one factor of interest since spatial and temporal localization of EPSINOID2 and FER in different tissues overlap, such as in non-hair cells or leaf trichomes. However, *fer* mutants show drastic root hair defects such as collapsed and burst hairs (Duan et al. 2010) which speaks against a possible EPSINOID2 action on FER. Nevertheless, it could be worthwhile to explore, for example, potential mis-targeting or localization of FER in *epsinoid2* mutants or overexpression lines specifically in non-hair cells. Investigation of its activating peptide RALF could also be of interest. Additionally, cell wall loosening or remodeling components could be possible downstream candidates of EPSINOID2.

Since there is only little known about non-hair cell-specific proteins downstream of patterning events, the search for potential downstream effectors of EPSINOID2 is very challenging. One known factor strongly expressed in non-hair cell files is the auxin influx transporter AUXIN RESISTANT1 (AUX1) which has been proposed to be important for the supply of auxin to hair cells (Bennett et al. 1996; Jones et al. 2009). Selection of the polar root hair initiation site at the basal end of the root hair cell where root hairs are formed is mediated by auxin which requires *AUX1* (Schiefelbein and Somerville 1990; Masucci and Schiefelbein 1994; Grebe et al. 2002). Additionally, normal root hair elongation also requires auxin supply (Pitts et al. 1998). It has been reported that BFA treatment can interfere with AUX1 localization at the plasma membrane in epidermal cells resulting in an evenly distributed localization in the cytosol (Grebe et al. 2002). Since EPSINOID2 is an ENTH domain protein which colocalizes with endosomal

structures and shows BFA sensitivity, it is likely involved in vesicle trafficking. Therefore, EPSINOID2 could influence correct localization of AUX1. This is contradicted by the fact that in *epsinoid2* mutants no obvious defects in root hair position or elongation were observed, however, this has not been analyzed in detail or quantified. Also, *aux1* mutants do produce a normal proportion of root hair cells (Masucci and Schiefelbein 1996). Nevertheless, other factors could compensate for loss of *EPSINOID2* and redundancies or crosstalk in hormonal pathways that affect root hair formation could mask loss of *AUX1* (reviewed in Vissenberg et al. 2020).

It has been proposed that root hair formation can occur in all epidermal cells after cell fate has been established, mediated, for example, by hormones and/or environmental factors (Masucci and Schiefelbein 1996; Schneider et al. 1997; Müller and Schmidt 2004; Savage et al. 2013). In a second scenario, EPSINOID2 could negatively act on root hair formation in response to biotic or abiotic stress or hormonal signaling. Since EPSINOID2 appears to affect root hair formation after cell fate determination, an involvement in the execution of non-hair specification is more likely in which EPSINOID2 could override the predetermined cell fate in adaption to environmental or endogenous cues. Nutrient availability can affect root hair development, for example, by altering the expression level of factors involved in root hair development (reviewed in Vissenberg et al. 2020 and Zhang et al. 2023). An essential limiting nutrient is nitrogen (N) which is available as ammonium (NH_4^+) and nitrate (NO_3^-). It has been shown that increasing nitrogen concentrations led to an increased root hair density and root hair length in Col-0 which involves NITRATE TRANSPORTER1.1 (NRT1.1) and AMMONIUM TRANSPORTERS (AMT1.1, AMT1.2, AMT1.3 and AMT2.1) (Vatter et al. 2015). In another study, it was revealed that decreasing trichoblast cell lengths but not ectopic root hair formation causes the increased root hair number, however, a difference in root hair length was not detected (Canales et al. 2017). It was also shown that loss of *NRT1.1* and both of its redundant downstream components *TGACG SEQUENCE-SPECIFIC BINDING PROTEIN 1* and *4* (*TGA1/TGA4*) exhibited a reduced response in root hair density to nitrate (Canales et al. 2017). It has been proposed that this nitrate signaling pathway involving NTR1.1 and TGA1/TGA4 induces *CPC* expression which mediates nitrate response by triggering root hair development (Canales et al. 2017). Since *EPSINOID2* is a downstream component of *CPC*, it is more likely that a response to nitrate would be a result of CPC action on root hair development. However, it is worthwhile to investigate EPSINOID2 behavior upon nitrate treatments, as initial experiments show an involvement in the plastic response to N availability (Sauer, unpublished).

Another essential nutrient is inorganic phosphorous (Pi). Low Pi availability results in increased root hair length and density due to increased root hair number in H position possibly as a result of shorter cells and additionally ectopic root hair formation (Bates and Lynch 1996; Ma et al. 2001; Müller and Schmidt 2004; Savage et al. 2013). There are contradicting reports about aberrant cortical cell number under phosphate deficient conditions, showing in one study normal number of cortical cells and in another study changes in cortical cell number. However, these observations might be due to differing compositions and pH of growth media (Ma et al. 2001; Müller and Schmidt 2004). The above-described root hair phenotypes, except for changes in root hair length, were also observed in *epsinoid2* mutants which makes analyses regarding a connection of *EPSINOID2* and phosphate starvation plausible. However, the CPC-like MYB transcription factor ENHANCER OF TRY AND CPC1 (ETC1) which acts partially redundant with TRY and CPC in epidermal cell fate determination has been reported to be involved in increased root hair formation in response to Pi starvation which would again potentially place *EPSINOID2* downstream of this network (Kirik et al. 2004; Savage et al. 2013; Rishmawi et al. 2018). Nevertheless, it has also been reported that *ETC1* is expressed in N cells similar as *CPC* but in contrast ETC1 protein does not move into neighboring H cells (Tominaga-Wada et al. 2017). Moreover, *ETC1* and surprisingly its homolog *ETC3*, which is normally barely expressed in roots and not involved in root epidermal patterning, are induced by Pi starvation whereas *CPC* and *TRY* expression is not affected (Simon et al. 2007; Ohmagari et al. 2020). This would make *ETC1* another interesting candidate to look at regarding genetic interaction with *EPSINOID2*, especially in combination with phosphate starvation (Tominaga-Wada et al. 2017).

The essential micro-nutrient Manganese (Mn) is important for many processes such as photosynthesis, hormone signaling and ROS scavenging (reviewed in Alejandro et al. 2020). Unlike Fe and Pi, Mn deficiency shows no other root hair phenotype than increased root hair density caused by ectopic root hair formation without notably affecting *GL2* expression. This has also been shown for ethylene treatments indicating another existing mechanism downstream of cell fate determination that confers plasticity to root hair development (Masucci and Schiefelbein 1996; Schmidt et al. 2000; Müller and Schmidt 2004; Wei Yang et al. 2008; Ohmagari et al. 2020). This makes Mn a valid candidate to investigate in association with EPSINOID2. Additionally, ethylene influence on EPSINOID2 action or vice versa could be investigated for completeness since high ethylene levels cause ectopic root hairs and the ethylene pathway acts downstream of cell fate specification although ethylene treatment causes

additional phenotypes not observed in *epsinoid2* mutants (Kieber et al. 1993; Tanimoto et al. 1995; Masucci and Schiefelbein 1996; Pitts et al. 1998).

All these candidate genes, nutrients or hormones could give more insight into either upstream or downstream EPSINOID2 action or regulation and could help to understand in which pathway EPSINOID2 is involved or what exact molecular function EPSINOID2 might have in root hair formation.

So far, an involvement of ENTH domain proteins in root hair formation has not been reported. However, several AP180 N-terminal homology (ANTH) domain proteins have been identified that are involved in pollen tube germination and elongation such as *Arabidopsis* ECA2, Endocytosis Adaptor of Pollen Tube 1 (EAP1), AP180 and *Oryza sativa* OsANTH3 (Zhao et al. 2010; Li et al. 2018; Muro et al. 2018; Kaneda et al. 2019; Kim and Jung 2023). Pollen tube elongation is a similar process as root hair growth in which unidirectional expansion of a long tubular cell requires, for example, highly polarized cytoplasm and vesicle trafficking (reviewed in Campanoni and Blatt 2007). Recently, ENTH domain protein Os01g62370 was identified in a Y2H screen as an interactor of *Germinating modulator of rice pollen* (GORI) which is a WD40 protein that is required for pollen tube growth by balancing secretion and endocytosis (Kim et al. 2021). Homozygous *gori-2* mutants exhibited reduced pollen germination and impaired tube growth which includes abnormal pectin distribution, in particular of de-esterified pectin in the apical region (Kim et al. 2021). Additionally, Os01g62370 was downregulated in *gori-2* mutants (Kim et al. 2021). In fact, Os01g62370 is the rice *EPSINOID2* ortholog which makes this a very interesting finding considering EPSINOID2 presumably being involved in membrane trafficking events and negative regulation of root hair formation. Therefore, it might be also worthwhile taking a closer look at *EPSINOID2* expression in pollen/pollen tube and a possible involvement in pollen tube growth.

4.4 *EPSINOID2* is regulated by different post-transcriptional and -translational mechanisms

EPSINOID2 seems to be targeted by miRNA844-3p

The idea of EPSINOID2 being a negative regulator of root hair formation led to analyses of a constitutive overexpression line *35S::ID2* in previous work. This unexpectedly gave rise to a hairy phenotype although *EPSINOID2* transcript levels were increased, speaking against transgene-mediated co-suppression at transcript level (Napoli et al. 1990; van der Krol et al. 1990; Larkin et al. 1994; Freimuth 2019). Overexpression was further investigated in this work

with GFP-tagged *EPSINOID2* expressed under 35S and a weaker UBI10 promoter, both showing almost no fluorescent signal, and *35S::ID2-GFP* again showed higher mRNA level but could not be detected on protein level. Assuming post-transcriptional or -translational down regulation of *EPSINOID2*, literature research revealed the so far little characterized miRNA844-3p targeting *EPSINOID2* in its 3rd exon (Rajagopalan et al. 2006). Additionally, *EPSINOID2* appeared to be upregulated in several miRNA biogenesis mutants such as *dcl1-15*, *dcl1-5*, *med20a* and *ago1-3*, indicating miRNA regulation of *EPSINOID2* (Kim et al. 2011; Seefried et al. 2014; Arribas-Hernández et al. 2016; Plotnikova et al. 2019). MiRNAs can regulate gene expression by slicing complementary target mRNA or inhibiting mRNA translation (reviewed in Guerra et al. 2015).

To address the question of miRNA regulation, several established approaches were used. *EPSINOID2* target sequence of miRNA844-3p was disrupted through silent mutations and then overexpressed. Both GFP-tagged as well as untagged miRNA-resistant *EPSINOID2* lines displayed a decreased root hair density and a strong signal in almost all cells was detected in GFP-tagged lines suggesting *EPSINOID2* is targeted and downregulated by miRNA844-3p. This was additionally supported by *STTM844* constructs exhibiting a similar reduction in root hair density as the miRNA-resistant overexpression constructs. Moreover, transcript levels and protein levels of miRNA-resistant *EPSINOID2* revealed an overexpression on both levels, and *STTM844* constructs showed quite normal transcript and higher protein levels as expected indicating that *EPSINOID2* is probably downregulated by miRNA844-3p through translational inhibition, which is in line with the results of the *35S::ID2* line. Furthermore, these results support the hypothesis of EPSINOID2 being a negative regulator of root hair formation. To further investigate the role of EPSINOID2 in suppression of root hair formation, a construct was generated at the end of this work with which miRNA-resistant *EPSINOID2* is ectopically expressed in H cells under the *MYC1* promoter (*MYC1::ID2-miR^R-GFP*) which will be analyzed in future work. It will be interesting to see whether this construct is able to suppress root hairs in H cells.

Full deletion CRISPR/Cas9 mutant *mir844* revealed a slightly increased mRNA level of *EPSINOID2*, however, contradicting the expectation of a decreased root hair density, analyses showed an increase. Additionally, overexpression of *MIR844* did not significantly change the amount of root hairs compared to wild type. These results are not in line with the observed decreased root hair density in lines where miRNA844-3p activity on *EPSINOID2* was presumably impaired. However, deletion and overexpression of the *MIR844* gene also affects the miRNA844-5p which could explain the root hair phenotype since action of miRNA844-5p

could directly or indirectly affect root hair density (Fahlgren et al. 2007). Besides, miRNA844-3p could have additional targets, even in other cell types, which also might influence root hairs. The miRNA target prediction tool psRNAtarget (Dai et al. 2018) returns around 97 putative target genes for miRNA844-5p and 86 for miRNA844-3p with *EPSINOID2* being the top target of miRNA844-3p and cytidinephosphate diacylglycerol synthase 3 (*CDS3*, AT4G26770) as well as an unknown U-box domain-containing protein kinase (AT5G51270) as top targets of miRNA844-5p. The latter was also identified as a miRNA844-5p target by Fahlgren et al. (2007). *CDS3* has been confirmed as a target of miRNA844-5p (Lee et al. 2015) and has been identified as a hair cell-specific gene in *Arabidopsis* root epidermis (Bruex et al. 2012). Lee et al. (2015) demonstrated that miRNA844 is involved in defense response to pathogens in *Arabidopsis*. Overexpression of *MIR844* led to a higher susceptibility to the pathogenic bacterium *Pseudomonas syringae* DC3000 and fungus *Botrytis cinerea*, and *MIR844* mutation (SALK_116570) led to more resistant plants. In line with this, miRNA844 was downregulated in plants infected with *P. syringae* or *B. cinerea* (Fahlgren et al. 2007; Lee et al. 2015). However, it is not clear from either study whether miRNA844-3p or -5p is downregulated. Moreover, the T-DNA of the Salk *mir844* mutant is inserted in the annotated promoter region of the downstream gene AT2G23348 as well as the *MIR844* gene itself (The Arabidopsis Information Resource (TAIR), https://seqviewer.arabidopsis.org/, on www.arabidopsis.org, 16.09.2023). This demonstrates the complexity of miRNA investigations, and it further shows that the results from this works' *MIR844* overexpression and deletion experiments might not reflect the actual miRNA844-3p action specifically on *EPSINOID2* or might mask miRNA844-3p effects. An excellent example where both miRNAs 5p and 3p (formally known as miRNA and miRNA*) are functional in two different pathways is miRNA393. It is involved in host immune response upon *P. syringae* infection (Zhang et al. 2011). MiRNA393-5p is loaded into AGO1 and regulates the PAMP-triggered immunity (PTI) by interfering with auxin signaling. In contrast, miRNA393-3p is loaded into AGO2 and targets the SNARE MEMB12 to promote secretion of PATHOGENESIS-RELATED GENE 1 (PR1) and thereby conferring immunity (Navarro et al. 2006; Zhang et al. 2011). These data are also an example for miRNA involvement in secretory trafficking.

A fundamental question was where *MIR844* is expressed in the root, however, no signal could be detected in two different transcriptional reporter lines, *MIR844::ER-GFP* and *MIR844::GUS*. Considering the reads in the study that identified miRNA844 by high-throughput pyrosequencing, it appears that miRNA844-3p and -5p with 8 and 5 reads, respectively, are very lowly expressed compared to the well-studied miRNA165a with 514

reads, the latter has been successfully detected with a GFP transcriptional reporter line (Rajagopalan et al. 2006; Carlsbecker et al. 2010). It should also be taken into consideration that the promoter length might have been too short for proper *MIR844* expression. As an alternative method, miRNA in situ hybridization with locked nucleic acid (LNA) could be used which confers more sensitivity to the detection of *MIR844* expression (Marco et al. 2019). An indirect method for visualization would be to investigate the spatial distribution of the miRNA for which a sensor construct is used in which the respective target sequence is incorporated into the 3'UTR of a reporter, such as GFP, which was initially presented in *Drosophila melanogaster* and also successfully utilized in *Arabidopsis* (Brennecke et al. 2003; Parizotto et al. 2004; Carlsbecker et al. 2010). In this work, the sensor construct for miRNA844-3p was designed as described in Parizotto et al. (2004) with nuclear-localized GFP containing one copy of the *EPSINOID2* target sequence in the 3'UTR expressed under the 35S promoter as well as an additional miRNA-resistant version of it. The results of three compared miR844-sensor lines and one miR844[R]-sensor line were inconclusive because variation of signal intensities between the three miR844-sensor lines and even within the same line was so high that a final conclusion could not be made. Two miR844-sensor lines showed very contradicting intensities whereas the third did not show a signal at all, therefore, no statement can be made about which line represents the true miRNA844-3p activity. The same is true for the miR844[R]-sensor line since only one line was analyzed. It must be noted that additionally the sample size was low. However, considering the strong 35S promoter activity and the presumably very low expression of *MIR844*, changes in GFP signal intensity might probably be very low or undetectable. The lack of signal in miR844-sensor line #1.1 appears to be a result of transgene-mediated silencing, a common problem with 35S promoter constructs (Napoli et al. 1990; Elmayan and Vaucheret 1996). It might be worthwhile to create new sensor constructs with a weaker ubiquitous promoter such as UBI10 or even with a root epidermis-specific promoter to get an idea of miRNA844-3p site of activity. This could also give insight into whether miRNA844-3p activity could be the reason for discrepancies between *EPSINOID2* mRNA and protein presence assuming *EPSINOID2* regulation through translational inhibition.

MiRNAs have a very broad range of biological functions and participate in normal plant growth and development as well as in responses to biotic and abiotic stress (reviewed in Dong et al. 2022 and Zhang et al. 2022). It has been proposed that evolutionarily young and/or less conserved miRNAs are usually expressed at very low levels under normal growth conditions compared to conserved plant miRNA families and this low abundance makes miRNA detection difficult (Rajagopalan et al. 2006; Fahlgren et al. 2007). Additionally, many miRNAs display

time- and tissue-specific expression as well as movement or stress-responsive up-/downregulation. For example miRNA399 is involved in Pi starvation response and upregulated in Pi-deprived plants but remains undetectable under normal growth conditions (Fujii et al. 2005; Bari et al. 2006; reviewed in Dong et al. 2022 and Zhang et al. 2022). In root development, several miRNAs have been identified influencing various processes such as primary root tip growth (miRNA160, miRNA167, miRNA165/166), lateral roots (miRNA164, miRNA167, miRNA399) and vascular patterning (miRNA165/166) (reviewed in Gautam et al. 2017; Dong et al. 2022). MiRNAs are also involved in hormonal pathways such as miRNA160 by targeting *AUXIN RESPONSE FACTORS 10* (*ARF10*) and *ARF16* which regulates root cap formation and lateral root development (Wang et al. 2005). In root and aboveground tissues, interference with miRNA160 regulation of *ARF17* leads to severe developmental defects (Mallory et al. 2005). As an example for abiotic stress, miRNA167 regulates lateral root growth in response to nitrogen (Gifford et al. 2008).

So far, no miRNA has been reported to be directly involved in root hair formation in *Arabidopsis*. There are several *Arabidopsis* miRNAs participating in hormonal pathways which might indirectly influence root hair development such as miRNA160-*ARF10/16/17* regulation of auxin signaling or ethylene-responsive miRNA319b-*MYB33* regulation (reviewed in Yan et al. 2022). In 2017, a study found that SERRATE (SE) which is part of the miRNA biogenesis machinery is a post-transcriptional regulator of root hair cell fate and hair elongation by promoting non-hair cell fate in a miRNA-dependent manner acting independently of CPC and WER, and also promoting root hair growth termination by stabilizing mRNAs (Foley et al. 2017). All together these studies represent only a small snippet of the whole miRNA network in plants yet demonstrate the great diversity of miRNA functions.

Given all this data, it is not unreasonable that both miRNA844-5p and -3p are functional and participating presumably in different pathways. The effect of miRNA844-3p might be more visible under certain stress conditions which could be employed to test for regulation of *EPSINOID2* by miRNA844-3p. All together the results of this work strongly suggest miRNA844-3p regulation of *EPSINOID2* which additionally strengthens the role of EPSINOID2 as a negative regulator in root hair formation.

EPSINOID2 protein presence is restricted to N cells

EPSINOID2 promoter is active in all root epidermal cells and *EPSINOID2* transcript was detected in both H and N cells. However, EPSINOID2 protein appears mostly restricted to N cells. This indicates that *EPSINOID2* mRNA is neither degraded in H cells nor moving from H

to N cells. Wada et al. (2002) revealed similar results only in an opposite manner for *CPC* whose promoter activity and transcript accumulation is restricted to N cells whereas CPC protein was detected in all epidermal cells. In a follow up study it was demonstrated that CPC moves from N to H cells via plasmodesmata (PD) (Kurata et al. 2005).

Three possible scenarios were proposed and investigated in this work: i) *EPSINOID2* translation is prevented by miRNA844-3p in H cells, ii) EPSINOID2 protein moves from H cells to N cells or iii) EPSINOID2 protein is rapidly degraded in H cells.

Action of miRNA844-3p on EPSINOID2 in H cells was analyzed with mNeon-tagged miRNA-resistant *EPSINOID2* expressed under its endogenous promoter giving inconclusive results as three independent lines showed differing results: on the one hand Neon signal in a N cell restricted pattern resembling the non-resistant GFP line, and on the other hand scattered signal in both cell types. These results suggest that miRNA844-3p action on *EPSINOID2* might not be the reason for the distinct protein localization in N cells. Therefore, it appears that a second mechanism regulates EPSINOID2 abundance independently from miRNA844-3p action.

Possible EPSINOID2 cell-to-cell mobility was addressed with 3xGFP-tagged *EPSINOID2* expressed under its endogenous promoter. Two independent still segregating T_2 lines exhibited differing signal intensities which was also observed for the *ID2::ID2-GFP* lines #6.3 and #12.3 and it must be considered that seedlings could have been heterozygous or homozygous for the transgene. However, interestingly, the GFP signal was present not only in N cells but also weakly in H cells though it was not as consistent as in N cells, and moreover, ID2-GFP was also detected at the cell plate presumably in H cells. These results points towards a possible movement of EPSINOID2 protein, however, further analyses are required to confirm this. These results are reminiscent of experiments with CPC movement with regard to the size exclusion limit (SEL) in which it was demonstrated that with increasing number of fused GFP molecules to CPC the signal got more and more restricted to N cells with only mild changes in 3xGFP-tagged lines and very strong impairment of CPC movement with 5xGFP (Kurata et al. 2005). To confirm EPSINOID2 movement, constructs with higher number of GFPs could be applied to see whether the pattern changes more drastically. An alternative method would be, for example, to block PDs by using an (inducible) constitutively active CALLOSE SYNTHASE 3 (CALS3) which leads to accumulation of callose at the PD thereby decreasing the PD diameter and reducing intercellular transport (Vatén et al. 2011; Daum et al. 2014).

EPSINOID2 appears to be targeted for proteasomal degradation

Post-translational degradation of EPSINOID2 was addressed with MG132 treatments which is a peptide aldehyde that binds the β1, β2 and β5 subunits of the 20S core particle (reviewed in Albornoz et al. 2019).

Treatments with MG132 led to an accumulation of ID2-GFP signal whereas treatments with protein synthesis inhibitor CHX led to a slight decrease. However, CHX treatments did not work properly. In a protocol for measuring protein half-time in *Arabidopsis*, a final concentration of 200 μM of CHX is recommended which is the double amount of what was used for ID2-GFP treatment (Guo and Yin 2019). Therefore, applied CHX concentrations might not have been sufficient to fully block protein synthesis. Additionally, MG132 treatment duration and/or concentrations could have been too low to develop its full potential. For example, B-BOX PROTEIN 21, which has been proposed to be targeted by the E3 ubiquitin ligase CONSTITUTIVELY PHOTOMORPHOGENIC 1 (COP1) for 26S proteasomal degradation in darkness, showed only a slight accumulation when treated with 50 μM MG132 and the full effect was only displayed with 100 μM (Xu et al. 2016). Nevertheless, these results point towards proteasomal degradation of EPSINOID2. It seems that this degradation is not the reason for differential abundance of EPSINOID2 protein and mRNA in the epidermis since in all treatments ID2-GFP showed the striped N cell-specific pattern. An example for regulated protein turnover in epidermal development has been shown for TRY, where seedlings have been treated with MG132 for 24 h, that in contrast to CPC is regulated by proteasomal degradation and loss of its C-terminus confers protein stability which leads to TRY accumulation and increased root hair numbers (Tominaga-Wada and Wada 2017). This also demonstrates that longer incubation with MG132 could give more clear results for EPSINOID2 protein abundance and turnover.

Further evidence for proteasomal degradation of EPSINOID2 lies in a KEN box motif (.KEN.) in its C-terminal region (MKENM) which appears to be conserved in many EPSINOID2 orthologs such as Os01g62370 which is involved in pollen tube growth (Kim et al. 2021). The KEN box is preferentially recognized by CDH1 recruiting the APC/C E3 ubiquitin ligase complex which leads to ubiquitination of the target protein and subsequent proteasomal degradation (Pfleger and Kirschner 2000). In fact, CCS52B, which is the B-type plant ortholog of CDH1, was identified as potential interactor of EPSINOID2 which is discussed below. Together these findings strongly support a potential proteasomal degradation of EPSINOID2, however, further analyses are required to confirm this. Experiments should be repeated with increased CHX concentration and generally longer incubation time as well as determination not

only by live cell imaging but also by western blot. Additional analyses could involve a version of EPSINOID2 in which the KEN box motif is mutated to determine if this confers stability to the EPSINOID2 protein and furthermore influences root hair density.

Taken together, all these results indicate that EPSINOID2 protein abundance is most likely affected by several different mechanisms acting in parallel. *EPSINOID2* expression and translation take place in all root epidermal cells and EPSINOID2 protein seems to move from H cells into N cells. In N cells, EPSINOID2 protein synthesis appears to be regulated by miRNA844-3p and proteasome-dependent degradation ensures EPSINOID2 protein turnover which suggests that EPSINOID2 protein levels might be important for its function.

EPSINOID2 shows characteristics of a haploinsufficient gene

An additional indication for tight control of protein levels is that EPSINOID2 appears to be a haploinsufficient gene which means that one wild-type allele is not sufficient to fully compensate the loss of the *EPSINOID2* gene (Mohr 1932; Veitia 2002). Heterozygous loss-of-function mutants *id2-1* and *id2-3* show the same increased root hair density as the homozygous mutants suggesting a dominant mutation. Furthermore, *id2-2* which is a knock-down mutant showed characteristics of a semi-dominant mutation with a less severe root hair phenotype in heterozygotes (Freimuth 2019). This is further evidence that EPSINOID2 protein levels seem to be critical for its function.

It has been proposed that haploinsufficiency or dominance is often linked to molecular or cellular players that are involved in processes dependent on correct protein concentrations and are sensitive to altered dosages which could, for example, lead to lower amounts of the protein insufficient to fully execute its biological function or to stoichiometric changes of macromolecular complexes or cellular networks (reviewed in Veitia and Birchler 2010). There are many known examples for haploinsufficient genes in *Drosophila*, yeast or humans which have different effects (reviewed in Johnson et al. 2019). For example, human glucose transporter 1 (GLUT1) is necessary for glucose supply to the brain which depends on GLUT1 dosage and reducing the amount by half leads to abnormal brain function (Seidner et al. 1998). Another example is the formation of heterotypic collagen fibrils in humans which requires certain stoichiometries of collagen V molecules. Here, lack of one *COL5A1* allele results in the connective-tissue disorder Ehlers-Danlos syndrome (EDS) (reviewed in Veitia and Birchler 2010).

In plants, however, specifically in *Arabidopsis*, there are only few known examples of haploinsufficient genes and typically their expression is tightly regulated and resulting proteins

are components of regulatory or signaling pathways, transcription factors or part of multimeric complexes (reviewed in Navarro-Quiles et al. 2023). For example, the *Arabidopsis* haploinsufficient gene *SHOU4* negatively regulates cellulose synthesis by interfering with exocytosis of cellulose synthases (CESAs) in a dosage-dependent manner (Polko et al. 2018). Another example, *GL3*, is haploinsufficient in the *WER* paralog mutant *glabra1-2* (*gl1-2*) and promotes trichome formation in a dosage-dependent manner in response to jasmonates (Yoshida et al. 2009). These examples underline the diversity of processes and effects of haploinsufficient genes. The observed haploinsufficiency of *EPSINOID2* and its potential dose-dependent action is in line with the discovered complex post-transcriptional regulation.

The complex regulation and apparently crucial protein level of EPSINOID2 might also be the reason why exhaustive attempts to rescue the hairy mutant phenotype of *id2-1* failed in the past (Freimuth 2019). In this work, a partial complementation of *id2-3* could be achieved with miRNA-resistant *EPSINOID2* expressed under its endogenous promoter. This is again in line with the above-mentioned findings that *EPSINOID2* is tightly regulated by different mechanisms and that its protein levels appear to be critical for its proper function. This partial rescue further corroborates that *EPSINOID2* is the causative gene for the observed root hair phenotype.

4.5 EPSINOID2 interacts with PME38 and CCS52B *in vitro*

Extensive search for EPSINOID2 interactors utilizing IP-MS/MS, Y2H screen and pull-down-MS/MS analyses led to a list of 18 potential interactors of which 5 (ACT2, RSW10, PLDα1, PME38 and CCS52B/FZR3) were tested in pull-down assays. In these assays, interaction of EPSINOID2 was tested negative for ACT2 and possibly for RSW10 and gave inconclusive results for PLDα1. However, as stated before interactions should additionally be tested with C-terminally tagged EPSINOID2 since tags at the N-terminus could prevent an interaction.

A weak positive *in vitro* interaction was detected for EPSINOID2 and PME38 in three independent experiments. Pectin methylesterases (PMEs), pectin methylesterase inhibitors (PMEIs), and polygalacturonases (PGs) mediate the modification and degradation of pectins (reviewed in Levesque-Tremblay et al. 2015). Synthesis of pectins starts in the Golgi where they also get highly methylesterified and are subsequently secreted from the TGN into the cell wall (reviewed in Ridley et al. 2001). Amount and distribution of methylesterification of pectins affects the mechanical properties of the cell wall (Willats et al. 2001). PMEs are located in the cell wall where they de-esterify homogalacturonans (HG) which are a major component of

pectins within the plant cell wall (reviewed in Micheli 2001). Removal of methylesters from HGs can have two opposing consequences: the free carboxyl groups can be cross-linked to other carboxyl groups of HGs by calcium leading to formation of a pectin gel thereby stiffening the cell wall or these HGs are degraded by PGs leading to softening of the cell wall (reviewed in Wolf et al. 2009). There are two classes of PMEs: type I PMEs that contain an N-terminally pro domain and type II PMEs that lack this domain (reviewed in Micheli 2001). Both types can additionally possess a signal peptide for secretion or a transmembrane domain at their N-terminus (reviewed in Micheli 2001). It has been proposed that the pro region is involved in PME folding, subcellular targeting or acts as an autoinhibitor during endomembrane trafficking (reviewed in Micheli 2001). Composition and mechanics of the plant cell wall determine cell size and shape, and changes such as tip growth of root hairs and pollen tubes involves remodeling of the cell wall which includes deposition and modification of pectins (reviewed in Levesque-Tremblay et al. 2015). It has been proposed that in pollen tube tip growth PME activity is inhibited at the apex leading to enrichment of esterified pectins whereas in lateral, mature regions PMEs are active resulting in more rigid walls (reviewed in Levesque-Tremblay et al. 2015). For example, PMEI2 is specifically located at the apical wall of the pollen tube whereas pollen specific PPME1 is only located in the lateral pollen tube wall (Röckel et al. 2008). In root hair tip growth, it has been shown that the auxin-induced receptor-like kinase ERULUS (ERU) acts as a negative regulator of PME activity (Schoenaers et al. 2018). The type I *PME3* promoter is ubiquitously active in leaves and stems of adult plants as well as roots of seedlings and loss-of-function *pme3-1* dark-grown seedlings showed less root hairs (Guénin et al. 2011; 2017).

PME38 is a type I PME which does not contain a transmembrane domain or signal peptide and so far nothing is known about its expression or function (Dedeurwaerder et al. 2009). GFP-fusion of *PME38* genomic sequence expressed under an approximately 600 bp promoter region did not show any signal in the root. This indicates that either *PME38* is not expressed in roots of seedlings, the promoter region of 600 bp was not sufficient for *PME38* expression, or *PME38* expression levels are too low to detect. Attempts of cloning 1 kb promoter region failed so far but should be continued to rule out that parts of the promoter were missing for proper expression. Expression levels could also have been too low under the utilized normal growth conditions; hence, several stress conditions or hormonal treatments could be applied to check upregulation of *PME38* since involvement of several plant PMEs and their regulatory PMEIs in biotic and abiotic stress responses has been shown (reviewed in Coculo and Lionetti 2022). However, gene expression data from the eFP browser (Winter et al. 2007) suggest *PME38*

expression in non-hair cells in the same zone as *EPSINOID2*, albeit at low levels (Figure S 6) (Brady et al. 2007a; Cartwright et al. 2009). Additionally, at the end of this work two independent T-DNA insertion lines *pme38-1* (SALK_017776, insertion in 1st exon) and *pme38-2* (SALK_016872C, insertion in 3rd exon) were obtained and homozygous mutants were established. Although it is not clear if these mutants are full knock-outs, initial root hair analyses revealed that *pme38-1* exhibited an increased root hair density compared to wild type which was comparable with the phenotype of *id2-3* (data not shown; Sauer and Freimuth, unpublished) and double mutants were generated for future analyses. These data point towards PME38 activity in roots and a possible role in negatively affecting root hair formation although secondary effects cannot be ruled out yet. Further analyses are necessary to investigate EPSINOID2 and PME38 protein and genetic interaction as well as their function as possible negative regulators in root hair formation.

A very strong *in vitro* interaction was repeatedly detected for EPSINOID2 and CCS52B/FZR3. This putative interaction is line with the upregulation of EPSINOID2 upon MG132 treatment which indicates proteasomal degradation. As mentioned above CCS52B/FZR3 is a B-type plant ortholog of animal CDH1 which is an co-activator subunit of APC/C in the ubiquitin/proteasome-dependent degradation pathway (Cebolla et al. 1999). Additionally, the identified KEN box in EPSINOID2 C-terminus, which is recognized by CDH1/CCS52, is another indicator for interaction with CCS52B and furthermore proteasome-dependent degradation of EPSINOID2.

In *Arabidopsis*, there are two more CDH1 orthologs of the A-type CCS52A1/FZR2 and CCS52A2/FZR1 (Cebolla et al. 1999; Tarayre et al. 2004; Fülöp et al. 2005). CCS52 has been first identified in *Medicago sativa* root nodules as a regulator of transition from cell cycle in proliferating cells to differentiation and it was proposed that CCS52 promotes endoreduplication in the development of organs (Cebolla et al. 1999). In *Arabidopsis*, both CCS52A1 and CCS52A2 isoforms are involved in endoreduplication, shown for CCS52A1 in trichomes and CCS52A2 pavement cells, during leaf development (Lammens et al. 2008; Kasili et al. 2010). In roots, *CCS52A1* is expressed in the elongation zone where it regulates the onset of cell differentiation promoting cell cycle exit, demonstrated by longer roots of *ccs52a1* mutant compared to wild type, and *CCS52A2* is expressed in the meristem maintaining the stem cell niche and repressing mitosis in the quiescent center (QC), as *ccs52a2* mutants exhibit disorganized root meristems and strongly impaired root growth (Vanstraelen et al. 2009; Takahashi et al. 2013).

Further investigations are necessary to confirm EPSINOID2 interaction with CCS52B *in vivo* and analyses of *CCS52B* expression and action in the root epidermis should be performed to see whether this interaction occurs during root development or in other organs since *EPSINOID2* is also expressed in aboveground tissue such as trichomes. However, the interaction of EPSINOID2 and CCS52B appears to be in a regulatory context rather than in relation with the molecular mode of action of EPSINOID2. All the data from this work strongly suggest post-translational regulation of EPSINOID2 presumably by proteasome-dependent degradation.

4.6 Outlook

In this project EPSINOID2, a member of a novel short ENTH domain protein subfamily, was analyzed intensively regarding its function and regulation. It was clearly demonstrated that *EPSINOID2* acts downstream of epidermal cell patterning as a negative regulator in root hair formation placing the epidermal cell fate network upstream of *EPSINOID2. EPSINOID2* is expressed in all epidermal cells but EPSINOID2-GFP seems to move from H cells to N cells where it accumulates. It was also shown that it is controlled by a complex regulatory network in which it is regulated on different levels by different mechanisms. Post-transcriptionally, *EPSINOID2* protein synthesis appears to be regulated by miRNA844-3p and post-translationally, EPSINOID2 seems to be targeted for proteasomal degradation, presumably through interaction of CCS52B with the identified KEN box motif in EPSINOID2 C-terminus. In general, the data suggest that EPSINOID2 protein level is critical for its proper function. It remains an open question what the exact molecular mode of action of EPSINOID2 is, especially considering its ENTH domain and possible involvement in endomembrane trafficking. Investigations of the potential interaction with PME38 could give more insight into how EPSINOID2 executes its function in root hair formation. Generally, hypothetical modes of action could be that EPSINOID2 competitively inhibits vesicle formation by non-productive interactions with components of the vesicle generation machinery, it could sequester or mis-target cargo that is relevant for root hairs to form, or it could remove root hair forming components. This should be one part of future investigations. Another part would be to get a better understanding of EPSINOID2 regulation by either miRNA844-3p or protein degradation. A third part should involve further analyses about EPSINOID2 placement in the root hair developmental network which should include responses to hormonal signaling and environmental stresses since an involvement in root hair plasticity is highly likely.

5. References

Alejandro, S.; Höller, S.; Meier, B. and Peiter, E. (2020). Manganese in Plants: From Acquisition to Subcellular Allocation. *Frontiers in Plant Science* **11**: 300.

Ali, M. S. and Baek, K.-H. (2020). Protective Roles of Cytosolic and Plastidal Proteasomes on Abiotic Stress and Pathogen Invasion. *Plants (Basel, Switzerland)* **9**: 832.

Alonso, J. M.; Stepanova, A. N.; Leisse, T. J.; Kim, C. J.; Chen, H.; Shinn, P.; Stevenson, D. K.; Zimmerman, J.; Barajas, P.; Cheuk, R.; Gadrinab, C.; Heller, C. et al. (2003). Genome-wide insertional mutagenesis of *Arabidopsis thaliana*. *Science* **301**: 653–657.

Al-Saharin, R.; Hellmann, H. and Mooney, S. (2022). Plant E3 Ligases and Their Role in Abiotic Stress Response. *Cells* **11**: 890.

Aniento, F.; Sánchez de Medina Hernández, V.; Dagdas, Y.; Rojas-Pierce, M. and Russinova, E. (2022). Molecular mechanisms of endomembrane trafficking in plants. *The Plant Cell* **34**: 146–173.

Arribas-Hernández, L.; Kielpinski, L. J. and Brodersen, P. (2016). mRNA Decay of Most Arabidopsis miRNA Targets Requires Slicer Activity of AGO1. *Plant Physiology* **171**: 2620–2632.

Ashery, U.; Bielopolski, N.; Barak, B. and Yizhar, O. (2009). Friends and foes in synaptic transmission: the role of tomosyn in vesicle priming. *Trends in Neurosciences* **32**: 275–282.

Assaad, F. F.; Qiu, J.-L.; Youngs, H.; Ehrhardt, D.; Zimmerli, L.; Kalde, M.; Wanner, G.; Peck, S. C.; Edwards, H.; Ramonell, K.; Somerville, C. R. and Thordal-Christensen, H. (2004). The PEN1 syntaxin defines a novel cellular compartment upon fungal attack and is required for the timely assembly of papillae. *Molecular Biology of the Cell* **15**: 5118–5129.

Bae, S.; Park, J. and Kim, J.-S. (2014). Cas-OFFinder: a fast and versatile algorithm that searches for potential off-target sites of Cas9 RNA-guided endonucleases. *Bioinformatics* **30**: 1473–1475.

Balcerowicz, D.; Schoenaers, S. and Vissenberg, K. (2015). Cell Fate Determination and the Switch from Diffuse Growth to Planar Polarity in *Arabidopsis* Root Epidermal Cells. *Frontiers in Plant Science* **6**: 1163.

Baluska, F.; Salaj, J.; Mathur, J.; Braun, M.; Jasper, F.; Samaj, J.; Chua, N. H.; Barlow, P. W. and Volkmann, D. (2000). Root hair formation: F-actin-dependent tip growth is initiated

by local assembly of profilin-supported F-actin meshworks accumulated within expansin-enriched bulges. *Developmental Biology* **227**: 618–632.

Bari, R.; Datt Pant, B.; Stitt, M. and Scheible, W.-R. (2006). PHO2, MicroRNA399, and PHR1 Define a Phosphate-Signaling Pathway in Plants. *Plant Physiology* **141**: 988–999.

Barrera-Rojas, C. H.; Rocha, G. H. B.; Polverari, L.; Pinheiro Brito, D. A.; Batista, D. S.; Notini, M. M.; da Cruz, A. C. F.; Morea, E. G. O.; Sabatini, S.; Otoni, W. C. and Nogueira, F. T. S. (2020). miR156-targeted *SPL10* controls Arabidopsis root meristem activity and root-derived *de novo* shoot regeneration via cytokinin responses. *Journal of Experimental Botany* **71**: 934–950.

Bassham, D. C.; Brandizzi, F.; Otegui, M. S. and Sanderfoot, A. A. (2008). The secretory system of Arabidopsis. *The Arabidopsis Book* **6**: e0116.

Bates, T. R. and Lynch, J. P. (1996). Stimulation of root hair elongation in *Arabidopsis thaliana* by low phosphorus availability. *Plant, Cell & Environment* **19**: 529–538.

Bennett, M. J.; Marchant, A.; Green, H. G.; May, S. T.; Ward, S. P.; Millner, P. A.; Walker, A. R.; Schulz, B. and Feldmann, K. A. (1996). *Arabidopsis AUX1* Gene: A Permease-Like Regulator of Root Gravitropism. *Science* **273**: 948–950.

Berger, F.; Haseloff, J.; Schiefelbein, J. and Dolan, L. (1998a). Positional information in root epidermis is defined during embryogenesis and acts in domains with strict boundaries. *Current Biology* **8**: 421–430.

Berger, F.; Hung, C. Y.; Dolan, L. and Schiefelbein, J. (1998b). Control of cell division in the root epidermis of *Arabidopsis thaliana*. *Developmental Biology* **194**: 235–245.

Bernhardt, C.; Lee, M. M.; Gonzalez, A.; Zhang, F.; Lloyd, A. and Schiefelbein, J. (2003). The bHLH genes *GLABRA3 (GL3)* and *ENHANCER OF GLABRA3 (EGL3)* specify epidermal cell fate in the *Arabidopsis* root. *Development* **130**: 6431–6439.

Bernhardt, C.; Zhao, M.; Gonzalez, A.; Lloyd, A. and Schiefelbein, J. (2005). The bHLH genes *GL3* and *EGL3* participate in an intercellular regulatory circuit that controls cell patterning in the *Arabidopsis* root epidermis. *Development* **132**: 291–298.

Bibikova, T. N.; Jacob, T.; Dahse, I. and Gilroy, S. (1998). Localized changes in apoplastic and cytoplasmic pH are associated with root hair development in *Arabidopsis thaliana*. *Development* **125**: 2925–2934.

Birnbaum, K.; Shasha, D. E.; Wang, J. Y.; Jung, J. W.; Lambert, G. M.; Galbraith, D. W. and Benfey, P. N. (2003). A gene expression map of the *Arabidopsis* root. *Science* **302**: 1956–1960.

Blilou, I.; Frugier, F.; Folmer, S.; Serralbo, O.; Willemsen, V.; Wolkenfelt, H.; Eloy, N. B.; Ferreira, P. C. G.; Weisbeek, P. and Scheres, B. (2002). The *Arabidopsis HOBBIT* gene encodes a CDC27 homolog that links the plant cell cycle to progression of cell differentiation. *Genes & Development* **16**: 2566–2575.

Brady, S. M.; Orlando, D. A.; Lee, J.-Y.; Wang, J. Y.; Koch, J.; Dinneny, J. R.; Mace, D.; Ohler, U. and Benfey, P. N. (2007a). A high-resolution root spatiotemporal map reveals dominant expression patterns. *Science* **318**: 801–806.

Brady, S. M.; Song, S.; Dhugga, K. S.; Rafalski, J. A. and Benfey, P. N. (2007b). Combining expression and comparative evolutionary analysis. The *COBRA* gene family. *Plant Physiology* **143**: 172–187.

Brennecke, J.; Hipfner, D. R.; Stark, A.; Russell, R. B. and Cohen, S. M. (2003). *bantam* Encodes a Developmentally Regulated microRNA that Controls Cell Proliferation and Regulates the Proapoptotic Gene *hid* in *Drosophila*. *Cell* **113**: 25–36.

Bruex, A.; Kainkaryam, R. M.; Wieckowski, Y.; Kang, Y. H.; Bernhardt, C.; Xia, Y.; Zheng, X.; Wang, J. Y.; Lee, M. M.; Benfey, P.; Woolf, P. J. and Schiefelbein, J. (2012). A gene regulatory network for root epidermis cell differentiation in Arabidopsis. *PLoS Genetics* **8**: e1002446.

Buchanan, B. B. (Hg.) (2015). Biochemistry & Molecular Biology of Plants. 2. ed. Rockville, Md., Chichester: American Society of Plant Biologists; Wiley Blackwell.

Budak, H. and Akpinar, B. A. (2015). Plant miRNAs: biogenesis, organization and origins. *Functional & Integrative Genomics* **15**: 523–531.

Campanoni, P. and Blatt, M. R. (2007). Membrane trafficking and polar growth in root hairs and pollen tubes. *Journal of Experimental Botany* **58**: 65–74.

Canales, J.; Contreras-López, O.; Álvarez, J. M. and Gutiérrez, R. A. (2017). Nitrate induction of root hair density is mediated by TGA1/TGA4 and CPC transcription factors in *Arabidopsis thaliana*. *The Plant Journal* **92**: 305–316.

Carlsbecker, A.; Lee, J.-Y.; Roberts, C. J.; Dettmer, J.; Lehesranta, S.; Zhou, J.; Lindgren, O.; Moreno-Risueno, M. A.; Vatén, A.; Thitamadee, S.; Campilho, A.;

Sebastian, J. et al. (2010). Cell signalling by microRNA165/6 directs gene dose-dependent root cell fate. *Nature* **465**: 316–321.

Cartwright, D. A.; Brady, S. M.; Orlando, D. A.; Sturmfels, B. and Benfey, P. N. (2009). Reconstructing spatiotemporal gene expression data from partial observations. *Bioinformatics* **25**: 2581–2587.

Cebolla, A.; Vinardell, J. M.; Kiss, E.; Oláh, B.; Roudier, F.; Kondorosi, A. and Kondorosi, E. (1999). The mitotic inhibitor *ccs52* is required for endoreduplication and ploidy-dependent cell enlargement in plants. *The EMBO Journal* **18**: 4476–4484.

Chen, H.; Fre, S.; Slepnev, V. I.; Capua, M. R.; Takei, K.; Butler, M. H.; Di Fiore, P. P. and Camilli, P. de (1998). Epsin is an EH-domain-binding protein implicated in clathrin-mediated endocytosis. *Nature* **394**: 793–797.

Chidambaram, S.; Müllers, N.; Wiederhold, K.; Haucke, V. and Mollard, G. F. von (2004). Specific interaction between SNAREs and epsin N-terminal homology (ENTH) domains of epsin-related proteins in trans-Golgi network to endosome transport. *The Journal of Biological Chemistry* **279**: 4175–4179.

Chidambaram, S.; Zimmermann, J. and Mollard, G. F. von (2008). ENTH domain proteins are cargo adaptors for multiple SNARE proteins at the TGN endosome. *Journal of Cell Science* **121**: 329–338.

Cho, H.-T. and Cosgrove, D. J. (2002). Regulation of root hair initiation and expansin gene expression in Arabidopsis. *The Plant Cell* **14**: 3237–3253.

Coculo, D. and Lionetti, V. (2022). The Plant Invertase/Pectin Methylesterase Inhibitor Superfamily. *Frontiers in Plant Science* **13**: 863892.

Collins, C. A.; LaMontagne, E. D.; Anderson, J. C.; Ekanayake, G.; Clarke, A. S.; Bond, L. N.; Salamango, D. J.; Cornish, P. V.; Peck, S. C. and Heese, A. (2020). EPSIN1 Modulates the Plasma Membrane Abundance of FLAGELLIN SENSING2 for Effective Immune Responses. *Plant Physiology* **182**: 1762–1775.

Cooper, G. M. (2000). The Mechanism of Vesicular Transport. In: Cooper, G. M., (Hg.) The Cell: A Molecular Approach, 2nd edition. Sunderland (MA): Sinauer Associates.

Cormack, R. G. H. (1949). The development of root hairs in angiosperms. *The Botanical Review* **15**: 583–612.

Cosgrove, D. J. (2000). Loosening of plant cell walls by expansins. *Nature* **407**: 321–326.

Craene, J.-O. de; Ripp, R.; Lecompte, O.; Thompson, J. D.; Poch, O. and Friant, S. (2012). Evolutionary analysis of the ENTH/ANTH/VHS protein superfamily reveals a coevolution between membrane trafficking and metabolism. *BMC Genomics* **13**: 297.

Cui, X.; Wang, S.; Huang, Y.; Ding, X.; Wang, Z.; Zheng, L.; Bi, Y.; Ge, F.; Zhu, L.; Yuan, M.; Yalovsky, S. and Fu, Y. (2022). *Arabidopsis* SYP121 acts as an ROP2 effector in the regulation of root hair tip growth. *Molecular Plant* **15**: 1008–1023.

Curtiss, M.; Jones, C. and Babst, M. (2007). Efficient cargo sorting by ESCRT-I and the subsequent release of ESCRT-I from multivesicular bodies requires the subunit Mvb12. *Molecular Biology of the Cell* **18**: 636–645.

Dai, X.; Zhuang, Z. and Zhao, P. X. (2018). psRNATarget: a plant small RNA target analysis server (2017 release). *Nucleic Acids Research* **46**: W49-W54.

Daum, G.; Medzihradszky, A.; Suzaki, T. and Lohmann, J. U. (2014). A mechanistic framework for noncell autonomous stem cell induction in *Arabidopsis*. *Proceedings of the National Academy of Sciences of the United States of America* **111**: 14619–14624.

Dedeurwaerder, S.; Menu-Bouaouiche, L.; Mareck, A.; Lerouge, P. and Guerineau, F. (2009). Activity of an atypical *Arabidopsis thaliana* pectin methylesterase. *Planta* **229**: 311–321.

Denninger, P.; Reichelt, A.; Schmidt, V. A. F.; Mehlhorn, D. G.; Asseck, L. Y.; Stanley, C. E.; Keinath, N. F.; Evers, J.-F.; Grefen, C. and Grossmann, G. (2019). Distinct RopGEFs Successively Drive Polarization and Outgrowth of Root Hairs. *Current Biology* **29**: 1854-1865.e5.

Deslauriers, S. D. and Larsen, P. B. (2010). FERONIA Is a Key Modulator of Brassinosteroid and Ethylene Responsiveness in *Arabidopsis* Hypocotyls. *Molecular Plant* **3**: 626–640.

Dettmer, J.; Hong-Hermesdorf, A.; Stierhof, Y.-D. and Schumacher, K. (2006). Vacuolar H+-ATPase Activity Is Required for Endocytic and Secretory Trafficking in *Arabidopsis*. *The Plant Cell* **18**: 715–730.

Di Cristina, M.; Sessa, G.; Dolan, L.; Linstead, P.; Baima, S.; Ruberti, I. and Morelli, G. (1996). The *Arabidopsis* Athb-10 (GLABRA2) is an HD-Zip protein required for regulation of root hair development. *The Plant Journal* **10**: 393–402.

Dolan, L.; Janmaat, K.; Willemsen, V.; Linstead, P.; Poethig, S.; Roberts, K. and Scheres, B. (1993a). Cellular organisation of the *Arabidopsis thaliana* root. *Development* **119**: 71–84.

Dolan, L.; Janmaat, K.; Willemsen, V.; Linstead, P.; Poethig, S.; Roberts, K. and Scheres, B. (1993b). Cellular organisation of the Arabidopsis thaliana root. *Development (Cambridge, England)* **119**: 71–84.

Donaldson, J. G.; Finazzi, D. and Klausner, R. D. (1992). Brefeldin A inhibits Golgi membrane-catalysed exchange of guanine nucleotide onto ARF protein. *Nature* **360**: 350–352.

Dong, Q.; Hu, B. and Zhang, C. (2022). microRNAs and Their Roles in Plant Development. *Frontiers in Plant Science* **13**: 824240.

Drake, M. T.; Downs, M. A. and Traub, L. M. (2000). Epsin binds to clathrin by associating directly with the clathrin-terminal domain. Evidence for cooperative binding through two discrete sites. *The Journal of Biological Chemistry* **275**: 6479–6489.

Drake, M. T. and Traub, L. M. (2001). Interaction of two structurally distinct sequence types with the clathrin terminal domain beta-propeller. *The Journal of Biological Chemistry* **276**: 28700–28709.

Duan, Q.; Kita, D.; Li, C.; Cheung, A. Y. and Wu, H.-M. (2010). FERONIA receptor-like kinase regulates RHO GTPase signaling of root hair development. *Proceedings of the National Academy of Sciences of the United States of America* **107**: 17821–17826.

Duckett, C. M.; Grierson, C.; Linstead, P.; Schneider, K.; Lawson, E.; Dean, C.; Poethig, S. and Roberts, K. (1994). Clonal relationships and cell patterning in the root epidermis of *Arabidopsis*. *Development* **120**: 2465.

Duncan, M. C.; Costaguta, G. and Payne, G. S. (2003). Yeast epsin-related proteins required for Golgi-endosome traffic define a gamma-adaptin ear-binding motif. *Nature Cell Biology* **5**: 77–81.

Elmayan, T. and Vaucheret, H. (1996). Expression of single copies of a strongly expressed 35S transgene can be silenced post-transcriptionally. *The Plant Journal* **9**: 787–797.

Escobar-Restrepo, J.-M.; Huck, N.; Kessler, S.; Gagliardini, V.; Gheyselinck, J.; Yang, W.-C. and Grossniklaus, U. (2007). The FERONIA receptor-like kinase mediates male-female interactions during pollen tube reception. *Science* **317**: 656–660.

Fahlgren, N.; Howell, M. D.; Kasschau, K. D.; Chapman, E. J.; Sullivan, C. M.; Cumbie, J. S.; Givan, S. A.; Law, T. F.; Grant, S. R.; Dangl, J. L. and Carrington, J. C. (2007). High-throughput sequencing of *Arabidopsis* microRNAs: evidence for frequent birth and death of *MIRNA* genes. *PLoS One* **2**: e219.

Fan, H.; Quan, S.; Ye, Q.; Zhang, L.; Liu, W.; Zhu, N.; Zhang, X.; Ruan, W.; Yi, K.; Crawford, N. M. and Wang, Y. (2023). A molecular framework underlying low-nitrogen-induced early leaf senescence in *Arabidopsis thaliana*. *Molecular Plant* **16**: 756–774.

Fendrych, M.; Synek, L.; Pečenková, T.; Toupalová, H.; Cole, R.; Drdová, E.; Nebesářová, J.; Šedinová, M.; Hála, M.; Fowler, J. E. and Žárský, V. (2010). The *Arabidopsis* Exocyst Complex Is Involved in Cytokinesis and Cell Plate Maturation. *The Plant Cell* **22**: 3053–3065.

Feng, W.; Kita, D.; Peaucelle, A.; Cartwright, H. N.; Doan, V.; Duan, Q.; Liu, M.-C.; Maman, J.; Steinhorst, L.; Schmitz-Thom, I.; Yvon, R.; Kudla, J. et al. (2018). The FERONIA Receptor Kinase Maintains Cell-Wall Integrity during Salt Stress through Ca2+ Signaling. *Current Biology* **28**: 666-675.e5.

Feng, Y.; Hiwatashi, T.; Minamino, N.; Ebine, K. and Ueda, T. (2022). Membrane trafficking functions of the ANTH/ENTH/VHS domain-containing proteins in plants. *FEBS Letters* **596**: 2256–2268.

Floris, M.; Mahgoub, H.; Lanet, E.; Robaglia, C. and Menand, B. (2009). Post-transcriptional regulation of gene expression in plants during abiotic stress. *International Journal of Molecular Sciences* **10**: 3168–3185.

Foley, S. W.; Gosai, S. J.; Wang, D.; Selamoglu, N.; Sollitti, A. C.; Köster, T.; Steffen, A.; Lyons, E.; Daldal, F.; Garcia, B. A.; Staiger, D.; Deal, R. B. et al. (2017). A Global View of RNA-Protein Interactions Identifies Post-transcriptional Regulators of Root Hair Cell Fate. *Developmental Cell* **41**: 204-220.e5.

Ford, M. G.; Pearse, B. M.; Higgins, M. K.; Vallis, Y.; Owen, D. J.; Gibson, A.; Hopkins, C. R.; Evans, P. R. and McMahon, H. T. (2001). Simultaneous binding of PtdIns(4,5)P2 and clathrin by AP180 in the nucleation of clathrin lattices on membranes. *Science* **291**: 1051–1055.

Ford, M. G. J.; Mills, I. G.; Peter, B. J.; Vallis, Y.; Praefcke, G. J. K.; Evans, P. R. and McMahon, H. T. (2002). Curvature of clathrin-coated pits driven by epsin. *Nature* **419**: 361–366.

Foreman, J.; Demidchik, V.; Bothwell, J. H. F.; Mylona, P.; Miedema, H.; Torres, M. A.; Linstead, P.; Costa, S.; Brownlee, C.; Jones, J. D. G.; Davies, J. M. and Dolan, L. (2003). Reactive oxygen species produced by NADPH oxidase regulate plant cell growth. *Nature* **422**: 442–446.

Freimuth, N. (2015). Funktionelle Charakterisierung von EPSIN-Homologen mit abweichenden C-Terminus in *Arabidopsis thaliana*. Bachelorarbeit. Universität Potsdam, Potsdam.

Freimuth, N. (2019). Functional analysis of the short ENTH domain protein EPSINOID2 and its potential role in root hair generation in *Arabidopsis thaliana*. Master thesis. Universität Potsdam, Potsdam.

Fujii, H.; Chiou, T.-J.; Lin, S.-I.; Aung, K. and Zhu, J.-K. (2005). A miRNA Involved in Phosphate-Starvation Response in *Arabidopsis*. *Current Biology* **15**: 2038–2043.

Fujimoto, M.; Arimura, S.; Ueda, T.; Takanashi, H.; Hayashi, Y.; Nakano, A. and Tsutsumi, N. (2010). *Arabidopsis* dynamin-related proteins DRP2B and DRP1A participate together in clathrin-coated vesicle formation during endocytosis. *Proceedings of the National Academy of Sciences of the United States of America* **107**: 6094.

Fülöp, K.; Tarayre, S.; Kelemen, Z.; Horváth, G.; Kevei, Z.; Nikovics, K.; Bakó, L.; Brown, S.; Kondorosi, A. and Kondorosi, E. (2005). Arabidopsis Anaphase-Promoting Complexes: Multiple Activators and Wide Range of Substrates Might Keep APC Perpetually Busy. *Cell Cycle* **4**: 4084–4092.

Galway, M. E.; Masucci, J. D.; Lloyd, A. M.; Walbot, V.; Davis, R. W. and Schiefelbein, J. W. (1994). The *TTG* gene is required to specify epidermal cell fate and cell patterning in the *Arabidopsis* root. *Developmental Biology* **166**: 740–754.

Gautam, V.; Singh, A.; Verma, S.; Kumar, A.; Kumar, P.; Mahima; **Singh, S.; Mishra, V. and Sarkar, A. K.** (2017). Role of miRNAs in root development of model plant *Arabidopsis thaliana*. *Indian Journal of Plant Physiology* **22**: 382–392.

Geldner, N.; Dénervaud-Tendon, V.; Hyman, D. L.; Mayer, U.; Stierhof, Y.-D. and Chory, J. (2009). Rapid, combinatorial analysis of membrane compartments in intact plants with a multicolor marker set. *The Plant Journal* **59**: 169–178.

Gifford, M. L.; Dean, A.; Gutierrez, R. A.; Coruzzi, G. M. and Birnbaum, K. D. (2008). Cell-specific nitrogen responses mediate developmental plasticity. *Proceedings of the National Academy of Sciences of the United States of America* **105**: 803–808.

Gladycheva, S. E.; Lam, A. D.; Liu, J.; D'Andrea-Merrins, M.; Yizhar, O.; Lentz, S. I.; Ashery, U.; Ernst, S. A. and Stuenkel, E. L. (2007). Receptor-mediated Regulation of Tomosyn-Syntaxin 1A Interactions in Bovine Adrenal Chromaffin Cells*. *The Journal of Biological Chemistry* **282**: 22887–22899.

Gleisner, M.; Kroppen, B.; Fricke, C.; Teske, N.; Kliesch, T.-T.; Janshoff, A.; Meinecke, M. and Steinem, C. (2016). Epsin N-terminal Homology Domain (ENTH) Activity as a Function of Membrane Tension. *The Journal of Biological Chemistry* **291**: 19953–19961.

Grebe, M.; Friml, J.; Swarup, R.; Ljung, K.; Sandberg, G.; Terlou, M.; Palme, K.; Bennett, M. J. and Scheres, B. (2002). Cell Polarity Signaling in *Arabidopsis* Involves a BFA-Sensitive Auxin Influx Pathway. *Current Biology* **12**: 329–334.

Grefen, C.; Donald, N.; Hashimoto, K.; Kudla, J.; Schumacher, K. and Blatt, M. R. (2010). A ubiquitin-10 promoter-based vector set for fluorescent protein tagging facilitates temporal stability and native protein distribution in transient and stable expression studies. *The Plant Journal* **64**: 355–365.

Grierson, C.; Nielsen, E.; Ketelaarc, T. and Schiefelbein, J. (2014). Root Hairs. *The Arabidopsis Book* **12**.

Guan, X.-Y.; Li, Q.-J.; Shan, C.-M.; Wang, S.; Mao, Y.-B.; Wang, L.-J. and Chen, X.-Y. (2008). The HD-Zip IV gene *GaHOX1* from cotton is a functional homologue of the *Arabidopsis GLABRA2*. *Physiologia Plantarum* **134**: 174–182.

Guénin, S.; Hardouin, J.; Paynel, F.; Müller, K.; Mongelard, G.; Driouich, A.; Lerouge, P.; Kermode, A. R.; Lehner, A.; Mollet, J.-C.; Pelloux, J.; Gutierrez, L. et al. (2017). AtPME3, a ubiquitous cell wall pectin methylesterase of *Arabidopsis thaliana*, alters the metabolism of cruciferin seed storage proteins during post-germinative growth of seedlings. *Journal of Experimental Botany* **68**: 1083–1095.

Guénin, S.; Mareck, A.; Rayon, C.; Lamour, R.; Assoumou Ndong, Y.; Domon, J.-M.; Sénéchal, F.; Fournet, F.; Jamet, E.; Canut, H.; Percoco, G.; Mouille, G. et al. (2011). Identification of pectin methylesterase 3 as a basic pectin methylesterase isoform involved in adventitious rooting in *Arabidopsis thaliana*. *New Phytologist* **192**: 114–126.

Guerra, D.; Crosatti, C.; Khoshro, H. H.; Mastrangelo, A. M.; Mica, E. and Mazzucotelli, E. (2015). Post-transcriptional and post-translational regulations of drought and heat response in plants: a spider's web of mechanisms. *Frontiers in Plant Science* **6**: 57.

Guo, H. and Yin, Y. (2019). Measuring Protein Half-life in *Arabidopsis thaliana*. *Bio-Protocol* **9**: e3318.

Haas, A. L.; Warms, J. V.; Hershko, A. and Rose, I. A. (1982). Ubiquitin-activating enzyme. Mechanism and role in protein-ubiquitin conjugation. *The Journal of Biological Chemistry* **257**: 2543–2548.

Haruta, M.; Sabat, G.; Stecker, K.; Minkoff, B. B. and Sussman, M. R. (2014). A peptide hormone and its receptor protein kinase regulate plant cell expansion. *Science* **343**: 408–411.

He, L. and Hannon, G. J. (2004). MicroRNAs: small RNAs with a big role in gene regulation. *Nature Reviews Genetics* **5**: 522–531.

Heberle, H.; Meirelles, G. V.; da Silva, F. R.; Telles, G. P. and Minghim, R. (2015). InteractiVenn: a web-based tool for the analysis of sets through Venn diagrams. *BMC Bioinformatics* **16**: 169.

Heider, M. R. and Munson, M. (2012). Exorcising the Exocyst Complex. *Traffic* **13**: 898–907.

Heinze, L.; Freimuth, N.; Rößling, A.-K.; Hahnke, R.; Riebschläger, S.; Fröhlich, A.; Sampathkumar, A.; McFarlane, H. E. and Sauer, M. (2020). EPSIN1 and MTV1 define functionally overlapping but molecularly distinct trans-Golgi network subdomains in *Arabidopsis*. *Proceedings of the National Academy of Sciences of the United States of America* **117**: 25880–25889.

Helms, J. B. and Rothman, J. E. (1992). Inhibition by brefeldin A of a Golgi membrane enzyme that catalyses exchange of guanine nucleotide bound to ARF. *Nature* **360**: 352–354.

Hershko, A. and Ciechanover, A. (1998). The ubiquitin system. *Annual Review of Biochemistry* **67**: 425–479.

Hershko, A.; Heller, H.; Elias, S. and Ciechanover, A. (1983). Components of ubiquitin-protein ligase system. Resolution, affinity purification, and role in protein breakdown. *The Journal of Biological Chemistry* **258**: 8206–8214.

Hirano, T.; Ebine, K.; Ueda, T.; Higaki, T.; Nakayama, T.; Konno, H.; Takigawa-Imamura, H. and Sato, M. H. (2020). The SYP123-VAMP727 SNARE complex is involved in the delivery of inner cell wall components to the root hair shank in Arabidopsis. *bioRxiv*: 2020.12.28.424500.

Hirst, J.; Miller, S. E.; Taylor, M. J.; Mollard, G. F. von and Robinson, M. S. (2004). EpsinR is an adaptor for the SNARE protein Vti1b. *Molecular Biology of the Cell* **15**: 5593–5602.

Hirst, J.; Motley, A.; Harasaki, K.; Peak Chew, S. Y. and Robinson, M. S. (2003). EpsinR: an ENTH domain-containing protein that interacts with AP-1. *Molecular Biology of the Cell* **14**: 625–641.

Holstein, S. E. H. and Oliviusson, P. (2005). Sequence analysis of *Arabidopsis thaliana* E/ANTH-domain-containing proteins: membrane tethers of the clathrin-dependent vesicle budding machinery. *Protoplasma* **226**: 13–21.

Hung, C. Y.; Lin, Y.; Zhang, M.; Pollock, S.; Marks, M. D. and Schiefelbein, J. (1998). A common position-dependent mechanism controls cell-type patterning and *GLABRA2* regulation in the root and hypocotyl epidermis of Arabidopsis. *Plant Physiology* **117**: 73–84.

Hurley, J. H. and Emr, S. D. (2006). THE ESCRT COMPLEXES: Structure and Mechanism of a Membrane-Trafficking Network. *Annual Review of Biophysics and Biomolecular Structure* **35**: 277–298.

Ichikawa, M.; Hirano, T.; Enami, K.; Fuselier, T.; Kato, N.; Kwon, C.; Voigt, B.; Schulze-Lefert, P.; Baluška, F. and Sato, M. H. (2014). Syntaxin of plant proteins SYP123 and SYP132 mediate root hair tip growth in *Arabidopsis thaliana*. *Plant & Cell Physiology* **55**: 790–800.

Itoh, T.; Koshiba, S.; Kigawa, T.; Kikuchi, A.; Yokoyama, S. and Takenawa, T. (2001). Role of the ENTH domain in phosphatidylinositol-4,5-bisphosphate binding and endocytosis. *Science* **291**: 1047–1051.

Johnson, A. F.; Nguyen, H. T. and Veitia, R. A. (2019). Causes and effects of haploinsufficiency. *Biological Reviews* **94**: 1774–1785.

Jones, A. R.; Kramer, E. M.; Knox, K.; Swarup, R.; Bennett, M. J.; Lazarus, C. M.; Leyser, H. M. O. and Grierson, C. S. (2009). Auxin transport through non-hair cells sustains root-hair development. *Nature Cell Biology* **11**: 78–84.

Jones, M. A.; Shen, J.-J.; Fu, Y.; Li, H.; Yang, Z. and Grierson, C. S. (2002). The Arabidopsis Rop2 GTPase is a positive regulator of both root hair initiation and tip growth. *The Plant Cell* **14**: 763–776.

Kalthoff, C.; Alves, J.; Urbanke, C.; Knorr, R. and Ungewickell, E. J. (2002a). Unusual structural organization of the endocytic proteins AP180 and epsin 1. *The Journal of Biological Chemistry* **277**: 8209–8216.

Kalthoff, C.; Groos, S.; Kohl, R.; Mahrhold, S. and Ungewickell, E. J. (2002b). Clint: a novel clathrin-binding ENTH-domain protein at the Golgi. *Molecular Biology of the Cell* **13**: 4060–4073.

Kaneda, M.; van Oostende-Triplet, C.; Chebli, Y.; Testerink, C.; Bednarek, S. Y. and Geitmann, A. (2019). Plant AP180 N-Terminal Homolog Proteins Are Involved in Clathrin-Dependent Endocytosis during Pollen Tube Growth in *Arabidopsis thaliana*. *Plant & Cell Physiology* **60**: 1316–1330.

Kang, Y. H.; Song, S.-K.; Schiefelbein, J. and Lee, M. M. (2013). Nuclear trapping controls the position-dependent localization of CAPRICE in the root epidermis of Arabidopsis. *Plant Physiology* **163**: 193–204.

Karas, B.; Amyot, L.; Johansen, C.; Sato, S.; Tabata, S.; Kawaguchi, M. and Szczyglowski, K. (2009). Conservation of *lotus* and Arabidopsis basic helix-loop-helix proteins reveals new players in root hair development. *Plant Physiology* **151**: 1175–1185.

Kasili, R.; Walker, J. D.; Simmons, L. A.; Zhou, J.; Veylder, L. de and Larkin, J. C. (2010). SIAMESE cooperates with the CDH1-like protein CCS52A1 to establish endoreplication in *Arabidopsis thaliana* trichomes. *Genetics* **185**: 257–268.

Katzmann, D. J.; Stefan, C. J.; Babst, M. and Emr, S. D. (2003). Vps27 recruits ESCRT machinery to endosomes during MVB sorting. *The Journal of Cell Biology* **162**: 413–423.

Kay, B. K.; Yamabhai, M.; Wendland, B. and Emr, S. D. (1999). Identification of a novel domain shared by putative components of the endocytic and cytoskeletal machinery. *Protein Science* **8**: 435–438.

Kevei, Z.; Baloban, M.; Da Ines, O.; Tiricz, H.; Kroll, A.; Regulski, K.; Mergaert, P. and Kondorosi, E. (2011). Conserved CDC20 cell cycle functions are carried out by two of the five isoforms in *Arabidopsis thaliana*. *PLoS One* **6**: e20618.

Kieber, J. J.; Rothenberg, M.; Roman, G.; Feldmann, K. A. and Ecker, J. R. (1993). *CTR1*, a negative regulator of the ethylene response pathway in Arabidopsis, encodes a member of the raf family of protein kinases. *Cell* **72**: 427–441.

Kim, Y. J.; Zheng, B.; Yu, Y.; Won, S. Y.; Mo, B. and Chen, X. (2011). The role of Mediator in small and long noncoding RNA production in *Arabidopsis thaliana*. *The EMBO Journal* **30**: 814–822.

Kim, Y.-J. and Jung, K.-H. (2023). WD40-domain protein GORI is an integrative scaffold that is required for pollen tube growth in rice. *Plant Signaling & Behavior* **18**: 2082678.

Kim, Y.-J.; Kim, M.-H.; Hong, W.-J.; Moon, S.; Kim, E.-J.; Silva, J.; Lee, J.; Lee, S.; Kim, S. T.; Park, S. K. and Jung, K.-H. (2021). GORI, encoding the WD40 domain protein, is required for pollen tube germination and elongation in rice. *The Plant Journal* **105**: 1645–1664.

Kirchhausen, T. (1993). Coated pits and coated vesicles — sorting it all out. *Current Opinion in Structural Biology* **3**: 182–188.

Kirchhausen, T.; Bonifacino, J. S. and Riezman, H. (1997). Linking cargo to vesicle formation. Receptor tail interactions with coat proteins. *Current Opinion in Cell Biology* **9**: 488–495.

Kirik, V.; Simon, M.; Huelskamp, M. and Schiefelbein, J. (2004). The *ENHANCER OF TRY AND CPC1* gene acts redundantly with *TRIPTYCHON* and *CAPRICE* in trichome and root hair cell patterning in *Arabidopsis*. *Developmental Biology* **268**: 506–513.

Kurata, T.; Ishida, T.; Kawabata-Awai, C.; Noguchi, M.; Hattori, S.; Sano, R.; Nagasaka, R.; Tominaga, R.; Koshino-Kimura, Y.; Kato, T.; Sato, S.; Tabata, S. et al. (2005). Cell-to-cell movement of the CAPRICE protein in *Arabidopsis* root epidermal cell differentiation. *Development* **132**: 5387–5398.

Kurepa, J. and Smalle, J. A. (2008). Structure, function and regulation of plant proteasomes. *Biochimie* **90**: 324–335.

Kwak, S.-H. and Schiefelbein, J. (2007). The role of the SCRAMBLED receptor-like kinase in patterning the *Arabidopsis* root epidermis. *Developmental Biology* **302**: 118–131.

Kwak, S.-H. and Schiefelbein, J. (2008). A feedback mechanism controlling SCRAMBLED receptor accumulation and cell-type pattern in *Arabidopsis*. *Current Biology* **18**: 1949–1954.

Kwak, S.-H.; Shen, R. and Schiefelbein, J. (2005). Positional signaling mediated by a receptor-like kinase in *Arabidopsis*. *Science* **307**: 1111–1113.

Kweon, D.-H.; Shin, Y.-K.; Shin, J. Y.; Lee, J.-H.; Lee, J.-B.; Seo, J.-H. and Kim, Y. S. (2006). Membrane topology of helix 0 of the Epsin N-terminal homology domain. *Molecules and Cells* **21**: 428–435.

Labun, K.; Montague, T. G.; Krause, M.; Torres Cleuren, Y. N.; Tjeldnes, H. and Valen, E. (2019). CHOPCHOP v3: expanding the CRISPR web toolbox beyond genome editing. *Nucleic Acids Research* **47**: W171-W174.

Lagos-Quintana, M.; Rauhut, R.; Lendeckel, W. and Tuschl, T. (2001). Identification of novel genes coding for small expressed RNAs. *Science* **294**: 853–858.

Lammens, T.; Boudolf, V.; Kheibarshekan, L.; Zalmas, L. P.; Gaamouche, T.; Maes, S.; Vanstraelen, M.; Kondorosi, E.; La Thangue, N. B.; Govaerts, W.; Inzé, D. and Veylder, L. de (2008). Atypical E2F activity restrains APC/CCCS52A2 function obligatory for endocycle onset. *Proceedings of the National Academy of Sciences of the United States of America* **105**: 14721–14726.

Lampropoulos, A.; Sutikovic, Z.; Wenzl, C.; Maegele, I.; Lohmann, J. U. and Forner, J. (2013). GreenGate---a novel, versatile, and efficient cloning system for plant transgenesis. *PLoS One* **8**: e83043.

Larkin, J. C.; Oppenheimer, D. G.; Lloyd, A. M.; Paparozzi, E. T. and Marks, M. D. (1994). Roles of the *GLABROUS1* and *TRANSPARENT TESTA GLABRA* Genes in Arabidopsis Trichome Development. *The Plant Cell* **6**: 1065–1076.

Larson, E. R.; Domozych, D. S. and Tierney, M. L. (2014). SNARE VTI13 plays a unique role in endosomal trafficking pathways associated with the vacuole and is essential for cell wall organization and root hair growth in arabidopsis. *Annals of Botany* **114**: 1147–1159.

Lauber, M. H.; Waizenegger, I.; Steinmann, T.; Schwarz, H.; Mayer, U.; Hwang, I.; Lukowitz, W. and Jürgens, G. (1997). The *Arabidopsis* KNOLLE Protein Is a Cytokinesis-specific Syntaxin. *The Journal of Cell Biology* **139**: 1485–1493.

Le Clainche, C.; Pauly, B. S.; Zhang, C. X.; Engqvist-Goldstein, Å. E. Y.; Cunningham, K. and Drubin, D. G. (2007). A Hip1R–cortactin complex negatively regulates actin assembly associated with endocytosis. *The EMBO Journal* **26**: 1199–1210.

Leavitt, R. G. (1904). Trichomes of the root in vascular cryptogams and angiosperms. *Proceedings of the Boston Society of Natural History* **31**: 273–313.

Lee, G.-J.; Kim, H.; Kang, H.; Jang, M.; Lee, D. W.; Lee, S. and Hwang, I. (2007). EpsinR2 interacts with clathrin, adaptor protein-3, AtVTI12, and phosphatidylinositol-3-phosphate. Implications for EpsinR2 function in protein trafficking in plant cells. *Plant Physiology* **143**: 1561–1575.

Lee, H. J.; Park, Y. J.; Kwak, K. J.; Kim, D.; Park, J. H.; Lim, J. Y.; Shin, C.; Yang, K.-Y. and Kang, H. (2015). MicroRNA844-Guided Downregulation of Cytidinephosphate Diacylglycerol Synthase3 (CDS3) mRNA Affects the Response of *Arabidopsis thaliana* to Bacteria and Fungi. *Molecular Plant-Microbe Interactions* **28**: 892–900.

Lee, M. M. and Schiefelbein, J. (1999). WEREWOLF, a MYB-Related Protein in *Arabidopsis*, Is a Position-Dependent Regulator of Epidermal Cell Patterning. *Cell* **99**: 473–483.

Lee, M. M. and Schiefelbein, J. (2002). Cell Pattern in the Arabidopsis Root Epidermis Determined by Lateral Inhibition with Feedback. *The Plant Cell* **14**: 611–618.

Lee, Y.; Kim, M.; Han, J.; Yeom, K.-H.; Lee, S.; Baek, S. H. and Kim, V. N. (2004). MicroRNA genes are transcribed by RNA polymerase II. *The EMBO Journal* **23**: 4051–4060.

Legendre-Guillemin, V.; Wasiak, S.; Hussain, N. K.; Angers, A. and McPherson, P. S. (2004). ENTH/ANTH proteins and clathrin-mediated membrane budding. *Journal of Cell Science* **117**: 9–18.

Levesque-Tremblay, G.; Pelloux, J.; Braybrook, S. A. and Müller, K. (2015). Tuning of pectin methylesterification: consequences for cell wall biomechanics and development. *Planta* **242**: 791–811.

Li, B.; Li, Y.; Liu, F.; Tan, X.; Rui, Q.; Tong, Y.; Qiao, L.; Gao, R.; Li, G.; Shi, R.; Li, Y. and Bao, Y. (2019). Overexpressed Tomosyn Binds Syntaxins and Blocks Secretion during Pollen Development1. *Plant Physiology* **181**: 1114–1126.

Li, H.; Luo, N.; Wang, W.; Liu, Z.; Chen, J.; Zhao, L.; Tan, L.; Wang, C.; Qin, Y.; Li, C.; Xu, T. and Yang, Z. (2018). The REN4 rheostat dynamically coordinates the apical and lateral domains of *Arabidopsis* pollen tubes. *Nature Communications* **9**: 2573.

Lin, Q.; Ohashi, Y.; Kato, M.; Tsuge, T.; Gu, H.; Qu, L.-J. and Aoyama, T. (2015). GLABRA2 Directly Suppresses Basic Helix-Loop-Helix Transcription Factor Genes with Diverse Functions in Root Hair Development. *The Plant Cell* **27**: 2894–2906.

Lin, Q.; Zhang, Z.; Wu, F.; Feng, M.; Sun, Y.; Chen, W.; Cheng, Z.; Zhang, X.; Ren, Y.; Lei, C.; Zhu, S.; Wang, J. et al. (2020). The APC/CTE E3 Ubiquitin Ligase Complex Mediates the Antagonistic Regulation of Root Growth and Tillering by ABA and GA. *The Plant Cell* **32**: 1973–1987.

Lin, Y. and Schiefelbein, J. (2001). Embryonic control of epidermal cell patterning in the root and hypocotyl of *Arabidopsis*. *Development* **128**: 3697–3705.

López-Bucio, J.; Cruz-Ramírez, A. and Herrera-Estrella, L. (2003). The role of nutrient availability in regulating root architecture. *Current Opinion in Plant Biology* **6**: 280–287.

Ma, Z.; Bielenberg, D. G.; Brown, K. M. and Lynch, J. P. (2001). Regulation of root hair density by phosphorus availability in *Arabidopsis thaliana*. *Plant, Cell & Environment* **24**: 459–467.

Mallory, A. C.; Bartel, D. P. and Bartel, B. (2005). MicroRNA-Directed Regulation of Arabidopsis *AUXIN RESPONSE FACTOR17* Is Essential for Proper Development and Modulates Expression of Early Auxin Response Genes. *The Plant Cell* **17**: 1360–1375.

Marco, C. F.; Skopelitis, D. S. and Timmermans, M. C. P. (2019). In Situ Localization of Small RNAs in Plants. In: de Folter, S., (eds) Plant MicroRNAs: Methods and Protocols. vol 1932: 159–173. New York, NY: Humana Press.

Mason, K.; LaMontagne-Mueller, E.; Sauer, M. and Heese, A. (2023). Arabidopsis clathrin adaptor EPSIN1 but not MODIFIED TRANSPORT TO THE VACOULE1 contributes to effective plant immunity against pathogenic *Pseudomonas* bacteria. *Plant Signaling & Behavior* **18**: 2163337.

Masucci, J. D.; Rerie, W. G.; Foreman, D. R.; Zhang, M.; Galway, M. E.; Marks, M. D. and Schiefelbein, J. W. (1996). The homeobox gene *GLABRA2* is required for position-dependent cell differentiation in the root epidermis of *Arabidopsis thaliana*. *Development* **122**: 1253–1260.

Masucci, J. D. and Schiefelbein, J. W. (1994). The *rhd6* Mutation of *Arabidopsis thaliana* Alters Root-Hair Initiation through an Auxin- and Ethylene-Associated Process. *Plant Physiology* **106**: 1335–1346.

Masucci, J. D. and Schiefelbein, J. W. (1996). Hormones act downstream of *TTG* and *GL2* to promote root hair outgrowth during epidermis development in the Arabidopsis root. *The Plant Cell* **8**: 1505–1517.

Menand, B.; Yi, K.; Jouannic, S.; Hoffmann, L.; Ryan, E.; Linstead, P.; Schaefer, D. G. and Dolan, L. (2007). An ancient mechanism controls the development of cells with a rooting function in land plants. *Science* **316**: 1477–1480.

Mendrinna, A. and Persson, S. (2015). Root hair growth: it's a one way street. *F1000Prime Peports* **7**: 23.

Micheli, F. (2001). Pectin methylesterases: cell wall enzymes with important roles in plant physiology. *Trends in Plant Science* **6**: 414–419.

Miller, S. E.; Collins, B. M.; McCoy, A. J.; Robinson, M. S. and Owen, D. J. (2007). A SNARE-adaptor interaction is a new mode of cargo recognition in clathrin-coated vesicles. *Nature* **450**: 570–574.

Mills, I. G.; Praefcke, G. J. K.; Vallis, Y.; Peter, B. J.; Olesen, L. E.; Gallop, J. L.; Butler, P. J. G.; Evans, P. R. and McMahon, H. T. (2003). EpsinR. An AP1/clathrin interacting protein involved in vesicle trafficking. *The Journal of Cell Biology* **160**: 213–222.

Mohr, O. L. (1932). On the potency of mutant genes and wild-type allelomorphs. *Proceedings of the 6th International Congress of Genetics* **1**: 190–212.

Molendijk, A. J.; Bischoff, F.; Rajendrakumar, C. S.; Friml, J.; Braun, M.; Gilroy, S. and Palme, K. (2001). *Arabidopsis thaliana* Rop GTPases are localized to tips of root hairs and control polar growth. *The EMBO Journal* **20**: 2779–2788.

Müller, M. and Schmidt, W. (2004). Environmentally Induced Plasticity of Root Hair Development in Arabidopsis. *Plant Physiology* **134**: 409–419.

Muro, K.; Matsuura-Tokita, K.; Tsukamoto, R.; Kanaoka, M. M.; Ebine, K.; Higashiyama, T.; Nakano, A. and Ueda, T. (2018). ANTH domain-containing proteins are required for the pollen tube plasma membrane integrity via recycling ANXUR kinases. *Communications Biology* **1**: 152.

Nagano, M.; Toshima, J. Y. and Toshima, J. (2023). Chapter 14 - Membrane shaping for clathrin-coated pits and endocytosis. In: Suetsugu, S., (Ed.) Plasma Membrane Shaping: 205–218: Academic Press.

Naito, Y.; Hino, K.; Bono, H. and Ui-Tei, K. (2015). CRISPRdirect: software for designing CRISPR/Cas guide RNA with reduced off-target sites. *Bioinformatics* **31**: 1120–1123.

Nakagawa, T.; Suzuki, T.; Murata, S.; Nakamura, S.; Hino, T.; Maeo, K.; Tabata, R.; Kawai, T.; Tanaka, K.; Niwa, Y.; Watanabe, Y.; Nakamura, K. et al. (2007). Improved Gateway binary vectors. High-performance vectors for creation of fusion constructs in transgenic analysis of plants. *Bioscience, Biotechnology, and Biochemistry* **71**: 2095–2100.

Napoli, C.; Lemieux, C. and Jorgensen, R. (1990). Introduction of a Chimeric Chalcone Synthase Gene into Petunia Results in Reversible Co-Suppression of Homologous Genes in trans. *The Plant Cell* **2**: 279–289.

Navarro, L.; Dunoyer, P.; Jay, F.; Arnold, B.; Dharmasiri, N.; Estelle, M.; Voinnet, O. and Jones, J. D. G. (2006). A Plant miRNA Contributes to Antibacterial Resistance by Repressing Auxin Signaling. *Science* **312**: 436–439.

Navarro-Quiles, C.; Lup, S. D.; Muñoz-Nortes, T.; Candela, H. and Micol, J. L. (2023). The genetic and molecular basis of haploinsufficiency in flowering plants. *Trends in Plant Science*.

Nebenführ, A.; Ritzenthaler, C. and Robinson, D. G. (2002). Brefeldin A: deciphering an enigmatic inhibitor of secretion. *Plant Physiology* **130**: 1102–1108.

Nguyen, H. H.; Lee, M. H.; Song, K.; Ahn, G.; Lee, J. and Hwang, I. (2018). The A/ENTH Domain-Containing Protein AtECA4 Is an Adaptor Protein Involved in Cargo Recycling from the trans-Golgi Network/Early Endosome to the Plasma Membrane. *Molecular Plant* **11**: 568–583.

Ohmagari, M.; Kono, Y. and Tominaga, R. (2020). Effect of phosphate starvation on *CAPRICE* homolog gene expression in the root of *Arabidopsis*. *Plant Biotechnology* **37**: 349–352.

Omidbakhshfard, M. A.; Omranian, N.; Ahmadi, F. S.; Nikoloski, Z. and Mueller-Roeber, B. (2012). Effect of salt stress on genes encoding translation-associated proteins in Arabidopsis thaliana. *Plant Signaling & Behavior* **7**: 1095–1102.

Parizotto, E. A.; Dunoyer, P.; Rahm, N.; Himber, C. and Voinnet, O. (2004). In vivo investigation of the transcription, processing, endonucleolytic activity, and functional relevance of the spatial distribution of a plant miRNA. *Genes & Development* **18**: 2237–2242.

Park, M.; Song, K.; Reichardt, I.; Kim, H.; Mayer, U.; Stierhof, Y.-D.; Hwang, I. and Jürgens, G. (2013). *Arabidopsis* μ-adaptin subunit AP1M of adaptor protein complex 1 mediates late secretory and vacuolar traffic and is required for growth. *Proceedings of the National Academy of Sciences of the United States of America* **110**: 10318–10323.

Park, M. Y.; Wu, G.; Gonzalez-Sulser, A.; Vaucheret, H. and Poethig, R. S. (2005). Nuclear processing and export of microRNAs in *Arabidopsis*. *Proceedings of the National Academy of Sciences of the United States of America* **102**: 3691–3696.

Park, W.; Li, J.; Song, R.; Messing, J. and Chen, X. (2002). CARPEL FACTORY, a Dicer homolog, and HEN1, a novel protein, act in microRNA metabolism in *Arabidopsis thaliana*. *Current Biology* **12**: 1484–1495.

Payne, C. T.; Zhang, F. and Lloyd, A. M. (2000). *GL3* Encodes a bHLH Protein That Regulates Trichome Development in Arabidopsis Through Interaction With GL1 and TTG1. *Genetics* **156**: 1349–1362.

Peyroche, A.; Antonny, B.; Robineau, S.; Acker, J.; Cherfils, J. and Jackson, C. L. (1999). Brefeldin A acts to stabilize an abortive ARF-GDP-Sec7 domain protein complex: involvement of specific residues of the Sec7 domain. *Molecular Cell* **3**: 275–285.

Pfleger, C. M. and Kirschner, M. W. (2000). The KEN box: an APC recognition signal distinct from the D box targeted by Cdh1. *Genes & Development* **14**: 655–665.

Pires, N. D.; Yi, K.; Breuninger, H.; Catarino, B.; Menand, B. and Dolan, L. (2013). Recruitment and remodeling of an ancient gene regulatory network during land plant evolution. *Proceedings of the National Academy of Sciences of the United States of America* **110**: 9571–9576.

Pitts, R. J.; Cernac, A. and Estelle, M. (1998). Auxin and ethylene promote root hair elongation in *Arabidopsis*. *The Plant Journal* **16**: 553–560.

Plotnikova, A.; Kellner, M. J.; Schon, M. A.; Mosiolek, M. and Nodine, M. D. (2019). MicroRNA Dynamics and Functions During Arabidopsis Embryogenesis. *The Plant Cell* **31**: 2929–2946.

Polko, J. K.; Barnes, W. J.; Voiniciuc, C.; Doctor, S.; Steinwand, B.; Hill, J. L.; Tien, M.; Pauly, M.; Anderson, C. T. and Kieber, J. J. (2018). SHOU4 Proteins Regulate Trafficking of Cellulose Synthase Complexes to the Plasma Membrane. *Current Biology* **28**: 3174-3182.e6.

Rajagopalan, R.; Vaucheret, H.; Trejo, J. and Bartel, D. P. (2006). A diverse and evolutionarily fluid set of microRNAs in *Arabidopsis thaliana*. *Genes & Development* **20**: 3407–3425.

Reiss, Y.; Kaim, D. and Hershko, A. (1988). Specificity of binding of NH2-terminal residue of proteins to ubiquitin-protein ligase. Use of amino acid derivatives to characterize specific binding sites. *The Journal of Biological Chemistry* **263**: 2693–2698.

Ridley, B. L.; O'Neill, M. A. and Mohnen, D. (2001). Pectins: structure, biosynthesis, and oligogalacturonide-related signaling. *Phytochemistry* **57**: 929–967.

Rishmawi, L.; Wolff, H.; Schrader, A. and Hülskamp, M. (2018). Sub-epidermal Expression of *ENHANCER OF TRIPTYCHON AND CAPRICE1* and Its Role in Root Hair Formation Upon Pi Starvation. *Frontiers in Plant Science* **9**: 1411.

Robinson, D. G. (1996). Clathrin-mediated trafficking. *Trends in Plant Science* **1**: 349–355.

Robinson, D. G.; Hinz, G. and Holstein, S. E. (1998). The molecular characterization of transport vesicles. *Plant molecular biology* **38**: 49–76.

Röckel, N.; Wolf, S.; Kost, B.; Rausch, T. and Greiner, S. (2008). Elaborate spatial patterning of cell-wall PME and PMEI at the pollen tube tip involves PMEI endocytosis, and reflects the distribution of esterified and de-esterified pectins. *The Plant Journal* **53**: 133–143.

Rosenthal, J. A.; Chen, H.; Slepnev, V. I.; Pellegrini, L.; Salcini, A. E.; Di Fiore, P. P. and Camilli, P. de (1999). The epsins define a family of proteins that interact with components of the clathrin coat and contain a new protein module. *The Journal of Biological Chemistry* **274**: 33959–33965.

Ryu, K. H.; Kang, Y. H.; Park, Y.; Hwang, I.; Schiefelbein, J. and Lee, M. M. (2005). The WEREWOLF MYB protein directly regulates *CAPRICE*transcription during cell fate specification in the *Arabidopsis* root epidermis. *Development* **132**: 4765–4775.

Sanderfoot, A. A. and Raikhel, N. V. (1999). The specificity of vesicle trafficking. Coat proteins and SNAREs. *The Plant Cell* **11**: 629–642.

Sauer, M. (2014). MTV1 Pull-down Assay in *Arabidopsis*. *Bio-Protocol* **4**.

Sauer, M.; Delgadillo, M. O.; Zouhar, J.; Reynolds, G. D.; Pennington, J. G.; Jiang, L.; Liljegren, S. J.; Stierhof, Y.-D.; Jaeger, G. de; Otegui, M. S.; Bednarek, S. Y. and Rojo, E. (2013). MTV1 and MTV4 encode plant-specific ENTH and ARF GAP proteins that mediate clathrin-dependent trafficking of vacuolar cargo from the trans-Golgi network. *The Plant Cell* **25**: 2217–2235.

Savage, N.; Yang, T. J. W.; Chen, C. Y.; Lin, K.-L.; Monk, N. A. M. and Schmidt, W. (2013). Positional signaling and expression of *ENHANCER OF TRY AND CPC1* are tuned to increase root hair density in response to phosphate deficiency in *Arabidopsis thaliana*. *PLoS One* **8**: e75452.

Scheres, B.; Benfey, P. and Dolan, L. (2002). Root development. *The Arabidopsis Book* **1**: e0101.

Schiefelbein, J.; Huang, L. and Zheng, X. (2014). Regulation of epidermal cell fate in Arabidopsis roots: the importance of multiple feedback loops. *Frontiers in Plant Science* **5**: 47.

Schiefelbein, J. W. and Somerville, C. (1990). Genetic Control of Root Hair Development in *Arabidopsis thaliana*. *The Plant Cell* **2**: 235–243.

Schindelman, G.; Morikami, A.; Jung, J.; Baskin, T. I.; Carpita, N. C.; Derbyshire, P.; McCann, M. C. and Benfey, P. N. (2001). COBRA encodes a putative GPI-anchored protein, which is polarly localized and necessary for oriented cell expansion in *Arabidopsis*. *Genes & Development* **15**: 1115–1127.

Schmidt, W.; Tittel, J. and Schikora, A. (2000). Role of hormones in the induction of iron deficiency responses in Arabidopsis roots. *Plant Physiology* **122**: 1109–1118.

Schneider, K.; Wells, B.; Dolan, L. and Roberts, K. (1997). Structural and genetic analysis of epidermal cell differentiation in *Arabidopsis* primary roots. *Development* **124**: 1789–1798.

Schoenaers, S.; Balcerowicz, D.; Breen, G.; Hill, K.; Zdanio, M.; Mouille, G.; Holman, T. J.; Oh, J.; Wilson, M. H.; Nikonorova, N.; Vu, L. D.; Smet, I. de et al. (2018). The Auxin-Regulated CrRLK1L Kinase ERULUS Controls Cell Wall Composition during Root Hair Tip Growth. *Current Biology* **28**: 722-732.e6.

Seefried, W. F.; Willmann, M. R.; Clausen, R. L. and Jenik, P. D. (2014). Global Regulation of Embryonic Patterning in Arabidopsis by MicroRNAs. *Plant Physiology* **165**: 670–687.

Seidner, G.; Alvarez, M. G.; Yeh, J. I.; O'Driscoll, K. R.; Klepper, J.; Stump, T. S.; Wang, D.; Spinner, N. B.; Birnbaum, M. J. and Vivo, D. C. de (1998). GLUT-1 deficiency syndrome caused by haploinsufficiency of the blood-brain barrier hexose carrier. *Nature Genetics* **18**: 188–191.

Sessions, A.; Burke, E.; Presting, G.; Aux, G.; McElver, J.; Patton, D.; Dietrich, B.; Ho, P.; Bacwaden, J.; Ko, C.; Clarke, J. D.; Cotton, D. et al. (2002). A high-throughput Arabidopsis reverse genetics system. *The Plant Cell* **14**: 2985–2994.

Simon, M.; Lee, M. M.; Lin, Y.; Gish, L. and Schiefelbein, J. (2007). Distinct and overlapping roles of single-repeat MYB genes in root epidermal patterning. *Developmental Biology* **311**: 566–578.

Skruzny, M.; Brach, T.; Ciuffa, R.; Rybina, S.; Wachsmuth, M. and Kaksonen, M. (2012). Molecular basis for coupling the plasma membrane to the actin cytoskeleton during clathrin-mediated endocytosis. *Proceedings of the National Academy of Sciences of the United States of America* **109**: E2533-42.

Skruzny, M.; Desfosses, A.; Prinz, S.; Dodonova, S. O.; Gieras, A.; Uetrecht, C.; Jakobi, A. J.; Abella, M.; Hagen, W. J.; Schulz, J.; Meijers, R.; Rybin, V. et al. (2015). An Organized Co-assembly of Clathrin Adaptors Is Essential for Endocytosis. *Developmental Cell* **33**: 150–162.

Song, J.; Lee, M. H.; Lee, G.-J.; Yoo, C. M. and Hwang, I. (2006). *Arabidopsis* EPSIN1 plays an important role in vacuolar trafficking of soluble cargo proteins in plant cells via interactions with clathrin, AP-1, VTI11, and VSR1. *The Plant Cell* **18**: 2258–2274.

Song, K.; Jang, M.; Kim, S. Y.; Lee, G.; Lee, G.-J.; Kim, D. H.; Lee, Y.; Cho, W. and Hwang, I. (2012). An A/ENTH domain-containing protein functions as an adaptor for clathrin-coated vesicles on the growing cell plate in Arabidopsis root cells. *Plant Physiology* **159**: 1013–1025.

Song, S.-K.; Ryu, K. H.; Kang, Y. H.; Song, J. H.; Cho, Y.-H.; Yoo, S.-D.; Schiefelbein, J. and Lee, M. M. (2011). Cell fate in the Arabidopsis root epidermis is determined by competition between WEREWOLF and CAPRICE. *Plant Physiology* **157**: 1196–1208.

Stegmann, M.; Monaghan, J.; Smakowska-Luzan, E.; Rovenich, H.; Lehner, A.; Holton, N.; Belkhadir, Y. and Zipfel, C. (2017). The receptor kinase FER is a RALF-regulated scaffold controlling plant immune signaling. *Science* **355**: 287–289.

Stewart, M. D.; Ritterhoff, T.; Klevit, R. E. and Brzovic, P. S. (2016). E2 enzymes: more than just middle men. *Cell Research* **26**: 423–440.

Sudakin, V.; Ganoth, D.; Dahan, A.; Heller, H.; Hershko, J.; Luca, F. C.; Ruderman, J. V. and Hershko, A. (1995). The cyclosome, a large complex containing cyclin-selective ubiquitin ligase activity, targets cyclins for destruction at the end of mitosis. *Molecular Biology of the Cell* **6**: 185–197.

Südhof, T. C. and Rothman, J. E. (2009). Membrane fusion. Grappling with SNARE and SM proteins. *Science* **323**: 474–477.

Sultana, M. M.; Dutta, A. K.; Tanaka, Y.; Aboulela, M.; Nishimura, K.; Sugiura, S.; Niwa, T.; Maeo, K.; Goto-Yamada, S.; Kimura, T.; Ishiguro, S.; Mano, S. et al. (2019). Gateway binary vectors with organelle-targeted fluorescent proteins for highly sensitive reporter assay in gene expression analysis of plants. *Journal of Biotechnology* **297**: 19–27.

Takahashi, N.; Kajihara, T.; Okamura, C.; Kim, Y.; Katagiri, Y.; Okushima, Y.; Matsunaga, S.; Hwang, I. and Umeda, M. (2013). Cytokinins control endocycle onset by promoting the expression of an APC/C activator in *Arabidopsis* roots. *Current Biology* **23**: 1812–1817.

Takatori, S. and Tomita, T. (2019). AP180 N-Terminal Homology (ANTH) and Epsin N-Terminal Homology (ENTH) Domains: Physiological Functions and Involvement in Disease.

In: Atassi, M. Zouhair Protein Reviews – Purinergic Receptors: Volume 20: 55–76. Cham: Springer International Publishing.

Tang, G.; Yan, J.; Gu, Y.; Qiao, M.; Fan, R.; Mao, Y. and Tang, X. (2012). Construction of short tandem target mimic (STTM) to block the functions of plant and animal microRNAs. *Methods* **58**: 118–125.

Tanimoto, M.; Roberts, K. and Dolan, L. (1995). Ethylene is a positive regulator of root hair development in *Arabidopsis thaliana*. *The Plant Journal* **8**: 943–948.

Tarayre, S.; Vinardell, J. M.; Cebolla, A.; Kondorosi, A. and Kondorosi, E. (2004). Two Classes of the Cdh1-Type Activators of the Anaphase-Promoting Complex in Plants: Novel Functional Domains and Distinct Regulation. *The Plant Cell* **16**: 422–434.

Tegtmeier, L. (2022). Functional analysis of ENTH domain proteins. Funktionelle Analyse der ENTH Proteine. Dissertation. Universität Potsdam, Potsdam.

Teh, O.-K.; Shimono, Y.; Shirakawa, M.; Fukao, Y.; Tamura, K.; Shimada, T. and Hara-Nishimura, I. (2013). The AP-1 μ adaptin is required for KNOLLE localization at the cell plate to mediate cytokinesis in Arabidopsis. *Plant & Cell Physiology* **54**: 838–847.

Tominaga, R.; Iwata, M.; Okada, K. and Wada, T. (2007). Functional analysis of the epidermal-specific MYB genes *CAPRICE* and *WEREWOLF* in *Arabidopsis*. *The Plant Cell* **19**: 2264–2277.

Tominaga-Wada, R.; Kurata, T. and Wada, T. (2017). Localization of ENHANCER OF TRY AND CPC1 protein in *Arabidopsis* root epidermis. *Journal of Plant Physiology* **214**: 48–52.

Tominaga-Wada, R. and Wada, T. (2017). Extended C termini of CPC-LIKE MYB proteins confer functional diversity in *Arabidopsis* epidermal cell differentiation. *Development* **144**: 2375–2380.

Toshima, J.; Toshima, J. Y.; Duncan, M. C.; Cope, M. J. T.; Sun, Y.; Martin, A. C.; Anderson, S.; Yates, J. R.; Mizuno, K. and Drubin, D. G. (2006). Negative Regulation of Yeast Eps15-like Arp2/3 Complex Activator, Pan1p, by the Hip1R-related Protein, Sla2p, during Endocytosis. *Molecular Biology of the Cell* **18**: 658–668.

van der Krol, A. R.; Mur, L. A.; Beld, M.; Mol, J. N. and Stuitje, A. R. (1990). Flavonoid genes in petunia. Addition of a limited number of gene copies may lead to a suppression of gene expression. *The Plant Cell* **2**: 291–299.

Vanstraelen, M.; Baloban, M.; Da Ines, O.; Cultrone, A.; Lammens, T.; Boudolf, V.; Brown, S. C.; Veylder, L. de; Mergaert, P. and Kondorosi, E. (2009). APC/C^{CCS52A} complexes control meristem maintenance in the *Arabidopsis* root. *Proceedings of the National Academy of Sciences of the United States of America* **106**: 11806–11811.

Vatén, A.; Dettmer, J.; Wu, S.; Stierhof, Y.-D.; Miyashima, S.; Yadav, S. R.; Roberts, C. J.; Campilho, A.; Bulone, V.; Lichtenberger, R.; Lehesranta, S.; Mähönen, A. P. et al. (2011). Callose Biosynthesis Regulates Symplastic Trafficking during Root Development. *Developmental Cell* **21**: 1144–1155.

Vatter, T.; Neuhäuser, B.; Stetter, M. and Ludewig, U. (2015). Regulation of length and density of *Arabidopsis* root hairs by ammonium and nitrate. *Journal of Plant Research* **128**: 839–848.

Veitia, R. A. (2002). Exploring the etiology of haploinsufficiency. *BioEssays* **24**: 175–184.

Veitia, R. A. and Birchler, J. A. (2010). Dominance and gene dosage balance in health and disease: why levels matter! *The Journal of Pathology* **220**: 174–185.

Vierstra, R. D. (2009). The ubiquitin–26S proteasome system at the nexus of plant biology. *Nature Reviews Molecular Cell Biology* **10**: 385–397.

Visintin, R.; Prinz, S. and Amon, A. (1997). CDC20 and CDH1: A Family of Substrate-Specific Activators of APC-Dependent Proteolysis. *Science* **278**: 460–463.

Vissenberg, K.; Claeijs, N.; Balcerowicz, D. and Schoenaers, S. (2020). Hormonal regulation of root hair growth and responses to the environment in Arabidopsis. *Journal of Experimental Botany* **71**: 2412–2427.

Wada, T.; Kurata, T.; Tominaga, R.; Koshino-Kimura, Y.; Tachibana, T.; Goto, K.; Marks, M. D.; Shimura, Y. and Okada, K. (2002). Role of a positive regulator of root hair development, *CAPRICE*, in *Arabidopsis* root epidermal cell differentiation. *Development* **129**: 5409–5419.

Wada, T.; Tachibana, T.; Shimura, Y. and Okada, K. (1997). Epidermal Cell Differentiation in *Arabidopsis* Determined by a *Myb* Homolog, *CPC*. *Science* **277**: 1113–1116.

Walker, A. R.; Davison, P. A.; Bolognesi-Winfield, A. C.; James, C. M.; Srinivasan, N.; Blundell, T. L.; Esch, J. J.; Marks, M. D. and Gray, J. C. (1999). The *TRANSPARENT TESTA GLABRA1* Locus, Which Regulates Trichome Differentiation and Anthocyanin Biosynthesis in Arabidopsis, Encodes a WD40 Repeat Protein. *The Plant Cell* **11**: 1337–1349.

Wang, J.; Gossing, M.; Fang, P.; Zimmermann, J.; Li, X.; Mollard, G. F. von; Niu, L. and Teng, M. (2011). Epsin N-terminal homology domains bind on opposite sides of two SNAREs. *Proceedings of the National Academy of Sciences of the United States of America* **108**: 12277–12282.

Wang, J.; Mei, J. and Ren, G. (2019). Plant microRNAs: Biogenesis, Homeostasis, and Degradation. *Frontiers in Plant Science* **10**: 360.

Wang, J.-W.; Wang, L.-J.; Mao, Y.-B.; Cai, W.-J.; Xue, H.-W. and Chen, X.-Y. (2005). Control of root cap formation by MicroRNA-targeted auxin response factors in Arabidopsis. *The Plant Cell* **17**: 2204–2216.

Wang, S.; Barron, C.; Schiefelbein, J. and Chen, J.-G. (2010). Distinct relationships between GLABRA2 and single-repeat R3 MYB transcription factors in the regulation of trichome and root hair patterning in Arabidopsis. *New Phytologist* **185**: 387–400.

Wang, Z.-P.; Xing, H.-L.; Dong, L.; Zhang, H.-Y.; Han, C.-Y.; Wang, X.-C. and Chen, Q.-J. (2015). Egg cell-specific promoter-controlled CRISPR/Cas9 efficiently generates homozygous mutants for multiple target genes in *Arabidopsis* in a single generation. *Genome Biology* **16**: 144.

Wasiak, S.; Legendre-Guillemin, V.; Puertollano, R.; Blondeau, F.; Girard, M.; Heuvel, E. de; Boismenu, D.; Bell, A. W.; Bonifacino, J. S. and McPherson, P. S. (2002). Enthoprotin: a novel clathrin-associated protein identified through subcellular proteomics. *The Journal of Cell Biology* **158**: 855–862.

Weber, T.; Zemelman, B. V.; McNew, J. A.; Westermann, B.; Gmachl, M.; Parlati, F.; Söllner, T. H. and Rothman, J. E. (1998). SNAREpins. Minimal Machinery for Membrane Fusion. *Cell* **92**: 759–772.

Wei Yang, T. J.; Perry, P. J.; Ciani, S.; Pandian, S. and Schmidt, W. (2008). Manganese deficiency alters the patterning and development of root hairs in *Arabidopsis*. *Journal of Experimental Botany* **59**: 3453–3464.

Weinmann, H.; Crews, C. (2020). Protein Degradation with New Chemical Modalities: The Royal Society of Chemistry.

Wendland, B.; Steece, K. E. and Emr, S. D. (1999). Yeast epsins contain an essential N-terminal ENTH domain, bind clathrin and are required for endocytosis. *The EMBO Journal* **18**: 4383–4393.

Widberg, C. H.; Bryant, N. J.; Girotti, M.; Rea, S. and James, D. E. (2003). Tomosyn Interacts with the t-SNAREs Syntaxin4 and SNAP23 and Plays a Role in Insulin-stimulated GLUT4 Translocation. *The Journal of Biological Chemistry* **278**: 35093–35101.

Willats, W. G.; Orfila, C.; Limberg, G.; Buchholt, H. C.; van Alebeek, G.-J. W.; Voragen, A. G..; Marcus, S. E.; Christensen, T. M.; Mikkelsen, J. D.; Murray, B. S. and Knox, J. P. (2001). Modulation of the Degree and Pattern of Methyl-esterification of Pectic Homogalacturonan in Plant Cell Walls: IMPLICATIONS FOR PECTIN METHYL ESTERASE ACTION, MATRIX PROPERTIES, AND CELL ADHESION. *The Journal of Biological Chemistry* **276**: 19404–19413.

Williamson, L. C.; Ribrioux, S. P.; Fitter, A. H. and Leyser, H. O. (2001). Phosphate Availability Regulates Root System Architecture in Arabidopsis. *Plant Physiology* **126**: 875–882.

Winter, D.; Vinegar, B.; Nahal, H.; Ammar, R.; Wilson, G. V. and Provart, N. J. (2007). An "Electronic Fluorescent Pictograph" browser for exploring and analyzing large-scale biological data sets. *PLoS One* **2**: e718.

Wolf, S.; Mouille, G. and Pelloux, J. (2009). Homogalacturonan Methyl-Esterification and Plant Development. *Molecular Plant* **2**: 851–860.

Woody, S. T.; Austin-Phillips, S.; Amasino, R. M. and Krysan, P. J. (2007). The WiscDsLox T-DNA collection: an arabidopsis community resource generated by using an improved high-throughput T-DNA sequencing pipeline. *Journal of Plant Research* **120**: 157–165.

Xie, Z.; Allen, E.; Fahlgren, N.; Calamar, A.; Givan, S. A. and Carrington, J. C. (2005). Expression of Arabidopsis *MIRNA* genes. *Plant Physiology* **138**: 2145–2154.

Xing, H.-L.; Dong, L.; Wang, Z.-P.; Zhang, H.-Y.; Han, C.-Y.; Liu, B.; Wang, X.-C. and Chen, Q.-J. (2014). A CRISPR/Cas9 toolkit for multiplex genome editing in plants. *BMC plant biology* **14**: 327.

Xu, D.; Jiang, Y.; Li, J.; Lin, F.; Holm, M. and Deng, X. W. (2016). BBX21, an *Arabidopsis* B-box protein, directly activates *HY5* and is targeted by COP1 for 26S proteasome-mediated degradation. *Proceedings of the National Academy of Sciences of the United States of America* **113**: 7655–7660.

Xu, F.-Q. and Xue, H.-W. (2019). The ubiquitin-proteasome system in plant responses to environments. *Plant, Cell & Environment* **42**: 2931–2944.

Yan, J.; Gu, Y.; Jia, X.; Kang, W.; Pan, S.; Tang, X.; Chen, X. and Tang, G. (2012). Effective small RNA destruction by the expression of a short tandem target mimic in *Arabidopsis*. *The Plant Cell* **24**: 415–427.

Yan, X.; Liu, X.; Cui, H. and Zhao, M. (2022). The roles of microRNAs in regulating root formation and growth in plants. *Journal of Integrative Agriculture* **21**: 901–916.

Yi, K.; Menand, B.; Bell, E. and Dolan, L. (2010). A basic helix-loop-helix transcription factor controls cell growth and size in root hairs. *Nature Genetics* **42**: 264–267.

Yoshida, Y.; Sano, R.; Wada, T.; Takabayashi, J. and Okada, K. (2009). Jasmonic acid control of GLABRA3 links inducible defense and trichome patterning in *Arabidopsis*. *Development* **136**: 1039–1048.

Yu, B.; Yang, Z.; Li, J.; Minakhina, S.; Yang, M.; Padgett, R. W.; Steward, R. and Chen, X. (2005). Methylation as a crucial step in plant microRNA biogenesis. *Science* **307**: 932–935.

Yu, F.; Qian, L.; Nibau, C.; Duan, Q.; Kita, D.; Levasseur, K.; Li, X.; Lu, C.; Li, H.; Hou, C.; Li, L.; Buchanan, B. B. et al. (2012). FERONIA receptor kinase pathway suppresses abscisic acid signaling in *Arabidopsis* by activating ABI2 phosphatase. *Proceedings of the National Academy of Sciences of the United States of America* **109**: 14693–14698.

Yu, Y.; Jia, T. and Chen, X. (2017). The 'how' and 'where' of plant microRNAs. *New Phytologist* **216**: 1002–1017.

Zhang, F.; Yang, J.; Zhang, N.; Wu, J. and Si, H. (2022). Roles of microRNAs in abiotic stress response and characteristics regulation of plant. *Frontiers in Plant Science* **13**: 919243.

Zhang, X.; Zhao, H.; Gao, S.; Wang, W.-C.; Katiyar-Agarwal, S.; Huang, H.-D.; Raikhel, N. and Jin, H. (2011). *Arabidopsis* Argonaute 2 regulates innate immunity via miRNA393*-mediated silencing of a Golgi-localized SNARE gene, *MEMB12*. *Molecular Cell* **42**: 356–366.

Zhang, Y.; Yang, Z.; Zhang, Z.; Li, Y.; Guo, J.; Liu, L.; Wang, C.; Fan, H.; Wang, B. and Han, G. (2023). Root Hair Development and Adaptation to Abiotic Stress. *Journal of Agricultural and Food Chemistry* **71**: 9573–9598.

Zhao, H.; Wang, X.; Zhu, D.; Cui, S.; Li, X.; Cao, Y. and Ma, L. (2012). A single amino acid substitution in IIIf subfamily of basic helix-loop-helix transcription factor AtMYC1 leads to trichome and root hair patterning defects by abolishing its interaction with partner proteins in *Arabidopsis*. *The Journal of Biological Chemistry* **287**: 14109–14121.

Zhao, Y.; an Yan; Feijó, J. A.; Furutani, M.; Takenawa, T.; Hwang, I.; Fu, Y. and Yang, Z. (2010). Phosphoinositides regulate clathrin-dependent endocytosis at the tip of pollen tubes in *Arabidopsis* and tobacco. *The Plant Cell* **22**: 4031–4044.

Zouhar, J. and Sauer, M. (2014). Helping hands for budding prospects. ENTH/ANTH/VHS accessory proteins in endocytosis, vacuolar transport, and secretion. *The Plant Cell* **26**: 4232–4244.

Zuker, M. (2003). Mfold web server for nucleic acid folding and hybridization prediction. *Nucleic Acids Research* **31**: 3406–3415.

6. Supporting information

6.1 Materials

Table S 1: Plant material

Plant material	AGI locus code	Ecotype	Vector	Description/Application	Reference/ Source
id2-1	AT3G46540	Col-0	-	T-DNA insertion mutant allele (Salk)	Alonso et al. 2003, Freimuth 2015
id2-3	AT3G46540	Col-0	pHEE401E	full deletion mutant (CRISPR/Cas9); pHEE401E was segregated out	generated in this work
ID2::ID2-GUS in Col-0	AT3G46540	Col-0	pGWB3	Analysis of expression pattern	generated in this work
ID2::ID2-GFP in Col-0	AT3G46540	Col-0	pGWB4	Translational reporter line for analyses of expression pattern and subcellular localization	generated in this work
ID2-1100::NLS-GFP in Col-0	AT3G46540	Col-0	pGWB565	Transcriptional reporter line	generated in this work
35S::ID2 in Col-0	AT3G46540	Col-0	pGWB402Ω	Untagged overexpression of *EPSINOID2* under 2x35S-Ω promoter	Freimuth 2019
35S::ID2-GFP in Col-0	AT3G46540	Col-0	pGWB405	GFP-tagged overexpression of *EPSINOID2* under 35S promoter	generated in this work
UBQ10::ID2-GFP in Col-0	AT3G46540	Col-0	pUBQ10-C-GFP	GFP-tagged overexpression of *EPSINOID2* under Ubiquitin-10 promoter	generated in previous work (unpublished)
35S::ID2-miR^R in Col-0	AT3G46540	Col-0	pGWB402Ω	miRNA-resistant overexpression line	generated in this work
35S::ID2-miR^R-GFP in Col-0	AT3G46540	Col-0	pGWB405	GFP-tagged miRNA-resistant overexpression line	generated in this work
ID2::ID2-miR^R in Col-0	AT3G46540	Col-0	pGWB401	miRNA-resistant *EPSINOID2* driven by its own promoter	generated in this work
ID2::ID2-miR^R-Neon in Col-0	AT3G46540	Col-0	pGWB401-mNeon	mNeon-tagged miRNA-resistant *EPSINOID2* driven by its own promoter	generated in this work

120

Plant material	AGI locus code	Ecotype	Vector	Description/Application	Reference/ Source
ID2::ID2-3xGFP in Col-0	AT3G46540	Col-0	pGWB401-3xGFP	analysis of potential *EPSINOID2* protein cell-to-cell movement	generated in this work
MYC1::ID2-miR^R-GFP in Col-0	AT3G46540	Col-0	pGWB401-GFP	hair cell-specific expression of miRNA-resistant *EPSINOID2*	generated in this work
ID2::ID2-miR^R id2-3	AT3G46540	Col-0	pGWB401	Complementation line	generated in this work
SCM::SCM-GFP	AT1G11130	Col-0, Ws	-	Marker line for *SCRAMBLED*; isolated from original line *scm-2 GL2::GUS SCM::SCM-GFP*	Kwak and Schiefelbein 2008; NACS (N66496)
WER::WER-GFP	AT5G14750	Col-0	pCB302	Translational marker line for *WEREWOLF*	Ryu et al. 2005; provided by Markus Grebe
WER::GFP	AT5G14750	Col-0	-	Transcriptional marker line for *WEREWOLF*; isolated from original line *myc1-1 WER::GFP*	Lee and Schiefelbein 1999; NASC (N67769)
CPC::CPC-Neon in Col-0/*id2-1*	AT2G46410	Col-0	pGWB401-mNeon	Translational marker line for *CAPRICE*	generated in this work
GL3::GL3-YFP	AT5G41315	Col-0	-	Translational marker line for *GLABRA3*	Bernhardt et al. 2005; NASC (N66494)
MYC1::GFP	AT4G00480	Col-0	-	Transcriptional marker line for *MYC1*	Bruex et al. 2012; provided by John Schiefelbein
GL2::GFP	AT1G79840	Col-0	-	Transcriptional marker line for *GLABRA2*	Lin and Schiefelbein 2001; provided by John Schiefelbein
SCM::SCM-GFP id2-1	AT1G11130	Col-0, Ws	-	*SCM* marker in *id2-1* mutant background; isolated from cross with original line *scm-2 GL2::GUS SCM::SCM-GFP*	generated in this work
WER::WER-GFP id2-1	AT5G14750	Col-0	-	*WER* marker in *id2-1* mutant background	generated in this work
WER::GFP id2-1	AT5G14750	Col-0	-	*WER* marker in *id2-1* mutant background	generated in this work
GL3::GL3-YFP id2-1	AT5G41315	Col-0	-	*GL3* marker in *id2-1* mutant background	generated in this work
MYC1::GFP id2-1	AT4G00480	Col-0	-	*MYC1* marker in *id2-1* mutant background	generated in this work

Plant material	AGI locus code	Ecotype	Vector	Description/Application	Reference/ Source
GL2::GFP id2-1	AT1G79840	Col-0	-	*GL2* marker in *id2-1* mutant background	generated in this work
scm-2	AT1G11130	Col-0	-	T-DNA insertion in third intron (SALK_086357)	Kwak and Schiefelbein 2008; NASC (N586357)
wer-1	AT5G14750	Col-2	-	point mutation in codon 93 (TGG → TGA)	Lee and Schiefelbein 1999; NASC (N6349)
cpc	AT2G46410	Col-0	-	T-DNA insertion in second exon (SAIL_310_C06)	Sessions et al. 2002; NASC (N873046)
gl3	AT5G41315	Col-0	-	T-DNA insertion in fifth exon (WiscDsLox412G05)	Woody et al. 2007; NASC (N854602)
gl3-1 egl3-1	AT5G41315, AT1G63650	Col-0, L*er*	-	*gl3-1*: point mutation in codon 378 (CAG → TAG) *egl3-1*: point mutation in codon 26 (TGG → TGA)	Bernhardt et al. 2003; NASC (N66490)
myc1-1	AT4G00480	Col-0	-	T-DNA insertion in second intron (SALK_057388)	Alonso et al. 2003; NASC (N557388)
gl2-2	AT1G79840	Col-0	-	T-DNA insertion in second intron (SALK_130213C)	Guan et al. 2008; NASC (N681725)
gl2-3	AT1G79840	Col-0	-	T-DNA insertion in second intron (SALK_039825C)	Wang et al. 2010; NASC (N665830)
id2-1 scm-2	AT1G11130	Col-0	-	*id2-1* crossed with *scm-2*	generated in this work
id2-1 wer-1	AT5G14750	Col-0, Col-2	-	*id2-1* crossed with *wer-1*	generated in this work
id2-1 cpc	AT2G46410	Col-0	-	*id2-1* crossed with *cpc*	generated in this work
id2-1 gl3	AT5G41315	Col-0	-	*id2-1* crossed with *gl3*	generated in this work
id2-1 gl3-1 egl3-1	AT5G41315, AT1G63650	Col-0, L*er*	-	*id2-1* crossed with *gl3-1 egl3-1*	generated in this work
id2-1 myc1-1	AT4G00480	Col-0	-	*id2-1* crossed with *myc1-1*	generated in this work
id2-1 gl2-3	AT1G79840	Col-0	-	*id2-1* crossed with *gl2-3*	generated in this work
ID2::ID2-GFP scm-2	AT1G11130	Col-0	pGWB4	*ID2::ID2-GFP* transformed into *scm-2*	generated in this work

122

Plant material	AGI locus code	Ecotype	Vector	Description/Application	Reference/ Source
ID2::ID2-GFP wer-1	AT5G14750	Col-0, Col-2	pGWB4	*ID2::ID2-GFP* #12.3 crossed with *wer-1*	generated in this work
ID2::ID2-GFP cpc	AT2G46410	Col-0	pGWB4	*ID2::ID2-GFP* transformed into *cpc*	generated in this work
ID2::ID2-GFP gl3	AT5G41315	Col-0	pGWB4	*ID2::ID2-GFP* transformed into *gl3*	generated in this work
ID2::ID2-GFP gl3-1 egl3-1	AT5G41315, AT1G63650	Col-0, Ler	pGWB4	*ID2::ID2-GFP* transformed into *gl3-1 egl3-1*	generated in this work
ID2::ID2-GFP myc1-1	AT4G00480	Col-0	pGWB4	*ID2::ID2-GFP* transformed into *myc1-1*	generated in this work
ID2::ID2-GFP gl2-2	AT1G79840	Col-0	pGWB4	*ID2::ID2-GFP* transformed into *gl2-2*	generated in this work
35S::STTM844 in Col-0	AT2G23347	Col-0	pGWB402Ω	Short tandem target mimic of miRNA844-3p target	generated in this work
35S::MIR844 in Col-0	AT2G23347	Col-0	pGWB402Ω	Overexpression of *MIR844*	generated in this work
MIR844::ER-GFP in Col-0	AT2G23347	Col-0	pGWB562	Transcriptional reporter line for *MIR844*	generated in this work
MIR844::GUS in Col-0	AT2G23347	Col-0	pGWB3	Transcriptional reporter line for *MIR844*	generated in this work
mir844	AT2G23347	Col-0	pHEE401E	full deletion mutant (CRISPR/Cas9); pHEE401E was segregated out	generated in this work
35S::NLS-GFP-miR844-sensor in Col-0	AT2G23347	Col-0	pGWB565	miRNA844-3p sensor construct	generated in this work
35S::NLS-GFP-miR844^R-sensor in Col-0	AT2G23347	Col-0	pGWB565	miRNA844-3p resistant sensor construct	generated in this work
UBI10::mCherry-RabA1g	AT3G15060	Col-0	pNIGEL	Wave129R; endosomal and cell plate marker	Geldner et al. 2009
VHA-a1::VHA-a1-RFP	AT2G28520	Col-0	pGTkan	VHA-a1-RFP; TGN marker	Dettmer et al. 2006
35S::mKO-CLC	AT2G40060	Col-0	pGWB8	mKO-CLC; TGN marker	Fujimoto et al. 2010
UBQ10::mCherry-RabF2b	AT4G19640	Col-0	pNIGEL	Wave2R; LE/PVC marker	Geldner et al. 2009
UBQ10::mCherry-SYP32	AT3G24350	Col-0	pNIGEL	Wave22R; Golgi marker	Geldner et al. 2009
PME38-600::PME38-GFP	AT4G00190	Col-0	pGWB401-GFP	Expression of genomic *PME38* under 612 bp promoter	generated in this work

Table S 2: Bacterial strains

Bacteria	Strain	Purpose
Escherichia coli	DH5α	Molecular cloning
Escherichia coli	BL21 (DE3) pLysS	Bacterial expression of recombinant proteins
Agrobacterium tumefaciens	GV3101	Stable and transient transformation of plants

Table S 3: Equipment

Equipment	Manufacturer
Applied Biosystems 2720 Thermal Cycler	Thermo Fisher Scientific, Waltham, MA, USA
Applied Biosystems ProFlex PCR-System, 3x32-Well	Thermo Fisher Scientific, Waltham, MA, USA
EasyPhor electrophoresis chambers	Biozym Scientific GmbH, Hessisch Oldendorf, Germany
Fujifilm Intelligent Dark Box	FUJIFILM Europe GmbH, Düsseldorf, Germany
Incubator	Memmert GmbH & Co. KG, Schwabach, Germany
Incubator	BINDER GmbH, Tuttlingen, Germany
Labgard Class II Laminar FlowBiological Safety Cabinet, Model NU-437-600E	NuAire, Inc., Plymouth, USA
Labinco test-tube rotator 528	Labinco BV, Breda, Netherlands
Mikro 200 Centrifuge	Hettich GmbH & Co.KG, Tuttlingen, Germany
Mini Trans-Blot Electrophoretic Transfer Cell	Bio-Rad Laboratories GmbH, München, Germany
Mini-PROTEAN Tetra Systems	Bio-Rad Laboratories GmbH, München, Germany
Mixer Mill MM 400	RETSCH GmbH, Haan, Deutschland
Molecular Imager Gel Doc XR+ System with Image Lab Software	Bio-Rad Laboratories GmbH, München, Germany
MSC-Advantage Class II Biological Safety Cabinet	Thermo Fisher Scientific, Waltham, MA, USA
NanoDrop OneC Mikrovolumen-UV/VIS-Spektralphotometer	Thermo Fisher Scientific, Waltham, MA, USA
neoLabLine Revolver Rotator D-6050	neoLab Migge GmbH, Heidelberg, Germany
Nikon D750	Nikon GmbH, Düsseldorf, Germany
Percival, Model CU-22L	CLF Plant Climatics, Wertingen, Germany
Percival, Model SE59-L2.3	CLF Plant Climatics, Wertingen, Germany
Power Pack Modell 250	Biometra, Göttingen, Germany
PowerPac 300	Bio-Rad Laboratories GmbH, München, Germany
Roller mixer RM 5K	SDI Germany GmbH, Ballrechten-Dottingen, Germany
Shaker Multitron Pro	INFORS HT, Einsbach, Germany
Sigma 3-18KS Centrifuge	Sigma Laborzentrifugen GmbH, Osterode am Harz, Germany

Equipment	Manufacturer
SIGMA 3K30 Centrifuge	SciQuip Ltd, Newtown, United Kingdom
Spectrophotometer GeneQuant 100	GE Healthcare GmbH, Freiburg, Germany
T100 Thermal Cycler	Bio-Rad Laboratories GmbH, München, Germany
Thermomixer comfort & compact	Eppendorf AG, Hamburg, Germany
TissueLyser II	QIAGEN, Hilden, Germany
Transferpette S	BRAND GmbH & Co. KG, Wertheim, Germany
Ultramat 2	SDI Germany GmbH, Cologne, Germany
Ultrasonic Homogenizer UP200Ht	Hielscher Ultrasonics GmbH, Teltow, Germany
Zeiss Axiophot	Carl Zeiss, Göttingen, Germany
Zeiss Axio Imager.M2	Carl Zeiss, Göttingen, Germany
Zeiss Axio Zoom.V16	Carl Zeiss, Göttingen, Germany
Zeiss LSM 880 Airyscan Fast	Carl Zeiss, Göttingen, Germany

Table S 4: Chemicals

Chemical	Manufacturer
1,4-Dithioerythritol (DTE)	Carl Roth GmbH + Co. KG, Karlsruhe, Germany
1,4-Dithiothreit (DTT)	Carl Roth GmbH + Co. KG, Karlsruhe, Germany
10X FastDigest (FD) Green Buffer	Thermo Fisher Scientific, Waltham, MA, USA
2-(N-morpholino)ethanesulfonic acid (MES)	Carl Roth GmbH + Co. KG, Karlsruhe, Germany
2-propanol	Carl Roth GmbH + Co. KG, Karlsruhe, Germany
4-(2-hydroxyethyl)-1-piperazineethanesulfonic acid (HEPES)	Carl Roth GmbH + Co. KG, Karlsruhe, Germany
Acetosyringone (AS)	Sigma-Aldrich Corporation, Taufkirchen, Germany
Agar-agar	Carl Roth GmbH + Co. KG, Karlsruhe, Germany
Agarose Standard	Carl Roth GmbH + Co. KG, Karlsruhe, Germany
Ammonium persulfate (APS)	Carl Roth GmbH + Co. KG, Karlsruhe, Germany
Brefeldin A (BFA)	Santa Cruz Biotechnology, Inc, Heidelberg, Germany
Bromphenol blue	SERVA Electrophoresis GmbH, Heidelberg, Germany
Coatosil 77	Momentive Performance Materials GmbH & Co. KG, Leverkusen, Germany
Coomassie brilliant blue R	Sigma-Aldrich Corporation, Taufkirchen, Germany
Cycloheximide	Carl Roth GmbH + Co. KG, Karlsruhe, Germany
Difco Beef extract	Becton, Dickinson & Company, Franklin Lakes, NJ, USA
Dimethylformamid (DMF)	Sigma-Aldrich Corporation, Taufkirchen, Germany
Dimethyl sulfoxide (DMSO)	Carl Roth GmbH + Co. KG, Karlsruhe, Germany
di-Sodium hydrogen phosphate (Na_2HPO_4)	Carl Roth GmbH + Co. KG, Karlsruhe, Germany
Ethanol absolute	VWR International GmbH, Darmstadt, Germany

Chemical	Manufacturer
Ethidium bromide solution 1 %	Carl Roth GmbH + Co. KG, Karlsruhe, Germany
Ethylenediaminetetraacetic acid (EDTA)	Carl Roth GmbH + Co. KG, Karlsruhe, Germany
Ethylene glycol-bis(β-aminoethyl ether)-N,N,N',N'-tetraacetic acid (EGTA)	Sigma-Aldrich Corporation, Taufkirchen, Germany
GeneRuler DNA Ladder Mix	Thermo Fisher Scientific, Waltham, MA, USA
GeneRuler 1 kb DNA Ladder	Thermo Fisher Scientific, Waltham, MA, USA
GeneRuler Low Range DNA Ladder	Thermo Fisher Scientific, Waltham, MA, USA
Glutathione−Agarose	Sigma-Aldrich Corporation, Taufkirchen, Germany
Glycerol	Carl Roth GmbH + Co. KG, Karlsruhe, Germany
Glycine	Carl Roth GmbH + Co. KG, Karlsruhe, Germany
Hydrochloric acid 37 % (HCl)	Carl Roth GmbH + Co. KG, Karlsruhe, Germany
Isopropyl-β-D-thiogalactopyranoside (IPTG)	Carl Roth GmbH + Co. KG, Karlsruhe, Germany
Magnesium chloride ($MgCl_2$)	Carl Roth GmbH + Co. KG, Karlsruhe, Germany
Magnesium sulphate ($MgSO_4$)	Carl Roth GmbH + Co. KG, Karlsruhe, Germany
Methanol (MeOH)	Sigma-Aldrich Corporation, Taufkirchen, Germany
MG-132	Sigma-Aldrich Corporation, Taufkirchen, Germany
Murashige & Skoog medium incl. vitamins (MS)	DUCHEFA Biochemie B.V., Haarlem, Netherlands
Orange G	Sigma-Aldrich Corporation, Taufkirchen, Germany
PageRuler Prestained Protein Ladder	Thermo Fisher Scientific, Waltham, MA, USA
Perfluorodecalin	Sigma-Aldrich Corporation, Taufkirchen, Germany
Phenylmethyl sulphonyl fluoride (PMSF)	Carl Roth GmbH + Co. KG, Karlsruhe, Germany
Plant agar	DUCHEFA Biochemie B.V., Haarlem, Netherlands
Ponceau S	Sigma-Aldrich Corporation, Taufkirchen, Germany
Potassium chloride (KCl)	Carl Roth GmbH + Co. KG, Karlsruhe, Germany
Potassium dihydrogen phosphate (KH_2PO_4)	Carl Roth GmbH + Co. KG, Karlsruhe, Germany
Potassium hydroxide (KOH)	Carl Roth GmbH + Co. KG, Karlsruhe, Germany
Powdered milk	Carl Roth GmbH + Co. KG, Karlsruhe, Germany
Protease Inhibitor Cocktail Set I (Calbiochem)	Merck KGaA, Darmstadt, Germany
Protein Marker VI (10 –245) prestained	AppliChem GmbH, Darmstadt, Germany
Rotiphorese Gel 30 (37.5:1)	Carl Roth GmbH + Co. KG, Karlsruhe, Germany
SDS Pellets	Carl Roth GmbH + Co. KG, Karlsruhe, Germany
Sodium chloride (NaCl)	Carl Roth GmbH + Co. KG, Karlsruhe, Germany
Sodium fluoride (NaF)	Carl Roth GmbH + Co. KG, Karlsruhe, Germany
Sodium hydroxide solution (NaOH)	Carl Roth GmbH + Co. KG, Karlsruhe, Germany
Sodium orthovanadate (Na_3VO_4)	Carl Roth GmbH + Co. KG, Karlsruhe, Germany
Sucrose	Fisher Scientific, Loughborough, U. K.
Tetramethylethylenediamine (TEMED)	Sigma-Aldrich Corporation, Taufkirchen, Germany
Trichloroacetic acid solution 20 % (TCA)	Carl Roth GmbH + Co. KG, Karlsruhe, Germany
Tris(hydroxymethyl)-aminomethane (Tris)	Carl Roth GmbH + Co. KG, Karlsruhe, Germany
Triton X-100	Sigma-Aldrich Corporation, Taufkirchen, Germany

Chemical	Manufacturer
Tryptone/Peptone ex casein	Carl Roth GmbH + Co. KG, Karlsruhe, Germany
TWEEN 20	Sigma-Aldrich Corporation, Taufkirchen, Germany
X-Gluc	Carl Roth GmbH + Co. KG, Karlsruhe, Germany
Yeast extract	Carl Roth GmbH + Co. KG, Karlsruhe, Germany

Table S 5: Solutions and buffer

Solution/Buffer	Composition	Application
Stock solutions	1 M Tris, pH 8.0 (HCl) 2 M NaCl 0.5 M EDTA, pH 8.0 (NaOH) 20 % (w/v) SDS 0.4 M IPTG 100 mM AS (in DMSO)	Solutions for buffers for floral-dip
Edward's buffer	200 mM Tris, pH 8.0 250 mM NaCl 25 mM EDTA, pH 8.0 0.5 % (w/v) SDS	DNA extraction
10x TE	50 ml: 5 ml 1 M Tris, pH 8.0 1 ml 0.5 M EDTA, pH 8.0	DNA extraction
Loading buffer	50 ml: 10 mg Orange G 27 ml glycerol 3 ml 1x TE	Agarose gel electrophoresis
50x TAE	2 M Tris 50 mM EDTA pH 8.0 (acetic acid)	Agarose gel electrophoresis
4x Stacking buffer	0.5 M Tris-Cl, pH 6.8 0.4 % (w/v) SDS	SDS-PAGE
4x Separation buffer	1.5 M Tris-Cl, pH 8.8 0.4 % (w/v) SDS	SDS-PAGE
3x Cracking buffer	30 % (v/v) Glycerol 30 % (v/v) 4x Stacking buffer 7 % (w/v) SDS 0.01 % (w/v) Bromophenol blue	Loading buffer for SDS-PAGE
10x Electrophoresis buffer (Laemmli buffer)	0.25 M Tris-base 1.92 M glycine 1 % (v/v) SDS	SDS-PAGE
Sample buffer	3x Cracking buffer 23 mg/ml DTE	Buffer for protein samples
PBS	1 L: 8 g NaCl 0.2 g KCl	Pull-down assay, Membrane stripping

Solution/Buffer	Composition	Application
	1.44 g Na_2HPO_4 0.24 g KH_2PO_4 pH 7.4 (HCl)	
Blocking buffer	5 % (w/v) powdered milk, in TBS-T	Western blot
Transfer buffer	50 mM Tris 150 mM glycine 10 % (v/v) MeOH	Western blot
Ponceau	0.2 % (w/v) Ponceau S 2 % (v/v) TCA	Western blot
TBS-T	20 mM Tris 170 mM NaCl pH 7.5 (HCl) 0.1 % (v/v) TWEEN20	Western blot
Stripping buffer	1 L: 15 g glycine 1 g SDS 10 ml Tween20 pH 2.2 (HCl)	Membrane stripping
Washing buffer	20 mM Tris-HCl, pH 8.0 100 mM NaCl 1 mM EDTA 1 mM DTT	Pull-down assay for pull-down-MS/MS
Plant extraction buffer	100 mM Tris-HCl, pH 8.0 100 mM NaCl 20 mM DTT 5 mM EGTA 5 mM EDTA 10 mM NaF 10 mM Na_3VO_4 0.5 % Triton X-100 1:200 Protease Inhibitor Cocktail Set I	Pull-down assay for pull-down-MS/MS
Binding buffer	20 mM HEPES 200 mM NaCl pH 7.5 (NaOH) 2 mM DTT (added freshly)	*In vitro* pull-down assay
Wash buffer	20 mM HEPES 200 mM NaCl pH 7.5 (NaOH) 2 mM DTT (added freshly) 1 mM EDTA (added freshly) 0.1 % Triton X-100	In vitro pull-down assay
Phosphate buffer (1 M)	100 ml: 12.02 g $Na_2HPO_4 \cdot 2H_2O$ 4.47 g $NaH_2PO_4 \cdot H_2O$ pH 7.0	GUS buffer

Solution/Buffer	Composition	Application
10x GUS	1 M Phosphate buffer, pH 7.0 100 mM EDTA 20 mM $K_3Fe(CN)_6$ 10 mM $K_4Fe(CN)_6 \cdot 3H_2O$ 1 % TritonX-100	GUS staining
Mounting media	10 % PBS, pH 8.5 90 % Glycerol	Tissue preparation for imaging

Table S 6: Culture media

Media	Composition (per liter)	Purpose
0.5x MS (Murashige & Skoog)	10 g sucrose 2.2 g MS 0.5 g MES pH 5.8 (KOH) 8 g plant agar (for solid media)	Cultivation of plants
LB (Lysogeny broth)	10 g tryptone 5 g yeast extract 10 g NaCl 15 g bacto agar (for solid media)	Cultivation of bacteria
SOB (Super Optimal Broth)	5 g NaCl 20 g tryptone 5 g yeast extract 2.5 ml 1 M KCl	Cultivation of bacteria
YEB (Yeast extract broth)	1 g yeast extract 5 g beef extract 5 g peptone 5 g sucrose 0.5 g $MgSO_4 \cdot 7\ H_2O$ pH 7.0 (KOH)	Cultivation of *Agrobacterium*

Table S 7: Reaction kits

Name	Manufacturer	Purpose
RNeasy Plant Mini Kit	QIAGEN, Hilden, Germany	RNA extraction
QIAprep Spin Miniprep Kit	QIAGEN, Hilden, Germany	Isolation and purification of DNA
RevertAid H Minus First Strand cDNA Synthesis Kit	Thermo Fisher Scientific, Waltham, MA, USA	cDNA synthesis
Monarch DNA Gel Extraction Kit	New England Biolabs GmbH, Frankfurt am Main, Germany	Extraction of DNA from agarose gels
Monarch PCR & DNA Cleanup Kit	New England Biolabs GmbH, Frankfurt am Main, Germany	Purification of PCR products
Monarch Plasmid Miniprep Kit	New England Biolabs GmbH, Frankfurt am Main, Germany	Isolation and purification of DNA
Gateway BP Clonase II Enzyme Mix (incl. Proteinase K)	Thermo Fisher Scientific, Waltham, MA, USA	BP reaction

Gateway LR Clonase II Enzyme Mix (incl. Proteinase K)	Thermo Fisher Scientific, Waltham, MA, USA	LR reaction
NEBuilder HiFi DNA Assembly Cloning Kit	New England Biolabs GmbH, Frankfurt am Main, Germany	DNA assembly of two fragments
Q5 High-Fidelity DNA Polymerase (incl. 5X Q5 Reaction Buffer)	New England Biolabs GmbH, Frankfurt am Main, Germany	Cloning PCR, PCR-based mutation
5X FIREPol Master Mix, 12.5 mM MgCl$_2$	Solis BioDyne, Tartu, Estonia	Genotyping PCR, semiquantitative RT-PCR, Colony PCR
DNase I, RNase-free (incl. 10x Reaction Buffer and EDTA)	Thermo Fisher Scientific, Waltham, MA, USA	DNase treatment of RNA
TNT T7 Quick Coupled Transcription/Translation System	Promega GmbH, Walldorf, Germany	*In vitro* translation
T4 DNA Ligase (incl. 10x Reaction Buffer)	New England Biolabs GmbH, Frankfurt am Main, Germany	CRISPR/Cas9 cloning and cloning of pBluescript-*ID2-CDS+Stop*
SuperSignal West Pico PLUS Chemiluminescent Substrate	Thermo Fisher Scientific, Waltham, MA, USA	Detection of HRP-conjugated antibodies

Table S 8: Antibiotics

Antibiotic	Manufacturer	Solvent	Concentration of stock solution [mg/ml]
Basta (Phosphinotricin)	DUCHEFA Biochemie B.V., Haarlem, Netherlands	H$_2$O	10
Carbenicillin Disodium	Formedium Ltd., Hunstanton, U.K.	H$_2$O	100
Hygromycin B	Carl Roth GmbH + Co. KG, Karlsruhe, Germany	H$_2$O	50
Kanamycin	Carl Roth GmbH + Co. KG, Karlsruhe, Germany	H$_2$O	50
Rifampicin	Sigma-Aldrich Corporation, Taufkirchen, Germany	DMSO	100
Spectinomycin dihydrochloride pentahydrate	Sigma-Aldrich Corporation, Taufkirchen, Germany	H$_2$O	50

Table S 9: Restriction enzymes

Name	Manufacturer
AfeI	Thermo Fisher Scientific, Waltham, MA, USA
BsaI	New England Biolabs GmbH, Frankfurt am Main, Germany
DpnI	Thermo Fisher Scientific, Waltham, MA, USA
FspI	Thermo Fisher Scientific, Waltham, MA, USA
HincII	New England Biolabs GmbH, Frankfurt am Main, Germany
HindIII	Thermo Fisher Scientific, Waltham, MA, USA
KpnI	Thermo Fisher Scientific, Waltham, MA, USA
MboI	Thermo Fisher Scientific, Waltham, MA, USA
MluI	Thermo Fisher Scientific, Waltham, MA, USA
NdeI	Thermo Fisher Scientific, Waltham, MA, USA
PsyI	Thermo Fisher Scientific, Waltham, MA, USA

PvuI	New England Biolabs GmbH, Frankfurt am Main, Germany
PvuII	Thermo Fisher Scientific, Waltham, MA, USA
ScaI	Thermo Fisher Scientific, Waltham, MA, USA
SphI	New England Biolabs GmbH, Frankfurt am Main, Germany
SsiI	Thermo Fisher Scientific, Waltham, MA, USA
XbaI	Thermo Fisher Scientific, Waltham, MA, USA
XhoI	New England Biolabs GmbH, Frankfurt am Main, Germany

Table S 10: Antibodies

Antibody	Manufacturer	Purpose
Rabbit anti-GST, polyclonal (diluted 1:1,000 in 3 % milk TBS-T)	Carl Roth GmbH + Co. KG, Karlsruhe, Germany	Primary antibody for western blot
Mouse anti-HALO, monoclonal (diluted 1:1,000 in 3 % BSA TBS-T)	Promega GmbH, Walldorf, Germany	Primary antibody for western blot
Rabbit anti-GFP, polyclonal IgG (diluted 1:250 in 3 % milk TBS-T)	Torrey Pines Biolabs, Inc., Houston, TX, USA	Primary antibody for western blot
Rabbit anti-ID2, antiserum pooled rabbit 1 + 2 (diluted 1:200 in 3 % milk TBS-T)	Davids Biotechnologie GmbH, Regensburg, Germany	Primary antibody for western blot
Goat anti-Mouse IgG-HRP (diluted 1:10,000 in 3 % milk TBS-T))	Santa Cruz Biotechnology, Inc, Heidelberg, Germany	HRP-conjugated secondary antibody for western blot
Goat anti-Rabbit IgG Antibody, HRP conjugate (diluted 1:10,000 in 3 % milk TBS-T)	Merck KGaA, Darmstadt, Germany	HRP-conjugated secondary antibody for western blot

Table S 11: Vectors

Vector	Resistance in bacteria	Resistance in plants	Description
pDONR221	Kanamycin	-	Donor vector (Gateway)
pGEX-2T-GW	Ampicillin/Carbenicillin	-	N-terminal GST tag; Destination vector (Gateway)
pGEX-C-GST	Ampicillin/Carbenicillin	-	modified pGEX-2T-GW for C-terminal GST tag; Destination vector (Gateway)
pGWB401	Spectinomycin	Kanamycin	no promoter, no tag; Destination vector (Gateway)
pGWB401-mNeon	Spectinomycin	Kanamycin	modified pGWB401 with no promoter and mNeon tag; Destination vector (Gateway)
pGWB401-GFP	Spectinomycin	Kanamycin	modified pGWB401 with no promoter and GFP tag; Destination vector (Gateway)
pGWB401-3xGFP	Spectinomycin	Kanamycin	modified pGWB401 with no promoter and 3xGFP tag; Destination vector (Gateway)
pGWB402Ω	Spectinomycin	Kanamycin	2xCaMV35S enhancer and omega, no tag; Destination vector (Gateway)

pGWB405	Spectinomycin	Kanamycin	CaMV35S promoter, C-terminal sGFP tag; addgene #74799
pGWB562	Spectinomycin	Hygromycin	no promoter, C-terminal ER-sGFP tag; kindly provided by Tsuyoshi Nakagawa; Sultana et al. 2019
pGWB565	Spectinomycin	Hygromycin	no promoter, C-terminal NLS-sGFP tag; kindly provided by Tsuyoshi Nakagawa; Sultana et al. 2019
pGWB3	Hygromycin	Hygromycin	no promoter, C-terminal GUS tag; Destination vector (Gateway)
pGWB4	Hygromycin	Hygromycin	no promoter, C-terminal sGFP tag; Destination vector (Gateway)
pUBQ10-C-GFP	Spectinomycin	BASTA	UBQ10 promoter, C-terminal GFP tag; Destination vector (Gateway), Grefen et al. 2010
pIX-HALO	Ampicillin/Carbenicillin	-	Gateway-compatible *in vitro* expression vector; N-terminal fusion of a Halo-Tag; Joseph Ecker Lab; ABRC stock CD3-1742, kindly provided by the group of Isabel Bäurle
pBluescript II Sk (+)	Ampicillin/Carbenicillin	-	Standard cloning vectors (phagemid) with f1 (+) orientation for rescue of sense strand ssDNA; used for in situ RNA hybridisation
pGBT9-GW	Ampicillin/Carbenicillin	-	N-terminal GAL4 binding domain for Y2H; kindly provided by Frederik Börnke
pGGC025	Ampicillin/Carbenicillin	-	provides 3xGFP; addgene #48830

Table S 12: Primers

All primers were ordered at Merck. All primers used for Gateway (GW) cloning system contain the appropriate *att* sequence overhangs at the 5' end of the forward primer (F) and the 3' end of the reverse primer (R), respectively. All SALK, Wisc or SAIL T-DNA insertion lines were genotyped with left border primers (L) for genomic sequences, the recommended left border primer for T-DNA insertion and the respective right border primers as recommended by the Salk Institute Genome Analysis Laboratory.

Primer	Sequence	Applications
AT3G46540-PR-F	GGACAAGTTTGTACAAAAAAGCAGGCTgcCACGATAATGTTATTGTATT	Forward primer with GW overhang binding approximately 1.1 kb upstream of *EPSINOID2* start codon; GW cloning of *ID2::ID2-GFP/-GUS* and *ID2-1100::NLS-GFP*
ID2-nonStop-GW-R	GGACCACTTTGTACAAGAAAGCTGGGTtATCTGTGTTCTCATCAAGCAAGACTAC	Reverse primer with GW overhang binding at the end of *EPSINOID2* gene without stop codon; GW cloning of *ID2::ID2-GFP/-GUS*
ID2-gen-miRNA-F	CCAACAGATTGACGAGAAAGG	Amplifying pENT221-*ID2-gen* w/o part that was synthesized
ID2-gen-miRNA-R	GCAGCCTTTGAAATGGACCC	Amplifying pENT221-*ID2-gen* w/o part that was synthesized
ID2-UTS1-F	ATATATGGTCTCGATTGACTAAAGAAATAGATCCAAgttttagagctagaaatagcaagttaaaat	Amplifying sgRNA cassette out of the pCBC-DT1T2 vector; overhang with site specific BsaI sites and included sgRNA UTS1 (19 nt w/o NGG)
ID2-UTS2-F	ATATATGGTCTCGATTGTGGAATTAATGGTAATTGGgttttagagctagaaatagcaagttaaaat	Amplifying sgRNA cassette out of the pCBC-DT1T2 vector; overhang with site specific BsaI sites and included sgRNA UTS2 (19 nt w/o NGG)
ID2-DTS1-R	ATTATTGGTCTCTAAACCttctttagacaactgccatcaatctcttagtcgactctaccaata	Amplifying sgRNA cassette out of the pCBC-DT1T2 vector; overhang with site specific BsaI sites and included sgRNA DTS1 (19 nt w/o NGG)
ID2-DTS2-R	ATTATTGGTCTCTAAACTCCGTAAATGGATGGTTCTcaatctcttagtcgactctaccaata	Amplifying sgRNA cassette out of the pCBC-DT1T2 vector; overhang with site specific BsaI sites and included sgRNA DTS2 (19 nt w/o NGG)
ID2-CRISPR-geno-R	ccgagtatgacggataccaag	Genotyping *id2-3* for *EPSINOID2* deletion
ID2-gen-ATG-F	ATGTCAATGATGAGCAGAACTCG	Genotyping *id2-3* for *EPSINOID2* deletion; Cloning *MYC1::ID2-miR^R-GFP*
Off-target1-UTS1-F	ttggtacggaggaggagacaacg	Checking for off targets caused by UTS1
Off-target2-UTS1-F	GCTGACCAATCAAGGTGGAGA	Checking for off targets caused by UTS1
Off-target1-UTS1-R	GCCTCAAGGAACTGTGTTGC	Checking for off targets caused by UTS1
Off-target2-UTS1-R	ggtgacgccataggtagagt	Checking for off targets caused by UTS1

Table S 12: Primers

All primers were ordered at Merck. All primers used for Gateway (GW) cloning system contain the appropriate *att* sequence overhangs at the 5' end of the forward primer (F) and the 3' end of the reverse primer (R), respectively. All SALK, Wisc or SAIL T-DNA insertion lines were genotyped with left border primers (L) for genomic sequences, the recommended left border primer for T-DNA insertion and the respective right border primers as recommended by the Salk Institute Genome Analysis Laboratory.

Primer	Sequence	Applications
Cas9-F	CGAAGGGCTACAAGGAGGTG	Genotyping for Cas9
Cas9-R	CTCGTAGAGGCCGGTAATCG	Genotyping for Cas9
ID2-PR-GW-R	GGACCACTTTGTACAAGAAAGCTGGGTtcttttcttcaaattattat caagaacc	Reverse primer for cloning of promoter constructs
ID2-Y208-GW-F	GGACAAGTTTGTACAAAAAAGCAGGCTgcTATAGGAA ATGTAATTCC	Cloning of fragment corresponding 65 aa of EPSINOID2 for antibody generation
ID2-G272-GW-R	GGACCACTTTGTACAAGAAAGCTGGGTtTTAACCCAAA AGTGGGTTTAC	Cloning of fragment corresponding 65 aa of EPSINOID2 for antibody generation
LBb1.3	ATTTTGCCGATTTCGGAAC	Recommended left border primer to amplify part of the T-DNA insertion of all SALK lines; used for genotyping
Wisc LB p745	CGTCCGCAATGTGTTATTAAGTTGTC	Recommended left border primer to amplify part of the T-DNA insertion of all Wisconsin lines; used for genotyping
Sail garlic LB3	tagcatctgaatttcataaccaatctcgatacac	Recommended left border primer to amplify part of the T-DNA insertion of all SAIL lines; used for genotyping
SALK_042677-R	TCAGTTGAGGCAATTGATGTG	Right border primer for genotyping *id2-1*
SALK_042677-L	TTTTGTTGCTATAACGGGACG	Left border primer for genotyping *id2-1*
MYC1-PR-F	GTACAAAAAAGCAGGCTgcCACGCCGGTTGAGTACAAA AGGGTTTGTC	Amplification of *MYC1* (AT4G00480) promoter for cloning *MYC1::ID2-miR^R-GFP* with GW
MYC1-PR-R	GAGTTCTGCTCATCATTGACATATCTAGATATCGTGAA GAACTGAATTTAAAAG	Amplification of *MYC1* (AT4G00480) promoter for cloning *MYC1::ID2-miR^R-GFP* with GW
pENT221-R	GTGGGCAGCCTGCTTTTTGTAC	Amplification of the pENT221-*ID2-ID2::ID2-miR^R* without the *EPSINOID2* promoter for cloning *MYC1::ID2-miR^R-GFP*

134

Table S 12: Primers

All primers were ordered at Merck. All primers used for Gateway (GW) cloning system contain the appropriate *att* sequence overhangs at the 5' end of the forward primer (F) and the 3' end of the reverse primer (R), respectively. All SALK, Wisc or SAIL T-DNA insertion lines were genotyped with left border primers (L) for genomic sequences, the recommended left border primer for T-DNA insertion and the respective right border primers as recommended by the Salk Institute Genome Analysis Laboratory.

Primer	Sequence	Applications
35S-GW-F	GGACAAGTTTGTACAAAAAAGCAGGCTgctgagactttcaaca aaggg	Amplification of 35S promoter from pGWB405 vector
35S-GW-R	GGACCACTTTGTACAAGAAAGCTGGGTttgttctctccaaatgaa atgaac	Amplification of 35S promoter from pGWB405 vector
TUB6β-F	ACTCTTCCCTGATCTTAGATATGAGC	semiquantitative RT-PCR, reference gene *TUB6β* (AT5G12250)
TUB6β-R	GTCTTCAAGGTTTCCAAGTATGTCA	semiquantitative RT-PCR, reference gene *TUB6β* (AT5G12250)
EF1α-F	TGAGCACGCTCTTCTTGCTTTCA	semiquantitative RT-PCR, reference gene *EF1α* (AT5G60390)
EF1α-R	GGTGGTGGCATCCATCTTGTTA	semiquantitative RT-PCR, reference gene *EF1α* (AT5G60390)
EPSINOID2-RTPCR-F	CTCATGGACCAGAGAGTGTTTC	semiquantitative RT-PCR; genotyping *id2-3* for *EPSINOID2* deletion
EPSINOID2-RTPCR-R	CATACCCGTCCTAGATTCCTCG	semiquantitative RT-PCR
ID2-geno-PR-F	GGAGTGAATTAGCTCAGCGG	Colony PCRs
M13-R	GGAAACAGCTATGACCATG	Colony PCRs
M13-F	GTAAAACGACGGCCAGTG	Colony PCRs
M13-21F	TGTAAAACGACGGCCAGT	Sequencing of all pENT221 constructs
M13-29R	CAGGAAAACAGCTATGACC	Sequencing of all pENT221 constructs
AT3G46540-R-1	ATCGGAAACACTCTCTGGTCC	Sequencing of pENT221-*ID2::ID2-gen*
CPC-GW-F	GGACAAGTTTGTACAAAAAAGCAGGCTgcctgcagatcttatac aaatc	Amplification of genomic *CPC* (AT2G46410) including 1.2 kb promoter region for GW cloning into pGWB401-mNeon
CPC-GW-R	GGACCACTTTGTACAAGAAAGCTGGGTtTTTCCTAAAA AAGTCTCTTCG	Amplification of genomic *CPC* (AT2G46410) including 1.2 kb promoter region for GW cloning into pGWB401-mNeon

135

Table S 12: Primers

All primers were ordered at Merck. All primers used for Gateway (GW) cloning system contain the appropriate *att* sequence overhangs at the 5' end of the forward primer (F) and the 3' end of the reverse primer (R), respectively. All SALK, Wisc or SAIL T-DNA insertion lines were genotyped with left border primers (L) for genomic sequences, the recommended left border primer for T-DNA insertion and the respective right border primers for T-DNA insertion as recommended by the Salk Institute Genome Analysis Laboratory.

Primer	Sequence	Applications
SCM-Sk_086357-L	GTTCCTGTGAGCTTGTTGTCC	Genotyping of *scm-2* T-DNA insertion line SALK_086357
SCM-Sk_086357-R	TATCACTTTGGGAGCACCATC	Genotyping of *scm-2* T-DNA insertion line SALK_086357
CPC-Sail_310_C06-L	TCTTCGTCTGTTGGCAAAAAC	Genotyping of *cpc* T-DNA insertion line SAIL_310_C06
CPC-Sail_310_C06-R	TTTTCTTTTCCTTTTCGAGCC	Genotyping of *cpc* T-DNA insertion line SAIL_310_C06
GL2-Salk-L	ACCACCGATCAGATCAGACAC	Genotyping of *gl2-2* and *gl2-3* T-DNA insertion lines SALK_130213 and SALK_039825
GL2-Salk-R	GGAGTTTTCGAGGTGGAGATC	Genotyping of *gl2-2* and *gl2-3* T-DNA insertion lines SALK_130213 and SALK_039825
GL3-Wisc-L	TTTTCTCAAGGTCATGAACCG	Genotyping of *gl3* T-DNA insertion line WiscDsLox412G05
GL3-WiscDsLox412G05-R	TTGGAGGAGTCGTTGAGATTG	Genotyping of *gl3* T-DNA insertion line WiscDsLox412G05
MYC1-Salk_057388-L	CTTGTTCTCCGCATATTGAGC	Genotyping of *myc1-1* T-DNA insertion line SALK_057388
MYC1-Salk_057388-R	tgaccaagtcaaccactctc	Genotyping of *myc1-1* T-DNA insertion line SALK_057388
WER-F	cttcatttgctcaaaattagtttctc	Genotyping primer for *wer-1* (spanning point mutation in codon 93 TGG → TGA); PCR product was digested with MboI
WER-R	TGAACCCAAAGTGAACTCAAGTAG	Genotyping primer for *wer-1* (spanning point mutation in codon 93 TGG → TGA); PCR product was digested with MboI
EGL3-F	ACGGTGCCGGACAATCTAAA	Genotyping primer for *egl3-1* (spanning point mutation in codon 26 TGG → TGA); PCR product was sequenced
EGL3-R	TCTCCCCACTCCAACACTct	Genotyping primer for *egl3-1* (spanning point mutation in codon 26 TGG → TGA); PCR product was sequenced

Table S 12: Primers

All primers were ordered at Merck. All primers used for Gateway (GW) cloning system contain the appropriate *att* sequence overhangs at the 5' end of the forward primer (F) and the 3' end of the reverse primer (R), respectively. All SALK, Wisc or SAIL T-DNA insertion lines were genotyped with left border primers (L) for genomic sequences, the recommended left border primer for T-DNA insertion and the respective right border primers as recommended by the Salk Institute Genome Analysis Laboratory.

Primer	Sequence	Applications
GL3-F	TGCGTTCACCAGTCGCTAAA	Genotyping primer for *gl3-1* (spanning point mutation in codon 378 CAG → TAG); PCR product was digested with SsiI
GL3-R	CATTCCTTGTGATGGTGCCG	Genotyping primer for *gl3-1* (spanning point mutation in codon 378 CAG → TAG); PCR product was digested with SsiI
mir844-CRISPR-F	gaaaccaattctctgtctctgt	Genotyping primer for *mir844* CRISPR/Cas9 deletion mutant
mir844-CRISPR-R	ccaacagcatagatcaaaggctaac	Genotyping primer for *mir844* CRISPR/Cas9 deletion mutant
MIR844-CRISPR-F	ATATATGGTCTCGATTGGAGTGAGTTCATGATGGTTgttttagagctagaaatagcaagttaaaat	CRISPR/Cas9-mediated deletion of *MIR844* gene
MIR844-CRISPR-R	ATTATTGGTCTCTAAACTAGACAACATTGAAAAGAAcaatctcttagtcgactctaccaata	CRISPR/Cas9-mediated deletion of *MIR844* gene
mir844-CRISPR-g-R	GTAGAAGAGACCACTCACCCTC	Genotyping primer for *mir844* CRISPR/Cas9 deletion mutant
miR844-PR-GW-F	GGACAAGTTTGTACAAAAAAGCAGGCTgcgctggggattgaagaaacg	Cloning of *MIR844* promotor for *MIR844::ER-GFP/GUS* reporter line
miR844-PR-GW-R	GGACCACTTTGTACAAGAAAGCTGGGTttaaccatcatgaactcactc	Cloning of *MIR844* promotor for *MIR844::ER-GFP/GUS* reporter line
ID2-CDS-KpnI-F	GATCGGTACCATGTCAATGATGAGCAGAAC	Restriction cloning of *ID2-CDS* into pBluescript II Sk (+)
ID2-CDSStop-XbaI-R	GATCTCTAGATTAATCTGTGTTCTCATCAAGC	Restriction cloning of *ID2-CDS* into pBluescript II Sk (+)
MIR844-stemloop-R	GGACCACTTTGTACAAGAAAGCTGGGTtagatgttgaaaagggggaaa	GW cloning of *MIR844* stemloop for miRNA844 overexpression
MIR844-stemloop-F	GGACAAGTTTGTACAAAAAAGCAGGCTgcgagtgagttcatgatggtta	GW cloning of *MIR844* stemloop for miRNA844 overexpression
3xGFP-pGBW401-F	acaaagtggttgataacagcatggtttctaaaggtgaagag	Amplification of 3xGFP from pGGC025

137

Table S 12: Primers

All primers were ordered at Merck. All primers used for Gateway (GW) cloning system contain the appropriate *att* sequence overhangs at the 5' end of the forward primer (F) and the 3' end of the reverse primer (R), respectively. All SALK, Wisc or SAIL T-DNA insertion lines were genotyped with left border primers (L) for genomic sequences, the recommended left border primer for T-DNA insertion and the respective right border primers as recommended by the Salk Institute Genome Analysis Laboratory.

Primer	Sequence	Applications
3xGFP-pGBW401-R	gggaaattcgagctcaagcttacttgtacagctcgtccatg	Amplification of 3xGFP from pGGC025
1xGFP-pGBW401-R	gggaaattcgagctcaagcttacttgtaaagctcatccatacc	Amplification of 1xGFP from pGGC025
3xGFP-Seq-R	ccactaccagaacctgatcc	Sequencing of 3xGFP constructs
ACT2-CDS-GW-F	GGACAAGTTTGTACAAAAAAGCAGGCTTAATGGCTGAGGCTGATGA	Amplification of *ACT2-CDS* for cloning HALO-tagged constructs using GW for *in vitro* translation
ACT2-CDS-GW-R	GGACCACTTTGTACAAGAAAGCTGGGTTGAAACATTTTCTGTGAACGATTCC	Amplification of *ACT2-CDS* for cloning HALO-tagged constructs using GW for *in vitro* translation
CHC1-CDS-GW-F	GGACAAGTTTGTACAAAAAAGCAGGCTTAATGGCGGCTGCTAAC	Amplification of *CHC1-CDS* for cloning HALO-tagged constructs using GW for *in vitro* translation
CHC1-CDS-GW-R	GGACCACTTTGTACAAGAAAGCTGGGTTGTAGCCGCCCATCG	Amplification of *CHC1-CDS* for cloning HALO-tagged constructs using GW for *in vitro* translation
WDL4-CDS-GW-F	GGACAAGTTTGTACAAAAAAGCAGGCTTAATGGCGTCCGAGGAT	Amplification of *WDL4-CDS* for cloning HALO-tagged constructs using GW for *in vitro* translation
WDl4-CDS-GW-R	GGACCACTTTGTACAAGAAAGCTGGGTTGCCTCCCACTACAACC	Amplification of *WDL4-CDS* for cloning HALO-tagged constructs using GW for *in vitro* translation
PVA12-CDS-GW-F	GGACAAGTTTGTACAAAAAAGCAGGCTTAATGAGTAACGAGCTTCTCAC	Amplification of *PVA12-CDS* for cloning HALO-tagged constructs using GW for *in vitro* translation
PVA12-CDS-GW-R	GGACCACTTTGTACAAGAAAGCTGGGTTTGTCCTCTTCATAATGTATCCCAG	Amplification of *PVA12-CDS* for cloning HALO-tagged constructs using GW for *in vitro* translation
ATMIN7-CDS-GW-F	GGACAAGTTTGTACAAAAAAGCAGGCTTAATGGCGGCTGGTG	Amplification of *MIN7-CDS* for cloning HALO-tagged constructs using GW for *in vitro* translation
ATMIN7-CDS-GW-R	GGACCACTTTGTACAAGAAAGCTGGGTTCTGTTGCAAAAGTGGCTTC	Amplification of *MIN7-CDS* for cloning HALO-tagged constructs using GW for *in vitro* translation

Table S 12: Primers

All primers were ordered at Merck. All primers used for Gateway (GW) cloning system contain the appropriate *att* sequence overhangs at the 5' end of the forward primer (F) and the 3' end of the reverse primer (R), respectively. All SALK, Wisc or SAIL T-DNA insertion lines were genotyped with left border primers (L) for genomic sequences, the recommended left border primer for T-DNA insertion and the respective right border primers as recommended by the Salk Institute Genome Analysis Laboratory.

Primer	Sequence	Applications
PME38-CDS-GW-F	GGGGACAAGTTTGTACAAAAAAGCAGGCTTAATGGTT TTCGGAAATGAAATGTGCG	Amplification of *PME38-CDS* for cloning HALO-tagged constructs using GW for *in vitro* translation
PME38-CDS-GW-R	GGGGACCACTTTGTACAAGAAAGCTGGGTTGAGATTG ATGGTGAAAGGCACTTTGG	Amplification of *PME38-CDS* for cloning HALO-tagged constructs using GW for *in vitro* translation
CNGC5-CDS-GW-F	GGACAAGTTTGTACAAAAAAGCAGGCTgcATGGCAGG GAAAAGAGAAAAC	Amplification of *CNGC5-CDS* for cloning HALO-tagged constructs using GW for *in vitro* translation
CNGC5-CDS-GW-R	GGACCACTTTGTACAAGAAAGCTGGGTtGTCAGCAGT GAAATCAGGCTC	Amplification of *CNGC5-CDS* for cloning HALO-tagged constructs using GW for *in vitro* translation
AP3D-CDS-GW-F	GGACAAGTTTGTACAAAAAAGCAGGCTgcATGTCGTC GTCTTCCACTTC	Amplification of *AP3D-CDS* for cloning HALO-tagged constructs using GW for *in vitro* translation
AP3D-CDS-GW-R	GGACCACTTTGTACAAGAAAGCTGGGTtCAAGAGAAA ATCTGGAATTATAAACTTG	Amplification of *AP3D-CDS* for cloning HALO-tagged constructs using GW for *in vitro* translation
SEC6-CDS-GW-F	GGACAAGTTTGTACAAAAAAGCAGGCTgcATGATGGT CGAAGATCTTGG	Amplification of *SEC6-CDS* for cloning HALO-tagged constructs using GW for *in vitro* translation
SEC6-CDS-GW-R	GGACCACTTTGTACAAGAAAGCTGGGTtAGTGAGTTTT CGCCACATAG	Amplification of *SEC6-CDS* for cloning HALO-tagged constructs using GW for *in vitro* translation
ECA4-CDS-GW-F	GGACAAGTTTGTACAAAAAAGCAGGCTgcATGGCTCC GAGTATTCGAAAAG	Amplification of *ECA4-CDS* for cloning HALO-tagged constructs using GW for *in vitro* translation
ECA4-CDS-GW-R	GGACCACTTTGTACAAGAAAGCTGGGTtGTAAGGATT GTTGTAGTAATACCCC	Amplification of *ECA4-CDS* for cloning HALO-tagged constructs using GW for *in vitro* translation
CNGC15-CDS-GW-F	GGACAAGTTTGTACAAAAAAGCAGGCTgcATGGGTTAT GGTAACTCAAGATCTG	Amplification of *CNGC15-CDS* for cloning HALO-tagged constructs using GW for *in vitro* translation
CNGC15-CDS-GW-R	GGACCACTTTGTACAAGAAAGCTGGGTtTTCACTAGAA AAATCTGGCTCTACTG	Amplification of *CNGC15-CDS* for cloning HALO-tagged constructs using GW for *in vitro* translation

Table S 12: Primers

All primers were ordered at Merck. All primers used for Gateway (GW) cloning system contain the appropriate *att* sequence overhangs at the 5' end of the forward primer (F) and the 3' end of the reverse primer (R), respectively. All SALK, Wisc or SAIL T-DNA insertion lines were genotyped with left border primers (L) for genomic sequences, the recommended left border primer for T-DNA insertion and the respective right border primers as recommended by the Salk Institute Genome Analysis Laboratory.

Primer	Sequence	Applications
CAP1-CDS-GW-F	GGACAAGTTTGTACAAAAAAGCAGGCTgcATGGCGCT AAGCATGCGAAAAG	Amplification of *CAP1-CDS* for cloning HALO-tagged constructs using GW for *in vitro* translation
CAP1-CDS-GW-R	GGACCACTTTGTACAAGAAAGCTGGGTtGTAAGGGTT GTTGTAGTAATAACCC	Amplification of *CAP1-CDS* for cloning HALO-tagged constructs using GW for *in vitro* translation
RSW10-CDS-GW-F	GGACAAGTTTGTACAAAAAAGCAGGCTgcATGGGTTCT GCATTCGATCC	Amplification of *RSW10-CDS* for cloning HALO-tagged constructs using GW for *in vitro* translation
RSW10-CDS-GW-R	GGACCACTTTGTACAAGAAAGCTGGGTtCCAAACCTA TCCTTGACGG	Amplification of *RSW10-CDS* for cloning HALO-tagged constructs using GW for *in vitro* translation
PLDa1-CDS-GW-F	GGACAAGTTTGTACAAAAAAGCAGGCTgcATGGCGCA GCATCTGTTGCAC	Amplification of *PLDα1-CDS* for cloning HALO-tagged constructs using GW for *in vitro* translation
PLDa1-CDS-GW-R	GGACCACTTTGTACAAGAAAGCTGGGTtGGTTGTAAG GATTGGAGGCAGG	Amplification of *PLDα1-CDS* for cloning HALO-tagged constructs using GW for *in vitro* translation
CCS52B-CDS-GW-F	GGACAAGTTTGTACAAAAAAGCAGGCTgcATGGCATC GCCACAGAGTACC	Amplification of *CCS52B-CDS* for cloning HALO-tagged constructs using GW for *in vitro* translation
CCS52B-CDS-GW-R	GGACCACTTTGTACAAGAAAGCTGGGTtCGGATCTGT GTCCTCCCCAATG	Amplification of *CCS52B-CDS* for cloning HALO-tagged constructs using GW for *in vitro* translation
BETA1-COP-CDS-GW-F	GGACAAGTTTGTACAAAAAAGCAGGCTgcATGGTTTTT CCTTTTCATTTGAGC	Amplification of *BETA1-COP-CDS* for cloning HALO-tagged constructs using GW for *in vitro* translation
BETA1-COP-CDS-GW-R	GGACCACTTTGTACAAGAAAGCTGGGTtGCTACTACCC TTTGTTTGAGG	Amplification of *BETA1-COP-CDS* for cloning HALO-tagged constructs using GW for *in vitro* translation
IRE-CDS-GW-F	GGACAAGTTTGTACAAAAAAGCAGGCTgcATGTCTAC GACGGAACCGTCG	Amplification of *IRE-CDS* for cloning HALO-tagged constructs using GW for *in vitro* translation
IRE-CDS-GW-R	GGACCACTTTGTACAAGAAAGCTGGGTtGTTTCGGGT CGAGGGGCTG	Amplification of *IRE-CDS* for cloning HALO-tagged constructs using GW for *in vitro* translation

Table S 12: Primers

All primers were ordered at Merck. All primers used for Gateway (GW) cloning system contain the appropriate *att* sequence overhangs at the 5' end of the forward primer (F) and the 3' end of the reverse primer (R), respectively. All SALK, Wisc or SAIL T-DNA insertion lines were genotyped with left border primers (L) for genomic sequences, the recommended left border primer for T-DNA insertion and the respective right border primers as recommended by the Salk Institute Genome Analysis Laboratory.

Primer	Sequence	Applications
VHA-A-CDS-GW-F	GGACAAGTTTGTACAAAAAAGCAGGCTgcATGCCGGCGTTTTACGGGAGG	Amplification of *VHA-A-CDS* for cloning HALO-tagged constructs using GW for *in vitro* translation
VHA-A-CDS-GW-R	GGACCACTTTGTACAAGAAAGCTGGGTtCCGAGTTTCATCTTCCAAAGCACG	Amplification of *VHA-A-CDS* for cloning HALO-tagged constructs using GW for *in vitro* translation
VHA-A1-CDS-GW-F	GGACAAGTTTGTACAAAAAAGCAGGCTgcATGGAGGAATTCTTAGATAAGTTGC	Amplification of *VHA-A1-CDS* for cloning HALO-tagged constructs using GW for *in vitro* translation
VHA-A1-CDS-GW-R	GGACCACTTTGTACAAGAAAGCTGGGTtGATTAAAGCGAAAGAGAAAGGC	Amplification of *VHA-A1-CDS* for cloning HALO-tagged constructs using GW for *in vitro* translation
PME38-gen-1000-GW-F	GGACAAGTTTGTACAAAAAAGCAGGCTgcGGTGGCATGAGTGTATCTTTG	Amplification of genomic *PME38* including 1049 bp promoter region for GW cloning into pGWB401-GFP
PME38-gen-600-GW-F	GGACAAGTTTGTACAAAAAAGCAGGCTgcgagtttccagatggaagattaggt	Amplification of genomic *PME38* including 612 bp promoter region for GW cloning into pGWB401-GFP
PME38-gen-GW-R	GGACCACTTTGTACAAGAAAGCTGGGTtGAGATTGATGGTGAAAGGCAC	Amplification of genomic *PME38* for GW cloning into pGWB401-GFP
Intron_FW MAF5	TTTTTTGCCCCCTTCGAATC	Check cDNA for genomic DNA contamination; Omidbakhshfard et al. 2012
Intron_REV MAF5	ATCTTCCGCCACCACATTGTAC	Check cDNA for genomic DNA contamination; Omidbakhshfard et al. 2012

Table S 13: Expendable items

Item	Manufacturer
96-well PCR plates	BRAND GMBH + CO KG, Wertheim, Germany
Adhesion slides, Menzel-Gläser, Polysine	Fisher Scientific GmbH, Schwerte, Germany
Amersham Protran 0.45 nitrocellulose western blotting membranes	GE Healthcare Europe GmbH, Freiburg, Germany
Autotube-Racks	Carl Roth GmbH + Co. KG, Karlsruhe, Germany
Biopsy embedding cassettes	Carl Roth GmbH + Co. KG, Karlsruhe, Germany
Cell culture dishes	VWR International GmbH, Darmstadt, Germany
Electroporation cuvettes for long electrodes, 2 mm, Peqlab	VWR International GmbH, Darmstadt, Germany
Gosselin™ Square Petri Dish, 120x120mm, Corning®	VWR International GmbH, Darmstadt, Germany
High Precision cover glasses (24 x 50 mm)	Paul Marienfeld GmbH & Co. KG, Lauda-Königshofen, Germany
Microscope slides (76 x 26 mm)	DURAN Glastechnik GmbH & Co. KG, Wertheim, Germany
PCR strips of 8 tubes	VWR International GmbH, Darmstadt, Germany
Pipette tips (10 µl, 200 µl, 1000 µl)	Biozym Scientific GmbH, Hessisch Oldendorf, Germany
Polypropylene Columns (5 ml)	QIAGEN, Hilden, Germany
Polypropylene tubes (13 ml, 15 ml und 50 ml)	Sarstedt AG & Co., Nümbrecht, Germany
Processing cassettes	Leica Biosystems Nussloch GmbH, Nussloch, Germany
Protein LoBind® Tubes (1.5 ml)	Eppendorf SE, Hamburg, Germany
Reaction tubes (1.5 ml and 2 ml)	Sarstedt AG & Co., Nümbrecht, Germany
Semi-micro cuvette, PS, 1.5 ml	BRAND GMBH + CO KG, Wertheim, Germany
Supelco glass beads, 2 mm	Merck KGaA, Darmstadt, Germany
Whatman Gel Blot Paper	GE Healthcare Europe GmbH, Freiburg, Germany

6.2 Methods

CRISPR/Cas9 full deletion mutants

The *id2-3* and *mir844* mutants were generated by using the CRISPR/Cas9 system using the adapted protocol provided by Daphne Goring from University of Toronto. SgRNAs UTS1/2 and DTS1/2 for *EPSINOID2* and UTS3 and DTS3 for *MIR844* were designed using CHOPCHOP (chopchop.cbu.uib.no, Labun et al. 2019) and CRISPRdirect (crispr.dbcls.jp, Naito et al. 2015) and are listed in Table S 14.

Table S 14: Target sequences for *EPSINOID2* and *MIR844* deletion.

Name	Target Sequence	Position	GC content	Efficiency	Off-targets according to Cas Offinder (MM = mis-match)
UTS1	ACTAAAGAAATAGATCCAAAGG	5'UTR of *ID2*	30 %	60 %	MM0: 1, MM1: 0, MM2: 0, MM3: 3
UTS2	TGGAATTAATGGTAATTGGTGG	5'UTR of *ID2*	35 %	65 %	MM0: 1, MM1: 0, MM2: 0, MM3: 2
DTS1	ATGGCAGTTGTCTAAAGAATGG	3'UTR of *ID2*	35 %	48 %	MM0: 1, MM1: 0, MM2: 0, MM3: 0
DTS2	AGAACCATCCATTTACGGATGG	4th exon of *ID2*	45 %	64 %	MM0: 1, MM1: 0, MM2: 0, MM3: 1
UTS3	GAGTGAGTTCATGATGGTTAGG	3' end of *MIR844*	40 %	53 %	MM0: 1, MM1: 0, MM2: 0, MM3: 0
DTS3	TTCTTTTCAATGTTGTCTAAGG	5' end of *MIR844*	30 %	40 %	MM0: 1, MM1: 0, MM2: 0, MM3: 0

Each sgRNA was included in primers to amplify the sgRNA cassette out of the pCBC-DT1T2 vector using the cloning PCR protocol.

Primer templates 5' to 3' for two sgRNAs:

Forward:

ATATATGGTCTCGATTG\\NNNNNNNNNNNNNNNNNNNN\\gttttagagctagaaatagcaagttaaaat

Reverse:

ATTATTGGTCTCTAAAC\\NNNNNNNNNNNNNNNNNNNN\\caatctcttagtcgactctaccaata

The first parts contain site-specific BsaI sites for Golden Gate cloning and the last parts overhangs complementary to the pCBC-DT1T2 backbone. The forward primer carries the first sgRNA (UTS) and the reverse primer the second sgRNA (DTS) without the PAM sequence represented as "N". Primers are listed in Table S 12. PCR products were cleaned using the Monarch DNA Gel Extraction Kit (NEB) and cloned into pHEE401E using the Golden Gate reaction as followed:

Golden Gate reaction:
- 1.5 µl Cutsmart buffer (NEB)
- 1.5 µl 10 mM ATP (NEB)
- 1.5 µl pHEE401E
- 150 ng PCR product (here: 1 µl each)
- 1 µl BsaI-HFv2 (NEB)
- 1 µl T4 DNA ligase (NEB, 2,000,000 units/ml)
- to 15 µl H_2O

Program:	37°C 5:00	⎤ 50 cycles
	16°C 5:00	⎦
	50°C 5:00	
	80°C 5:00	

Afterwards 4 µl of the reactions were transformed into DH5α and plated on LB medium containing Kanamycin. The resulting products were transformed into *A. tumefaciens* and subsequently introduced into Col-0 via floral dipping (protocols see below).

After obtaining homozygous full deletion lines, plants were checked for off-targets predicted by Cas-OFFinder (www.rgenome.net/cas-offinder, Bae et al. 2014) which are listed in detail in Table S 15.

Table S 15: Predicted off-targets from sgRNAs used for *EPSINOID2* and *MIR844* deletion.

Target	Off-target	Off-target sequence	Position	Corresponding Locus
UTS1	1	ACTAAAcAAATAGAagCAAAGG	Chr 4: 8213317	intergenic region
UTS1	2	ACTcAtGAAATAGATCgAATGG	Chr 1: 27084817	AT1G71960 (ABCG25, ATP-BINDING CASETTE G25)

Genotyping PCR

PCR reaction:	5.5 µl	H_2O
	3 µl	Primer mix
	0.5 µl	DMSO
	3 µl	Template (extracted DNA)
	3 µl	5X FIREPol Master Mix

PCR program:	94°C 2:30	
	94°C 0:25	
	55°C 0:25	⎤
	72°C 1:20 (0:30 per kb)	⎥ 34 cycles
	72°C 7:00	⎦
	15°C ∞	

Annealing temperature was used as required for the respective primer pair and elongation time was adjusted to the respective length of the product size.

Cloning PCR

PCR reaction:
30.5 µl	H_2O
10 µl	5x Q5 Reaction Buffer
1 µl	10 mM dNTP Mix
5 µl	Primer mix
1.5 µl	DMSO
1.5 µl	Template DNA
0.5 µl	Q5 High-Fidelity DNA Polymerase

PCR program:

98°C   0:30
98°C   0:10
55°C   0:30
72°C   1:30   (0:30 per kb)   ⎤
72°C   7:00   ⎥ 35 cycles
15°C   ∞

The 50 µl PCR reaction was divided into two 25 µl batches in an 8-well PCR strip.

PCR for testing the DNaseI-treated RNA

PCR reaction:
10 µl	H_2O
2 µl	Intron-specific primer mix
1 µl	DNaseI-treated RNA
3 µl	5x FIREPol MasterMix

PCR program:

94°C   2:30
94°C   0:25
65°C   0:25   ⎤ Start: 65°C, decrease 1°C every 2 cycles
72°C   0:30   ⎥ 30 cycles
72°C   7:00   ⎦
15°C   ∞

PCR for testing the cDNA

PCR reaction:
10 µl	H_2O
2 µl	Primer mix for the respective reference gene

1 µl	1:10 diluted cDNA
3 µl	5x FIREPol MasterMix

PCR program:

94°C	2:30	
94°C	0:25	
57°C	0:25	
72°C	0:30	30 cycles
72°C	7:00	
15°C	∞	

Semiquantitative RT-PCR

PCR reaction:

26.6 µl	H₂O
6.7 µl	Primer mix for *EPSINOID2*
6.7 µl	cDNA
10.0 µl	5x FIREPol MasterMix

PCR program:

94°C	2:30		
94°C	0:25		
55°C	0:25	28 cycles	
72°C	0:30		
10°C	1:00	Sampling	
94°C	0:25		4 x
55°C	0:25	2 cycles	
72°C	0:30		
10°C	1:00		

8.5 µl from each sample were taken after 28, 30, 32, 34 and 36 cycles, mixed with 3 µl loading buffer and loaded onto an agarose gel.

BP reaction

Donor vector for all constructs was Gateway pDONR221.

BP reaction:

1 µl   pDONR221

2 µl   PCR product

| 1 µl | 1X TE buffer |
| 1 µl | Gateway BP Clonase II Enzyme Mix |

After mixing and centrifuging, the reaction was incubated overnight at room temperature and stopped by adding 1 µl ProteinaseK and incubation for 10 min at 37°C the next day. The resulting vector carrying the sequence of interest is designated as pENT221.

Transformation of chemical competent *E. coli* DH5α

50 µl cells were unfrozen on ice and 2.5 µl of BP or LR reaction were added. Cells were incubated for 20 min on ice and subsequently a heat shock was performed for 60 s at 42°C in a thermomixer. After 3 min on ice, 1 ml liquid SOB media was added. After 1 h incubation at 37°C and 250 rpm, the cells were centrifuged for 1 min at 5,000 rpm and most of the supernatant was discarded. The pellet was resuspended in approximately 100 µl of the left-over supernatant and the cells were plated on LB media with the appropriate antibiotics (Table S 8) and incubated over night at 37°C.

LR reaction

In the LR reaction, the gene of interest was transferred from the respective pENT221 into the desired Gateway-compatible destination vector.

LR reaction:

1 µl	pENT221
2 µl	Destination vector
1 µl	1X TE buffer
1 µl	Gateway LR Clonase II Enzyme Mix

The reaction was shortly mixed, centrifuged and incubated for 4 h at room temperature. The reaction was terminated with 1 µl ProteinaseK and incubation for 10 min at 37°C.

DNA Quantification using the GeneRuler 1 kb DNA ladder

For approximate DNA quantification of PCR fragments, the GeneRuler 1 kb DNA ladder was used as recommended in the NEBuilder HiFi DNA Assembly Cloning Kit.

5 µl of the PCR product and 5 µl of the GeneRuler 1 kb DNA ladder were loaded on 1 % agarose gel. According to the GeneRuler manual, concentration of the ladder is 0.1 µg/µl. By loading 5 µl a final mass of 0.5 µg of the ladder runs in the gel. After electrophoresis, intensity

of the fragments band was compared to the bands of the ladder. For calculation of the final DNA concentration of the loaded sample, the corresponding ng/0.5 µl value of the band with the same intensity was used. With this concentration the amount of DNA in pmol was then calculated applying the formula (1) below in which N is the number of nucleotides in bp and 600 pg/pmol is the average molecular weight of a nucleotide pair.

$$\mu g \, DNA \, \cdot \, \frac{pmol}{660 \, pg} \, \cdot \, \frac{10^6 \, pg}{1 \, \mu g} \, \cdot \, \frac{1}{N} = pmol \, DNA \qquad (1)$$

The amount of DNA in pmol was needed to assemble two fragments using the NEBuilder HiFi DNA Assembly Cloning Kit (NEB).

DNA Assembly of fragments with the NEBuilder HiFi DNA Assembly Cloning Kit
The following recommendations for assembly of 2 fragments were considered: the total amount of fragments should be between 0.03 and 0.2 pmol, the DNA ratio of vector:insert should be 1:2 and the mass of the vector should be 50 - 100 ng. The reaction was set up as described in the NEBuilder HiFi DNA Assembly protocol and incubated at 50°C for 15 min and afterwards stored at -20°C.

Transformation of electrocompetent *A. tumefaciens* GV3101
50 µl electrocompetent *A. tumefaciens* GV3101 cells were unfrozen on ice and pipetted into an electroporation cuvette (2 mm, VWR). 2 µl of the plasmid were added and cells were mixed by flicking the cuvette. After 2 min incubation on ice, cells were transformed using the Ec2 program of the MicroPulser Electroporator (BioRad). After the pulse, 1 ml SOB was immediately mixed with the bacteria in the cuvette, the cells were decanted into a 1.5 ml tube and incubated for 2 h at 28°C and 350 rpm. The bacteria were then centrifuged for 2 min at 5,000 rpm, most of the supernatant was discarded and the pellet resuspended in approximately 100 µl of the remaining supernatant. The bacteria were plated on solid YEB media containing rifampicin (Rif, 100 µg/ml) and the appropriate antibiotics for the selection of the transformed cells carrying the construct. Colonies grew for 2 days at 28°C in an incubator.

Stable transformation of *A. thaliana* using the floral-dip method
Cultivation of plants:
Seeds of *A. thaliana* Col-0, homozygous *id2-1* or *id2-3* mutants were directly sown on soil. 4 plants grew for approximately 3-4 weeks in small pots and for each construct 4-5 pots were

used for transformation. One week prior transformation, the main inflorescence stem was cut to increase the number of unopened buds which should improve transformation efficiency. Before dipping, plants were removed from the growth chamber and siliques were cut off.

Cultivation of *A. tumefaciens* and floral dipping:

Single colonies of A. tumefaciens carrying the construct of interest were picked and grown in 10 ml liquid YEB media with rifampicin and the appropriate selection antibiotics at 28°C and 250 rpm overnight. In a 1 L flask, 200 ml liquid YEB were prepared with the appropriate selection antibiotic in a 1:250 concentration and the overnight culture was added. The bacteria were incubated for 4 h at 28°C and 250 rpm. 2 h prior the transformation, 200 µl acetosyringone of a 100 mM stock solution (100 µM) and before floral dipping, 8 g sucrose (4 %) and 100 µl Coatosil 77 (0.05 %) were added to the culture. Plants were dipped into the culture in a beaker to cover all floral buds in bacterial solution and plant trays were covered with plastic lids for one night in the growth chamber. T_1 transgenic plants were selected on MS media containing the appropriate antibiotics.

Expression of recombinant proteins in *E. coli*

5 ml liquid LB medium in a 13 ml tube containing carbenicillin (100 µg/ml) was inoculated with a single colony of BL21 cells containing the desired construct. The bacteria were grown at 37°C and 220 rpm overnight and OD_{600} of the 1:10 diluted cultures was measured with a photometer the next day. The respective volume of the overnight culture corresponding to a final OD 0.1 was added to 300 ml fresh LB medium containing carbenicillin (100 µg/ml) in a 1 L flask. Bacteria were grown at 30°C and 220 rpm until an OD 0.6 was reached and 1 ml sample was taken. After induction with 75 µl 0.4 M Isopropyl β-D-1-thiogalactopyranoside (IPTG), the cultures grew for another 3 h at 30°C and 220 rpm. Another 1 ml sample was taken before harvesting the culture. After 15 min on ice, cultures were split into two for each construct and centrifuged in 50 ml falcons at 5,000 rpm 4°C for 5 min. The supernatant was discarded, and pellets were washed with 4°C cold sterile water and subsequent centrifugation at 5,000 rpm 4°C for 5 min. The supernatant was discarded again. Pellets were weighed and stored at -80°C.

In vitro translation

All reactions were set up as 25 µl assays in low bind reaction tubes using 20 µl TNT T7 Quick MasterMix, 0.7 µl 1 mM Methionine, a volume of the plasmid corresponding to ~500 ng and a volume of ddH_2O to reach the final volume. Samples were vortexed, spin down, incubated for 90 min at 30°C and afterwards immediately frozen at -80°C.

Sample treatment

Samples for SDS-PAGE were treated with 3x Cracking buffer (Table S 5) which was complemented with 23 mg/ml Dithioerythritol (DTE), referred to as sample buffer. All samples taken before induction and before harvesting from protein expression in BL21 were centrifuged for 5 min at 9,000 rpm. After discarding the supernatant, pellets were resuspended in 200 µl sample buffer and boiled for 5 min at 95°C and 900 rpm and stored at -20°C. Plants samples were frozen in liquid nitrogen and ground in different volumes of sample buffer depending on the desired concentration. Samples were then centrifuged at 13,000 rpm for a few minutes and the supernatant was boiled as described before and frozen at -20°C.

Pull-down assay for MS/MS

To extract expressed recombinant proteins which serve as bait in the pull-down assay, bacteria had to be lysed. Pelleted bacterial cultures were resuspended in 15 ml ice cold extraction buffer and cells were subsequently disrupted using a sonicator. The lysate of each construct was transferred into 10 1.5 ml tubes and centrifuged at 4°C and 12,000 rpm for 25 min. 150 µl of the supernatant of each construct were taken as a control for protein expression and mixed with 75 µl sample buffer, incubated for 5 min at 95°C and stored at -20°C. Next, Poly-Prep columns were prepared for pull-down experiments. For reconstitution of glutathione beads, 9 ml washing buffer were added to 95.2 mg dry glutathione agarose beads. After 10 min swelling, 3 ml were loaded onto the columns (one column per construct). Columns were washed twice with 5 ml washing buffer. The supernatants of the centrifuged bacterial lysates were loaded onto the columns and incubated at 4°C for 1 h in a rotating wheel. Columns were drained and subsequently washed 6 times with 5 ml 4°C cold washing buffer. 1 ml washing buffer was added to each column. Each bait protein was distributed into three 1.5 ml tubes (350 µl) and stored at -80°C.

For plant extracts, *Arabidopsis* Col-0 were grown in three independent batches for 7 days on MS media. From each experiment, 1 g plant material was frozen in liquid nitrogen, ground and 2 ml plant extraction buffer were added. Extracts were centrifuged at 4°C and 20,000x g for 20 min. The beads with the bait protein were rebuffered with the plant extraction buffer and the supernatant was removed. 800 µl of each plant extract supernatant was added to each bait protein and then incubated at 4°C for 1.5 h in a rotating wheel. Afterwards beads were washed 9 times with 1 ml washing buffer, which was removed at the end, and the beads were stored at -80°C. Samples were then transferred to the IGZ for analysis.

In vitro **pull-down assay**

The pull-down assay with *in vitro* translated and GST-tagged proteins were performed according to the following protocol: The expressed GST-tagged bait proteins were extracted and bound to glutathione beads as described above. Bait proteins bound to beads were distributed in 1.5 ml reaction tubes with a final 1 mg beads/100 µl buffer density. After spinning down the beads, the supernatant was removed and 200 µl binding buffer (Table S 5) was added. Bait beads were then mixed thoroughly and 100 µl were distributed into two low protein bind tubes. 640 µl binding buffer was then added to the 25 µl in vitro protein prey mix. 300 µl of that mix was added to each bait protein tube and the rest was kept on ice. Samples were incubated for 1 h at 4°C in a rotating wheel. Afterwards, 50 µl of the in vitro translated prey protein was mixed with 50 µl sample buffer (Table S 5), referred to as "Input" sample. The incubated bait-prey mix was spun down. 50 µl of the supernatant were mixed with 50 µl sample buffer, referred to as "FlowThrough (FT)" sample. The rest of the supernatant was removed. The beads were washed three times with 500 µl wash buffer (Table S 5) for 5 min each at room temperature. After centrifuging, the supernatant was removed completely and 50 µl sample buffer was added, referred to as "Eluate (EL)" sample. All samples were heated at 75°C for 10 min and analyzed in a western blot.

Incubation with antibodies

Incubation and washing steps were done in a rotator (neoLab) or on a roller mixer (CAT). After SDS-PAGE and western blot, the membrane was blocked for one hour with blocking buffer (Table S 5) and depending on antibodies and samples incubated one hour or overnight with the respective primary antibody (Table S 10). Afterwards the membrane was washed three times for 10 min with TBS-T (Table S 5), followed by 1 h incubation with the appropriate HRP-conjugated secondary antibody (Table S 10). The membrane was then washed again three times for 10 min in TBS-T and bound antibodies were detected with the SuperSigna West Pico PLUS Chemiluminescent Substrate (Thermo Scientific). Pictures were taken in the Fujifilm Intelligent Dark Box with an Atik 460 EX camera.

Mild membrane stripping for antibody removal and restaining

To re-incubate a membrane with another antibody after western blot and initial detection with an antibody, the "western blot membrane stripping for restaining protocol" from abcam was used. Accordingly, the membrane was incubated with freshly prepared mild stripping buffer for

10 min. This step was repeated. The membrane was then washed twice with PBS for 10 min and twice with TBS-T for 5 min. Afterwards the membrane was ready for blocking and all subsequent steps for detection.

6.3 Results
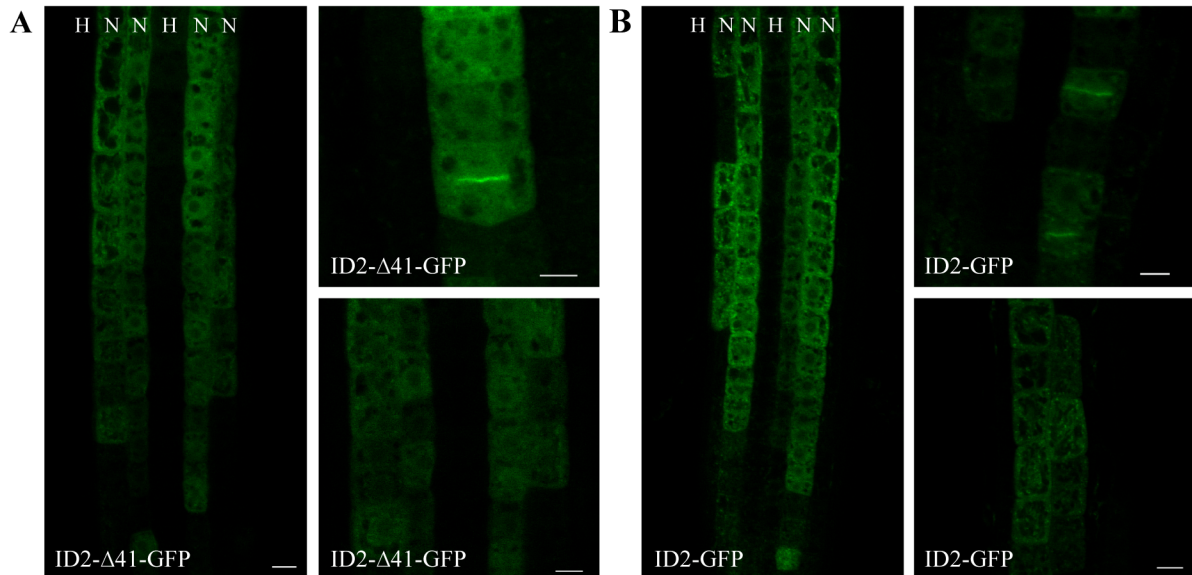
**Figure S 1: Comparison of ID2-GFP and ID2-Δ41-GFP signal.**

Expression pattern of *ID2::ID2-GFP* and *ID2::ID2-Δ41-GFP* in 7-day-old *Arabidopsis* seedling roots. Scale bars = 10 μm. (A) ID2-Δ41-GFP showed a specific signal in non-hair cell files of the root epidermis in the meristematic and transition to elongation zone. Subcellularly, the signal is mostly cytosolic and ID2-Δ41-GFP localizes to the growing cell plate in dividing cells. (B) *ID2-GFP* exhibits the same expression pattern in the root epidermis. ID2-GFP signal is also cytosolic, and it localizes to the cell plate, however, the full length ID2-GFP shows stronger punctate structures in the cytosol reminiscent of endosomal structures.
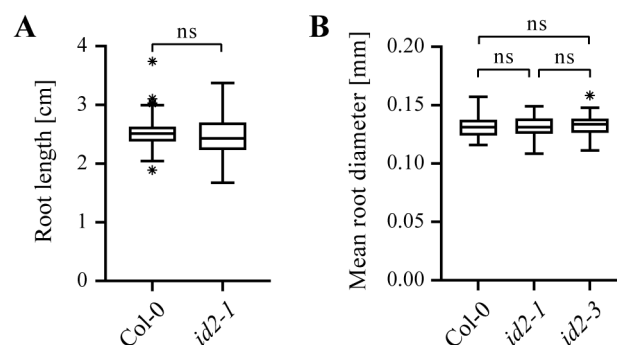
Figure S 2: Loss of *EPSINOID2* does not cause changes in root length or diameter.

Root length and diameter were determined in 7-day-old *Arabidopsis* seedlings in three independent experiments which were pooled. Asterisks indicate outliers. (A) *id2-1* did not show an aberrant root length from wild type (76 < n < 85). (B) Both *epsinoid2* mutants showed no significant difference in mean root diameter compared to Col-0 (71 < n < 89).
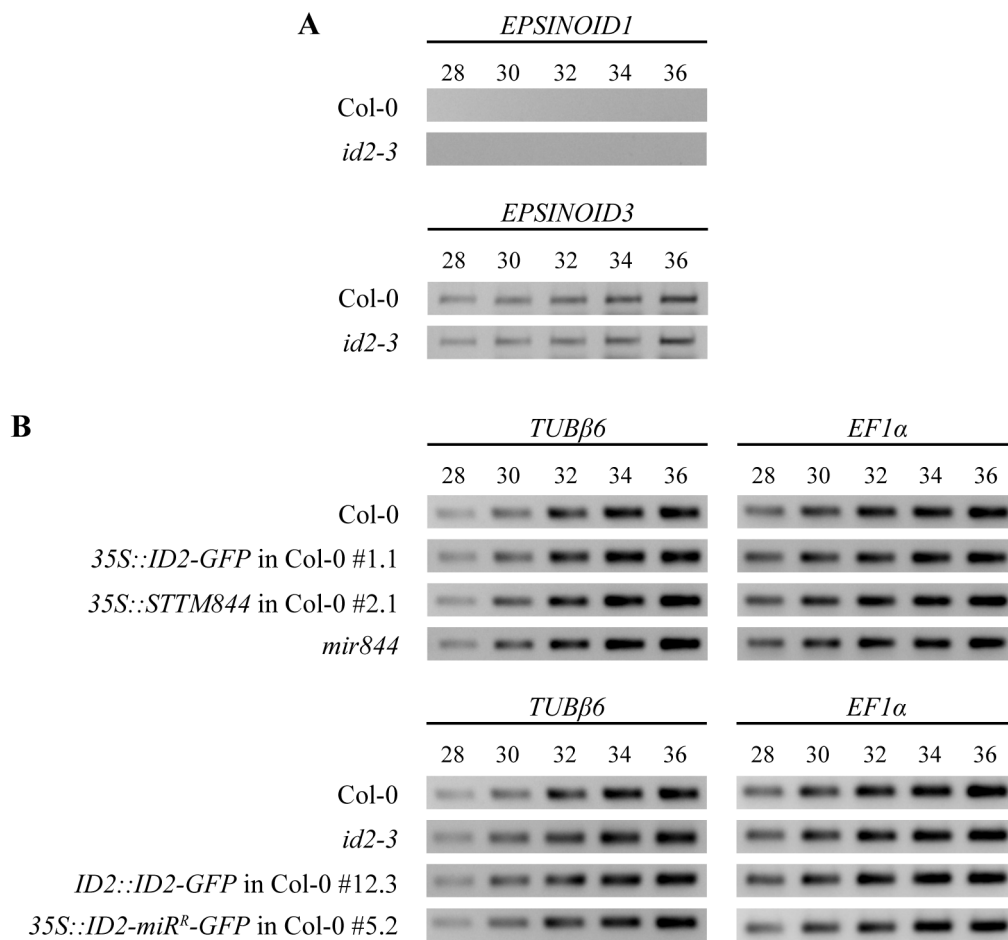
Figure S 3: Semiquantitative RT-PCRs of *id2-3* and *ID2* transformants.

(A) *EPSINOID1* and *3* are not upregulated in *id2-3* mutants. Note that *EPSINOID1* is not expressed in roots at all (Freimuth 2015). (B) Semiquantitative RT-PCR with specific primers for housekeeping genes *TUB6β* and *EF1α* show no increased mRNA levels in either *id2-3* mutant or *ID2* transformants, respectively.
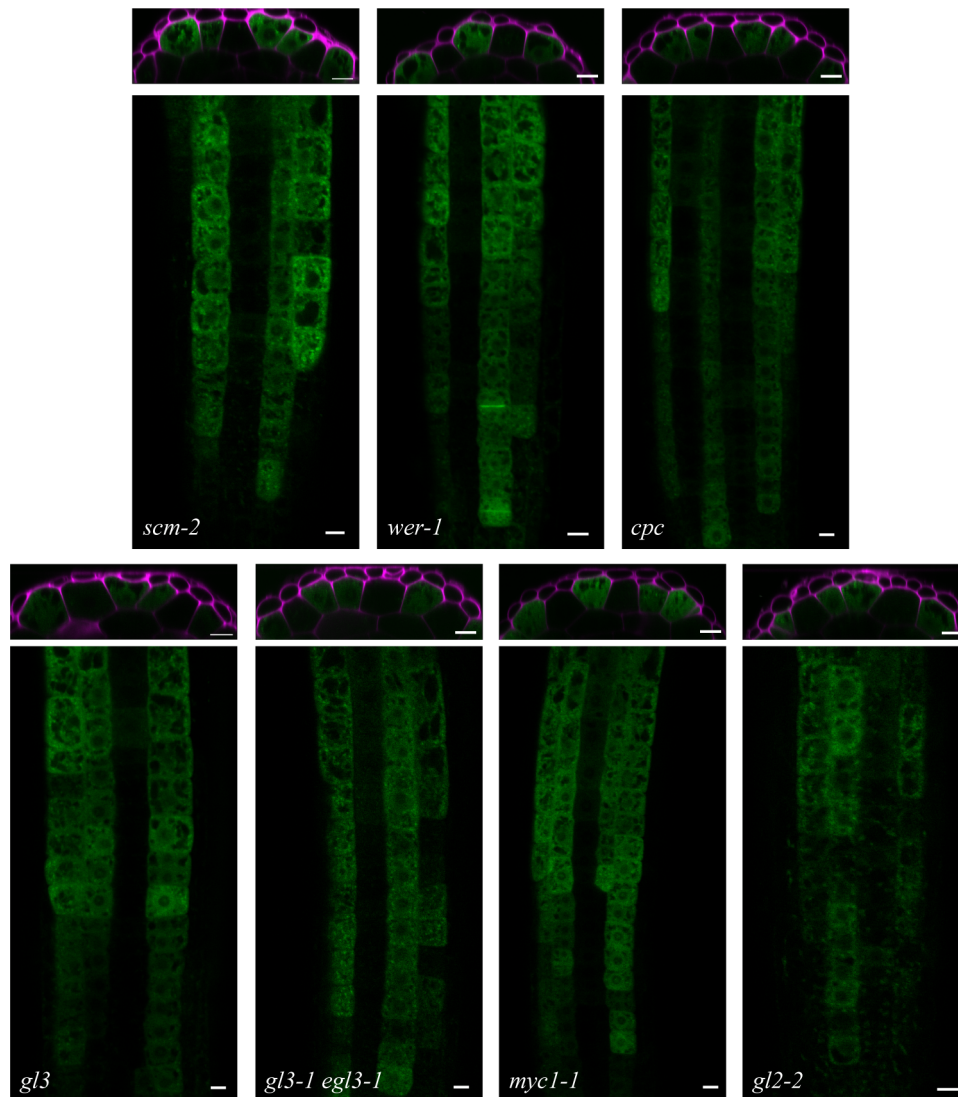
Figure S 4: Backcrosses of *ID2::ID2-GFP* transformants in root hair mutant background.

The analyzed *ID2::ID2-GFP* transformants in root hair mutant background were crossed with Col-0 to test whether the specific expression pattern of *ID2::ID2-GFP* can be restored to ensure that the ID2-GFP signal in root hair mutants is caused by the mutant background. 5-day-old seedlings of the F1 backcrosses were analyzed and, in all lines, the specific non-hair cell pattern of ID2-GFP was restored. Cell walls were stained with propidium iodide. Scale bars = 10 μm.
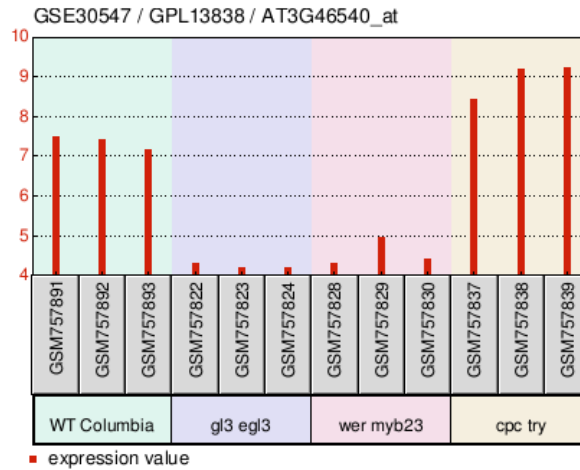
Figure S 5: Expression data of *EPSINOID2* from the *Arabidopsis* root epidermis in different backgrounds. Expression values of *EPSINOID2* in the root epidermis are shown from three different biological replicates of Columbia wild type (WT), *gl3 egl3*, *wer myb23* and *cpc try* mutant seedlings (Bruex et al. 2012). Data were analyzed and graph was obtained using the GEO2R web tool from NCBI.
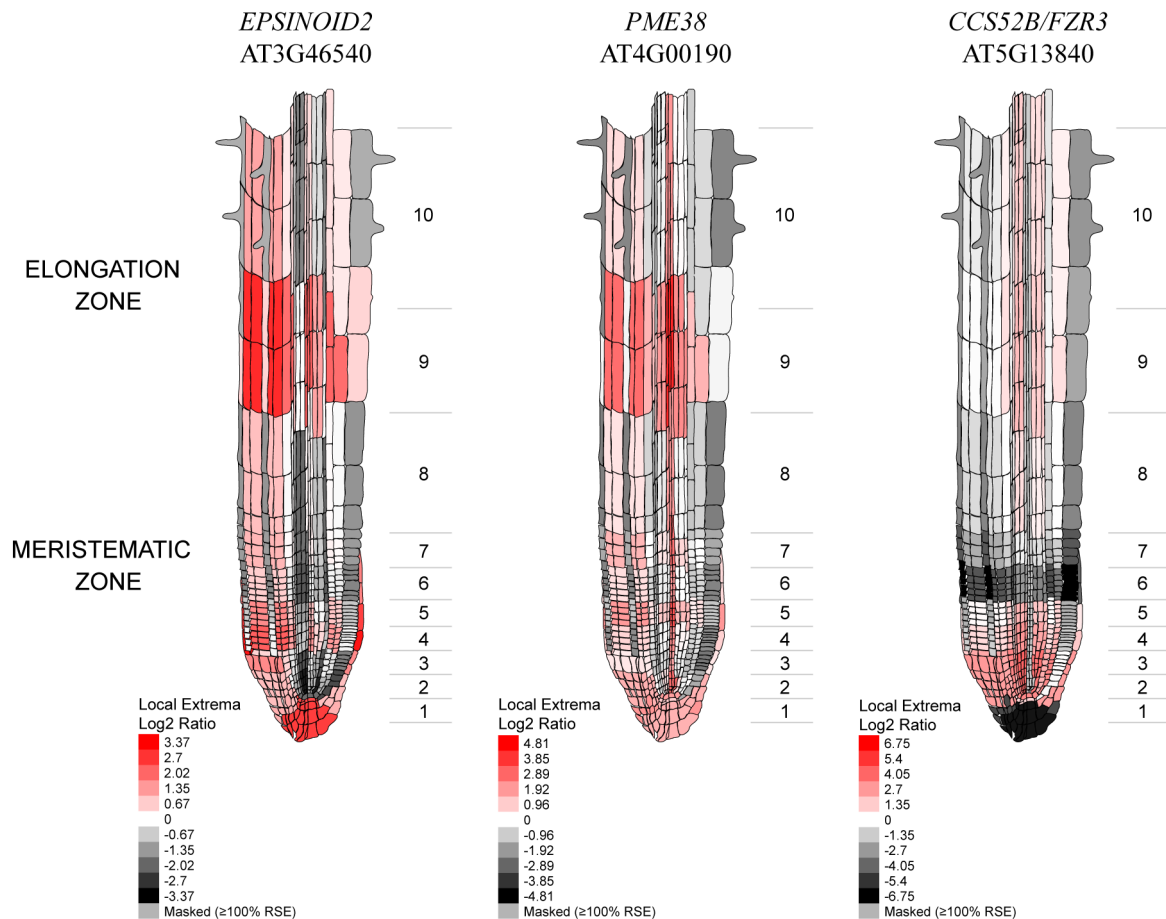
Figure S 6: Cell-type-specific expression data of *EPSINOID2*, *PME38* and *CCS52B* in the *Arabidopsis* root. Cell-type-specific relative gene expression data visualized by the eFP browser (Winter et al. 2007; Brady et al. 2007a; Cartwright et al. 2009). Both, *EPSINOID2* and *PME38* show higher expression in non-hair cells in the transition to the elongation zone. *CCS52B* appears to be expressed very weakly in roots according to these datasets.

Selbstständigkeitserklärung

Hiermit bestätige ich, Nina Freimuth, durch meine Unterschrift, dass die eingereichte Dissertation mit dem Titel

Elucidating the suppression of root hair formation
by a member of a novel, short ENTH protein family
in *Arabidopsis thaliana*

von mir selbstständig und nur mit Hilfe der angegebenen Quellen angefertigt worden ist.

Die von mir vorgelegte Dissertation ist bisher an keiner anderen Hochschule eingereicht worden.

Potsdam, den 19.11.2023   **……………………………**

                                 Nina Freimuth